On the dichotomic collective behaviors of large populations of pulse-coupled firing oscillators

PhD Dissertation by

Alexandre Mauroy

Systems and Modeling Research Unit
Department of Electrical Engineering and Computer Science
Faculty of Applied Sciences
University of Liège, Belgium

Jury members:

Prof. L. Wehenkel (Chair)
Prof. R. Sepulchre (Advisor)
Prof. D. Aeyels (UGent)
Prof. D. Angeli (Imperial College London, United Kingdom)
Prof. J.-M. Coron (Université Pierre et Marie Curie, France)
Prof. T. Gilet (ULg)
Prof. L. Praly (Mines ParisTech, France)

Abstract

The study of populations of pulse-coupled firing oscillators is a general and simple paradigm to investigate a wealth of natural phenomena, including the collective behaviors of neurons, the synchronization of cardiac pacemaker cells, or the dynamics of earthquakes. In this framework, the oscillators of the network interact through an instantaneous impulsive coupling: whenever an oscillator fires, it sends out a pulse which instantaneously increments the state of the other oscillators by a constant value.

There is an extensive literature on the subject, which investigates various model extensions, but only in the case of *leaky integrate-and-fire oscillators*. In contrast, the present dissertation addresses the study of other integrate-and-fire dynamics: general *monotone integrate-and-fire dynamics* and *quadratic integrate-and-fire dynamics*.

The main contribution of the thesis highlights that the populations of oscillators exhibit a *dichotomic collective behavior*: either the oscillators achieve perfect synchrony (slow firing frequency) or the oscillators converge toward a phase-locked clustering configuration (fast firing frequency). The dichotomic behavior is established both for finite and infinite populations of oscillators, drawing a strong parallel between discrete-time systems in finite-dimensional spaces and continuous-time systems in infinite-dimensional spaces.

The first part of the dissertation is dedicated to the study of monotone integrate-and-fire dynamics. We show that the dichotomic behavior of the oscillators results from the monotonicity property of the dynamics: the monotonicity property induces a *global contraction* property of the network, that forces the dichotomic behavior. Interestingly, the analysis emphasizes that the contraction property is captured through a 1-norm, instead of a (more common) quadratic norm.

In the second part of the dissertation, we investigate the collective behavior of quadratic integrate-and-fire oscillators. Although the dynamics is not monotone, an "average" monotonicity property ensures that the collective behavior is still dichotomic. However, a global analysis of the dichotomic behavior is elusive and leads to a standing conjecture. A local stability analysis circumvents this issue and proves the dichotomic behavior in particular situations (small networks, weak coupling, etc.). Surprisingly, the local stability analysis shows that specific integrate-and-fire oscillators exhibit a non-dichotomic behavior, thereby suggesting that the dichotomic behavior is not a general feature of every network of pulse-coupled oscillators.

The present thesis investigates the remarkable dichotomic behavior that emerges from networks of pulse-coupled integrate-and-fire oscillators, putting emphasis on the stability properties of these particular networks and developing theoretical results for the analysis of the corresponding dynamical systems.

Résumé

Les populations d'oscillateurs impulsivement couplés constituent un paradigme simple et général pour étudier une multitude de phénomènes naturels, tels que les comportements collectifs des neurones, la synchronisation des cellules pacemaker du coeur, ou encore la dynamique des tremblements de terre. Dans ce contexte, les oscillateurs interagissent au sein du réseau par le biais d'un couplage instantané: quand un oscillateur décharge, il envoie vers les autres oscillateurs une impulsion qui incrémente instantanément leur état par une valeur constante.

Diverses extensions du modèle ont été intensément étudiées dans la littérature, mais seulement dans le cas d'oscillateurs *leaky integrate-and-fire*. Afin de pallier cette restriction, le présent manuscrit traite de l'étude d'autres dynamiques *integrate-and-fire*: les dynamiques générales *integrate-and-fire monotones* et les dynamiques *integrate-and-fire quadratiques*.

La contribution principale de la thèse met en évidence le *comportement d'ensemble dichotomique* selon lequel s'organisent les populations d'oscillateurs: soit les oscillateurs atteignent un état de synchronisation parfaite (taux de décharge lent), soit ils convergent vers une configuration de *clustering* en blocage de phase (taux de décharge rapide). Ce comportement dichotomique est établi aussi bien pour des populations finies que pour des populations infinies, ce qui démontre un parallèle élégant entre des systèmes en temps-discret dans des espaces de dimension finie et des systèmes en temps-continu dans des espaces de dimension infinie.

La première partie du manuscrit se concentre sur l'étude des dynamiques *integrate-and-fire* monotones. Dans ce cadre, nous montrons que le comportement dichotomique résulte de la propriété de monotonicité des oscillateurs. Cette dernière induit une propriété de *contraction globale*, elle-même engendrant le comportement dichotomique. En outre, l'analyse révèle que la propriété de contraction est capturée par une norme 1, au lieu d'une norme quadratique (plus usuelle).

Dans la seconde partie de la thèse, nous étudions le comportement d'ensemble d'oscillateurs *integrate-and-fire* quadratiques. Bien que la dynamique ne soit plus monotone, une propriété de monotonicité "en moyenne" implique que le comportement collectif est encore dichotomique. Alors qu'une analyse de stabilité globale s'avère être difficile et conduit à plusieurs conjectures, une analyse locale permet de prouver le comportement dichomique dans certaines situations (réseaux de petite taille, couplage faible, etc.). De plus, l'analyse locale prouve que des oscillateurs *integrate-and-fire* particuliers ne s'organisent pas suivant un comportement dichotomique, ce qui suggère que ce dernier n'est pas une caractéristique générale de tous les réseaux d'oscillateurs impulsivement couplés.

En résumé, la thèse étudie le remarquable comportement dichotomique qui émerge des réseaux d'oscillateurs *integrate-and-fire* impulsivement couplés, mettant ainsi l'emphase sur les propriétés de stabilité desdits réseaux et développant les résultats théoriques nécessaires à l'étude mathématique des systèmes dynamiques correspondants.

Acknowledgments

dw3 nṯr n.ṯn, thank you.

It is my pleasant duty to put on record my thanks and gratitude to all of those who have contributed to make this thesis a pleasant, enriching, and even exciting experience.

First and foremost, I am heartily thankful to my advisor, Rodolphe Sepulchre, who always maintained the (unstable) equilibrium between strictness and humanity that characterizes a conscientious mentor concerned about his students' wellness. This thesis would not have been possible without his invaluable advice, his permanent support, and his unwavering enthusiasm. Moreover, I acknowledge him for his encouragements to learn new (supposedly scientific) topics, even as far from dynamical systems theory as Ancient Egyptian language.

I also mention with gratitude the help which I have received from Jean-Michel Coron (Université Pierre et Marie Curie, France), Paul Van Dooren (UCL), and Quentin Louveaux. Faced with important issues, I have greatly benefited from their inestimable expertise.

I am very grateful to Julien Hendrickx (UCL). His support along with his interest for the present research have been a real source of motivation.

I am also indebted to my (former and present) colleagues at University of Liège, who have all contributed to create a stimulating work environment in a warm and friendly atmosphere. In particular, it was a real pleasure to share the office with Michel Journée and Anne Collard, two different but very nice people. Many thanks also to Christian Bastin for his enjoyable company; to Silvère Bonnabel for the nice climbing evenings together with informal discussions on scientific and personal matters; to Boris Defourny for interesting (and often funny) conversations; to Guillaume Drion for lively debates on (potentially) philosophical subjects; to Gilles Meyer for his prompt and efficient solutions to so many technical problems; to Bamdev Mishra for being the most faithful member of our UMP (University-restaurant Mangeur Party); to Pierre Sacré for his precious help through various scientific interactions; to Alain Sarlette for his invaluable encouragement and his sound advice; to Laura Trotta for all these (un)intended events that brought a hint of freshness and humor within the research group. Occasional discussions in the corridors and good moments with Damien Ernst, Florence Belmudes, Raphaël Fonteneau, and Mohamed Boutaayamou were also greatly appreciated. Finally, a special thank goes to Marcus Drosson for the mutual sharing of our respective problems and achievements, resulting in a friendly support throughout all these years of studies.

I gratefully acknowledge Joelle Tran for her careful reading of the first draft and for her valuable comments.

I wish to express my sincere gratitude to the members of the Jury: Louis Wehenkel (chair), Rodolphe Sepulchre (advisor), Dirk Aeyels (UGent), David Angeli (Imperial College London, United Kingdom), Jean-Michel Coron (Université Pierre et Marie Curie, France), Tristan Gilet (ULg), and Laurent Praly (Mines ParisTech, France).

Major financial support was provided by an FNRS fellowship and the Belgian Network DYSCO (Dynamical Systems, Control, and Optimization), funded by the Interuniversity Attraction Poles Programme, initiated by the Belgian State, Science Policy Office.

Last but not least, I offer my regards and blessing to my family. I owe my parents many thanks for unconditional support and devotion over all these years. Completing this thesis is also an occasion to remember all those moments with my grandfather, Marcel Mauroy, spent sharing our common passion for science and mathematics. Finally, my deepest gratitude goes to my future wife, my sweet Priscilla, whose love has been, by far, the most precious encouragement.

Contents

Chapter 1

Introduction

"*In the longer run, network thinking will become essential to all branches of science as we struggle to interpret the data pouring in from neurobiology, genomics, ecology, finance and the World-Wide Web.*" Such is the conclusion of a 2001 Nature article by S. H. Strogatz [105], that illustrates to what degree analyzing complex networks to predict or design their collective behavior has become an essential question. One decade later, network theory is more than ever a central and overwhelming research thematic in many scientific disciplines.

From artificial to natural networks

In recent times, the synthesis of collective behaviors in artificial networks has attracted great interest. In particular, numerous engineering applications have motivated leaderless coordination of multi-agent systems. Without leader and without external control, the agents interact within an autonomous network to *reach a consensus*: to compute a common average of local measurements (sensor networks), to align according to a common heading angle (unmanned aerial vehicles), or to achieve a common task (cooperative robotics). The *consensus problem* thematic and the synthesis of collective motions have led to intensive research in the engineering control community (e.g. [52, 66, 76, 98, 113], see the introduction in [94] for an overview).

Artificial networks are, first and foremost, a mere (and pale) imitation of nature, which was and is still an inexhaustible source of inspiration for the design of leaderless multi-agent systems. In a number of natural phenomena, collective behaviors spontaneously emerge from the network, in spite of the absence of leader. The puzzling unity of schools of fish or flocks of birds is such an intriguing example [91].

Among the multitude of natural networks, the most fascinating ones are undoubtedly the (biological) neural networks, that have largely inspired the machine learning community (see e.g. the Hopfield model [46]). Above all, the human brain is the biggest network ever studied, with billions of neurons individually connected to about ten thousands of others. Interestingly, the difficulties to unveil the brain mysteries arise not only from the intricate architecture of the huge neural network, but also because the essential functioning mechanisms are still unknown. For instance, it is not clear how information is processed in the brain, a fundamental issue known as the *neuronal coding problem*. (The reader may refer to the monograph [35] for a comprehensive overview on neural networks.)

It is an unquestionable fact that every brain mechanism does not rely on the individual

behavior of a neuron, but on the ensemble behavior of many neurons. As an illustration, particular collective behaviors have been pointed out to explain some vision mechanisms (*feature binding problem* [30, 38]). Pathologies such as epilepsy or Parkinson disease arise from abnormal collective behaviors [116]. As a consequence, a main challenge in neuroscience is to highlight how the intrinsic properties of the neuron, for which accurate models are well-known (e.g. Hodgkin-Huxley model [45]), influence the global ensemble behavior of the whole network, a behavior that is recorded, for instance, in an electroencephalography.

Neural networks exhibit a wealth of collective behaviors, among which two are particularly remarkable: *synchronization* and *clustering*. Synchronization is a coherent and organized behavior emerging from a (apparently) disorganized network [106]. Many other natural mechanisms rely on synchronization: heart pacemaker cells of the heart [86], insulin-secreting cells in the pancreas [100], flashing fireflies [15], chirping crickets [120], clapping audiences, etc. In contrast, clustering is a fragmentation of the collective behavior in locally synchronized but well separated subgroups. It is observed in various situations: swarm behavior of animals or social insects [91, 119], yeast cell cycle [9], opinion dynamics in social science [43], etc.

In the above context, the present dissertation is a mathematical study of the collective behaviors in large networks inspired from neural networks, with a particular attention to both synchronization and clustering behaviors. The general objective is to *highlight the relationships between the microscopic properties of the individual agents and the macroscopic ensemble phenomena of the whole network.*

Networks of coupled oscillators

A general paradigm to analyze and understand a large variety of natural phenomena is to study networks of *coupled oscillators*. Acoustic vibrations, circadian rhythms, or economic cycles are such explicit examples that clearly illustrate the omnipresence of oscillators. As a consequence, networks of coupled oscillators are often the underlying mechanisms of numerous phenomena: they play a key role in neuroscience [35], but also in other fields of biology (e.g. heart pacemaker cells [86]), in mechanics (e.g. coupled Huygens pendula [49]), in physics (e.g. Josephson-junction arrays [123]), in civil engineering (e.g. pedestrian excitation of bridges [68]), etc.

The study of coupled oscillators is not trivial, but appears to be a *complex issue*. Indeed, the network simplicity is only apparent: although the oscillators are characterized by a simple individual dynamics, they are usually connected through a *nonlinear coupling*. They may therefore exhibit intricate collective behaviors, whose complexity is amplified by the network size. In particular, the robustness of the collective behaviors in heterogeneous networks is a mathematical puzzle that has attracted intense research interest (e.g. Kuramoto model [59, 104]).

In a more specific framework than the general context of coupled oscillators, the present thesis is dedicated to the study of models of coupled *phase oscillators*. Under mild assumptions, an oscillatory system, however complex it is, can be turned into a phase oscillator [125]. The sensitivity of the phase oscillator to external perturbations is expressed through the so-called *phase response curve*, a well-known tool that biologists (for instance) can directly compute with real experiments (see [102]). In this context, a fundamental question is

to quantify, through the phase response curve, the robustness of the phase oscillator to external perturbations [40]. Investigating the collective behaviors in networks of coupled phase oscillators, where each oscillator is perturbed by the neighboring oscillators, is perfectly in line with this important robustness issue.

Impulsive coupling

There exist many examples of oscillators that do not interact through a continuous and permanent coupling, but that influence (and are influenced by) the network only during a tiny fraction of their cycle (e.g. yeast cells populations [9]). It is particularly so when the oscillators send out fast pulses (e.g. spiking neurons [35]), a situation where the coupling is almost instantaneous.

In 1975, Peskin proposed a model of *instantaneous impulsive coupling* [86], assuming that a pulse emitted by an oscillator causes an *instantaneous increment* to the state of the other oscillators (the oscillators are *pulse-coupled*). Initially introduced to model pacemaker cells of the heart, impulsive coupling was successfully applied to spiking neurons [35], flashing fireflies [15], earthquakes dynamics [82], etc. and even to unsupervised classification problems [92].

Impulsive coupling is always associated to *firing oscillators*. The emission of the pulses corresponds to a fast part of the oscillator dynamics —the so-called *firing* — that contrasts with the slow remaining part of the dynamics. The most popular model studied in this context is the *integrate-and-fire oscillator* [57, 63], whose evolution is characterized by a rise to an upper threshold and an instantaneous reset to a lower threshold (the firing). Networks of pulse-coupled integrate-and-fire oscillators were initially studied by Mirollo and Strogatz [75], a seminal paper that initiated abundant research on diverse extensions of the original model (e.g. reduced interconnectivity [25, 26, 28, 36, 84, 108, 110], delays [33, 109], non-instantaneous interactions [3, 12, 118, 128], non-identical oscillators [10, 19, 24, 97]).

From the original model of Peskin to the most recent studies, the pulse-coupled oscillators are assumed to be *leaky* integrate-and-fire oscillators [63], an integrate-and-fire dynamics that is popular but restrictive with respect to the wide diversity of natural phenomena. For instance, a leaky dynamics is a caricature of the real dynamics of a neuron, which may exhibit various behaviors, such as excitability. However, in spite of the numerous extensions of the original model, *studies of more general integrate-and-fire oscillators are surprisingly rare*. In this context, significant results on more general dynamics are missing.

To fill in this lack, the present dissertation addresses the study of *more general dynamics*, thereby paving the way to investigate the *relationship between the dynamics of the oscillators and the collective behaviors of the network.*

1.1 Contributions of the dissertation

The major contribution of the dissertation is to highlight the collective *dichotomic behavior* observed in networks of pulse-coupled integrate-and-fire oscillators: the oscillators either achieve *perfect synchrony* (low firing frequency) or converge to a *clustering behavior* (high firing frequency). In this context, the thesis considers *monotone* integrate-and-fire dynamics and (non-monotone) *quadratic* integrate-and-fire dynamics, and aims at answering the following questions:

- In the case of *monotone* dynamics, why is the collective behavior dichotomic ?

  The dissertation investigates general monotone dynamics, including the leaky integrate-and-fire dynamics, and shows that the monotonicity property of the dynamics induces a global *contraction property* of the network. This contraction property formally explains the dichotomic behavior of the oscillators.

- In the case of *quadratic* integrate-and-fire oscillators, why is the collective behavior still dichotomic (in spite of the non-monotone dynamics) ?

  The dissertation goes beyond the monotonicity assumptions by investigating the *non-monotone* quadratic integrate-and-fire dynamics, a well-known generalization of the leaky integrate-and-fire dynamics [32]. To the author's knowledge, the dynamics has never been considered with an impulsive coupling. However, such a study is of interest since the dynamics can model an excitable behavior instead of the oscillatory behavior.

  The study demonstrates that the quadratic integrate-and-fire oscillators are characterized by the dichotomic behavior. Even though the dynamics is non-monotone, the dichotomic behavior results from the "average" monotonicity property of the dynamics.

More specifically, the main points and contributions of the dissertation are summarized as follows.

- For monotone oscillators, the *global stability results* obtained in the thesis contrast with the weaker local results of the existing literature. Interestingly, they rely on 1-*norms instead of more usual quadratic norms*. Even though the use of non-quadratic norms in stability theory is not novel (see e.g. [44, 87, 88]), the framework presented throughout the thesis could possibly open new avenues for the general study of dynamical systems with monotonicity properties.

- The study of quadratic integrate-and-fire oscillators is a complex issue, and a *strong conjecture* on the global stability problem is investigated. However, several local stability results circumvent the open problems, still highlighting the dichotomic behavior of the quadratic integrate-and-fire oscillators.

- Surprisingly, the dichotomic behavior is *not a general property* in networks of pulse-coupled integrate-and-fire oscillators. An example of integrate-and-fire oscillator is provided, whose dynamics is similar to quadratic integrate-and-fire dynamics and that is not characterized by a dichotomic behavior. As a consequence of the result, some properties of small networks are not observed with larger networks.

- Throughout the dissertation, the results are extended to the study of a continuum of oscillators: the stability results in finite-dimensional spaces are naturally extended to nonlinear partial differential equations in infinite-dimensional spaces. In this context, a *strong parallel* is established *between finite and infinite* populations, and *between discrete-time and continuous-time* dynamical systems.

1.2 Outline of the dissertation

The dissertation is organized as follows (a more detailed summary is given at the beginning of each chapter).

Chapter 2 presents a general overview on firing oscillators models, with a particular emphasis on several integrate-and-fire models. The second part of the chapter is devoted to phase reduction techniques, that reduce firing oscillators to harmonic (phase) oscillators characterized by a particular phase response curve.

Chapter 3 introduces the mathematical tools involved in the study of pulse-coupled oscillators. General results on the collective behaviors of the networks are presented, that require no specific assumption on the dynamics of the oscillators. In particular, the dichotomic behavior is studied for networks of two oscillators.

Chapter 4 considers the case of monotone dynamics, providing global stability results that ensure convergence toward (phase-locked) clustering configurations. Various approaches suggest that a 1-norm is the most appropriate framework to capture the global network properties. Finally, the robustness of the clustering configurations is investigated in the case of heterogeneous networks.

Chapter 5 extends the global stability results of Chapter 4 to infinite populations of pulse-coupled oscillators. Stability results characterize the nonlinear continuity equation that describes the evolution of the infinite population, still highlighting the dichotomic behavior of the oscillators.

Chapter 6 focuses on the collective behaviors of quadratic integrate-and-fire oscillators. The chapter conjectures the (global) dichotomic behavior of the oscillators and provides partial results on the local stability problem. Another model is proposed, which is similar to the quadratic integrate-and-fire model but which does not exhibit a dichotomic behavior.

Chapter 7 is devoted to the weak coupling limit. Under the weak coupling assumption, general stability criteria are obtained, both for finite and infinite populations. The stability criteria not only solve the conjecture on quadratic integrate-and-fire oscillators but are also applied to very general models (Hodgkin-Huxley dynamics, delays, etc.). Finally, some results related to the averaged dynamics of the oscillators are presented in the last part of the chapter.

Chapter 8 concludes the manuscript, summarizing the achievements of the thesis and raising some research perspectives.

Publications: The main results of the thesis can be found in the following publications.

- The material of Chapter 4 is published in [73];
- The material of Chapter 5 can be found in [72];
- The material of Chapter 6 is published in [70] and in [74];

- The material of Chapter 7 is published in [74].

1.3 Conventions and notations

Abbreviations. The acronyms used in the thesis are defined as follows.

FN	Fitzhugh-Nagumo
HH	Hodgkin-Huxley
iPRC	infinitesimal phase response curve
LHS	left hand side
LIF	leaky integrate-and-fire
PDE	partial differential equation
PRC	phase response curve
QIF	quadratic integrate-and-fire

Stability. Stability theory plays a key role in the present dissertation. For a comprehensive overview of Lyapunov stability theory and for detailed definitions of *(asymptotic) stability*, *local stability*, *global stability*, etc., the reader may refer to the reference book [55]. Throughout the manuscript, the term "asymptotic" is omitted, so that "stability" always means "asymptotic stability". In addition, a system will be said *anti-stable* if the corresponding backward-time system is stable.

Notations. Given a scalar variable x and a scalar function f, one uses the following notations:

$\Re\{x\}$, $\Im\{x\}$	real and imaginary parts of x
$x^\dagger$	complex conjugate of x
$\lfloor x \rfloor$	integer part of x
$\lceil x \rceil$	smallest integer such that $\lceil x \rceil \geq x$
x^+	next iterate of a discrete-time map
$\dot{f}$	first derivative of f with respect to time
f', f''	first and second derivatives of f with respect to a phase variable
$\hat{f}_n$	nth Fourier coefficient of f

Vectors and matrix are denoted by bold symbols. Given the vector $\mathbf{x}$ and the matrix $\mathbf{M}$, one defines the general notations:

$\mathbf{x}^T$, $\mathbf{M}^T$	transpose of $\mathbf{x}$ and $\mathbf{M}$
$\mathbf{M}^\dagger$	conjugate transpose of $\mathbf{M}$
$\|\mathbf{M}\|_\infty$	infinity norm of $\mathbf{M}$
$\|\mathbf{x}\|_{(1)}$, $\|\mathbf{M}\|_{(1)}$	1-norm (introduced in Section 4.2.1) of $\mathbf{x}$ and $\mathbf{M}$
$\|\mathbf{x}\|_{(2)}$, $\|\mathbf{M}\|_{(2)}$	quadratic norm (introduced in Section 4.2.2) of $\mathbf{x}$ and $\mathbf{M}$

For the sake of simplicity, the most frequent symbols used in the manuscript are listed below.

i	unit imaginary number $\sqrt{-1}$
j, k, l, n	integers used in various situations (mainly subscripts)
N	number of oscillators
N_g	number of clusters
x	state variable
t	time variable
F	vector field of an integrate-and-fire oscillator, i.e. $\dot{x} = F(x)$
S, γ	parameters of F
$\underline{x}$, $\overline{x}$	lower and upper thresholds of the integrate-and-fire dynamics
ϵ, K	coupling strengths in finite and infinite populations
θ	phase variable
ω	natural frequency
$\mathbf{\Theta}$	phase configuration of the network
θ^*, $\mathbf{\Theta}^*$	phase-locked configurations (fixed point)
$\rho(\theta, t)$	density of the oscillators
$J(\theta, t)$	flux of the oscillators
$\rho^*(\theta)$, $J^*(\theta)$	stationary density and stationary flux
$f(\theta)$	evolution function of the integrate-and-fire oscillator
$Z(\theta)$	infinitesimal phase response curve
$h(\theta)$	scalar firing map
$\mathbf{H}(\mathbf{\Theta})$	multidimensional firing map
$\mathbf{I}$	identity matrix
$\mathbf{J}$	Jacobian matrix
$\mathbf{L}$	linear map (defined in Section 3.4.2)
$\mathbf{N}$	nonlinear map (defined in Section 3.4.2)
$\mathcal{V}$	Lyapunov function
$p(z)$	polynomial function
λ	eigenvalue or root of polynomial p
$\check{h}$, $\check{\mathbf{H}}$, $\check{\theta}$, $\check{\mathbf{\Theta}}^*$	notations corresponding to the conservative situation (Section 6.3)

Chapter 2

Models of interacting firing oscillators

As a preliminary to the results developed in the sequel, this chapter presents a brief overview of the oscillators characterized by a fast firing phenomenon (e.g. spiking neurons [35], heart pacemaker cells [86], etc.). Section 2.1 describes general (multidimensional) models of firing oscillators, including the Hodgkin-Huxley model and the Fitzhugh-Nagumo model. Phase reduction techniques are developed in Section 2.2, which shows how general (firing) oscillators can be turned into phase oscillators evolving on the circle. Section 2.3 introduces the well-known integrate-and-fire models as reductions of multidimensional firing models. Finally, networks of interacting firing oscillators are briefly described in Section 2.4, as well as the two main behaviors that emerge from such networks.

2.1 General models of firing oscillators

An oscillator is a dynamical system whose state asymptotically evolves on a (stable) *limit cycle*. Consider a (nonlinear) state dynamics

$$\dot{\mathbf{x}} = \mathbf{F}(\mathbf{x}), \quad \mathbf{x} \in \mathbb{R}^n$$

with a periodic orbit (or *limit cycle*) $\mathbf{x}^\gamma(t)$ of period T, such that $\mathbf{x}^\gamma(t+T) = \mathbf{x}^\gamma(t)$ for all t. If the limit cycle is stable, any trajectory close to the limit cycle converges to the limit cycle: the system behaves as an oscillator.

In mathematical neuroscience, an oscillator model usually describes the periodic *firing* of a neuron under a constant external current. A *firing oscillator* is characterized by a limit cycle with contrasting *slow* and *fast* parts. This is illustrated in the following well-known example.

Example 2.1.1 (Hodgkin-Huxley (HH) model)**.** A. L. Hodgkin and A. F. Huxley proposed a four-dimensional conductance-based model for the membrane voltage dynamics of the squid giant axon [45]. Taking into account the main ionic currents (ions Na^+ and K^+) and a leakage

current through the cell membrane, the dynamics is given by

$$\begin{aligned} C\dot{V} &= -\bar{g}_{\mathrm{Na}}(V - V_{\mathrm{Na}})m^3h - \bar{g}_{\mathrm{K}}(V - V_{\mathrm{K}})n^4 - g_{\mathrm{L}}(V - V_L) + I_b \\ \dot{m} &= \alpha_m(V)(1-m) - \beta_m(V)m \\ \dot{h} &= \alpha_h(V)(1-h) - \beta_h(V)h \\ \dot{n} &= \alpha_n(V)(1-n) - \beta_n(V)n \end{aligned}$$

with

$$\begin{aligned} \alpha_m(V) &= (0.1V - 2.5)/[1 - \exp(2.5 - 0.1V)] \\ \beta_m(V) &= 4\exp(-V/18) \\ \alpha_h(V) &= 0.07\exp(-V/20) \\ \beta_h(V) &= 1/[1 + \exp(3 - 0.1V)] \\ \alpha_n(V) &= (0.01V - 0.1)/[1 - \exp(1 - 0.1V)] \\ \beta_n(V) &= 0.125\exp(-V/80) \end{aligned}$$

and

$V_{\mathrm{Na}} = 115\,\mathrm{mV}$, $V_{\mathrm{K}} = -12\,\mathrm{mV}$, $V_{\mathrm{L}} = 10.6\,\mathrm{mV}$, $\bar{g}_{\mathrm{Na}} = 120\,\mathrm{mS/cm^2}$, $\bar{g}_{\mathrm{K}} = 36\,\mathrm{mS/cm^2}$, $\bar{g}_{\mathrm{L}} = 0.3\,\mathrm{mS/cm^2}$, $C = 1\,\mu\mathrm{F/cm^2}$.

For some values of the (external) baseline current I_b — a standard value is $I_b = 10$ mA, the system has a stable limit cycle characterized by a "slow" voltage increase followed by a fast *action potential*, a short event in which the voltage rapidly increases and decreases (Figure 2.1). In particular, when the maximum value $\overline{V} \approx 30$ mV is reached, the voltage quasi-instantaneously falls to the minimum value $\underline{V} \approx -70$ mV. This fast "reset" from the maximum value $\overline{V}$ to the minimum value $\underline{V}$ is a *firing* — the oscillator is said to *fire*, a phenomenon that is typical of neuron behaviors. ◇

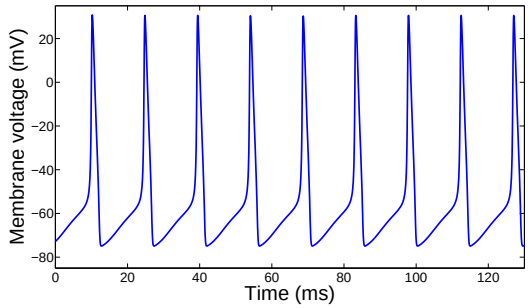

Figure 2.1: With an external current $I_b = 10$ mA, the Hodgkin-Huxley model has a periodic behavior (firing oscillator). When the membrane voltage reaches the maximum value $\overline{V} \approx 30$ mV, it is (quasi)-instantaneously reset to the minimum value $\underline{V} \approx -70$ mV: the oscillator *fires*.

Since it provides a realistic model of the firing dynamics characterizing an action potential, the HH model is probably the most used and studied model in mathematical neuroscience.

Numerous extensions of the model have also been considered in the last decades, incorporating, for instance, other ion channels (see e.g. [27]). On the other hand, similar but simpler models are also widely used in computational neuroscience, similar in their *firing* behavior and simpler in their lower dimension (for an overview, refer to [50, 54]). In two dimensions, examples of such models are the Morris-Lecar model [77] and the FitzHugh-Nagumo (FN) model [34, 78].

Example 2.1.2 (Fitzhugh-Nagumo (FN) model)**.** Initially suggested by R. Fitzhugh, the FN model is a relaxation model characterized by the two-dimensional dynamics

$$\begin{aligned} \dot{V} &= V - V^3/3 - U + I_b\,, \\ \dot{U} &= \tau^{-1}(V + a - b\,U)\,, \end{aligned}$$

where V is the membrane voltage and U is a recovery variable. The parameters are usually $a = 0.7$, $b = 0.8$, and $\tau^{-1} = 0.08$.

For some values of the (external) baseline current (e.g. $I_b = 1$), there is a limit cycle. Provided that $\tau^{-1} \ll 1$, the dynamics has two (strongly) separated time scales, resulting in a sharp time evolution that characterizes a firing behavior (see Figure 2.2). ◇

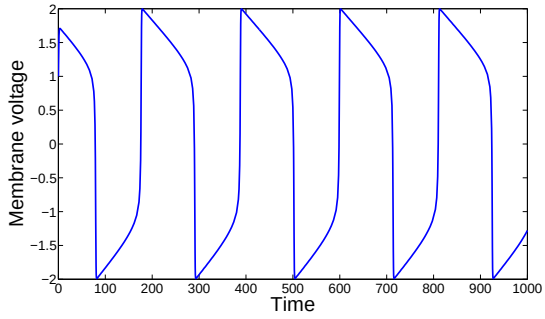

Figure 2.2: With an external current $I_b = 1$ and $\tau^{-1} = 0.01$, the FN model has a periodic firing behavior.

2.2 Phase reduction

The multidimensional dynamics of the firing oscillators often leads to an intricate mathematical analysis, especially when large networks of coupled oscillators are considered. In this context, phase reduction techniques are widely used for the study of interacting oscillators. Phase reduction turns *multidimensional state* oscillators into *one-dimensional phase* oscillators whose sensitivity to external perturbations is given by the so-called *phase response curve*, a well-known mathematical tool especially used for biological systems [50, 125] (see [102] for a review).

According to Winfree [125], a dynamical system characterized by an asymptotically stable limit cycle can be assimilated to a phase oscillator in a neighborhood of the limit cycle, as long as the perturbations (to which the system is subjected) are weak enough. On the limit

cycle, a phase $\theta \in S^1(0, 2\pi)$ is assigned to the oscillator and is related to the ratio of time spent on the cycle to the period T of the limit cycle. In the case of firing oscillators, a phase $\theta = 0$ corresponds by convention to the point of the limit cycle where the firing occurs. (Even though the phase is scaled to 2π, so that a complete revolution on the limit cycle corresponds to a phase variation of 2π, the phase cannot be assimilated to an angular measurement of the position on the limit cycle.) The transformation reduces the multidimensional state dynamics $\dot{\mathbf{x}} = \mathbf{F}(\mathbf{x})$, $\mathbf{x} \in \mathbb{R}^n$, to a *one-dimensional phase dynamics* $\dot{\theta} = \omega$, with the natural frequency $\omega = 2\pi/T$.

If an oscillator with state $\mathbf{x}^\gamma$ on the limit cycle is subject to a small perturbation $\mathbf{\Delta x}$, it leaves the limit cycle — its state becomes $\mathbf{x}^\gamma + \mathbf{\Delta x}$ — and then, asymptotically reaches the limit cycle, but with a certain phase shift $\Delta\theta$ compared with the unperturbed trajectory (Figure 2.3). The phase shift, which depends on the phase θ at the perturbation time, is given by the *phase response curve* (PRC) $Z_{\mathbf{\Delta x}} : S^1(0, 2\pi) \mapsto \mathbb{R}$. In other words, the PRC expresses a perturbation of the state as a *perturbation of the phase*.

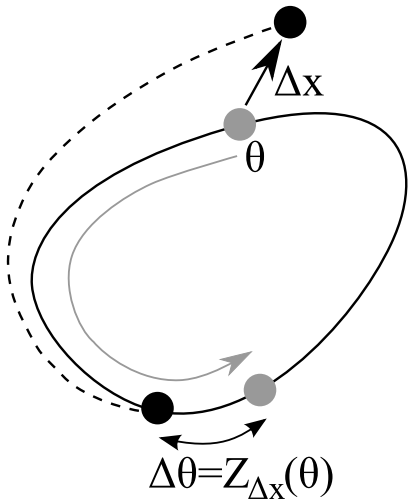

Figure 2.3: At phase θ, the oscillator is subject to a small perturbation $\mathbf{\Delta x}$ and leaves the limit cycle. When reaching the limit cycle, the perturbed oscillator (black) has a phase delay $\Delta\theta = Z_{\mathbf{\Delta x}}(\theta)$ compared with the unperturbed oscillator (gray).

For a given model, there are as many PRC's as there are perturbations $\mathbf{\Delta x}$. A particular PRC is the *infinitesimal* PRC (iPRC). It corresponds to an infinitesimal perturbation in the unit direction $\hat{\mathbf{e}}$, $\|\hat{\mathbf{e}}\| = 1$. (In models of neurons, the perturbation direction is usually a perturbation of the membrane voltage state.) The iPRC $Z : S^1(0, 2\pi) \mapsto \mathbb{R}$ is given by the directional derivative

$$Z(\theta) = \hat{\mathbf{e}} \cdot \frac{\partial \theta}{\partial \mathbf{x}}(\mathbf{x}^\gamma(\theta)) \,,$$

with the gradient $\frac{\partial \theta}{\partial \mathbf{x}} = \left(\frac{\partial \theta}{\partial x_1} \cdots \frac{\partial \theta}{\partial x_n}\right)$ evaluated on the limit cycle.

The iPRC is of interest for several reasons. It is an intrinsic characteristic of the oscillators that allows to classify the dynamics into two categories [31, 42]. In addition, there exist several numerical tools to compute the iPRC and analytical expressions can also be obtained for integrate-and-fire dynamics (see below). The iPRC of HH oscillators and FN oscillators is

shown in Figure 2.4.

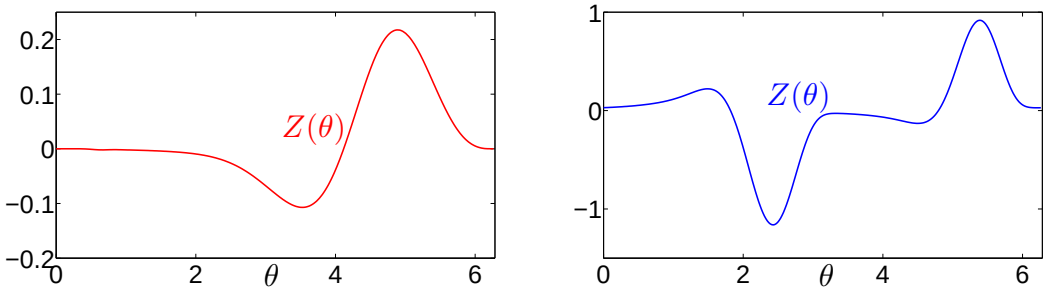

(a) Hodgkin-Huxley (HH) oscillator (b) Fitzhugh-Nagumo (FN) oscillator

Figure 2.4: The iPRC of HH oscillators and FN oscillators is numerically computed with the usual parameters and with a baseline current $I_b = 10$ mA (HH) and $I_b = 1$ (FN). (The numerical computations have been performed by Pierre Sacré.)

The iPRC is of paramount importance for the study of coupled oscillators. Indeed, the iPRC corresponds to the oscillator sensitivity to an external continuous input (e.g. a coupling between neighboring oscillators). Consider the general multidimensional dynamics

$$\dot{\mathbf{x}} = \mathbf{F}(\mathbf{x}) + u(t)\,\hat{\mathbf{e}}\,, \quad \mathbf{x} \in \mathbb{R}^n\,,$$

where $u(t)$ is the external input. Then, the phase dynamics can be written as (see [13] for more details)

$$\dot{\theta} = \omega + Z(\theta)\,u(t)\,, \tag{2.1}$$

with an error of the order of $\max_t |u(t)|^2$ [61]. The phase dynamics (2.1) is valid in good approximation, without the second-order correction, provided that the external input is weak.

Although the present dissertation focuses on the study of an impulsive coupling, which is generally neither continuous nor weak, the iPRC is widely used in Chapter 5 and in Chapter 7. The other results presented in this thesis rely on the use of convenient mathematical tools, based on a specific PRC and developed in Chapter 3.

2.3 Integrate-and-fire oscillators

First introduced in [57, 63], the *integrate-and-fire* models appear as a one-dimensional reduction of multidimensional firing dynamics. Since it enables the deepest mathematical studies in large networks of interacting oscillators, the model has attracted considerable interest and is still abundantly used in current research. In the present dissertation, we mainly focus on this model.

2.3.1 Reduction to an integrate-and-fire dynamics

A straightforward phase reduction of a multidimensional firing model does not exploit the firing dynamics. In contrast, the one-dimensional *integrate-and-fire* model is obtained by ap-

proximating the fast firing phenomenon by a reset while focusing on the "slow" state evolution between two firings. More precisely, the integrate-and-fire model can be seen as the result of a reduction process in two steps (see Figure 2.5):

1. Approximation of the firing. The time spent on the (fast) firing part of the limit cycle (from B to A) is negligible with respect to the time spent on the rest of the cycle (from A to B). Then, an oscillator in B can be instantaneously reinjected in A, a good approximation that yields a *discontinuous limit cycle with reset*.

2. Phase reduction. A phase reduction is performed in the vicinity of the discontinuous limit cycle A-B, associating a phase $\theta = 0$ to point A and a phase $\theta = 2\pi$ to point B. The approximated iPRC is discontinuous and can be obtained analytically.

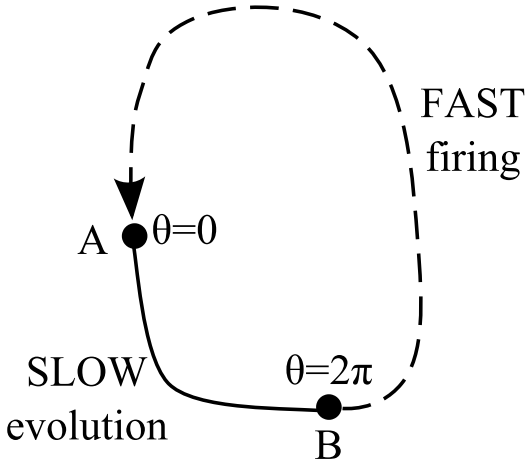

Figure 2.5: Since the firing from B to A is much faster than the dynamics between A and B, the firing can be replaced in good approximation by a reset. Then, a phase reduction is performed in the vicinity of the discontinuous limit cycle A-B.

The reduction presented above is illustrated by the following example.

Example 2.3.1 (Limit cycle close to a Homoclinic bifurcation)**.** In [13], limit cycles close to a homoclinic bifurcation are approximated by a discontinuous limit cycle, to which corresponds a discontinuous iPRC.

A homoclinic bifurcation occurs when there exists, for a given parameter value, a homoclinic orbit to a saddle point with real eigenvalues. At the bifurcation, a limit cycle appears. Assuming that there is a single unstable eigenvalue λ_u such that $\lambda_u < |\lambda_{s_j}|$, with λ_{s_j} being the stable eigenvalues, the limit cycle is stable [39]. Since the trajectory is much slower near the saddle point, the limit cycle is discontinuous in good approximation and the iPRC can be approximated by the discontinuous function (see [13] for more details)

$$Z(\theta) = C\,\omega \exp\left(\frac{2\pi\lambda_u}{\omega}\right) \exp\left(-\lambda_u \frac{\theta}{\omega}\right) , \tag{2.2}$$

where $C > 0$ is a model-dependent constant.

In the popular Morris-Lecar model [77], which is among the most widely used conductance-based models in computational neuroscience, a homoclinic bifurcation can occur for low external currents [93, 115]. ◇

Remark 2.3.1. In the literature, most of studies on finite networks of integrate-and-fire oscillators use a phase variable defined between 0 and 1. For consistency purposes, a unique definition of the phase has been adopted throughout the manuscript: the phase is defined on the circle $S^1(0, 2\pi)$. ◇

As mentioned in [1], the main interest of the integrate-and-fire model relies on a separation of time scales. Whereas a complex dynamics (e.g. the HH dynamics) models the whole behavior of the oscillator, including the firings, the simplified dynamics of the integrate-and-fire model only refers to the behavior between the firings, since the firings are considered as additional resets.

The approximation is relevant, especially when considering a network of coupled firing oscillators. In this case, the behavior of the whole network does not depend on the fast firings but on the state evolution between two firings. In addition, the approximation reduces the computational cost of numerical simulations and dramatically simplifies theoretical studies.

2.3.2 Relation between state dynamics and phase dynamics

The integrate-and-fire dynamics are usually expressed as *one-dimensional state dynamics between two threshold values*: a scalar state variable x monotonically increases between two thresholds $\underline{x}$ and $\overline{x}$, according to the dynamics

$$\dot{x} = F(x), \quad \text{with } F(x) > 0, \forall x \in [\underline{x}, \overline{x}]. \tag{2.3}$$

Upon reaching the upper threshold $\overline{x}$, the state is instantaneously reset to the lower threshold $\underline{x}$. Roughly speaking, the oscillator *integrates* between the two thresholds and *fires* when reaching the upper threshold (Figure 2.6).

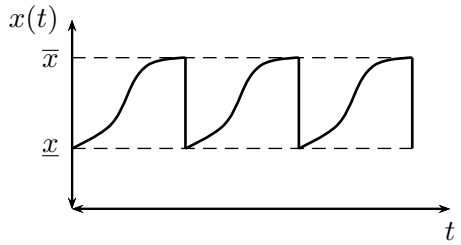

Figure 2.6: Time evolution of the state of an integrate-and-fire oscillator.

The above one-dimensional state dynamics is equivalent to a phase dynamics (e.g. obtained through the reduction process explained in Section 2.3.1). Indeed, there is a trivial change of variable between the one-dimensional state $x \in [\underline{x}, \overline{x}]$ and the phase $\theta \in S^1(0, 2\pi)$: the phase is determined from the state by rescaling in such a way that $\theta = 0$ corresponds to the low threshold $x = \underline{x}$ and that the (unperturbed) oscillator satisfies $\dot{\theta} = \omega$, where $\omega = 2\pi/T$

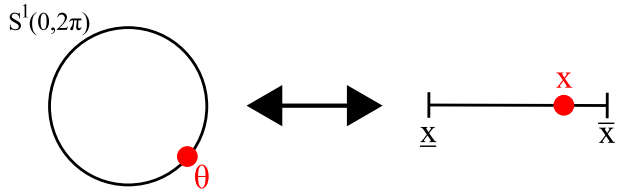

Figure 2.7: There is a bijection between the state $x \in [\underline{x}, \overline{x}]$ and the phase $\theta \in S^1(0, 2\pi)$. In particular, the state $\underline{x}$ (resp. $\overline{x}$) corresponds to the phase $\theta = 0^+$ (resp. $2\pi^-$).

is the natural frequency of the oscillator (Figure 2.7).

The state-phase relation is given by the function $f \in [0, 2\pi] \mapsto [\underline{x}, \overline{x}]$ defined as

$$f(\theta) \triangleq \phi^{-1}(\theta/\omega) = x\,. \tag{2.4}$$

The function $\phi(x)$ corresponds to the time required by the state $x(t)$, solution of $\dot{x} = F(x)$, $x(0) = \underline{x}$, to reach the value x, that is

$$\phi(x) = \int_{\underline{x}}^{x} \frac{1}{F(s)}\, ds, \quad \phi(\overline{x}) = T = \frac{2\pi}{\omega}\,. \tag{2.5}$$

In addition, the iPRC is related to F through the analytical expression (see [13, 32])

$$Z(\theta) = \frac{d\theta}{dx} = \frac{\omega}{F(f(\theta))}\,. \tag{2.6}$$

It is noticeable that, disregarding the fact that the integrate-and-fire model is the reduction of a multidimensional model, the infinitesimal iPRC requires no assumption of a weak input, since the trajectories always remain on the unidimensional cycle $[\underline{x}, \overline{x}]$.

2.3.3 Monotone dynamics and leaky integrate-and-fire (LIF) model

There exist several integrate-and-fire models, at which correspond different dynamics $\dot{x} = F(x)$ that determine the ensemble behavior of the coupled oscillators. First and foremost, the models characterized by a monotone vector field $dF/dx < 0\ \forall x \in [\underline{x}, \overline{x}]$ or $dF/dx > 0\ \forall x \in [\underline{x}, \overline{x}]$ are extensively studied in the present dissertation (see Chapter 4 and Chapter 5). By slight abuse of terminology, we will refer in the sequel to *monotone (integrate-and-fire) oscillators* for integrate-and-fire oscillators with a monotone vector field.

A typical monotone integrate-and-fire model is the leaky integrate-and-fire (LIF) model. The LIF model is the most popular integrate-and-fire model and is a direct *simplification of the Hodgkin-Huxley model* [2]. It models a neuron membrane as a capacitor C in parallel with a resistor R that allows a leaky current through the membrane-capacitor. To this electrical system, driven by an external current I, corresponds the dynamics

$$\dot{V} = -\frac{V}{CR} + \frac{I}{C}$$

where V is the membrane voltage. A firing occurs when $V = \overline{V}$ and the voltage is then reset to $V = \underline{V}$. Modulo an appropriate change of variable, the state model is of the general form

$$\dot{x} = S + \gamma x\,, \quad x \in [\underline{x}, \overline{x}]\,, \tag{2.7}$$

with $\gamma < 0$, $\underline{x} = 0$, and $\overline{x} = 1$. Equation (2.7) corresponds to the integrate-and-fire model (2.3) with the monotone decreasing vector field $F(x) = S + \gamma x$. In order to have $F(x) > 0$ $\forall\, x \in [\underline{x}, \overline{x}]$, we suppose that $S > 0$ and $S > -\gamma$ (driven current I sufficiently high).

The "leaky" nature of the model relates to the negative value γ ($dF/dx < 0$), corresponding to a concave-down time evolution of the oscillator [Figure 2.8 (a)]. In contrast, positive values of γ ($dF/dx > 0$) would result in a concave-up time evolution of the oscillator [Figure 2.8 (b)]. In the neuroscience context for instance, it is experimentally observed that time evolutions of the membrane potential (of a neuron) actually is neither concave-up nor concave-down. Considering concave-up time evolutions instead of the usual concave-down evolution is one of the key contribution of the thesis. The distinction between concave-up and concave-down time evolution indeed plays a key role in the collective behavior emerging from the network of coupled oscillators.

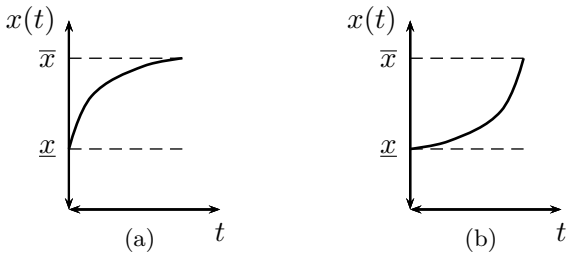

Figure 2.8: The time evolution of integrate-and-fire oscillators is (a) concave-down when $dF/dx < 0$ and (b) concave-up when $dF/dx > 0$.

The monotone oscillators are characterized by the following properties.

Curvature property. Some attention is put on the curvature of f, which plays a key role in the collective behavior of the coupled oscillators. It follows from (2.5) and (2.4) that

$$f' = \frac{1}{\omega}\left(\frac{d\phi}{dx}\right)^{-1} = \frac{F}{\omega} > 0\,, \tag{2.8}$$

where f' denotes the first derivative of f with respect to the phase θ. The relation (2.8) implies the following property of the function f.

Property 1. *If F is monotone increasing (resp. decreasing) on $[\underline{x}, \overline{x}]$, then the evolution f is concave-up (resp. concave-down) on $[0, 2\pi]$.*

The curvature property of f corresponds to the curvature of the time evolution of the oscillator.

Infinitesimal PRC. Since the derivative of the iPRC is given by

$$Z'(\theta) = -\frac{dF}{dx}\Big(f(\theta)\Big)\frac{1}{F(f(\theta))}\,, \tag{2.9}$$

the iPRC inherits the monotonicity property of the F.

Property 2. *If F is monotone increasing (resp. decreasing) on $[\underline{x}, \overline{x}]$, then the iPRC is monotone decreasing (resp. increasing).*

These properties are illustrated with the LIF model (and its "nonleaky" analog with $\gamma > 0$). The function f and the (monotone) iPRC is shown in Figure 2.9. In addition, the iPRC is given by

$$Z(\theta) = \frac{\omega}{S}\exp\left(-\frac{\gamma\,\theta}{\omega}\right) \quad \text{with} \quad \omega = 2\pi\,\gamma\left[\log\left(\frac{S+\gamma}{S}\right)\right]^{-1}. \tag{2.10}$$

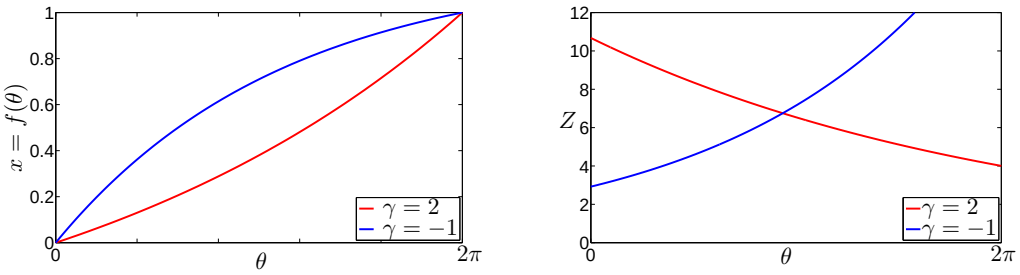

(a) Function f (b) iPRC

Figure 2.9: (a) The monotone oscillators $\dot{x} = 1.2 + \gamma\,x$, $x \in [0, 1]$, are characterized by (a) a function f with a curvature of constant sign and (b) a monotone iPRC.

The reader will note that the phase reduction of oscillators close to a homoclinic bifurcation (Example 2.3.1) leads to a monotone iPRC and therefore yields another example of monotone oscillators.

2.3.4 QIF and "QIF-like" integrate-and-fire dynamics

A main motivation of the present dissertation is the study of the QIF model (see Chapter 6 and Chapter 7). The QIF model, first proposed in [32], is probably the second most popular integrate-and fire model after the LIF model (see for instance [14, 65, 111]). The model is characterized by a quadratic membrane voltage dynamics, given by

$$C\dot{V} = q(V - V_{th})^2 + I - I_{th}\,, \tag{2.11}$$

where V_{th} and I_{th} are respectively the voltage and current thresholds and q is a fixed parameter. A firing occurs whenever $V = \overline{V}$ and the voltage is then reset to $V = \underline{V}$. Modulo an appropriate change of variables, the state model is of the general form

$$\dot{x} = S + x^2\,, \quad x \in [\underline{x}, \overline{x}]\,. \tag{2.12}$$

Equation (2.12) corresponds to the integrate-and-fire model (2.3) with the quadratic vector field $F(x) = S + x^2$. Even though the firing and reset values $\overline{V}$ and $\underline{V}$ are known constants, the thresholds $\underline{x}$ and $\overline{x}$ have arbitrary values that depend on V_{th}. For $\underline{x} \to -\infty$ and $\overline{x} \to \infty$, the QIF model corresponds to the so-called Θ-neuron, which is a canonical type I neuron model [31]. In addition, the QIF model is a simplified version of the Izhikevich model [50, 51], a two-dimensional quadratic integrate-and-fire model described by the quadratic dynamics (2.11), but where a recovery current I_{th} is a second state variable evolving according to a linear integrate-and-fire dynamics. Depending on the chosen parameters values, the Izhikevich model exhibit most of the fundamental behaviors of neurons (e.g. burst, resonator, etc.).

A main interest of the QIF model relies on the fact that the model can capture both an oscillatory or an excitable behavior. When $S > 0$ (or equivalently $I > I_{th}$), $F(x)$ is strictly positive on $[\underline{x}, \overline{x}]$ and the model is an oscillator. When $S < 0$ (or equivalently $I < I_{th}$), the model exhibits a different regime. Without any external perturbation, the state converges to the resting value $x = -\sqrt{|S|}$. Then, assuming it receives a sufficiently large perturbation, the state may exceed $\sqrt{S}$ and then rises and fires at $x = \overline{x}$ before finally going back to the initial rest value (Figure 2.10). In this situation, the behavior is not oscillatory but excitable, a feature that is encountered, for instance, within neural populations. In the present work, we investigate networks of QIF units in the oscillatory regime, paving the way for a further study of the excitable regime.

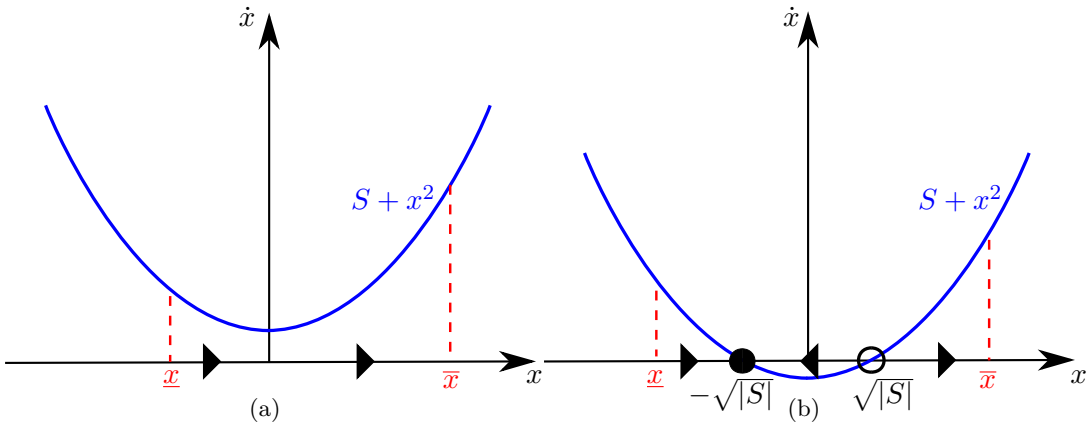

Figure 2.10: The QIF model is characterized (a) by an oscillator behavior when $S > 0$ and (b) by an excitable behavior when $S < 0$.

The QIF model is fundamentally different from the LIF model in that its state dynamics is not monotone. While monotone oscillators benefit from monotonicity properties that yield strong results on coupled populations, a mathematical study of coupled QIF oscillators leads to open problems and is actually one of the main challenges that motivated the work presented in the dissertation.

"QIF-like" oscillators. To get a deeper insight into the problem arising from the study of QIF oscillators, other "QIF-like" integrate-and-fire dynamics are considered. They satisfy

the following assumption.

Assumption 1. *$F(\cdot) : [\underline{x}, \overline{x}] \mapsto \mathbb{R}$ is continuous, positive, even, and strictly increasing on $[0, \overline{x}]$.*

The QIF model satisfies Assumption 1. Other representative models of this class are shown in Figure 2.11. The *exponential* model, defined by $F(x) = S\,\exp(x^2)$, $S > 0$, is characterized by a shape similar to the QIF model. The *piecewise linear* model, defined by $F(x) = S + \gamma|x|$, $S, \gamma > 0$, is a direct generalization of the linear LIF model.

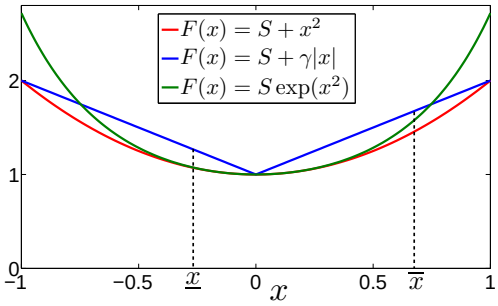

Figure 2.11: Three models (quadratic, exponential, and piecewise linear) satisfying Assumption 1.

Curvature property. The function f of QIF and "QIF-like" oscillators is characterized by the following property.

Property 3. *Assume that the dynamics satisfies Assumption 1. If $\underline{x}+\overline{x} > 0$ (resp. $\underline{x}+\overline{x} < 0$), then the function f is concave-up in the mean (resp. concave-down in the mean), that is*

$$\int_0^{2\pi} f''(\theta)\,d\theta = f'(2\pi) - f'(0) = \frac{F(\overline{x}) - F(\underline{x})}{\omega} > 0 \quad (\textit{resp.} \ < 0)\,. \tag{2.13}$$

Property 3 is illustrated in Figure 2.12 in the case of QIF oscillators.

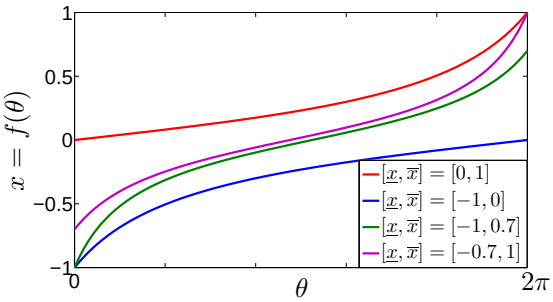

Figure 2.12: The function f of QIF oscillators ($S = 0.1$) is both concave-down and concave-up. It is concave-down in the mean for $\underline{x} + \overline{x} < 0$ and concave-up in the mean for $\underline{x} + \overline{x} > 0$.

Infinitesimal PRC. The iPRC corresponding to QIF and "QIF-like" oscillators is characterized by the following property.

Property 4. *An integrate-and-fire model satisfying Assumption 1 has an iPRC with a vertical reflection symmetry, that is*

$$Z(\theta) = Z_e(\theta - \overline{\theta}) \quad \forall \theta \in [0, 2\pi]\,, \tag{2.14}$$

where $Z_e(\cdot)$ is an even function on $\mathbb{R}$. To the inequality $\overline{x}+\underline{x} > 0$ (resp. $\overline{x}+\underline{x} < 0$) corresponds the inequality $\overline{\theta} < \pi$ (resp. $\overline{\theta} > \pi$).

In addition, consider two models (a) and (b) with the thresholds satisfying $\underline{x}_{(a)} = -\overline{x}_{(b)}$ and $\overline{x}_{(a)} = -\underline{x}_{(b)}$ (opposite values $\underline{x} + \overline{x}$). Then, they are characterized by mirrored iPRC's, that is, $\overline{\theta}_{(b)} = 2\pi - \overline{\theta}_{(a)}$ and $Z_{(b)}(\theta) = Z_{(a)}(2\pi - \theta)$.

Proof. Since F is even, it follows from (2.5) that

$$\phi(-x) = -\phi(x) + \phi(-\underline{x})\,. \tag{2.15}$$

Consequently, (2.4) leads to

$$f(\theta) = -f(\,-\theta + \omega\,\phi(-\underline{x}))$$

and setting $\overline{\theta} = \omega\,\phi(-\underline{x})/2$, one obtains

$$f(\overline{\theta} + \theta) = -f(\overline{\theta} - \theta)\,. \tag{2.16}$$

Since F is even, the iPRC (2.6) satisfies

$$Z(\overline{\theta} + \theta) = Z(\overline{\theta} - \theta)\,.$$

The condition $\underline{x} + \overline{x} > 0$ implies $\phi(-\underline{x}) < \phi(\overline{x}) = T$, and $\overline{\theta} < \pi$.

For the two models (a) and (b), it is straightforward that $\omega_{(a)} = \omega_{(b)} = \omega$. In addition, (2.5) implies $\phi_{(a)}(x) = \phi_{(a)}(-\overline{x}_{(a)}) + \phi_{(b)}(x)$ or, given (2.15),

$$\phi_{(b)}(x) = \phi_{(a)}(x) + \frac{2\pi}{\omega} - \phi_{(a)}(-\underline{x}_{(a)})\,. \tag{2.17}$$

It follows that

$$\overline{\theta}_{(b)} = \frac{\omega}{2}\phi_{(b)}(-\underline{x}_{(b)}) = \frac{\omega}{2}\phi_{(b)}(\overline{x}_{(a)}) = 2\pi - \frac{\omega}{2}\phi_{(a)}(-\underline{x}_{(a)}) = 2\pi - \overline{\theta}_{(a)}\,,$$

which concludes the proof. □

Property 4 can be verified for the QIF model and for the piecewise linear model, for instance. It is illustrated in Table 2.1 and Figure 2.13.

QIF model $F(x) = S + x^2$	Piecewise linear model $F(x) = S + \gamma\|x\|$
$Z_e(\theta) = \frac{\omega}{S}\cos^2\left(\frac{\sqrt{S}}{\omega}\theta\right)$	$Z_e(\theta) = \frac{\omega}{S}\exp\left(-\frac{\gamma}{\omega}\|\theta\|\right)$
$\overline{\theta} = -\dfrac{2\pi\arctan\left(\underline{x}/\sqrt{S}\right)}{\arctan\left(\overline{x}/\sqrt{S}\right) - \arctan\left(\underline{x}/\sqrt{S}\right)}$	$\overline{\theta} = \dfrac{2\pi\log\left(\left(S-\gamma\underline{x}\right)/S\right)}{\log\left(\left(S-\gamma\underline{x}\right)/S\right) + \log\left(\left(S+\gamma\overline{x}\right)/S\right)}$
$\omega = 2\pi\sqrt{S}\Big/\left[\arctan\frac{\overline{x}}{\sqrt{S}} - \arctan\frac{\underline{x}}{\sqrt{S}}\right]$	$\omega = 2\pi\gamma/\log\left(\dfrac{\left(S-\gamma\underline{x}\right)\left(S+\gamma\overline{x}\right)}{S^2}\right)$

Table 2.1: "QIF-like" models satisfy Property 4, that is, the iPRC is of the form $Z(\theta) = Z_e(\theta - \overline{\theta})$. (The computations are not shown.)

◇

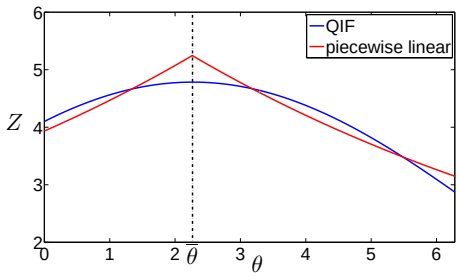

Figure 2.13: The iPRC of "QIF-like" oscillators has a mirror symmetry with respect to phase $\overline{\theta}$.

The properties of the oscillators (curvature and iPRC) are of paramount importance to determine the behavior of the coupled oscillators. We conclude the section by summarizing them in the following equivalent statements (to which we will indistinctly refer in the sequel):

- For monotone oscillators:
  1. The vector field $F(x)$ is monotone increasing (resp. decreasing) on $[\underline{x}, \overline{x}]$;
  2. (Property 1) The function f (2.4) are concave-up (resp. concave-down) on $[0, 2\pi]$;
  3. (Property 2) The iPRC is monotone decreasing (resp. increasing).

- For "QIF-like" oscillators satisfying Assumption 1:
  1. The vector field $F(x)$ has a positive (resp. negative) mean slope on $[\underline{x}, \overline{x}]$, that is $\underline{x} + \overline{x} > 0$ (resp. $\underline{x} + \overline{x} < 0$);
  2. (Property 3) The function f (2.4) are concave-up (resp. concave-down) in the mean;
  3. (Property 4) The iPRC is characterized by $\overline{\theta} < \pi$ (resp. $\overline{\theta} > \pi$) in (2.14).

2.4 Networks of interacting oscillators

Thanks to simplified models and to phase reduction, a single firing oscillator has a simple behavior. Within a network, it interacts with the other oscillators through a *nonlinear coupling*, that may however yield complex ensemble behaviors.

2.4.1 Networks and couplings

We study networks of N interacting oscillators, each of them characterized by its own state $\mathbf{x}_k$ or equivalently by its own phase θ_k, with the labels $k \in \mathcal{N} = \{1, \dots, N\}$. Connected to the oscillators $j \in \mathcal{N}_k \subseteq \mathcal{N}$, oscillator k has a dynamics

$$\dot{\theta}_k = \omega_k + \Omega_k^{\text{coupling}}(\theta_{j \in \mathcal{N}_k}) \,, \tag{2.18}$$

where $\Omega_k^{\text{coupling}}$ is the phase coupling term, that can be derived from a state coupling through a PRC. If the coupling always triggers a phase advance to the oscillators, that is $\Omega_k^{\text{coupling}} > 0$, it is an *excitatory* coupling. If it always triggers a phase delay, that is $\Omega_k^{\text{coupling}} < 0$, it is an *inhibitory* coupling.

In the present dissertation, we mainly consider that the oscillators are identical and therefore characterized by equal natural frequencies $\omega_k = \omega$ for all $k \in \mathcal{N}$ (homogeneous population). In addition, assuming that the network is dense enough, we consider in good approximation that each oscillator is connected to every other (that is, $\mathcal{N}_k = \mathcal{N}$ or $\mathcal{N}_k = \mathcal{N} \setminus \{k\}$) — the coupling is said *all-to-all* or *global*. Studying sparse network topologies is an interesting problem which has led to numerous studies, but it is beyond the scope of the present dissertation.

The particular coupling investigated in this thesis is an *impulsive* coupling (developed in detail in Chapter 3), a coupling that is closely related to the dynamics of firing oscillators. While the impulsive coupling is discontinuous in essence, the study, however, leads to the analysis of a continuous coupling (Chapter 5) and of a "Kuramoto-like" coupling (Chapter 7), for which the oscillators are coupled through their phase differences.

2.4.2 Collective behaviors

Networks of N coupled firing oscillators can exhibit several ensemble behaviors on the torus $S^1 \times S^1 \times \cdots \times S^1 = \mathbb{T}^N$. The two extreme behaviors are *synchronization* and *phase-locked anti-synchronization* (or *phase-locking*). While synchronized oscillators are gathered, anti-synchronized oscillators are spread on the circle (Figure 2.14).

Definition 1 (Synchronization)**.** N firing oscillators are *synchronized* if they all fire at the same time. That is, if $\theta_k = 0$, $k \in \mathcal{N}$, then $\theta_j = 0$ for all $j \in \mathcal{N}$.

In the case of identical oscillators, the oscillators have the same phase $\theta_1 = \theta_2 = \cdots = \theta_N$ forever.

Definition 2 (Phase-locking)**.** N firing oscillators are *phase-locked* if, at each firing of any oscillator, the $N-1$ other oscillators have phases with fixed values $\{\theta_1^*, \ldots, \theta_{N-1}^*\}$ (with the convention $0 < \theta_k^* < \theta_{k+1}^* < 2\pi$).

The indices of the phase-locked phases are not related to the indices of the different oscillators. At each firing, there may be a permutation of the oscillators in the phase-locked configuration, so that a same locked phase θ_k^* (k fixed) may be assigned to different oscillators. If the oscillators homogeneously spread on $S^1(0, 2\pi)$, that is $\theta_k^* = 2\pi k/N$, the phase-locked configuration is a *splay state*. In some situations, groups of oscillators (instead of single oscillators) are phase-locked: this is a phase-locked *clustering* configuration.

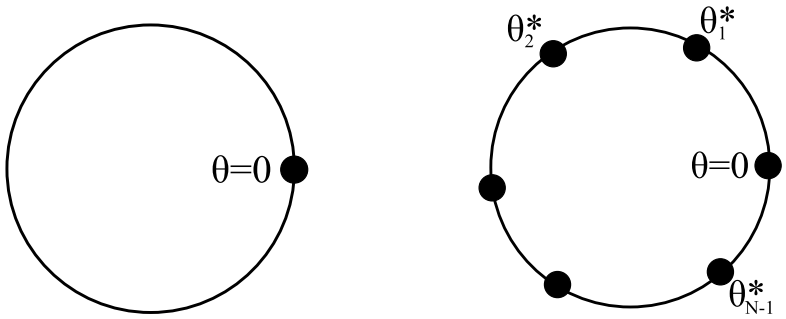

Figure 2.14: (a) Synchronization: all the oscillators fire simultaneously. (b) Phase-locking: at each firing, the oscillators have fixed but different phases.

Other collective behaviors — periodic, quasiperiodic, chaotic — are also observed in networks of coupled oscillators. But throughout this thesis, emphasis is put on the two extreme behaviors (synchronization and phase-locked anti-synchronization). In the next chapter, we show how oscillators interacting through an impulsive coupling achieve either synchronization or phase-locked anti-synchronization, and are thereby characterized by an interesting *dichotomy*.

Chapter 3

Impulsive coupling and firing maps

Impulsive coupling is a natural way of coupling firing oscillators. In a neural network, firing neurons interact by sending out action potential (spikes) that modify the state of the other connected oscillators. Given the very short time length of the spikes, the coupling is almost instantaneous and is considered in good approximation as an impulsive coupling.

As an introduction to impulsive coupling, this chapter presents general results on identical pulse-coupled integrate-and-fire oscillators. In Section 3.1, impulsive coupling is introduced in detail. Section 3.2 describes the clustering phenomenon exhibited by identical pulse-coupled oscillators and shows that the network may be characterized by an interesting dichotomic behavior — the oscillators either synchronize or converge toward a phase-locked clustering configuration. Using a discrete-time one-dimensional map that describes the evolution of the network at each firing (the so-called *firing map*), Section 3.3 proves that two pulse-coupled oscillators exhibit the dichotomic behavior. Next, Section 3.4 performs a preliminary study of large networks and provides some general properties of the multidimensional generalization of the above-mentioned firing map.

The main contribution of the chapter is to highlight (i) the dichotomic behavior of two monotone or "QIF-like" oscillators and (ii) the existence of phase-locked clustering configurations in large populations.

3.1 Impulsive coupling

Impulsive coupling (or pulse-coupling) was first proposed by Peskin to model pacemaker cells in the heart [86]. In the case of integrate-and-fire oscillators, it was defined as follows. Whenever an oscillator fires, it sends out a pulse that causes an *instantaneous increment* $\epsilon < \overline{x} - \underline{x}$ to the state of all other oscillators (all-to-all coupling). The coupling strength ϵ is constant, usually positive (excitatory coupling), and does not depend on the oscillator emitting the pulse, even though one assumes some heterogeneity in the network. If, after receiving the pulse, the incremented state of an oscillator exceeds the upper threshold, then it is also reset to the lower threshold with the firing oscillator — there is an *absorption* (Figure 3.1).

Similarly to [75], some assumptions are adopted in the sequel. We assume that an absorbed oscillator does not emit a pulse before reaching the threshold again. By this assumption, we prevent "avalanche" phenomena which could ignite a chain reaction of firings. In addition,

the coupling is not additive: when N oscillators fire simultaneously, the resulting pulse is always ϵ, and not $n\epsilon$. The two assumptions do not modify the coupling mechanisms and have no significant influence on the network behavior.

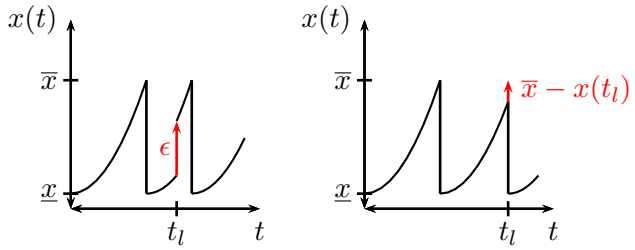

Figure 3.1: (a) When an oscillator fires (at time t_l), it increments the state of the other oscillators by a value $\epsilon > 0$. (b) If $x(t_l) > \overline{x} - \epsilon$, there is an absorption.

The impulsive coupling is summarized by the jump rule

$$x_j(t) = \overline{x} \Rightarrow x_k(t^+) = \begin{cases} x_k(t^-) + \epsilon & \text{if } x_k(t^-) < \overline{x} - \epsilon \\ \underline{x} & \text{if } x_k(t^-) \geq \overline{x} - \epsilon \end{cases} \quad \forall k \neq j \in \mathcal{N}.$$

In the sequel, we consider the case of identical oscillators — the generalization of the impulsive coupling to nonidentical oscillators is direct. Between the two thresholds, the dynamics of the pulse-coupled integrate-and-fire oscillators is given by

$$\dot{x}_k = F(x_k) + \epsilon \sum_{\substack{j=1 \\ j \neq k}}^{N} \sum_{l=0}^{\infty} \delta(t - t_l^{(j)}), \quad x \in [\underline{x}, \overline{x}]. \tag{3.1}$$

The Dirac functions δ model the pulses that increment the state of oscillator k at the firing times $t_l^{(j)}$, that is, when an oscillator $j \neq k$ fires. Equivalently, the phase dynamics expresses as

$$\dot{\theta}_k = \omega + Z_\epsilon(\theta_k) \sum_{\substack{j=1 \\ j \neq k}}^{N} \sum_{l=0}^{\infty} \delta(t - t_l^{(j)}), \tag{3.2}$$

where Z_ϵ is the PRC related to an impulsive perturbation. This particular PRC can be analytically derived from the iPRC (2.6) (Figure 3.2):

$$Z_\epsilon(\theta) = \int_{f(\theta)}^{f(\theta)+\epsilon} \frac{d\theta}{dx}(s)\, ds = \int_{f(\theta)}^{f(\theta)+\epsilon} Z\Big(f^{-1}(s)\Big)\, ds = \omega \int_{f(\theta)}^{f(\theta)+\epsilon} \frac{1}{F(s)}\, ds. \tag{3.3}$$

In Figure 3.2, the oscillator receiving the pulse jumps from phase θ to phase

$$f^{-1}\Big(f(\theta) + \epsilon\Big) = \theta + Z_\epsilon(\theta).$$

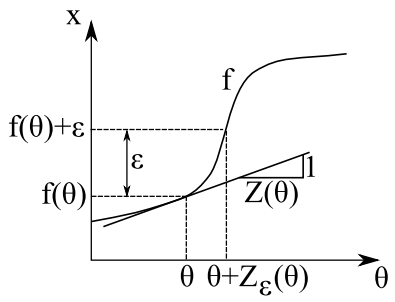

Figure 3.2: The PRC Z_ϵ corresponds to the phase advance of an oscillator whose state is instantaneously incremented by ϵ. The PRC Z_ϵ is derived from the iPRC Z.

Remark 3.1.1. Impulsive coupling can also be applied to models other than the integrate-and-fire models. But in the case of multidimensional dynamics, the PRC Z_ϵ cannot be derived from the iPRC and must be computed numerically. ◇

Remark 3.1.2. The reader will easily verify that the phase dynamics (3.2) particularizes the general phase dynamics (2.18), with

$$\Omega_k^{\text{coupling}}(\theta_{j\in\mathcal{N}}) = Z_\epsilon(\theta_k) \sum_{\substack{j=1 \\ j\neq k}}^{N} \omega_j \, \delta(\theta_j) \, .$$

◇

Pulse-coupled integrate-and-fire oscillators are hybrid models: they are the compositions of a continuous flow $\dot{\theta}_k = \omega \ \forall k$ (between two firings) with a discrete jump $\theta_k^+ = \theta_k + Z_\epsilon(\theta_k)$ (at each firing). Between two firings, the oscillators are all uncoupled. They rigidly rotate on the circle, so that the *phase* difference $\theta_k - \theta_j$ between any pair $\{j, k\}$ of oscillators remains constant. When a firing occurs, the state of the oscillators instantaneously jumps to other values; the *state* difference $x_k - x_j$ is conserved through this event.

Since it only affects the network at precise firing times, the impulsive coupling presents a great advantage. By "omitting" the time intervals between two firings, where nothing happens, one only retains information on the network configuration at the precise firing times. The continuous-time model is then turned into a *discrete-time* model, a framework that not only dramatically simplifies numerical simulations (from speed, memory, and precision points of view) but also retains the only information needed to perform an efficient analysis of the network. This will be developed in detail in Section 3.3.

A wealth of extensions of the original impulsive coupling can be found in literature. Topologies different from the all-to-all topology have been abundantly studied [36, 108, 110]: chain topology [84], ring topology [28], two-dimensional lattices [26], random topology [25, 82]. Several studies introduce delayed transmissions between the oscillators [33, 109] or consider non-instantaneous interactions, where the delta-like pulses are replaced by smooth α-functions [3, 12, 118, 128]. The effect of a partial reset (no absorption but residual charges after the firing) is also investigated in [56]. However, the vast majority of these studies only consider

the LIF dynamics ($\dot{x} = S + \gamma\, x$, with $\gamma < 0$). In contrast, the main contribution of the present dissertation extends the analysis of pulse-coupled oscillators to different dynamics.

3.2 Absorptions, synchronization, and clustering

Numerical simulations show that networks of identical pulse-coupled integrate-and-fire oscillators are usually characterized by a strong *dichotomic behavior*. After a transient evolution, the oscillators either perfectly synchronize (*synchronization* behavior) or gather into several *clusters*, in a phase-locked anti-synchronized configuration (*clustering* behavior) (Figure 3.3). Synchronization of pulse-coupled oscillators was first rigorously studied in the seminal paper of Mirollo and Strogatz [75]. The existence of the clustering behavior was reported in studies on delayed LIF models (see e.g. [33, 117]), and in [73] for non-delayed models with concave-up time evolution (instead of the usual concave-down evolution of the LIF oscillator).

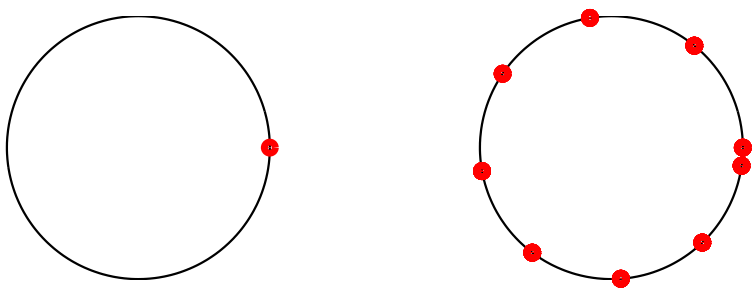

(a) (b)

Figure 3.3: "Snapshot" configuration of $N = 100$ oscillators: (a) the oscillators perfectly synchronize (one cluster); (b) the oscillators gather in 9 phase-locked clusters. Each dot represents a cluster of oscillators.

The behavior of the network is an evolution in two stages: the initial *formation of the clusters* through the absorption phenomenon and the *evolution of the clusters* toward either synchronization or phase-locked clustering.

3.2.1 Absorptions and clusters

The initial evolution of large networks of pulse-coupled oscillators is typically dominated by the absorption phenomenon: each firing oscillator absorbs nearby oscillators and creates a cluster. After an absorption, the oscillator that has just fired and all those that it has absorbed subsequently have the same phase forever — since they are identical. They therefore aggregate in a cluster. Since we made the assumption of nonadditive coupling strength, the cluster actually behaves as a single oscillator. (In the following, we sometimes make no distinction between a single oscillator and a cluster.) In addition, the number of clusters — denoted by N_g — is bounded, as shown in the following lemma.

Lemma 3.2.1. *In a network of N pulse-coupled integrate-and-fire oscillators with pulse strength $0 < \epsilon < \overline{x} - \underline{x}$, the number of clusters N_g is bounded by*

$$N_g \leq N_{g,\max} \triangleq \min\left(\left\lceil \frac{\overline{x} - \underline{x}}{\epsilon} \right\rceil, N\right) \tag{3.4}$$

where $\lceil X \rceil$ corresponds to the smallest integer such that $\lceil x \rceil \geq x$.

Proof. Consider a cluster that has just fired, with a state $x_g = \underline{x}$. Each time a new firing occurs, a (possibly new) cluster is reset to $\underline{x}$ and the state x_g of the first cluster is increased by ϵ. After n_f firings, there are $n_f + 1$ clusters (or single oscillators) in $[\underline{x}, x_g]$ and $x_g \geq \underline{x} + n_f\,\epsilon$. In the best conditions, $x_g = \underline{x} + n_f\,\epsilon$ and the first cluster will not fire again as long as

$$\underline{x} + n_f\,\epsilon < \overline{x}, \tag{3.5}$$

so that the maximal number of firings is

$$n_{f,\max} = \left\lceil \frac{\overline{x} - \underline{x}}{\epsilon} - 1 \right\rceil. \tag{3.6}$$

There are therefore at most $N_{g,\max} = n_{f,\max} + 1$ clusters in $[\underline{x}, x_g < \overline{x}]$. If $n_{f,\max} + 1$ exceeds the initial number N of oscillators, then $N_{g,\max} = N$. □

The number of clusters depends on the size of the interval $[\underline{x}, \overline{x}]$ and on the coupling strength ϵ. The result can be compared with the clustering configurations observed in a yeast cell model introduced in [9], configurations whose number of clusters is determined by the size of specific interaction regions.

Clustering is also observed in various other models. However, a cluster is usually a group of interacting agents that asymptotically converge toward a consensus value (see e.g. [5, 43, 119]). In networks of pulse-coupled oscillators, though, a cluster is created in finite time since it is a consequence of the absorption mechanism.

Remark 3.2.1 (Effect of the network topology)**.** In the present dissertation, we only consider a complete network topology ("all-to-all" coupling). Since the clusters are created by the aggregation of oscillators which are absorbed by the firing of one oscillator, only connected oscillators will aggregate in a cluster. The number N_g and the composition of the clusters therefore depend not only on the initial conditions but also on the network connectivity. In particular, the number of clusters N_g may exceed the maximum value $N_{g,\max}$ given by (3.4) if the coupling is not "all-to-all". Furthermore, the clusters may disappear in weakly connected networks by lack of local aggregation. Numerical simulations suggest that the clusters configurations are preserved if the network connectivity is sufficiently high. In such situations, the network connectivity only affects the speed of convergence to phase-locked clusters configurations, as shown in [110]. ◇

3.2.2 Evolution toward either synchronization or clustering

After the initial absorptions, the N_g clusters evolve as N_g single oscillators. Possibly characterized by a dichotomic behavior, they achieve either synchronization or phase-locked clustering (Figure 3.3). The dichotomic behavior depends on the curvature of the oscillators time evolution (see Section 2.3.3). The synchronization behavior is observed for oscillators with a

concave-down time evolution (in the mean) while the phase-locked clustering behavior is observed for oscillators with a *concave-up* time evolution (in the mean). As shown in Chapter 6, the dichotomic behavior is not observed with every integrate-and-fire dynamics, but is a common feature of a large class of integrate-and-fire models.

Synchronization. The clusters themselves coalesce under further absorptions, an aggregating process that persists until a unique cluster remains, the synchronized state. Then, the remaining cluster (the synchronized oscillators) fires at the frequency $\omega_{\text{sync}} = \omega$, where ω is the natural frequency of the oscillators.

Phase-locked clustering As the opposite behavior, every cluster tends to maximize the distance with respect to the neighboring clusters, and the network asymptotically converges toward a phase-locked anti-synchronized configuration. Assuming that the phase-locked configuration is $\{0, \theta_1^*, \theta_2^*, \cdots, \theta_{N_g-1}^*\}$ (at the firing of any cluster), the clusters fire periodically at a frequency

$$\omega_{\text{clust}} = \frac{2\pi\,\omega}{2\pi - \theta_{N_g-1}^*}\,. \tag{3.7}$$

Since the phase of each cluster is at least increased by a value $2\pi - \theta_{N_g-1}^*$ between two successive firings, the phase-locked phase $\theta_{N_g-1}^*$ satisfies $2\pi - \theta_{N_g-1}^* < 2\pi/N_g$ and it follows that $\omega_{\text{clust}} > N_g\,\omega$. The phase-locked clustering is thus characterized by a *high firing frequency*, whereas the synchronization behavior is characterized by a *low firing frequency*.

3.3 The case of two oscillators

To understand the dichotomic behavior described in the preceding section, the case of two oscillators is first considered. The "discrete-time" character of the pulse-coupled integrate-and-fire oscillators is fully exploited when considering a discrete-time map, the so-called *firing map*, that was originally introduced in [75]. The convergence properties of the firing map determine whether the network achieves synchronization or phase-locked clustering.

3.3.1 Firing map

While disregarding the continuous evolution between two firings, the firing map expresses the phase differences of the two oscillators at the successive firing times. For instance, the network configuration $(0, \theta)$ is mapped to $(h(\theta), 0)$ at the next firing, where $h(\theta)$ is the firing map.

To compute the firing map, one considers the two oscillators A and B, whose initial configuration $(0, \theta)$ is given in Figure 3.4 (a). When oscillator B is about to fire [Figure 3.4 (b)], oscillator A has a phase $2\pi - \theta$, since the phase difference between the two oscillators has remained constant. After the firing of oscillator B [Figure 3.4 (c)], oscillator A jumps to phase

$$\theta^+ = h(\theta) \triangleq f^{-1}\Big(f(2\pi - \theta) + \epsilon\Big)\,. \tag{3.8}$$

The firing map is directly related to the PRC Z_ϵ. Considering Figure 3.2, one has

$$h(\theta) = 2\pi - \theta + Z_\epsilon(2\pi - \theta)\,. \tag{3.9}$$

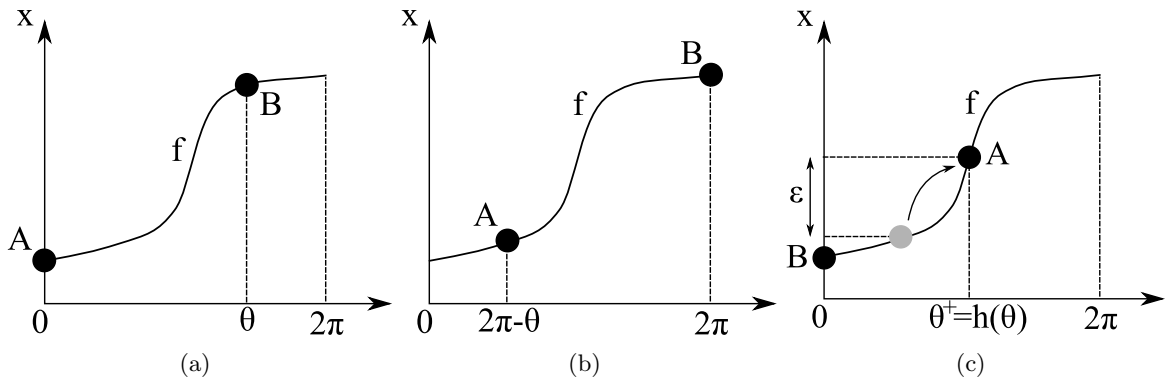

Figure 3.4: (a) Oscillator A fires; (b) Oscillator B is about to fire; (c) Oscillator B fires.

Properties. The firing map has the following general properties.

1. The firing map is defined only if $f(2\pi - \theta) + \epsilon < \overline{x}$. Its domain is thus $[\beta_1, 2\pi]$, with $\beta_1 = 2\pi - f^{-1}(\overline{x} - \epsilon)$. If $0 < \theta \leq \beta_1$, there will be an absorption at the next firing and the two oscillators will synchronize.

2. The firing map is monotone decreasing (Figure 3.5). The time derivative is given by

$$h'(\theta) = -\frac{f'(2\pi - \theta)}{f'\Big(h(\theta)\Big)} = -\frac{F\Big(f(2\pi - \theta)\Big)}{F\Big(f(2\pi - \theta) + \epsilon\Big)} < 0\,, \tag{3.10}$$

   where the last equality follows from (2.8).

3. The monotonicity property of the firing map implies that the firing map is invertible. In addition, since the firing map is decreasing, it is characterized by a unique fixed point $\theta^* = h(\theta^*)$. The fixed point corresponds to a situation in which an oscillator has a fixed phase at the firing of the other oscillator: this corresponds to the phase-locked behavior. Hence, the dichotomic behavior is linked to stability of the fixed point. If the fixed point is attracting, the network configuration asymptotically converges toward the phase-locked configuration. If the fixed point is repelling, the distance $\theta - \theta^*$ from the fixed point grows at each firing until $\theta \leq \beta_1$, and an absorption synchronizes the two oscillators.

3.3.2 Dichotomic behavior of monotone oscillators

In case of monotone integrate-and-fire oscillators with an increasing vector field ($dF/dx > 0$), the positive curvature of the function f implies a strong *contraction* property of the firing map. The result is summarized as follows.

Property 5. *If the function f is concave-up on $[0, 2\pi]$, then the firing map* (3.8) *is a contraction on $[\beta_1, 2\pi]$.*

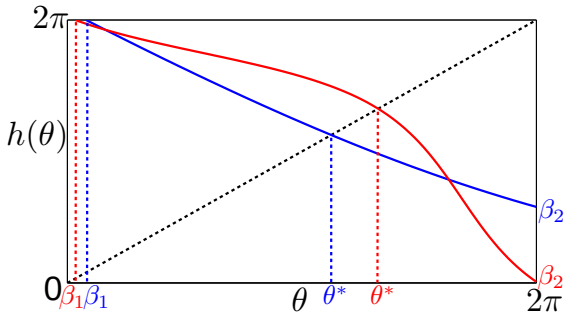

Figure 3.5: Two firing maps [of oscillators with a monotone decreasing dynamics (blue) and of QIF oscillators (red)]. Each firing map is monotone decreasing in $[\beta_1, 2\pi]$ and has a unique fixed point.

Proof. By construction, the application (3.8) maps the interval $[\beta_1, 2\pi]$ onto the interval $[\beta_2, 2\pi]$, with $\beta_2 = h(2\pi) = f^{-1}(\underline{x} + \epsilon)$. In addition, it follows from (3.10) that the firing map satisfies

$$-1 < h'(\theta) < 0 \quad \forall \theta \in [\beta_1, 2\pi]\,, \tag{3.11}$$

since f' is strictly increasing and $h(\theta) > 2\pi - \theta$ by construction. By the mean value theorem, one has

$$|h(\theta) - h(\psi)| \leq |h'(\xi)|\,|\theta - \psi|$$

for some $\xi \in [\theta, \psi]$ and the firing map is a contraction on $[\beta_1, 2\pi]$ with the Lipschitz constant $\max_{\xi \in [\beta_1, 2\pi]} h'(\xi)$, which concludes the proof. □

Property 5 can be added to the equivalent properties of monotone integrate-and-fire models (Properties 1 and 2). Next, the behavior of two monotone oscillators with $dF/dx > 0$ is characterized by the following proposition.

Proposition 3.3.1. *Consider two pulse-coupled identical integrate-and-fire oscillators $\dot{x} = F(x)$ characterized by a monotone increasing F. Then either an absorption occurs at the first firing or both oscillators asymptotically converge to the phase-locked difference θ^*, the unique fixed point of the firing map h.*

Proof. If there is no absorption at the first firing, an absorption will never occur since $\beta_2 > \beta_1$ by the contraction property. In this case, by the contraction mapping theorem (see e.g. [55]), the unique fixed point θ^* of the firing map is a global attractor for the dynamics $\theta^+ = h(\theta)$. □

As a counterpart of this result, it is equivalent to show that the firing map is expanding for concave-down functions f (decreasing $dF/dx < 0$), leading to the synchronization of the two oscillators. This highlights the dichotomic behavior and its dependence on the curvature of the function f (the derivative dF/dx).

3.3.3 Dichotomic behavior of "QIF-like" oscillators

In case of integrate-and-fire oscillators with "QIF-like" dynamics (satisfying Assumption 1), the firing map is not a contraction. However, the firing map satisfies an important property.

A well-chosen translation of the firing map has a reflection symmetry with respect to the bisectrix (Figure 3.6). The property is summarized as follows.

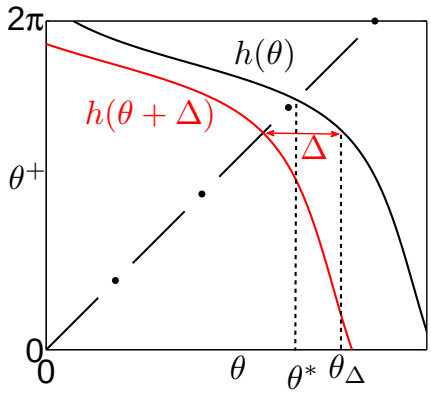

Figure 3.6: The scalar firing map has an important property: the map $h(\theta+\Delta)$ has a reflection symmetry with respect to the bisectrix.

Property 6. *Pulse-coupled integrate-and-fire oscillators satisfying Assumption 1 have a firing map* (3.8) *that verifies*

$$h(\cdot + \Delta) = h^{-1}(\cdot) - \Delta\,, \tag{3.12}$$

where (Δ, θ_Δ) *is the unique solution of*

$$\begin{cases} \theta_\Delta - h(\theta_\Delta) = \Delta \\ |h'(\theta_\Delta)| = 1 \end{cases}. \tag{3.13}$$

The value Δ *has the same sign as* $\underline{x} + \overline{x}$*. Moreover,*

$$|h'(\theta)| < 1 \quad \forall \theta < \theta_\Delta\,. \tag{3.14}$$

Proof. From (2.16), it follows that

$$f(\theta) = -f(-\theta + 2\overline{\theta}) \tag{3.15}$$

and

$$f^{-1}(-x) = -f^{-1}(x) + 2\overline{\theta}\,. \tag{3.16}$$

Properties (3.16) and (3.15) lead to

$$\begin{aligned} h^{-1}(\theta) &= 2\pi - f^{-1}\Big(f(\theta) - \epsilon\Big)\,, \\ &= 2(\pi - \overline{\theta}) + f^{-1}\Big(-f(\theta) + \epsilon\Big)\,, \\ &= 2(\pi - \overline{\theta}) + f^{-1}\Big(f(-\theta + 2\overline{\theta} + \epsilon\Big)\,, \\ &= 2(\pi - \overline{\theta}) + h\Big(\theta + 2(\pi - \overline{\theta})\Big)\,. \end{aligned}$$

Setting

$$\Delta = 2(\pi - \overline{\theta})\,, \tag{3.17}$$

one obtains (3.12). In addition, Property 4 implies that $\overline{\theta} < \pi$, or equivalently $\Delta > 0$ if $\underline{x} + \overline{x} > 0$.
Equations (3.13) and (3.17) lead to the equality $f(\theta_\Delta - 2\pi + 2\overline{\theta}) = f(2\pi - \theta_\Delta) + \epsilon$. According to (3.15), one obtains $-f(2\pi - \theta_\Delta) = f(2\pi - \theta_\Delta) + \epsilon$ and it follows from (3.10) that $|h'(\theta_\Delta)| = 1$. Since $dF/dx > 0$ for $x > 0$, one has $|h'(\theta)| < 1$ for $\theta < \theta_\Delta$. □

Property 6 can be added to the equivalent properties of models satisfying Assumption 1 (Properties 3 and 4). The result is of paramount importance since the condition $\Delta > 0$ ($\underline{x} + \overline{x} > 0$) determines the global stability of the firing map, and then the behavior of the two oscillators. This is summarized in the following proposition.

Proposition 3.3.2. *Consider two pulse-coupled identical integrate-and-fire oscillators with a dynamics satisfying Assumption 1. (i) If $\underline{x} + \overline{x} > 0$, either an absorption occurs at the first firing or both oscillators asymptotically converge to the phase-locked difference θ^*, the unique fixed point of the firing map h. (ii) If $\underline{x} + \overline{x} < 0$, the two oscillators achieve synchronization.*

Proof. We consider the case $\underline{x} + \overline{x} > 0$. If there is no absorption at the first firing, an absorption will never occur since Property 6 yields

$$\beta_1 = h^{-1}(2\pi) = h(2\pi + \Delta) + \Delta < h(2\pi) = \beta_2 \,,$$

which follows from (3.12), (3.14), and $\Delta > 0$.
Next, we proceed in two steps to prove that the fixed point $\theta^* = h(\theta^*)$ is a global attractor.

Step 1: We show that the firing map $h(\cdot)$ has no nontrivial 2-periodic orbits, that is

$$h(\theta) = h^{-1}(\theta) \tag{3.18}$$

admits no other solution but the fixed point θ^*. In the plane $(\theta, h(\theta) = \theta^+)$, a rotation of $-\pi/4$ of the axes results in a change of variables

$$(\theta, \theta^+) \mapsto (\tilde{\theta}, \tilde{\theta}^+) = \frac{\sqrt{2}}{2}(\theta - \theta^+, \theta + \theta^+) \,.$$

It turns the bisectrix into the $\tilde{\theta}^+$-axis — that is, $\tilde{\theta} = 0$ — and the firing map $h(\theta)$ becomes the map $\tilde{h}(\tilde{\theta})$. The assumption (3.12) expresses as

$$\tilde{h}\left(\frac{\Delta}{\sqrt{2}} + \tilde{\theta}\right) = \tilde{h}\left(\frac{\Delta}{\sqrt{2}} - \tilde{\theta}\right) \quad \forall \tilde{\theta}$$

and (3.14) is rewritten as

$$\tilde{h}'(\tilde{\theta}) > 0 \quad \forall \tilde{\theta} < \frac{\Delta}{\sqrt{2}} \,.$$

These two properties imply that the equation $\tilde{h}(\tilde{\theta}) = \tilde{h}(-\tilde{\theta})$, which is equivalent to (3.18), has no other solution but $\tilde{\theta} = 0$ (which corresponds to the fixed point θ^*). Hence, the return map $R \triangleq h \circ h$ has a unique fixed point.

Step 2: The fixed point $\theta^* = h(\theta^*)$ cannot be greater than $\theta_\Delta = h(\theta_\Delta) + \Delta$ since $\Delta > 0$ and $h' < 0$. Then, $\theta^* < \theta_\Delta$ implies that $|h'(\theta^*)| < 1$, according to (3.14). It follows that the derivative of the return map satisfies $R'(\theta^*) = [h'(\theta^*)]^2 < 1$. Moreover, it holds

that $R'(\theta) = h'(h(\theta))h'(\theta) > 0$. Since, in addition, the return map has only one fixed point $R(\theta^*) = \theta^*$, it can be written that

$$\begin{cases} \theta^* < R(\theta) < \theta & \text{if } \theta > \theta^*, \\ \theta < R(\theta) < \theta^* & \text{if } \theta < \theta^*. \end{cases}$$

This leads to

$$|R(\theta) - R(\theta^*)| = |R(\theta) - \theta^*| < |\theta - \theta^*| \quad \forall \theta \neq \theta^*$$

and the fixed point of R is globally attracting. For every $e > 0$, there exist integers n_1 and n_2 such that, for all θ,

$$\begin{cases} |R^n(\theta) - \theta^*| = |h^{2n}(\theta) - \theta^*| < e & \text{for } n \geq n_1, \\ |R^n(h(\theta)) - \theta^*| = |h^{2n+1}(\theta) - \theta^*| < e & \text{for } n \geq n_2. \end{cases}$$

It follows that, for every $e > 0$, there exists an integer $n_3 = \max(2n_1, 2n_2 + 1)$ such that $|h^n(\theta) - \theta^*| < e$ for $n \geq n_3$ and for all θ. Then, one has $\lim_{n\to\infty} |h^n(\theta) - \theta^*| = 0$.

In the case $\underline{x} + \overline{x} < 0$, the proof follows on similar lines to show that the fixed point is globally repelling, which leads to the absorption of an oscillator by the other. □

The global stability properties of the firing map still imply the dichotomic behavior of the two oscillators. The fixed point of the firing map is globally attracting (or globally repelling), a property that is shared with the firing map of monotone oscillators. In the present case, the vector field F is neither monotone increasing nor monotone decreasing, but the dichotomic behavior depends on whether the vector field is increasing *in the mean* or decreasing *in the mean*.

The firing map is not characterized by a contraction property, as it is for monotone oscillators, but is contracting over the phase interval $[0, \theta_\Delta]$ and expanding over the complementary interval $[\theta_\Delta, 2\pi]$. A rough parallelism can be established. While concave-up time evolution (of oscillators with monotone increasing dynamics) leads to a contracting firing map, a time evolution that is *concave-up in the mean* leads to a firing map that is *contracting "on average"*, since the interval $[\beta_1, 2\pi]$ is mapped onto the smaller interval $[\beta_2, 2\pi]$.

3.4 Large networks

In large populations, the oscillators aggregate in several clusters that subsequently evolve according to the dynamics of a multidimensional firing map.

3.4.1 Number of clusters

As mentioned in Section 3.2, the initial behavior of a large population of oscillators is dominated by the absorptions that create the clusters. The number of clusters N_g depends on the initial configuration of the network. It is determined by the following algorithm, based on successive iterations of the firing map (3.8).

1. $N_g := 1$; $\mathcal{N} = \{1, \ldots, N\}$;

2. $\theta_{\max} := \max\{\theta_k \,|\, k \in \mathcal{N}\}$;

3. Remove from $\mathcal{N}$ all indices k such that $\theta_k > \theta_{\max} - 2\pi + f^{-1}(\overline{x} - \epsilon)$;

4. Shift oscillators to next firing position $\theta_k := f^{-1}\big(f(2\pi + \theta_k - \theta_{\max}) + \epsilon\big)$ for $k \in \mathcal{N}$;

5. if $\mathcal{N} = \varnothing$;
   - then stop;
   - else $N_g := N_g + 1$ and return to 2.

From the above algorithm, it is immediate to see that, if the initial conditions satisfy

$$\max_{k=1,\dots,N} \theta_k - \min_{k=1,\dots,N} \theta_k < 2\pi - f^{-1}(\overline{x} - \epsilon) = \beta_1 \,,$$

then all the oscillators will be close enough to be absorbed by the first firing and form only one cluster ($N_g = 1$). On the other hand, $N_g = N_{g,\max}$ (see Lemma 3.2.1) if the oscillators are homogeneously distributed — e.g., a high number of oscillators with randomly distributed phases.

3.4.2 Multidimensional firing map

While the evolution of two oscillators/clusters is dictated by the firing map (3.8) — that we denote in the sequel as the *scalar* firing map — the evolution of $N_g > 2$ clusters is dictated by a $(N_g - 1)$-*dimensional* firing map.

Let the clusters phases be the components of the vector $\mathbf{\Theta} = (\theta_1, \theta_2, \cdots, \theta_{N_g-1}) \in (0, 2\pi)^{N_g-1}$. The $(N_g - 1)$-dimensional firing map is a direct generalization of the scalar firing map and expresses as

$$\mathbf{H}(\mathbf{\Theta}) = \begin{cases} \theta_1^+ &= h(\theta_{N_g-1}) \\ \theta_2^+ &= h(\theta_{N_g-1} - \theta_1) \\ &\vdots \\ \theta_{N_g-1}^+ &= h(\theta_{N_g-1} - \theta_{N_g-2}) \end{cases} . \tag{3.19}$$

In this framework, a given index is not always assigned to the same cluster. Whenever a cluster fires, it receives the index 0 — its phase $\theta_0 = 0$ is omitted in (3.19) — and an index $k \in \{1, \cdots, N_g - 1\}$ is assigned to the $N_g - 1$ remaining clusters, according to the phase ordering

$$\theta_0 = 0 < \theta_1 < \theta_2 < \cdots < \theta_{N_g-1} < 2\pi \,. \tag{3.20}$$

Since the oscillators are identical, the order of the clusters is never modified, and a cyclic permutation of the indices is performed at each firing. To summarize, the successive iterations of the firing map describe the evolution of the relative phase differences between the clusters, phase differences that are only modified at each firing.

The $(N_g - 1)$ dimensional firing map is characterized by some general properties.

Domain and absorptions. The domain of the scalar firing map h restricts the domain of the (N_g-1)-dimensional firing map. If the phase difference $\theta_{N_g-1}-\theta_k \leq \beta_1$, an absorption will occur at the next firing. The (N_g-1)-dimensional firing map is thus defined on the domain

$$\mathcal{U} = \Big\{ \Theta \in (0,2\pi)^{N_g-1} \,|\, \theta_k < \theta_{k+1}, k = 1,\dots,N_g-2 \text{ and } \theta_{N_g-1}-\theta_{N_g-2} > \beta_1 \Big\} \,. \tag{3.21}$$

When an absorption occurs, the number of clusters decreases from N_g to $\tilde{N}_g < N_g$. The (N_g-1)-dimensional vector $\boldsymbol{\Theta} = (\theta_1, \theta_2, \cdots, \theta_{\tilde{N}_g-1}, \cdots, \theta_{N_g-1})$ is projected onto a $(\tilde{N}_g-1)$-dimensional subspace, according to the projection

$$\mathcal{P}_{\text{absp}}\Big((\theta_1, \theta_2, \cdots, \theta_{\tilde{N}_g-1}, \cdots, \theta_{\tilde{N}_g-1})\Big) = (\theta_1, \theta_2, \cdots, \theta_{\tilde{N}_g-1}, 0, \cdots, 0) \,.$$

The evolution of the $\tilde{N}_g$ remaining distinct clusters is subsequently described by the $(\tilde{N}_g-1)$-dimensional firing map $\mathbf{H}'(\boldsymbol{\Theta}')$, with $\boldsymbol{\Theta}' = [\theta_1, \theta_2, \cdots, \theta_{\tilde{N}_g-1}] \in (0,2\pi)^{\tilde{N}_g-1}$.

Fixed point. The fixed point $\mathbf{H}(\boldsymbol{\Theta}^*) = \boldsymbol{\Theta}^*$ corresponds to a phase-locked clustering configuration of the network — at each firing, the phases of the clusters are fixed. The following result establishes, in full generality, the existence and the uniqueness of the fixed point.

Proposition 3.4.1. *The fixed point of the* (N_g-1)*-dimensional firing map* (3.19)*, with* $1 < N_g \leq N_{g,\max}$*, exists and is unique in* $\mathcal{U}$*.*

Proof. We proceed in three steps.

Step 1: Let $B_1(\theta) = \theta$ and $B_k(\theta) = \theta - h(B_{k-1}(\theta))$ for $k = 2,\dots,N_g$. We prove the following property. For $k = 1\dots,N_g$, there exists a value $0 \leq \theta_k^c$ such that $B_k(\theta_k^c) = 0$ and such that $B_k'(\theta) > 0$ and $0 < B_k(\theta) < 2\pi \;\forall \theta \in [\theta_k^c, 2\pi)$. This is trivial for $B_1(\theta) = \theta$, with $\theta_1^c = 0$. Considering the property to be true for B_{k-1} with $k \in \{2\dots,N_g\}$, we proceed by induction. One first obtains

$$B_k'(\theta) = 1 - h'\Big(B_{k-1}(\theta)\Big) B_{k-1}'(\theta) > 0 \quad \forall \theta \in [\theta_{k-1}^c, 2\pi] \tag{3.22}$$

since $h(\cdot)$, evaluated on $B_{k-1}(\theta) \in [0,2\pi]$, is strictly decreasing. Then, noting that $\theta_{k-1}^c < 2\pi$ and that $h(0) > 2\pi$ by construction, we have

$$B_k(\theta_{k-1}^c) = \theta_{k-1}^c - h\Big(B_{k-1}(\theta_{k-1}^c)\Big) = \theta_{k-1}^c - h(0) < 0 \,. \tag{3.23}$$

Moreover, one easily computes that

$$B_k(2\pi) = 2\pi - f^{-1}\Big(\underline{x} + (k-1)\epsilon\Big) > 0 \tag{3.24}$$

since $k \leq N_g \leq N_{g,\max} < (\overline{x}-\underline{x})/\epsilon + 1$. As a consequence of (3.22), (3.23), (3.24), and the continuity of B_k, there exists a unique θ_k^c, with $\theta_{k-1}^c < \theta_k^c < 2\pi$, such that $B(\theta_k^c) = 0$. Noting that $B_k(2\pi) < 2\pi$, it follows that $0 \leq B_k(\theta) < 2\pi \;\forall \theta \in [\theta_k^c, 2\pi)$.

Step 2: A fixed point of the firing map (3.19) satisfies

$$\theta_k^* = h\Big(B_k(\theta_{N_g-1}^*)\Big), \quad k = 1,\dots,N_g-1 \,. \tag{3.25}$$

One deduces that the condition (3.20) implies $0 < \theta_n^* - \theta_k^* < 2\pi$, or equivalently

$$0 < B_k(\theta^*_{N_g-1}) < 2\pi, \quad k = 1, \dots, N_g - 1\,. \tag{3.26}$$

Moreover, it also holds

$$B_{N_g}(\theta^*_{N_g-1}) = 0\,. \tag{3.27}$$

According to the above properties of B_k, the value $\theta^*_{N_g-1} = \theta^c_{N_g}$ exists and is the unique solution of (3.27) which fulfills all the conditions (3.26). The values θ_k^* are then explicitly determined by (3.25).

Step 3: One verifies that the fixed point does not violate the ordering conditions (3.20). First, we have

$$\theta_1^* = h\Big(B_1(\theta^*_{N_g-1})\Big) = h(\theta^*_{N_g-1}) > 0\,.$$

Furthermore, knowing that

$$h\Big(B_2^*(\theta^*_{N_g-1})\Big) = h\bigg(\theta^*_{N_g-1} - h\Big(B_1(\theta^*_{N_g-1})\Big)\bigg) > h(\theta^*_{N_g-1}) = h\Big(B_1^*(\theta^*_{N_g-1})\Big)\,,$$

the other relations follow by induction. If $h(B_k(\theta^*_{N_g-1})) < h(B_{k+1}(\theta^*_{N_g-1}))$ for $k = 1, \dots, N_g - 1$, then

$$\begin{aligned} h\Big(B_{k+2}(\theta^*_{N_g-1})\Big) &= h\bigg(\theta^*_{N_g-1} - h\Big(B_{k+1}(\theta^*_{N_g-1})\Big)\bigg) \\ &> h\bigg(\theta^*_{N_g-1} - h\Big(B_k(\theta^*_{N_g-1})\Big)\bigg) = h\Big(B_{k+1}(\theta^*_{N_g-1})\Big)\,. \end{aligned}$$

At last, one has $\theta^*_{N_g-1} < 2\pi$, which concludes the proof. □

Remark 3.4.1. Without the upper bound $N_g < N_{g,\max}$, the firing map has still a unique fixed point on $[0, h^{-1}(0)]^{N_g-1}$, for any $N_g \in \mathbb{N}_0$. But in this case, the fixed point may have some components beyond 2π, and does not necessary lies in $\mathcal{U}$. ◇

The result of Proposition 3.4.1 is very general since it makes no assumption on the dynamics of the integrate-and-fire oscillators. In addition, it implies that the network can exhibit only a very limited number of phase-locked clustering configurations.

Corollary 3.4.1. *A network of N pulse-coupled integrate-and-fire oscillators has only $N_{g,\max}$ (3.4) different phase-locked clustering configurations. Moreover, a phase-locked configuration is unique for a given number of clusters.*

Proof. The case $N_g = 1$ corresponds to the unique synchronized behavior. Lemma 3.2.1 implies that $N_g < N_{g,\max}$. Then, the assumption of Proposition 3.4.1 is satisfied and it follows that there exists only one phase-locked clustering configuration for each number $N_g < N_{g,\max}$. □

From a practical (numerical) point of view, the system $\mathbf{H}(\mathbf{\Theta}^*) = \mathbf{\Theta}^*$ can be easily solved to obtain the fixed point. Once the scalar equation (3.27) solved to obtain $\theta^*_{N_g-1}$, the $N_g - 2$ remaining θ_k^*'s are explicitly given by (3.25). This property, as well as the proof of Proposition 3.4.1, is due to the particular *chain structure* of the firing map.

Particular structure. One of the remarkable properties of the firing map (3.19) is its particular structure. The firing map is indeed the composition

$$\mathbf{H} = \mathbf{N} \circ \mathbf{L} \tag{3.28}$$

of a linear map $\mathbf{L}$, corresponding to the oscillators shift between two firings, with a nonlinear map $\mathbf{N}$, corresponding to the impulsive interaction of the oscillators at a firing (Figure 3.7). The linear map is a dynamical application defined by the $(N_g - 1) \times (N_g - 1)$ companion matrix

$$\mathbf{L} = \begin{pmatrix} 0 & \dots & 0 & 1 \\ -1 & 0 & 0 & 1 \\ & \ddots & & \vdots \\ 0 & & 0 & \vdots \\ 0 & 0 & -1 & 1 \end{pmatrix} \tag{3.29}$$

and provides the firing map $\mathbf{H}$ with a *multidimensional chain structure*. The nonlinear map is a repeated static nonlinearity $\mathbf{N}(\zeta) = (h(\zeta_1), \cdots, h(\zeta_{N_g-1}))$, where h is the scalar firing map previously defined for two oscillators. The linear map corresponds to the uniform rotation of the oscillators between two firings (continuous flow of the hybrid model) and the nonlinear map is related to the impulsive coupling at each firing (instantaneous jump of the hybrid model).

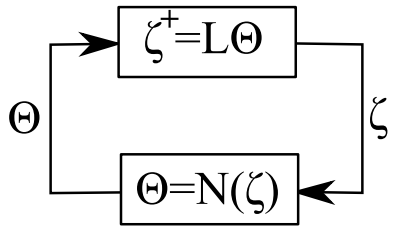

Figure 3.7: The firing map is the (feedback) combination of a linear (dynamical) map $\mathbf{L}$ with a static nonlinearity $\mathbf{N}$.

Stability properties. The stability properties of the firing map are of paramount importance to investigate the collective behavior emerging from the network. For instance, a globally (anti-)stable fixed point leads to a dichotomic behavior of large networks. Given the particular feedback structure of the firing map (Figure 3.7), the stability problem is also related to absolute stability questions (see [55] for an overview).

While the linear map $\mathbf{L}$ somehow accounts for the "multidimensional architecture" of the firing map, it provides no stability property. This is illustrated by the dynamics of uncoupled oscillators. Setting $\epsilon = 0$ in (3.8) yields $h(\theta) = 2\pi - \theta$ and the phase difference between two configurations $\mathbf{\Theta}$ and $\mathbf{\Psi}$ evolves as

$$(\mathbf{\Theta} - \mathbf{\Psi})^+ = -\mathbf{L}\,(\mathbf{\Theta} - \mathbf{\Psi})\,. \tag{3.30}$$

The linear map thereby governs the rigid rotation of the oscillators, a marginally stable behavior that converges toward no particular configuration. This is also suggested by the property

$$(-\mathbf{L})^{N_g} = \mathbf{I}\,,$$

where **I** is the identity, property that shows no net influence of the linear map after N_g steps.

In contrast, it is the static nonlinearity **N** that governs the stability properties of the firing map **H**. The static nonlinearity is related to the firing instants, where the impulsive coupling modifies the relative configuration of the network. The map is directly derived from the scalar firing map, for which strong global stability results have been established. Then, a relevant question is *which properties of the scalar firing map induce the stability of the* $(N_g - 1)$*-dimensional firing map.*

In other words:

- Q1. For monotone integrate-and-fire oscillators, is the $(N_g - 1)$-dimensional firing map characterized by a *contraction* property?
- Q2. For "QIF-like" integrate-and-fire oscillators (satisfying Assumption 1), is the fixed point of the $(N_g - 1)$-dimensional firing map *globally stable* whenever $\underline{x} + \overline{x} > 0$ (evolution concave-up in the mean)?

In the rest of the present dissertation, we tackle these two questions, focusing on large populations of oscillators and investigating whether a dichotomic behavior characterizes two oscillators (or clusters) as well as $N_g > 2$ clusters. Under mild additional assumptions, Chapter 4 provides a positive answer to question Q1. Interestingly, the answer of question Q2 depends on further properties of F, a result which means that large networks of pulse-coupled oscillators are not all characterized by a dichotomic behavior. The extension of the stability properties of the scalar firing map to higher dimensions depends on finer properties on the scalar firing map. In addition, Chapter 6 shows that the second question leads to open problems, especially in the case of QIF oscillators.

Chapter 4

Global analysis of monotone integrate-and-fire oscillators

In 1975, Peskin originally applied impulsive coupling to LIF oscillators [86] and conjectured that the network always synchronizes. The conjecture was proved fifteen years later by Mirollo and Strogatz [75], under the more general assumption of monotone *decreasing* F (*concave-down* time evolution). In contrast, we show that a monotone *increasing* F (*concave-up* time evolution) leads to a phase-locked clustering behavior. The study of monotone increasing dynamics, presented in the present chapter, complements the previous analysis and highlights the dichotomic behavior of monotone oscillators.

Systems of two oscillators are characterized by a dichotomic behavior, an observation that follows from the contraction property of the scalar firing map (see Chapter 3). The present chapter extends this result and shows that large networks of monotone oscillators are characterized by the same properties as the simple networks of two oscillators: the multidimensional firing map has also a contraction property and large populations are also characterized by the dichotomic behavior.

The chapter is organized as follows. In Section 4.1, we discuss some properties of the dichotomic behavior, properties that are induced by the monotone dynamics of the oscillators. Section 4.2 presents the main result of the chapter. The contraction property of the multidimensional firing map is established for a well-chosen 1-norm. A link between the contraction property and absolute stability theory is established in Section 4.3. Finally, the robustness of the phase-locked clustering configuration in heterogeneous populations of monotone oscillators is investigated in Section 4.4.

The main contributions of the chapter are (i) the contraction property of the multidimensional firing map, for identical monotone oscillators and (ii) the study of heterogeneous populations of monotone oscillators. The main results presented in the chapter are published in [73].

4.1 Dichotomic behavior

Networks of identical monotone integrate-and-fire oscillators exhibit the dichotomic behavior: either they achieve perfect synchrony (decreasing F, concave-down time evolution) or they converge toward a phase-locked clustering configuration (increasing F, concave-up time

evolution).

4.1.1 Synchronization

Identical pulse-coupled integrate-and-fire oscillators with a concave-down time evolution achieve perfect synchrony, a result that was proved in [75]:

Theorem 4.1.1 (Mirollo and Strogatz, 1990)**.** *For almost all initial conditions, a system of identical pulse-coupled integrate-and-fire oscillators $\dot{x} = F(x)$, with a monotone decreasing vector field $dF/dx < 0$ on $[\underline{x}, \overline{x}]$ (concave-down time evolution), approaches a state in which all the oscillators are firing synchronously.*

4.1.2 Phase-locked clustering

If the initial conditions are randomly distributed, all the oscillators are not absorbed during a unique initial firing. Under this condition, numerical simulations suggest that *all* networks of integrate-and-fire oscillators with a concave-up time evolution converge toward a phase-locked clustering configuration.

As a first observation, the number of absorptions is bounded and two clusters cannot merge through an absorption. This property, summarized in the following proposition, precludes the synchronization of the whole network by an aggregating process of the clusters.

Proposition 4.1.1. *In a network of N identical integrate-and-fire oscillators $\dot{x} = F(x)$ characterized by $dF/dx > 0$ on $[\underline{x}, \overline{x}]$ (concave-up time evolution), a cluster of more than one oscillator cannot be absorbed by any firing oscillator. Consequently, there are at most $N_{g,\max}$ (3.4) absorptions.*

Proof. Consider a cluster A that has just been created through the firing of one of its oscillators. At this time, the cluster has the state $\underline{x}$ and the states of the other oscillators are all increased by ϵ. In particular, the state of its preceding oscillator/cluster B is greater than $\underline{x}+\epsilon$ and the state difference $x_B - x_A > \epsilon$. In order to prove that B cannot absorb A at its next firing, one has to show that the state difference remains greater than ϵ until B fires. At each intermediate firing that occurs before the firing of B, the states of A and B are both increased by ϵ and $x_B - x_A$ remains unchanged. Moreover, between two successive intermediate firings, the phases of both A and B are increased by a same value $\Delta\theta$, a process that increases the state difference :

$$f\Big(f^{-1}(x_B) + \Delta\theta\Big) - f\Big(f^{-1}(x_A) + \Delta\theta\Big) > f\Big(f^{-1}(x_B)\Big) - f\Big(f^{-1}(x_A)\Big) = x_B - x_A\,,$$

where the inequality holds since the evolution function f is concave-up. Hence, the state difference remains greater than ϵ and the cluster A is not absorbed by the firing of B.
Since the absorptions only create new clusters, the number of absorptions cannot exceed N_g, whose bound is $N_{g,\max}$ by Lemma 3.2.1. □

Proposition 4.1.1 shows that the network cannot achieve synchrony and implies that the N_g clusters evolve according to a unique $(N_g - 1)$-dimensional firing map, since the number of clusters cannot decrease. However, the above result implies nothing on the convergence of the N_g clusters toward the phase-locked clustering configuration, so that a stability analysis of the $(N_g - 1)$-dimensional firing map is needed.

A preliminary answer to the stability question is provided by the following proposition.

Proposition 4.1.2. *If the evolution function f is concave-up on $[0, 2\pi]$, then the Jacobian matrix $\mathbf{J}(\boldsymbol{\Theta})$ of the corresponding $(N_g - 1)$-firing map, $N_g > 1$, has all its eigenvalues inside the unit disk, for all $\boldsymbol{\Theta} \in \mathcal{U}$. Consequently, the fixed point of the $(N_g - 1)$-dimensional firing map is locally asymptotically stable.*

Proof. The Jacobian matrix $\mathbf{J}$ is

$$\mathbf{J} = \begin{pmatrix} 0 & \dots & 0 & h'_0 \\ -h'_1 & 0 & 0 & h'_1 \\ 0 & \ddots & 0 & \vdots \\ 0 & 0 & -h'_{N_g-2} & h'_{N_g-2} \end{pmatrix},$$

with $h'_0 = |h'(\theta_{N_g-1})|$ and $h'_k = |h'(\theta_{N_g-1} - \theta_k)|$ for $k = 1, \dots, N_g - 2$. The characteristic polynomial of $\mathbf{J}$ expresses as

$$p(z) = z^{N_g-1} + h'_{N_g-2} z^{N_g-2} + h'_{N_g-3} h'_{N_g-2} z^{N_g-3} + \cdots + \prod_{k=1}^{N_g-2} h'_k z + \prod_{k=0}^{N_g-2} h'_k \,. \tag{4.1}$$

It follows from Property 5 [see (3.11)] that $h'_k < 1$ for $k = 0, \dots, N_g - 2$. By the Eneström-Kakeya theorem[1] [48], the polynomial has all its roots inside the unit disk. Then, all the eigenvalues are inside the unit disk, which concludes the proof. □

The above result follows from the important Property 5 (i.e. $|h'| < 1$) that characterizes the scalar firing map of monotone integrate-and-fire oscillators.

Remark 4.1.1. Owing to the special structure $\mathbf{H} = \mathbf{N} \circ \mathbf{L}$ of the firing map (see Chapter 3), the Jacobian matrix can be decomposed as the matrix product $\mathbf{J} = -\mathbf{D}\,\mathbf{L}$, with $\mathbf{D}$ a diagonal matrix whose entries are the derivatives h'_k. The diagonal matrix $\mathbf{D}$ is related to the nonlinear part $\mathbf{N}$ of the firing map and provides the Jacobian matrix with stability properties. ◇

Proposition 4.1.2 implies that the Jacobian matrix is stable everywhere in $\mathcal{U}$, a property that restricts the behavior of the firing map. It follows from the Jacobian matrix property that the trajectories are not chaotic and, in addition, there exists no nontrivial periodic orbit (the proof is not detailed in the present manuscript).

However, the Jacobian matrix property is a local property which does not prove that the fixed point is a global attractor. In the case of synchronization, the local property implies that every set is mapped onto a set of greater measure and thereby shows that the trajectories must leave $\mathcal{U}$ after successive iterations (this results in an absorption). This property was directly used in [75] to prove Theorem 4.1.1. In the case of phase-locked clustering, each set converges toward a set of zero measure, but this does not imply that the trajectories converge toward a fixed point. As a consequence, the Jacobian property cannot be used directly to prove the convergence toward a phase-locked configuration. Such a property even leads to strong conjectures in dynamical systems theory (Jacobian conjectures [20, 101]). Even though the firing map is *locally* contracting everywhere in $\mathcal{U}$ — the measure of infinitesimal volumes is decreasing along each solution — it is not obvious whether the firing map is *globally* contracting. We tackle this issue in the next section.

[1] If $p(z) = \sum_{k=0}^{n} p_k z^k$ is a polynomial such that $p_n \geq p_{n-1} \geq \cdots \geq p_0 > 0$, then $p(z)$ does not vanish in $|z| > 1$.

4.2 Global contraction: from a quadratic norm to a 1-norm

In the case of two oscillators, the scalar firing map is a contraction, with $|h'| < 1$ (Property 5). In the sequel, we prove that the $(N_g - 1)$-dimensional firing map is also a contraction. The question is not trivial since the contraction property must be defined with respect to a distance, for instance derived from a particular norm, and it is a priori not obvious which norm to consider. After initially considering a more usual *quadratic norm*, we show that, surprisingly, a *1-norm* is more convenient to express the contraction property of the firing map.

4.2.1 Contraction with respect to a quadratic norm

The contraction property of the $(N_g - 1)$-dimensional firing map is first investigated with respect to a quadratic vector norm. Exploiting the particular structure $\mathbf{H} = \mathbf{N} \circ \mathbf{L}$ of the firing map, we introduce a norm such that the induced distance between two trajectories is invariant during the rigid rotation of the oscillators between two firings (map $\mathbf{L}$), but varies only under the instantaneous jump triggered by a firing (map $\mathbf{N}$). One considers the quadratic vector norm

$$\|\mathbf{x}\|_{(2)} = \sqrt{\mathbf{x}^T \mathbf{Q} \mathbf{x}}\,, \tag{4.2}$$

where the $(N_g - 1) \times (N_g - 1)$ matrix $\mathbf{Q}$ is chosen in such a way that the linear map $\mathbf{L}$ is an isometry, that is

$$\|\mathbf{L}\mathbf{x}\|_{(2)} = \|\mathbf{x}\|_{(2)} \quad \forall \mathbf{x} \quad \text{or equivalently} \quad \mathbf{L}^T \mathbf{Q} \mathbf{L} = \mathbf{Q}\,. \tag{4.3}$$

A matrix satisfying (4.3) corresponds to the Laplacian matrix of a graph with a chain structure — the reader will remember that the linear map $\mathbf{L}$ provides the firing map with a chain structure — and is given by

$$\mathbf{Q} = \begin{pmatrix} 2 & -1 & 0 & \dots & 0 \\ -1 & 2 & -1 & \ddots & 0 \\ 0 & \ddots & \ddots & \ddots & 0 \\ 0 & \ddots & -1 & 2 & -1 \\ 0 & \dots & 0 & -1 & 2 \end{pmatrix}. \tag{4.4}$$

One verifies that the norm is well-defined since the matrix $\mathbf{Q}$ is positive definite:

$$\mathbf{x}^T \mathbf{Q} \mathbf{x} = x_1^2 + \sum_{k=1}^{N_g - 2} (x_k - x_{k+1})^2 + x_{N_g - 1}^2 > 0$$

for all $\mathbf{x} \neq (0, \dots, 0)$. From the vector norm, one also derives the induced matrix norm

$$\|\mathbf{A}\|_{(2)} = \max_{\mathbf{x} \neq \mathbf{0}} \frac{\|\mathbf{A}\mathbf{x}\|_{(2)}}{\|\mathbf{x}\|_{(2)}}\,. \tag{4.5}$$

Under some assumptions, we show that the $(N_g - 1)$-dimensional firing map is a contraction with respect to the norm (4.2). This is the statement of Theorem 4.2.1. To prove the result,

the special structure of the firing map is exploited: while the linear map $\mathbf{L}$ is an isometry with respect to the considered norm (4.3), the nonlinear map $\mathbf{N}$ induces the contraction property of the firing map. As a preliminary to the result, the following lemma provides a useful property of the norm of particular diagonal matrices.

Lemma 4.2.1. *For any integer $n = 0, \dots, N_g-1$, let $\mathbf{D}_n^{(0,1)} = diag\{d_k\}$ be a $(N_g-1)\times(N_g-1)$ diagonal matrix, with $d_k = 0$ for $k \leq n$ and $d_k = 1$ for $k > n$. Then*

$$\max_{n\in\{0,\dots,N_g-1\}} \|\mathbf{D}_n^{(0,1)}\|_{(2)} \leq \frac{N_g+1}{2\sqrt{N_g}}\,.$$

Proof. The proof of Lemma 4.2.1 can be found in Appendix A.1. □

As a consequence of Lemma 4.2.1, some diagonal matrices with entries less than one are not a contraction in the proposed norm. Then, the condition $|h'| < 1$ (fulfilled whenever f is concave-up) is not sufficient to establish the contraction (of the nonlinear map $\mathbf{N}$) and a more restrictive assumption is necessary. This is summarized in the following theorem.

Theorem 4.2.1. *If the bounds $\underline{h} = \min_{\theta\in[0,2\pi]} |h'(\theta)|$ and $\overline{h} = \max_{\theta\in[0,2\pi]} |h'(\theta)|$ satisfy*

$$\frac{\overline{h}-\underline{h}}{1-\underline{h}} < \frac{2\sqrt{N_g}}{N_g+1} \tag{4.6}$$

and if

$$h''(\theta) > 0 \quad \forall\theta\in[0,2\pi] \quad or \quad h''(\theta) < 0 \quad \forall\theta\in[0,2\pi]\,, \tag{4.7}$$

then the (N_g-1)-dimensional firing map (3.19), with $N_g > 2$, is a contraction in $\mathcal{U}$ for the quadratic norm (4.2).

Proof. Let $\mathbf{\Theta} = (\theta_1, \dots, \theta_{N_g-1})$, $\mathbf{\Psi} = (\psi_1, \dots, \psi_{N_g-1})$, and define $\theta_0 = \psi_0 = 0$. For each $k \in \{1, \dots, N_g-1\}$, one has

$$\theta_k^+ - \psi_k^+ = h(\theta_{N_g-1} - \theta_{k-1}) - h(\psi_{N_g-1} - \psi_{k-1})$$

or, by the mean value theorem,

$$\theta_k^+ - \psi_k^+ = h'(\xi_k)\left[(\theta_{N_g-1} - \psi_{N_g-1}) - (\theta_{k-1} - \psi_{k-1})\right]$$

for some $\xi_k \in [\theta_{N_g-1} - \theta_{k-1}, \psi_{N_g-1} - \psi_{k-1}]$. In vector form, it follows that

$$\mathbf{H}(\mathbf{\Theta}) - \mathbf{H}(\mathbf{\Psi}) = -\mathbf{D}\,\mathbf{L}\,(\mathbf{\Theta} - \mathbf{\Psi})\,,$$

with the diagonal matrix

$$\mathbf{D} = \mathrm{diag}\left\{|h'(\xi_1)|, \dots, |h'(\xi_{N_g-1})|\right\}\,. \tag{4.8}$$

Next, we obtain

$$\|\mathbf{H}(\mathbf{\Theta}) - \mathbf{H}(\mathbf{\Psi})\|_{(2)} = \|\mathbf{D}\mathbf{L}(\mathbf{\Theta} - \mathbf{\Psi})\|_{(2)} \leq \|\mathbf{D}\|_{(2)}\|\mathbf{L}(\mathbf{\Theta} - \mathbf{\Psi})\|_{(2)} = \|\mathbf{D}\|_{(2)}\|(\mathbf{\Theta} - \mathbf{\Psi})\|_{(2)}\,,$$

where the last equality follows from (4.3), the isometry property of $\mathbf{L}$.

It remains to prove that $\|\mathbf{D}\|_{(2)} < 1$. The assumption (4.7) implies that the ξ_k's are ordered and, as a consequence, that the entries of the diagonal matrix $\mathbf{D}$ (4.8) are ordered. Given the symmetry $\mathbf{Q}(k,l) = \mathbf{Q}(l,k) = \mathbf{Q}(N_g - l, N_g - k)$, we consider without lack of generality that the firing map is concave-up, so that the entries of $\mathbf{D}$ are increasing. As a consequence, any admissible matrix $\mathbf{D}$ can be expressed as a convex combination of the matrices $\mathbf{D}_n^{(\underline{h},\overline{h})} = \mathrm{diag}\{d_k\}$, with $d_k = \underline{h}$ for $k \leq n$ and $d_k = \overline{h}$ for $k > n$. It follows that

$$\|\mathbf{D}\|_{(2)} = \left\| \sum_{n=0}^{N_g-1} \alpha_n \mathbf{D}_n^{(\underline{h},\overline{h})} \right\|_{(2)} \leq \sum_{n=0}^{N_g-1} \alpha_n \|\mathbf{D}_n^{(\underline{h},\overline{h})}\|_{(2)} \leq \max_{n\in\{0,\dots,N_g-1\}} \|\mathbf{D}_n^{(\underline{h},\overline{h})}\|_{(2)}, \tag{4.9}$$

where $\alpha_n \geq 0$ and $\sum_n \alpha_n = 1$. Moreover, since $\mathbf{D}_n^{(\underline{h},\overline{h})} = \underline{h}\,\mathbf{I} + (\overline{h} - \underline{h})\,\mathbf{D}_n^{(0,1)}$, one has

$$\|\mathbf{D}\|_{(2)} \leq \underline{h}\,\|\mathbf{I}\|_{(2)} + (\overline{h} - \underline{h}) \max_{n\in\{0,\dots,N_g-1\}} \|\mathbf{D}_n^{(0,1)}\|_{(2)} \leq \underline{h} + (\overline{h} - \underline{h}) \frac{N_g + 1}{2\sqrt{N_g}}\,,$$

where the last inequality follows from Lemma 4.2.1. Finally, the assumption (4.6) implies $\|\mathbf{D}\|_{(2)} < 1$, which concludes the proof. □

At this stage, the contraction property of the scalar firing map does not perfectly extend to the $(N_g - 1)$-dimensional firing map. In Theorem 4.2.1, additional assumptions are required, assumptions that are not needed for the contraction property of the scalar firing map. While assumption (4.7) is a mild technical assumption (satisfied by LIF oscillators, for instance), assumption (4.6) is more restrictive. In addition, the greater the number of clusters N_g, the more restrictive the condition (4.6). Since N_g has an upper bound $N_{g,\max}$ (3.4), the condition (4.6) slightly restricts the model parameters for which the firing map is a contraction. However, in the case of a weak coupling $\epsilon << 1$, the upper bound $N_{g,\max}$ may be very high and the assumption (4.6) imposes very restrictive lower and upper bounds on the derivative of the scalar firing map.

The question is whether another distance is more appropriate to capture the contraction property of the $(N_g - 1)$-dimensional firing map, under assumptions that do not depend on the number of clusters N_g. The answer is positive, through a particular 1-norm inspired from the quadratic norm (4.2).

4.2.2 Contraction with respect to a 1-norm

To improve on Theorem 4.2.1, we introduce a norm for which the linear map $\mathbf{L}$ is still an isometry, but for which the contraction property induced by the nonlinear part $\mathbf{N}$ is satisfied under milder assumptions, independently of the number N_g.

Instead of the quadratic norm (4.2)

$$\|\mathbf{x}\|_{(2)}^2 = x_1^2 + \sum_{k=1}^{N_g-2} (x_k - x_{k+1})^2 + x_{N_g-1}^2\,,$$

we replace the squares $(\cdots)^2$ by absolute values $|\cdots|$ and propose the 1-norm

$$\|\mathbf{x}\|_{(1)} = |x_1| + \sum_{k=1}^{N_g-2} |x_k - x_{k+1}| + |x_{N_g-1}|\,, \tag{4.10}$$

with the induced matrix norm

$$\|\mathbf{A}\|_{(1)} = \max_{\mathbf{x}\neq\mathbf{0}} \frac{\|\mathbf{A}\mathbf{x}\|_{(1)}}{\|\mathbf{x}\|_{(1)}} .$$

The linear map $\mathbf{L}$ is still an isometry for the norm (4.10). Noting $\mathbf{y} = \mathbf{L}\mathbf{x}$, one verifies

$$\|\mathbf{y}\|_{(1)} = |y_1| + \sum_{k=1}^{N_g-2} |y_{k+1} - y_k| + |y_{N_g-1}| = |x_{N_g-1}| + |x_1| + \sum_{k=1}^{N_g-2} |x_{k+1} - x_k| = \|\mathbf{x}\|_{(1)} .$$

The 1-norm is more appropriate than the quadratic norm to express the contraction property of the firing map. Whereas Lemma 4.2.1 shows that the quadratic norm of the special diagonal matrices $\mathbf{D}_n^{(0,1)}$ can exceed one (and increases with the number N_g), the following lemma shows that the 1-norm never exceeds one, for any number N_g.

Lemma 4.2.2. *For any integer $n = 0, \ldots, N_g-1$, let $\mathbf{D}_n^{(0,1)} = diag\{d_k\}$ be a $(N_g-1)\times(N_g-1)$ diagonal matrix, with $d_k = 0$ for $k \leq n$ and $d_k = 1$ for $k > n$. Then, one has*

$$\begin{aligned} \|\mathbf{D}_{N_g-1}^{(0,1)}\|_{(1)} &= 0 \\ \|\mathbf{D}_n^{(0,1)}\|_{(1)} &= 1 \quad \textit{for} \quad n < N_g - 1 . \end{aligned}$$

Proof. The proof of Lemma 4.2.2 can be found in Appendix A.2. □

The following theorem establishes the contraction property of the $(N_g - 1)$-dimensional firing map without the restrictive assumption (4.6) on the bounds of the scalar firing map.

Theorem 4.2.2. *If $|h'(\theta)| < 1 \ \forall\theta \in [0, 2\pi]$ (f is concave-up) and if*

$$h''(\theta) > 0 \quad \forall\theta \in [0, 2\pi] \quad \textit{or} \quad h''(\theta) < 0 \quad \forall\theta \in [0, 2\pi] ,$$

then the $(N_g - 1)$-dimensional firing map (3.19) is a contraction in $\mathcal{U}$ for the 1-norm (4.10).

Proof. The proof follows on similar lines as the proof of Theorem 4.2.1. Since $\mathbf{L}$ is an isometry, one obtains $\|\mathbf{H}(\boldsymbol{\Theta}) - \mathbf{H}(\boldsymbol{\Psi})\|_{(1)} \leq \|\mathbf{D}\|_{(1)}\|(\boldsymbol{\Theta} - \boldsymbol{\Psi})\|_{(1)}$ and it remains to prove that $\|\mathbf{D}\|_{(1)} < 1$. Given the curvature assumption on h, the matrix $\mathbf{D}/\|\mathbf{D}\|_\infty$ — with $\|\mathbf{D}\|_\infty < 1$ since $|h'| < 1$ — is expressed as the convex combination of the matrices $\mathbf{D}_n^{(0,1)}$, $n = 0, \ldots, N_g - 1$. Similarly to (4.9), one has

$$\frac{\|\mathbf{D}\|_{(1)}}{\|\mathbf{D}\|_\infty} \leq \max_{n\in\{0,\ldots,N_g-1\}} \|\mathbf{D}_n^{(0,1)}\|_{(1)}$$

and, by Lemma 4.2.2, $\|\mathbf{D}\|_{(1)} \leq \|\mathbf{D}\|_\infty < 1$, which concludes the proof. (Actually, it is easy to see that $\|\mathbf{D}\|_{(1)} = \|\mathbf{D}\|_\infty$.) □

Theorem 4.2.2 shows that a particular distance between any two trajectories is decreasing with time. While the distance is conserved between the firings (rigid rotation of the oscillators), the distance strictly decreases at every instantaneous firing.

Theorem 4.2.2 implies that the fixed point of the firing map is a global attractor. It thus extends Property 3.3.1 to large populations of oscillators. Insofar as more than one cluster is formed during the initial absorptions stage, the clusters always converge to a phase-locked clustering state. This is summarized in the following theorem.

Theorem 4.2.3. *Consider a network of N identical pulse-coupled integrate-and-fire oscillators $\dot{x} = F(x)$ characterized by (i) a monotone vector field $dF/dx > 0$ on $[\underline{x}, \overline{x}]$ (concave-up evolution) and (ii) a scalar firing map with a curvature of constant sign. Then either an absorption occurs at the first firing and synchronizes all the oscillators, or the network asymptotically converges to a phase-locked clustering configuration.*

Proof. The proof follows from Theorem 4.2.2, through the contraction mapping theorem (see e.g. [55]), and from Proposition 4.1.1. □

As a key result of this chapter, Theorem 4.2.2 implies Theorem 4.2.3 (phase-locked clustering), a result that can be seen as the counterpart of Theorem 4.1.1 (synchronization) and that highlights the dichotomic behavior of pulse-coupled monotone integrate-and-fire oscillators.

4.3 A link to absolute stability theory

The present section is a brief digression about the absolute stability problem related to the analysis of the firing map. The stability results obtained within this framework are not stronger than the contraction property with respect to the 1-norm, a property that remains the main contribution of this chapter. However, in this section, we show that the results previously obtained with the quadratic norm (Section 4.2.1) are related to absolute stability results.

In nonlinear control theory, absolute stability problem is related to feedback systems with a static nonlinearity. The systems are said absolutely stable if they are globally stable for any nonlinearity satisfying a given condition (for instance, a sector condition). In the pulse-coupled oscillators context, we have seen that the firing map has a particular structure, interpreted as the feedback interconnection between a linear dynamical system $\mathbf{L}$ and a nonlinear static system $\mathbf{N}$ (Figure 3.7). As a consequence, some absolute stability results are applied in the present context and show the global stability of the firing map, in the case of monotone oscillators. (More details about absolute stability can be found in [55].)

Considering the notations of Figure 3.7, we propose the change of variables

$$\begin{aligned} \mathbf{x} &= \boldsymbol{\Theta} - \boldsymbol{\Theta}^* \\ \mathbf{y} &= \zeta - \mathbf{L}\boldsymbol{\Theta}^* , \end{aligned}$$

where $\boldsymbol{\Theta}^*$ is the fixed point of the firing map, that is $\boldsymbol{\Theta}^* = \mathbf{H}(\boldsymbol{\Theta}^*) = \mathbf{N}(\mathbf{L}\boldsymbol{\Theta}^*)$. In the new variables, the two systems

$$\begin{aligned} \zeta^+ &= \mathbf{L}\boldsymbol{\Theta} \\ \boldsymbol{\Theta} &= \mathbf{N}(\zeta) \end{aligned}$$

become

$$\mathbf{y}^+ = \mathbf{L}\mathbf{x} \tag{4.11}$$

$$\mathbf{x} = \mathbf{N}(\mathbf{y} + \mathbf{L}\boldsymbol{\Theta}^*) - \boldsymbol{\Theta}^* \triangleq -\boldsymbol{\Phi}(\mathbf{y}) . \tag{4.12}$$

The feedback interconnection of the two systems is represented in Figure 4.1. The linear dynamical system (4.11) is characterized by the transfer function $\mathbf{G}(e^{i\omega}) = \mathbf{L}e^{-i\omega}$. The static

nonlinearity $\mathbf{\Phi}$ (4.12) satisfies $\mathbf{\Phi}(\mathbf{0}) = \mathbf{0}$, thanks to the change of variables. The convergence to the fixed point $\mathbf{\Theta}^*$ corresponds in the new variables to the convergence to $(\mathbf{x}, \mathbf{y}) = (\mathbf{0}, \mathbf{0})$.

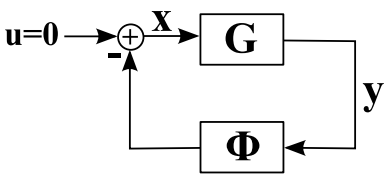

Figure 4.1: The firing map is the feedback interconnection of a linear system, whose transfer function is $\mathbf{G}(e^{i\omega}) = \mathbf{L}e^{-i\omega}$, with a static nonlinearity $\mathbf{\Phi}(\mathbf{y})$.

Each component of the repeated nonlinearity $\mathbf{N}(\zeta) = (h(\zeta_1), \cdots, h(\zeta_{N_g-1}))$ is monotone decreasing, since the scalar firing map is monotone decreasing. Then, the components Φ_k of the repeated nonlinearity $\mathbf{\Phi}$ are all monotone increasing. In addition, they are slope restricted, since they are characterized by slopes between $\underline{h} = \min_{\theta\in[0,2\pi]} |h'(\theta)|$ and $\overline{h} = \max_{\theta\in[0,2\pi]} |h'(\theta)|$. The nonlinearity thereby satisfies the sector condition (Figure 4.2)

$$[\Phi_k(y_k) - \underline{h}y_k][\Phi_k(y_k) - \overline{h}y_k] \leq 0\,. \tag{4.13}$$

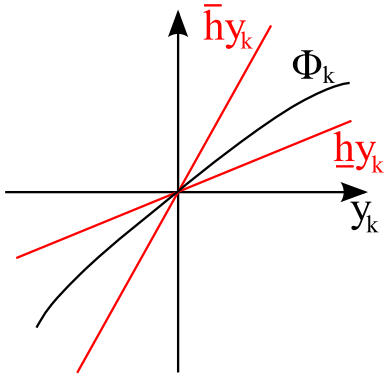

Figure 4.2: The static nonlinearity $\mathbf{\Phi}$ satisfies the sector condition.

Since the sector condition (4.13) is fulfilled, the well-known *circle criterion* (see [55, 124]) provides conditions on $\underline{h}$ and $\overline{h}$ to establish the absolute stability of the system (4.11)-(4.12). It follows from the circle criterion that the origin (corresponding to the fixed point of the firing map) is globally stable if

$$\mathbf{G}(\mathbf{I} + \underline{h}\mathbf{G})^{-1} \tag{4.14}$$

is stable (all the poles are inside the unit circle) and if

$$(\mathbf{I} + \underline{h}\mathbf{G}^\dagger)(\mathbf{I} + \overline{h}\mathbf{G}) + \left[(\mathbf{I} + \underline{h}\mathbf{G})(\mathbf{I} + \overline{h}\mathbf{G})\right]^\dagger > 0\,, \tag{4.15}$$

where $\mathbf{G}^\dagger$ holds for the conjugate transpose of $\mathbf{G}$.

Stability of (4.14) is easily verified. Since $\det[\mathbf{G}(e^{i\omega})] = \det[\mathbf{L}]e^{-i\omega} = e^{-i\omega}$ does not encircle the point $-1/\underline{h} < -1$, it follows from the multivariable Nyquist criterion [17] that (4.14) is stable.

Condition (4.15) is a passivity condition that yields

$$\mathbf{I} + \underline{h}\overline{h} + \frac{1}{2}(\underline{h} + \overline{h})\left(\mathbf{L}e^{-i\omega} + \mathbf{L}^T e^{i\omega}\right) > 0 \quad \forall\omega\,. \tag{4.16}$$

Condition (4.16) is a slope restriction of the nonlinearity. It provides a general condition on the bounds $\underline{h}$ and $\overline{h}$ (slope restriction of the nonlinearity) to ensure the global stability of the origin for the system (4.11)-(4.12), that is, to ensure the global stability of the fixed point for the firing map. The condition is compared with the results obtained in Section 4.2.1, for different dimensions.

- In one dimension, the theory confirms the known results on the global stability of the scalar firing map. Indeed, condition (4.16) leads to

  $$1 + \underline{h}\overline{h} + (\underline{h} + \overline{h})\cos\omega > 0 \quad \forall\omega$$

  and is satisfied for any $\underline{h} < \overline{h} < 1$. It is noticeable that, for a non-monotone dynamics with $\overline{h} > 1$, the condition is not satisfied. Although we know that the fixed point is globally stable for "QIF-like" dynamics (Proposition 3.3.2), the circle criterion fails to prove this result.

- In two dimensions, condition (4.16) becomes

  $$\begin{pmatrix} 1 + \underline{h}\overline{h} & -\underline{h}\overline{h} - i\,(\underline{h} + \overline{h})\sin\omega \\ -\underline{h}\overline{h} + i\,(\underline{h} + \overline{h})\sin\omega & 2\underline{h}\overline{h} + (\underline{h} + \overline{h})\cos\omega + 1 \end{pmatrix} > 0 \quad \forall\omega\,.$$

  Straightforward computations show that the above condition is actually equivalent to the condition $\|\mathbf{D}\|_{(2)} < 1$, with the quadratic norm (4.2) and the diagonal matrix $\mathbf{D} = \mathrm{diag}\{d_k\}$, $\underline{h} < d_k < \overline{h}$. In two dimensions, the circle criterion and the quadratic norm introduced in Section 4.2.1 lead to the same results, imposing condition (4.6) on the bounds $\underline{h}$ and $\overline{h}$.

- In three dimensions, condition (4.16) yields

  $$\begin{pmatrix} 1 + \underline{h}\overline{h} & -\frac{\underline{h}+\overline{h}}{2}e^{i\omega} & \frac{\underline{h}+\overline{h}}{2}e^{-i\omega} - \underline{h}\overline{h} \\ -\frac{\underline{h}+\overline{h}}{2}e^{-i\omega} & 1 + \underline{h}\overline{h} & -\underline{h}\overline{h} - i\,(\underline{h} + \overline{h})\sin\omega \\ \frac{\underline{h}+\overline{h}}{2}e^{i\omega} - \underline{h}\overline{h} & -\underline{h}\overline{h} - i\,(\underline{h} + \overline{h})\sin\omega & 3\underline{h}\overline{h} + (\underline{h} + \overline{h})\cos\omega + 1 \end{pmatrix} > 0 \quad \forall\omega\,. \tag{4.17}$$

  Straightforward computations show that, even though the condition is similar to the condition $\|\mathbf{D}\|_{(2)} < 1$, it is however slightly more restrictive on the bounds $\underline{h}$ and $\overline{h}$. For instance, when $\underline{h} = 0$, the quadratic norm ensures global stability provided that $\overline{h} < 2/\sqrt{6} \approx 0.816$ while (4.17) requires that $\overline{h} < 0.806$ (Figure 4.3).

  The condition obtained with the circle criterion is more restrictive because it imposes no condition on the second derivative Φ_k'', and thereby on h'' — in contrast, the quadratic norm approach imposes condition (4.7) on h''. Thus, should the scalar firing map violate

the mild assumption (4.7), the quadratic norm would fail to prove the global stability of the firing map, but the circle criterion proves the global stability under the stronger slope restriction (4.17) (instead of (4.6)). (Condition (4.7) is only used to prove that the entries of (4.8) are ordered, a property that is always satisfied in two dimensions.) In addition, when the second derivative condition is satisfied, the resulting order on the Φ_k''s could be taken into account by introducing a multiplier in the absolute stability criterion [127]. In this situation, the condition on the bounds $\underline{h}$ and $\overline{h}$ would be relaxed.

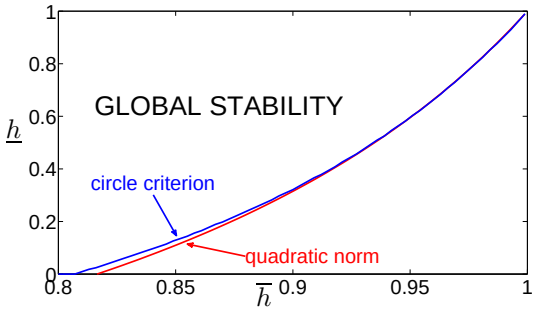

Figure 4.3: Global stability of the fixed point is proved if the couple $(\overline{h}, \underline{h})$ is above the curve. The circle criterion imposes a (slightly) more restrictive condition (on $\underline{h}$ and $\overline{h}$) than the quadratic norm.

- As the system dimension increases, condition (4.16) is increasingly conservative (similarly to the contraction property with respect to the quadratic norm).

The results are similar to those obtained with the quadratic norm (Section 4.2.1), a fact that is logical since the passivity condition (4.15) is related to the existence of a quadratic Lyapunov function, through the Kalman-Yakubovich-Popov (KYP) lemma [53, 89, 126] (see also [55]). In addition, absolute stability theory clearly implies that a *quadratic norm cannot characterize the contraction property in full generality*. Instead, a non-quadratic norm must be considered ([87] similarly shows that non-quadratic polyhedral Lyapunov functions yield less conservative stability conditions than the circle criterion). The study thereby reinforces our statement that the 1-norm is appropriate to capture the dynamics of monotone oscillators.

4.4 Heterogeneous populations

In this chapter, we have shown that the firing map has strong contraction properties that imply a strong dichotomic behavior for identical (monotone) pulse-coupled oscillators. A natural extension to these results is to discuss the robustness of the behavior against some heterogeneity within the network, considering that the frequency ω_k of each oscillator is randomly distributed.

Networks of nonidentical oscillators are characterized by intricate behaviors — as a generic example, the Kuramoto model [4, 59, 104] clearly illustrates the complexity of heterogeneous

networks. In case of integrate-and-fire oscillators, the persistence of synchrony in heterogeneous populations has been investigated and has also lead to complex problems. For instance, [114] showed that, in heterogeneous populations with smooth pulse interactions, synchrony is not achieved and the population breaks into two subpopulations.

In case of impulsive coupling, Peskin [86] first conjectured — in addition to its conjecture on identical oscillators — that the network of oscillators with a concave-down time evolution always converges to synchronization even if the oscillators are not quite identical. Some simplified models were analyzed in [10]. Later on, for oscillators characterized by a constant velocity $\dot{x}_k = F(x_k) = S_k$, Senn et al. [97] found sufficient conditions for synchrony. However, the time evolution of these oscillators has no curvature and synchronization is not induced by the impulsive coupling in itself but by the frequency differences and by the absorption mechanism. An answer to Peskin's conjecture was given in 2008 by Chang et al. [19]. The authors proposed sufficient (but not necessary) conditions to ensure the synchronization of nonidentical oscillators with concave-down time evolutions. In addition, they also showed that oscillators with concave-up time evolutions can synchronize, provided that their discrepancies and their curvature are small. (Results of [19, 97] show that the curvature of the time evolution is not a strict indicator of synchronization, as it happened to be for identical oscillators.)

As it is explained above, there is abundant (though incomplete) literature about synchronization in heterogeneous populations of pulse-coupled oscillators. On the other hand, less work has been performed on the phase-locked clustering behavior in heterogeneous populations. In this section, we therefore focus on the clustering behavior, showing that this global behavior of identical oscillators (induced by strong contraction properties of the firing map) is robust and still persists for nonidentical oscillators.

4.4.1 Two oscillators

The case of two different interacting oscillators has been studied in [28]. The authors proved frequency locking when the frequencies are close enough for the oscillators to fire alternately ($1:1$ entrainment).

Since the oscillators are different, they are associated with different firing maps h_1 and h_2. For $1:1$ entrainment, the two firing maps are applied alternately, so that one considers the two return maps $R_1 = h_1 \circ h_2$ and $R_2 = h_2 \circ h_1$. The return maps determine the evolution of one oscillator at the successive firings of the other oscillator. For oscillators with concave-up time evolution, the return maps have a unique stable fixed point, resulting in the unique phase-locked behavior described in [28]. Other firing patterns exist for larger frequency differences between the two oscillators, each resulting in a different combination of the two firing maps. Each firing pattern corresponds to a different return map and results in a different phase-locked behavior.

This analysis suggests that a detailed description of the dynamics of a population of N different oscillators quickly becomes intricate as the number of oscillators grows.

4.4.2 Clustering behavior in large populations

In large populations, the clusters are affected by the heterogeneity of the oscillators. For identical oscillators, an absorption is irreversible and a cluster can be assimilated to a single oscillator. In contrast, nonidentical oscillators that have fired together can subsequently

separate and clusters can be modified or even destroyed. Coupling and heterogeneity have opposite influences: while the former creates clusters through the absorption mechanism, the latter tends to destroy them.

In the sequel, we report on numerical observations about the clustering behavior of a (large) population of oscillators. We simulated the behavior of $N = 100$ integrate-and-fire oscillators with the monotone individual dynamics

$$\dot{x_k} = S + \gamma x_k \,, \quad x_k \in [0,1] \quad k = 1, \ldots, N \,,$$

where $\gamma > 0$. The parameters $S_k > 0$ are randomly distributed — Gaussian distribution of mean $\mu(S_k)$ and standard deviation $\sigma(S_k)$ — so that frequency variations appear across the population. To study the robustness of clustering against the population heterogeneity, we kept a fixed distribution for the parameters S_k (individual discrepancies) and a constant value for ϵ (coupling strength), but we varied the parameter γ (identical for the N oscillators). The parameter γ is a key feature of the oscillators. It determines the curvature of the time evolution of the oscillators and affects the relative importance of the coupling strength versus the frequency distribution.

Clustering configurations are still observed in heterogeneous populations (Figure 4.4). Whereas each cluster can be considered as a unique oscillator in case of identical oscillators, the clusters of nonidentical oscillators spread over a finite range $[\theta_a, \theta_b]$ due to the frequency discrepancies. A cluster is now defined as a set of oscillators that fire together. It is characterized by its slowest and its fastest oscillator, respectively determining the lower bound θ_a and the upper bound θ_b of the cluster interval. The range of each cluster gradually broadens as the elapse time increases since the last absorption.

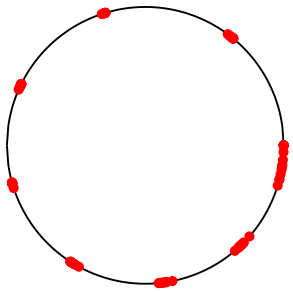

Figure 4.4: "Snapshot" clustering behavior in a population of $N = 100$ oscillators [$\gamma = 0.5$, $\mu(S_k) = 0.99$, $\sigma(S_k) = 0.19$, $\epsilon = 0.11$]. The clusters broaden during their evolution on the circle.

An important difference with respect to the identical case is the existence of *traveling oscillators*. An oscillator trapped within a cluster will return close to its initial position every N_g firings — that is, each time the same cluster fires. In contrast, a traveling oscillator will visit all clusters and its state evolution after N_g firings will therefore drift across the entire phase range. The number of traveling oscillators is a qualitative measure of the clustering level. Figure 4.5 illustrates the fraction of traveling oscillators as a function of the parameter

γ and clearly shows the presence of three distinct situations: total clustering ($\gamma > \gamma_c$), partial clustering ($\gamma_{nc} < \gamma < \gamma_c$), and weak clustering ($\gamma < \gamma_{nc}$).

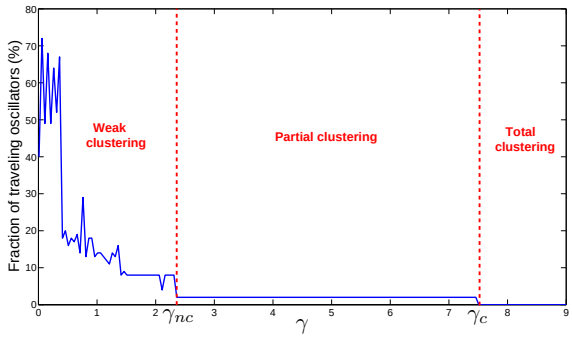

Figure 4.5: Fraction of traveling oscillators in a population of $N = 100$ oscillators [$\mu(S_k) = 3.2$, $\sigma(S_k) = 1.6$, $\epsilon = 0.11$] as a function of the parameter γ. The fraction is 2% over the range $[\gamma_{nc}, \gamma_c]$.

Total clustering Beyond the critical value γ_c, the coupling strength induces a sufficient coherence in the population to prevent any oscillator exchange between the clusters. Each oscillator is trapped within a cluster, in which it stays indefinitely, and fires at the frequency of the fastest oscillator of the cluster. The oscillators discrepancies are dominated by the absorption phenomena and the network asymptotically converges to a phase-locked configuration. Figure 4.6 illustrates this situation of total clustering and shows that the position of each oscillator is fixed at each firing of the same cluster (every N_g firings).

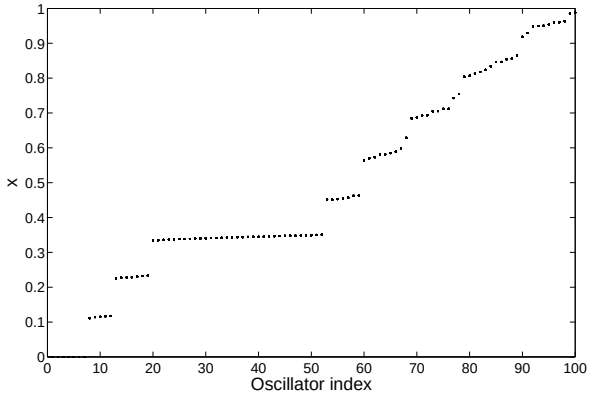

Figure 4.6: Total clustering in a population of $N = 100$ oscillators [$\mu(S_k) = 3.2$, $\sigma(S_k) = 1.6$, $\epsilon = 0.11$] for strong coherence ($\gamma = 8 > \gamma_c$). Each dot represents the value of x_k every $N_g = 9$ firings. The single dot per oscillator indicates a phase-locked configuration (transient behavior is not shown).

Partial clustering For values between γ_{nc} and γ_c, the fastest oscillators travel across the clusters. They are fast enough to catch up the preceding cluster and to be trapped by its next absorption. This partial clustering situation is shown in Figure 4.7. Among the whole population, only two oscillators are traveling. The 98 remaining oscillators stay in a fixed cluster in steady state. However, their positions are not perfectly constant every N_g firings because of the two traveling oscillators. Indeed, since the frequency of a cluster is uniquely determined by the frequency of its fastest oscillator, a (fast) traveling oscillator jumping from one cluster to another modifies the frequency of the clusters. During the exchange, the traveling oscillator decreases the frequency of the cluster it is leaving while possibly speeding up the cluster it has just joined. As a consequence, this drift of traveling oscillators modifies the firing times of the clusters and affects the exact location of a given oscillator every N_g firings. Nevertheless, the clustering configuration is still very visible. Moreover, this partial clustering configuration remarkably extends over a broad range of the parameter γ, as illustrated in Figure 4.5, and therefore presents an outstanding robustness to frequency discrepancies across the population.

Weak clustering Below the critical value γ_{nc}, the number of traveling oscillators grows rapidly and a large fraction of the population travels across the different clusters (Figure 4.8). This results in a situation of weak clustering, in which clusters are less visible. As the coherence parameter γ decreases to 0, clustering tends to disappear. Figure 4.5 suggests that the transition from partial clustering (few traveling oscillators) to no clustering (most of the oscillators are traveling) rapidly occurs below the critical value γ_{nc}, in a nonmonotonic way and with strong fluctuations. Despite its strong robustness over the broad partial clustering range, clustering is violently destroyed below the value γ_{nc}.

4.4.3 Periodic behaviors

The period of the clustering behavior is the number of firings T_f required by the oscillators to recover their exact original locations. For N identical oscillators, the clusters have fixed positions at each firing of any cluster and the period $T_f = 1$. With two different (but quite similar) oscillators, which fire in an entrainment mode $1:1$, the phase of an oscillator at the firing of the other oscillator is constant and the period $T_f = 2$. When considering a population of N nonidentical oscillators, the periodicity of the steady state depends on the clustering situation and appears to be an indirect measure of the level of clustering.

Total clustering ($\gamma > \gamma_c$) leads to a firing period $T_f = N_g$, since each oscillator has a fixed position at each firing of the same cluster. The apparition of traveling oscillators in the situation of partial clustering considerably increases the periodicity because the exchanges between the clusters affect the firing frequency of the clusters. With a single traveling oscillator, the firing period expresses as

$$T_f = N_g N_f, \tag{4.18}$$

where $N_f + 1$ is the number of times the traveling oscillator fires before returning to its initial cluster. While the traveling oscillator fires $N_f + 1$ times, the clusters fire one time less, i.e. N_f times, and the firing mode is thus

$$N_f + 1 : N_f : \cdots : N_f \,. \tag{4.19}$$

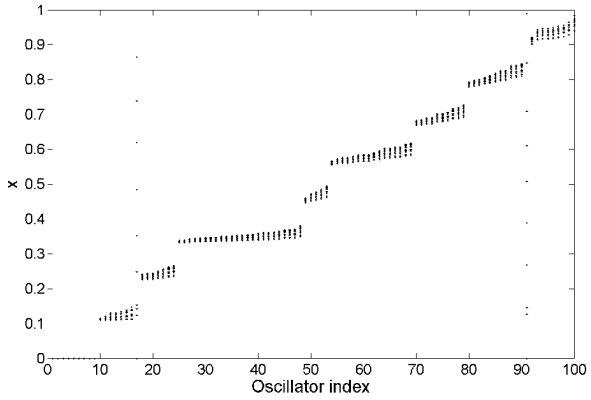

Figure 4.7: Partial clustering in a population of $N = 100$ oscillators [$\mu(S_k) = 3.2$, $\sigma(S_k) = 1.6$, $\epsilon = 0.11$] for intermediate coherence ($\gamma_{nc} < \gamma = 4 < \gamma_c$). Dots have the same meaning as in Figure 4.6. Oscillators 17 and 91 are traveling while the 98 remaining ones are nearly phase-locked.

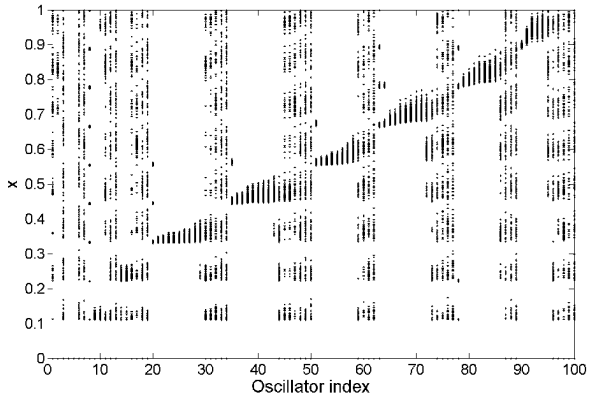

Figure 4.8: Weak clustering in a population of $N = 100$ oscillators [$\mu(S_k) = 3.2$, $\sigma(S_k) = 1.6$, $\epsilon = 0.11$] for small coherence ($\gamma = 0.5 < \gamma_{nc}$). Dots have the same meaning as in Figure 4.6. About half of the oscillators are traveling.

After the total number of $N_g N_f$ firings, each cluster has the same frequency as at the beginning and recovers its initial exact location, a situation that ends the period.

With more than one traveling oscillator, the firing period may considerably increase. For instance, two traveling oscillators require N_{f_1} and N_{f_2} firings, respectively, to return within their initial cluster. However, since generally $N_{f_1} \neq N_{f_2}$, T_f must adjust so that the two traveling oscillators are simultaneously in their initial cluster. This requires the existence of integers n and m such that

$$\sum_{k=1}^{n} N_{f_1}^{(k)} = \sum_{k=1}^{m} N_{f_2}^{(k)} \triangleq N_c \tag{4.20}$$

and the total firing period is then

$$T_f = N_g N_c \,. \tag{4.21}$$

The integers n and m can be very high, so that a rapid adjustment of N_{f_1} and N_{f_2} is not always observed, leading to quasiperiodic behaviors. Table 4.1 illustrates the firing periodicity as a function of the parameter γ in a population of nonidentical oscillators with a narrow frequency distribution. Although only two oscillators are traveling in the range $\gamma \in [0.05, 0.35]$ (partial clustering), the total period T_f may be very large for small values of γ. For $\gamma = 0.05$, the firing period cannot be computed and the behavior is (nearly) aperiodic. These numerical observations still emphasize that partial clustering occurs over a broad range of the coherence parameter γ (weak clustering was never observed numerically in the example of Table 4.1) and can coexist with (almost) aperiodic firing patterns.

Slope γ	Firing period T_f	N_c	Number of firings N_{f1}	Number of firings N_{f2}
0.45	9	/	/	/
0.4	333	37	37	/
0.35	1080	120	20-24-29-20-27	65-55
0.3	405	45	21-24	45
0.25	396	44	19-25	44
0.2	369	41	20-21	41
0.15	1962	218	20-21-20-19-22-20-19-19-20-18-20	38-38-35-38-35-34
0.1	4464	...	...	...
0.05	>100 000	...	...	...

Table 4.1: Firing period and values N_{f1} and N_{f2} for various values of the coherence parameter γ with $N = 100$, $\mu(S_k) = 1$, $\sigma(S_k) = 0.1$, $\epsilon = 0.11$. In the current case, the number of clusters is $N_g = 9$.

4.5 Conclusion

In this chapter, emphasis has been put on the dichotomic behavior of the network, since we showed that the network can exhibit a phase-locked clustering behavior in addition to the well-known synchronization behavior. For identical oscillators, the phase-locked clustering behavior is a global behavior that is induced by the strong contraction properties of the firing

map. [Global stability of the firing map is summarized in Table 4.2, with the respective assumptions imposed by the different approaches.] The strong properties of identical oscillators enforce a (total/partial) clustering behavior for weak and medium discrepancies, showing the robustness of the clustering configuration against frequency discrepancies across the network.

Method	Assumption on h'	Assumption on h''
quadratic norm (4.2)	conservative condition (4.6)	mild condition (4.7)
circle criterion	very conservative condition (4.16)	/
1-norm (4.10)	contracting scalar firing map ($\lvert h' \rvert < 1$)	mild condition (4.7)

Table 4.2: The 1-norm is the most appropriate to capture the contraction property of the scalar firing map.

A mathematical analysis of heterogeneous populations is actually much more involved (as it is suggested in Section 4.4.1). Even though the partial clustering behavior may appear as a "simple" behavior, a mathematical characterization of the periodic configuration is intractable — at least by means of the firing maps, since the order between the oscillators is not preserved, and thus not known — and it is even more the case for the situation of weak clustering. In case of synchronization, partially synchronized behaviors can also appear, whose mathematical analysis is very challenging.

An efficient way to study heterogeneous populations is to consider the continuum limit of an infinite number of oscillators (mean-field approximation). Within this framework, mathematical tools exist to study the effect of heterogeneity on the behaviors. For instance, partial synchronization of LIF pulse-coupled populations has been recently studied in [24]. In addition, the discrepancies between the oscillators can be approximated when considering a noisy dynamics, a stochastic extension that is compatible with the continuum limit [3].

In the present dissertation, we do not focus on the case of nonidentical oscillators. However, in the next chapter, we propose to extend the global analysis of finite homogeneous populations to a global analysis of infinite homogeneous populations (continuum limit), possibly opening the way for future research on heterogeneous populations.

Chapter 5

Global analysis for a continuum of monotone oscillators

In the present chapter, we investigate the behavior of infinite populations of monotone oscillators. When the number of oscillators is very large, the population is well-approximated by a continuum of $N \to \infty$ oscillators (*thermodynamic limit*), a technique known as the *mean-field approximation* [112] and often used to study large populations of phase oscillators [13] and, more specifically, of integrate-and-fire oscillators [81].

In case of impulsive coupling, several studies (e.g. [3, 12, 11, 60, 117]) provide stability results for infinite populations of LIF oscillators. Although these studies extend the analysis to delayed transmissions, they merely rely on a linear *local* analysis. In contrast, we present in this chapter *global* stability results for infinite populations of monotone oscillators (including the LIF oscillators).

The global analysis of finite populations (Chapter 4) is extended to infinite populations, so that a perfect *parallel* is drawn between finite populations and infinite populations. In addition, the analysis shows the coherence between a *discrete* approach (relying on the discrete-time firing map) and a *continuous* approach (relying on a continuous-time transport equation).

Beyond the analysis of pulse-coupled monotone oscillators, the theory developed in the chapter leads to general results on partial differential equations (PDE). The analysis focuses on transport equations with a monotone dynamics (derived from a monotone iPRC) and provides existence, uniqueness, and global stability results for the stationary solution of the PDE.

The chapter is organized as follows. In Section 5.1, we derive the transport equation for the continuum of pulse-coupled oscillators. Section 5.2 presents numerical experiments showing that the continuum model is characterized by a dichotomic behavior. In addition, existence and uniqueness results are obtained for the stationary solution of the PDE. Sections 5.3 and 5.4 are quite technical. In Section 5.3, a strict Lyapunov function is proposed, which is induced by a *total variation distance* and which is inspired from the results of Chapter 4. In Section 5.4, we perform the convergence analysis of populations of monotone oscillators. Finally, the parallel between finite and infinite populations, as well as some extensions of the model, are discussed in Section 5.5.

The main contribution of the chapter is the global analysis of the PDE, a result that is obtained through a particular Lyapunov function and that highlights the parallel between

finite and infinite populations. The results presented in the chapter can be found in [72].

5.1 A transport equation for pulse-coupled oscillators

In this section, we derive the transport equation (continuity equation) for general pulse-coupled oscillators (not necessary monotone integrate-and-fire oscillators). We obtain a nonlinear PDE, whose nonlinearity is induced by the impulsive coupling. The derivation of the model is standard and similar developments are found in [3, 13, 60].

5.1.1 Phase density equation

For the sake of generality, we consider phase oscillators on the circle $S^1(0, 2\pi)$ characterized by the phase dynamics (2.1), that is here denoted as $\dot{\theta} = v(\theta, t)$. At this stage, no assumption is made on the particular phase dynamics that corresponds to integrate-and-fire oscillators.

In the (thermodynamic) limit of a large number of $N \to \infty$ oscillators, the infinite population is a continuum characterized by a phase density function

$$\rho(\theta, t) \geq 0 \ \in C^0(L^1(0, 2\pi); \mathbb{R}^+)\,,$$

with the quantity $\rho(\theta, t)d\theta$ being the fraction of oscillators with a phase between θ and $\theta + d\theta$ at time t. The density is nonnegative and satisfies the normalization

$$\int_0^{2\pi} \rho(\theta, t)\, d\theta = 1 \quad \forall t\,.$$

The time evolution of the density obeys the well-known continuity equation

$$\frac{\partial}{\partial t}\rho(\theta, t) = -\frac{\partial}{\partial \theta}\Big(v(\theta, t)\, \rho(\theta, t)\Big)\,. \tag{5.1}$$

In the above equation, the function

$$v(\theta, t)\, \rho(\theta, t) \triangleq J(\theta, t) \tag{5.2}$$

is the (nonnegative) flux $J(\theta, t) \geq 0 \ \in C^0(L^1(0, 2\pi); \mathbb{R}^+)$. The quantity $J(\theta, t)dt$ represents the fraction of oscillators flowing through phase θ between time t and $t + dt$. Since the phase θ is defined on $S^1(0, 2\pi) \equiv \mathbb{R} \bmod 2\pi$, the flux must satisfy the boundary conditions

$$J(0, t) = J(2\pi, t) \triangleq J_0(t) \quad \forall t\,. \tag{5.3}$$

For the sake of simplicity, we use in the sequel the notation J_0 to denote the boundary flux (5.3). For oscillators firing at phase $\theta = 0$, $J_0(t)$ is also called the *firing rate* of the oscillators. It plays a key role for the impulsive coupling.

5.1.2 Continuous impulsive coupling

For a high number of oscillators ($N \gg 1$), we define the impulsive coupling (3.1) with a coupling strength ϵ inversely proportional to the number of oscillators, that is $\epsilon = K/N$. This precaution prevents the coupling to increase with the number of oscillators: the constant K corresponds to the net influence of the whole population through the coupling, whatever the number of oscillators. In the thermodynamic limit $N \to \infty$, for instance, each oscillator of the infinite population sends out an infinitesimal spike $\epsilon \to 0$ when firing.

Within large populations of integrate-and-fire oscillators, the influence of a single oscillator is negligible. It follows that the sums in (3.1) can be considered over the whole population, so that the dynamics becomes

$$\dot{x}_k = F(x_k) + K \frac{1}{N} \sum_{j=1}^{N} \sum_{l=0}^{\infty} \delta(t - t_l^{(j)}) \,, \quad x \in [\underline{x}, \overline{x}] \,. \tag{5.4}$$

Next, observing that the oscillators crossing $\theta = 0$ at the firing times $t_l^{(j)}$ induce a (discontinuous) flux $J_0(t) = \frac{1}{N} \sum_j \sum_l \delta(t - t_l^{(j)})$, we rewrite (5.4) as

$$\dot{x}_k = F(x_k) + K \, J_0(t) \,. \tag{5.5}$$

In other words, the impulsive coupling is a coupling identical for all the oscillators and *proportional to the firing rate* J_0.

In case of infinite populations, the dynamics of the oscillators is still given by (5.5). But now, the flux is continuous, so that the coupling is a continuous-time function. The coupling is interpreted as an infinite sum of infinitesimal spikes that result from the uninterrupted firings of the continuum. Since the coupling corresponds to a continuous-time input $u^{\text{imp}}(t) = K \, J_0(t)$, the phase reduction is performed directly with the infinitesimal iPRC and the phase dynamics (2.1) is given by

$$\dot{\theta} = v(\theta, t) = \omega + K \, Z(\theta) \, J_0(t) \,. \tag{5.6}$$

Actually, it follows from (3.3) that $Z_\epsilon \approx \epsilon \, Z(\theta) = K/N \, Z(\theta)$ when $\epsilon \ll 1$, so that (5.6) is equivalent to the phase dynamics (3.2).

Remark 5.1.1. It is of interest to investigate the effect of an inhibitory coupling (negative coupling constant) instead of an excitatory coupling (negative coupling constant). In the case of finite populations, an inhibitory coupling leads to ill-defined situations. In contrast, a noticeable advantage of the continuum model is that one can consider positive an excitatory coupling as well as an inhibitory coupling with infinite populations. In this context, we see below that the sign of the coupling strength influences the behavior, as does the dynamics of the oscillators. ◇

The final PDE for the continuum of pulse-coupled oscillators is derived as follows. At phase $\theta = 0$, (5.2) and (5.6) yield the relationship

$$J_0(t) = v(0, t) \, \rho(0, t) = [\omega + K \, Z(0) \, J_0(t)] \, \rho(0, t) \tag{5.7}$$

and the flux J_0 is explicitly given by

$$J_0(t) = \frac{\omega \, \rho(0, t)}{1 - K \, Z(0) \, \rho(0, t)} \,.$$

The continuity equation (5.1) thus leads to the nonlinear PDE for the density

$$\frac{\partial \rho(\theta,t)}{\partial t} = -\omega \frac{\partial \rho(\theta,t)}{\partial \theta} - \frac{K\,\omega\,\rho(0,t)}{1-K\,Z(0)\,\rho(0,t)} \frac{\partial}{\partial \theta}\Big(Z(\theta)\,\rho(\theta,t)\Big)\,. \tag{5.8}$$

The boundary condition (5.3) is expressed in terms of density as

$$\frac{\rho(0,t)}{1-K\,Z(0)\,\rho(0,t)} = \frac{\rho(2\pi,t)}{1-K\,Z(2\pi)\,\rho(2\pi,t)} \left(= \frac{J_0(t)}{\omega}\right)\,. \tag{5.9}$$

The reader will notice that, in contrast to the periodicity condition on the flux, no periodicity is assumed on the density $\rho(\theta,t)$. [In particular, $\rho(0,t) \neq \rho(2\pi,t)$ if $Z(0) \neq Z(2\pi)$.]

The density of the pulse-coupled oscillators evolves according to the nonlinear PDE (5.8) with the boundary condition (5.9). The PDE is studied in detail in the rest of the chapter, with a particular attention to the case of monotone iPRC. Observe that a monotone iPRC implies that $Z(0) \neq Z(2\pi)$.

5.2 A dichotomic behavior

Under the monotonicity assumption on the iPRC, the PDE exhibits a dichotomic asymptotic behavior, that depends on the coupling sign ($K > 0$ or $K < 0$) and on the derivative Z' (or equivalently dF/dx).

5.2.1 Asymptotic behavior

Without coupling ($K = 0$), the last term of (5.8) disappears and the PDE is a standard transport equation. Its solution is a rigid translation of the initial density $\rho(\theta,0)$ with a constant velocity ω, that is, a traveling wave $\rho(\theta,t) = \rho((\theta-\omega t) \bmod 2\pi, 0)$. In this case, any solution is periodic (with period $2\pi/\omega$) and the system is marginally stable. This situation is equivalent to (3.30), where the motion of a finite population of uncoupled oscillators is only dictated by the linear map $\mathbf{L}$.

When the oscillators are coupled, the last term of (5.8) modifies the transport equation. Under the influence of the coupling, the velocity depends on both time and phase and the density is thereby "stretched" or "compressed". This is illustrated when computing the total time derivative along a characteristic curve $\Lambda(t)$ defined by $\dot{\Lambda} = v(\Lambda(t),t)$, that is

$$\frac{\partial \rho}{\partial t} + \frac{\partial \rho}{\partial \theta} v(\Lambda(t),t) = \frac{d\rho}{dt} = -\rho(\Lambda(t),t)\,J_0(t)\,K\,Z'(\Lambda(t))\,, \tag{5.10}$$

where (5.8) and (5.9) have been used. The total derivative shows that the density is modified on a characteristic curve whenever the iPRC is not a constant. In addition to the rigid translation, the density undergoes a nonlinear transformation, possibly leading to asymptotic convergence to a particular density function corresponding to a particular stationary organization of the oscillators.

The total derivative (5.10) gives clear insight that the sign of the derivative $K\,Z'$ is of first importance. In fact, the sign of $K\,Z'$ will enforce a dichotomic behavior. The condition $K\,Z'(\theta) < 0\ \forall \theta \in [0,2\pi]$ — or $K\,dF/dx > 0\ \forall x \in [\underline{x},\overline{x}]$ — will be shown to enforce convergence to a *uniform flux* $J(\theta,t) = J^*$ on $S^1(0,2\pi)$. This situation, corresponding to the maximal

spreading of the oscillators on the circle, is called the *asynchronous state* [3, 117] (Figure 5.1). In contrast, the reverse condition $K\,Z'(\theta) > 0\ \forall\theta \in [0, 2\pi]$ — or $K\,dF/dx < 0\ \forall x \in [\underline{x}, \overline{x}]$ — will be shown to enforce convergence to a *delta-like flux* (Figure 5.2). This situation, characterized by the synchronization of all the oscillators, is the *synchronous state*.

We remark that reversing the coupling sign ($K > 0$ or $K < 0$) has the same effect as reversing the monotonicity of F ($dF/dx > 0$ or $dF/dx < 0$).

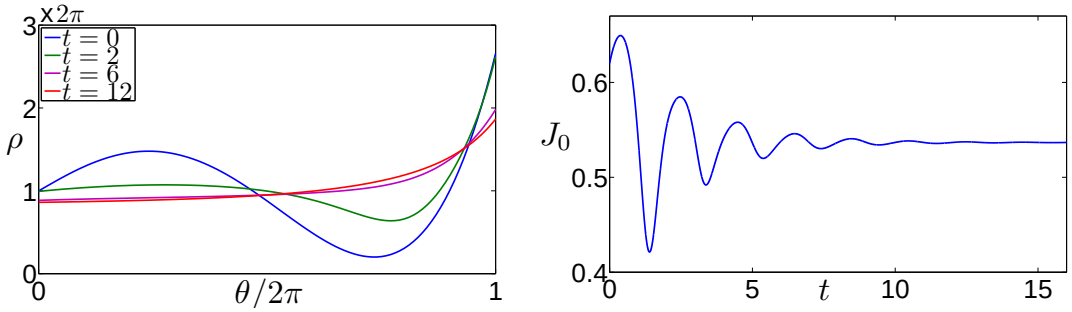

(a) Density (b) Flux

Figure 5.1: When $K\,Z' < 0$, the solution converges to the asynchronous state. With the monotone LIF dynamics $\dot{x} = 2.1 - 2\,x$, $x \in [0, 1]$ and with an inhibitory coupling $K = -0.1 < 0$, the function $K\,Z$ is monotone decreasing. (a) The density converges to a stationary solution ρ^* and (b) the flux $J_0(t)$ tends to a constant value $J^* \approx 0.53$.

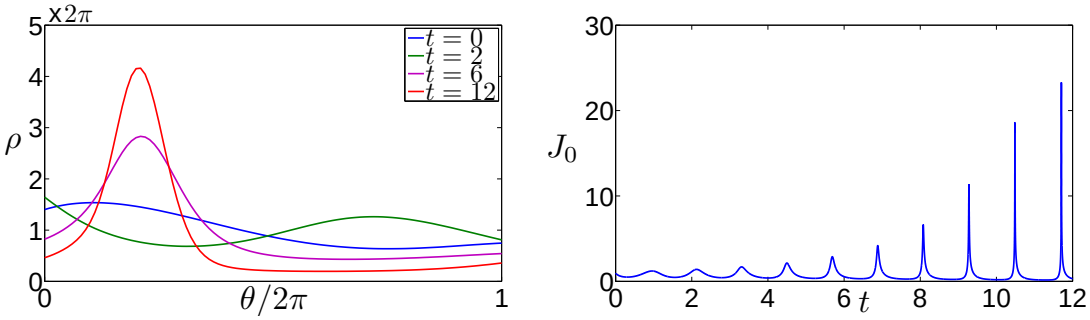

(a) Density (b) Flux

Figure 5.2: When $K\,Z' > 0$, the solution converges to the synchronous state. With the same LIF dynamics as in Fig. 5.1, but with an excitatory coupling $K = 0.1 > 0$, the function $K\,Z$ is monotone increasing. (a) The density converges to a synchronous solution and (b) the flux $J_0(t)$ tends to a Dirac function.

The two asymptotic behaviors — synchronous and asynchronous states — are the exact analog of the synchronization and phase-locked clustering behaviors of finite populations (Sections 3.2 and 4.1). This is obvious in the case of synchronization, that occurs for both finite and infinite populations when $K > 0$ and $dF/dx < 0$. Asynchronous state and phase-locked clustering are also equivalent behaviors, that both occur when $K > 0$ and $dF/dx > 0$. They

are both anti-synchronized behaviors, for which the clusters/oscillators evenly spread over the circle $S^1(0, 2\pi)$. In addition, the firing frequency (3.7) of the clustering configuration is well-approximated by $\omega_{\text{clust}} \approx 2\pi\, J^*$ if the number of clusters N_g is very high (when $\epsilon \ll 1$).

The only difference between the two behaviors is that clustering is not observed in infinite populations. The absorption mechanism is here ill-defined and the clusters correspond to singularities in the continuum of oscillators. As a consequence, one has to prevent absorptions from creating clusters through well-chosen parameters and initial conditions.

Remark 5.2.1 (Marginal stability)**.** The limit case between the two situations corresponds to a constant iPRC (neither increasing nor decreasing), yielding a total derivative (5.10) that is equal to zero, as in the uncoupled case. In this case, the velocity $v(t) = \omega + K\, Z J_0(t)$ does not depend on the phase and the density thereby undergoes a rigid translation. Any solution evolves periodically and the stationary solution is marginally stable. An equivalent situation for finite populations is investigated in Section 6.3. ⋄

5.2.2 Stationary asynchronous state

The stationary fixed point of the firing map corresponds to the phase-locked clustering configuration. Similarly, the stationary solution of the PDE (5.1), characterized by a constant flux $J(\theta, t) = J^*$, corresponds to the asynchronous state.

It follows from (5.7) that the stationary density must satisfy

$$\rho^*(\theta) = \frac{J^*}{\omega + K\, Z(\theta) J^*}\,. \tag{5.11}$$

[This density could also be made uniform by a proper change of variable under which the velocity $\dot\theta = \omega + K\, Z(\theta) J^*$ becomes constant (see Section 6.6.1).] The stationary asynchronous state thus exists if there exists a value $J^* > 0$ so that the stationary density is nonnegative

$$\frac{J^*}{\omega + K\, Z(\theta) J^*} \geq 0\,, \quad \forall \theta \in [0, 2\pi] \tag{5.12}$$

and normalized

$$\int_0^{2\pi} \frac{J^*}{\omega + K\, Z(\theta) J^*} d\theta = 1\,. \tag{5.13}$$

The following proposition gives necessary and sufficient conditions to ensure the existence and uniqueness of the stationary solution.

Proposition 5.2.1. *A stationary flux $J^* > 0$ satisfying the conditions (5.12) and (5.13) exists if and only if the inequality*

$$\lim_{\substack{s \to r \\ s > r}} \int_0^{2\pi} \frac{1}{K\, Z(\theta) + s}\, d\theta > 1 \tag{5.14}$$

is satisfied with

$$r \triangleq \begin{cases} 0 & \text{if } K\, Z(\theta) \geq 0 \quad \forall \theta \in [0, 2\pi]\,, \\ \left| \min_{\theta \in [0, 2\pi]} \Big(K\, Z(\theta) \Big) \right| & \text{otherwise}\,. \end{cases}$$

Moreover, the solution is unique when it exists.

Proof. Inequality (5.12) implies that the velocity $\omega + K\,Z(\theta)J^*$ is strictly positive, so that

$$J^* \in \mathcal{J} \triangleq \left(0, \lim_{\substack{s \to r \\ s > r}} \frac{\omega}{s}\right) .$$

The function

$$W(J) = \int_0^{2\pi} \frac{J}{\omega + K\,Z(\theta)J}\, d\theta$$

satisfies $W(0) = 0$, is continuous on $\mathcal{J}$, and is strictly increasing on $\mathcal{J}$ since

$$\frac{dW}{dJ} = \int_0^{2\pi} \frac{\omega}{[\omega + K\,Z(\theta)J]^2}\, d\theta > 0 \quad \forall J \in \mathcal{J}\,.$$

As a consequence, the equation $W(J) = 1$, which is equivalent to condition (5.13), has a (unique) solution $J^* \in \mathcal{J}$ if and only if

$$\lim_{\substack{s \to r \\ s > r}} W(\omega/s) = \lim_{\substack{s \to r \\ s > r}} \int_0^{2\pi} \frac{1}{K\,Z(\theta) + s} d\theta > 1\,,$$

which concludes the proof. □

Proposition 5.2.1 implies that the coupling constant K must be bounded. For integrate-and-fire oscillators, the bounds on the coupling constant are computed analytically and are given in the following corollary.

Corollary 5.2.1. *For integrate-and-fire dynamics $\dot{x} = F(x)$, a stationary flux $J^* > 0$ fulfilling the conditions (5.12) and (5.13) exists if the coupling constant satisfies*

$$\lim_{\substack{s \to F_{\min} \\ s < F_{\min}}} \int_{\underline{x}}^{\overline{x}} \frac{s}{s - F(x)} dx < K < \overline{x} - \underline{x}\,, \tag{5.15}$$

with $F_{\min} = \min_{x \in [\underline{x}, \overline{x}]} (F(x))$.

Proof. If the coupling is excitatory ($K > 0$), it follows from (2.6) that $K\,Z(\theta) \geq 0\ \forall \theta \in [0, 2\pi]$, so that $r = 0$. Then, the condition (5.14) of Proposition 5.2.1 can be rewritten as

$$\int_0^{2\pi} \frac{1}{K\,Z(\theta)}\, d\theta = \int_{\underline{x}}^{\overline{x}} \frac{1}{K}\, dx > 1\,,$$

or equivalently

$$K < \overline{x} - \underline{x}\,. \tag{5.16}$$

If the coupling is inhibitory ($K < 0$), it follows on similar lines that Proposition 5.2.1 implies the lower bound in (5.15). □

The upper bound in (5.15) leads to a more intuitive interpretation of the condition (5.14) in Proposition 5.2.1. Consider that, after its firing, an oscillator of the continuum requires a time ΔT to have a state increase equal to $\overline{x} - \underline{x}$ and to fire again. Since the whole population fires within the time interval ΔT, the time integration of the coupling term $u^{\text{imp}} = K\,J_0(t)$ in the dynamics $\dot{x} = F(x) + u^{\text{imp}}$ shows that the coupling induces over the time interval a state

increase equal to K. Then, a coupling $K = \overline{x} - \underline{x}$ implies that the natural dynamics $\dot{x} = F(x)$ cannot increase the state. One must have $\Delta T = 0$, so that the velocity of the oscillator is infinite. For finite populations, this situation is equivalent to "avalanche" phenomena igniting a chain reaction of firings [when absorbed oscillators are allowed to emit a pulse (see Section 3.1)]. On the other hand, condition (5.16), which is equivalent to $\epsilon < (\overline{x} - \underline{x})/N$, prevents absorptions from creating clusters.

Example 5.2.1. Corollary 5.2.1 is applied to different integrate-and-fire dynamics. It follows from straightforward computations that the asynchronous state exists

- for LIF oscillators, if $-\infty < K < 1$;
- for QIF oscillators, if $-\infty < K < \overline{x} - \underline{x}$;
- for the vector field $F(x) = S + |x|^{1/2}$ (with $\underline{x} < 0$ and $\overline{x} > 0$), if

$$-2S\left(\sqrt{-\underline{x}} + \sqrt{\overline{x}}\right) < K < \overline{x} - \underline{x}\,.$$

$\diamond$

5.3 A strict Lyapunov function induced by the total variation distance

Lyapunov analysis is a classical approach to study the stability of nonlinear PDE's (see e.g. [21, 22]). In this section, we extend the global stability results of Chapter 4 to construct a strict Lyapunov function for the PDE (5.8). The Lyapunov function, inspired by the 1-norm introduced in Section 4.2.2, is a L^1 distance interpreted as the *total variation distance between quantile densities*. The relevance of this distance in the present context is in contrast with the results of [99] showing that the total variation distance is constant for systems of conservation laws (except for those of a very particular class introduced in [107]).

5.3.1 Quantile density

The description of the population configuration, through the density $\rho(\theta)$, is not similar to the description of finite populations, through the vector $\mathbf{\Theta} = (\theta_1, \cdots, \theta_{N-1})$. While the former corresponds to the "amount" of oscillators as a function of the phase, the latter corresponds to the phase as a function of the oscillator index. To establish an equivalence between finite and infinite populations, we introduce an index for infinite populations of oscillators and use the concept of *quantile function*.

For infinite populations, the oscillators can be continuously labeled on the interval $I \triangleq [0, 1]$ and an oscillator index $\varphi \in I$ is defined as follows. Given a density function $\rho : [0, 2\pi] \mapsto \mathbb{R}^+$, the cumulative density function $P(\theta) : [0, 2\pi] \mapsto I \triangleq [0, 1]$, defined as

$$P(\theta) = \int_0^\theta \rho(s)\, ds\,,$$

attributes an index $\varphi = P(\theta) \in I$ to each oscillator with phase θ. In particular, an index $\varphi = 0$ (resp. $\varphi = 1$) is attributed to the oscillator at phase $\theta = 0$ (resp. $\theta = 2\pi$).

Next, to complete the equivalent description of infinite populations, we introduce the quantile function (widely used in statistics [85]): the quantile function $Q : I \mapsto [0, 2\pi]$ is the inverse cumulative density function, that is,

$$Q(\varphi) = P^{-1}(\varphi) = \inf\{\theta | P(\theta) \geq \varphi\} .$$

The (continuous) quantile function is equivalent to the (discrete) description $\mathbf{\Theta}$ of finite populations. Indeed, for a finite number of N distinct oscillators — for sake of simplicity, we consider that no cluster is created — the phases θ_k are the N-quantiles $\theta_k = Q_k^{(N)}$, that is

$$\mathbf{\Theta} = (\theta_1, \cdots, \theta_{N-1}) = \left(Q_1^{(N)}, \cdots, Q_{N-1}^{(N)}\right) . \tag{5.17}$$

When the number of oscillators tends to infinity, the N-quantiles are replaced by the continuous quantile function Q. (Roughly speaking, the quantile function plays the role of the vector $\mathbf{\Theta}$ with an infinity of components.)

As the analog of the density ρ, the *quantile density function* [85], also called *sparsity function*, is the function $q : I \mapsto \mathbb{R}^+$ that satisfies (see Figure 5.3)

$$Q(\varphi) = \int_0^{\varphi} q(s)\, ds .$$

The quantile density function, which is the derivative of the quantile function, expresses the increase of phase per unit increase of oscillator index. The density function is linked to the quantile density function by the relationship

$$q(\varphi) = \frac{dQ}{d\varphi} = \frac{1}{\rho(Q(\varphi))} . \tag{5.18}$$

In order to avoid some ill-defined cases, the condition $\rho > 0$ must be satisfied on $[0, 2\pi]$.

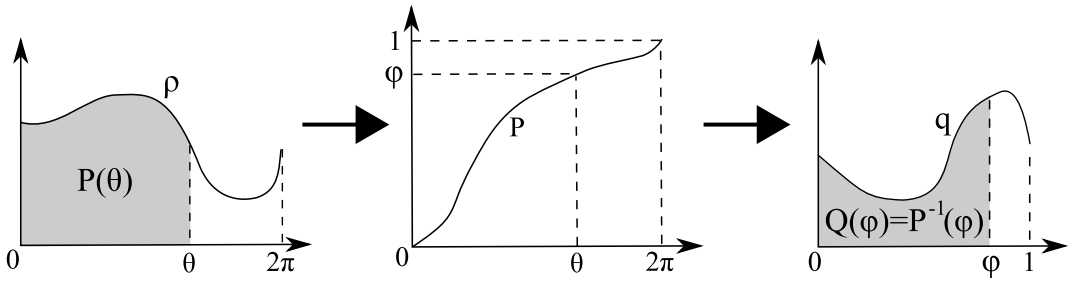

Figure 5.3: The density function $\rho(\theta)$ (left) has a cumulative density $P(\theta)$ (center). The quantile function $Q(\varphi) = P^{-1}(\varphi)$ is the cumulative density function of the quantile density function $q(\varphi)$ (right).

The reader will notice that, as the oscillators density $\rho(\theta, t)$ depends on time in (5.1), the corresponding quantile function and quantile density function also depend on time and are then rigorously defined as the two-variable functions $Q(\varphi, t)$ and $q(\varphi, t)$. But for notational convenience, the time variable is omitted when clear for the context. In addition, we denote the quantile function and the quantile density associated to the stationary density (5.11) by Q^* and q^* respectively.

5.3.2 Total variation distance

The 1-norm introduced in Section 4.2.2 to study finite populations of monotone oscillators leads to a L^1 distance (between quantile densities) in the case of infinite populations, that can be interpreted as a *total variation distance*.

For a finite population of N distinct oscillators, the 1-norm (4.10) induces a simple Lyapunov function for the system: the distance (induced by the 1-norm) between a configuration $\boldsymbol{\Theta}$ and the fixed point $\boldsymbol{\Theta}^*$. It is expressed as

$$\mathcal{V}^{(N)} = \left|Q_1^{(N)} - Q_1^{*(N)}\right| + \sum_{k=1}^{N-2} \left|\left(Q_k^{(N)} - Q_{k+1}^{(N)}\right) - \left(Q_k^{*(N)} - Q_{k+1}^{*(N)}\right)\right| + \left|Q_{N-1}^{(N)} - Q_{N-1}^{*(N)}\right| , \quad (5.19)$$

where the components θ_k are replaced by the N-quantiles (5.17). In the limit $N \to \infty$, the continuous equivalent of (5.19) corresponds to the L^1-distance between the quantile density functions:

$$\mathcal{V}(\rho) = \int_0^1 \left|\frac{\partial Q}{\partial \varphi} - \frac{dQ^*}{d\varphi}\right| d\varphi = \|q - q^*\|_{L^1} \quad \forall \rho > 0 \in C^0([0, 2\pi]) . \quad (5.20)$$

In contrast with the case of finite populations, there is no additional term corresponding to the boundaries, since $Q(0) = Q^*(0) = 0$ and $Q(1) = Q^*(1) = 2\pi$. In addition, the second equality is obtained through (5.18). One verifies that $\mathcal{V}(\rho) = 0 \Leftrightarrow q = q^*$ a.e. $\Leftrightarrow \rho = \rho^*$ a.e.

Theorem 4.2.2 shows that, under mild conditions, quantity (5.19) decreases at the successive firings of the oscillators, given the contraction property of the 1-norm. We claim that, for infinite populations, the continuous equivalent (5.20) also decreases at the successive firings of the continuum, that is, (5.20) decreases continuously with time. The main result of this chapter will thus establish (5.20) as a good Lyapunov function for the PDE (5.8).

The Lyapunov function (5.20) is interpreted as a total variation distance. Indeed, the total variation distance between two random variables corresponds to the L^1-distance between the corresponding density functions (see [29] for further details). The notion of total variation distance becomes clearer when one removes the integral from the expression (5.20). To do so, we first introduce the *critical points* $\varphi_c^{(k)}$ $(k = 1, \ldots, N_c)$ as the values corresponding to the extreme differences between the two functions Q and Q^*. Formally, the critical points satisfy

$$\left.\frac{\partial Q}{\partial \varphi}\right|_{\varphi=\varphi_c^{(k)}} = \left.\frac{dQ^*}{d\varphi}\right|_{\varphi=\varphi_c^{(k)}} \quad \text{or equivalently} \quad q(\varphi_c^{(k)}) = q^*(\varphi_c^{(k)}) \quad (5.21)$$

and

$$\begin{aligned} (-1)^k \frac{\partial Q}{\partial \varphi} &\geq (-1)^k \frac{dQ^*}{d\varphi} \qquad \forall \varphi \in [\varphi_c^{(k-1)}, \varphi_c^{(k)}] \\ (-1)^k \frac{\partial Q}{\partial \varphi} &> (-1)^k \frac{dQ^*}{d\varphi} \qquad \text{for some } \varphi \in (\varphi_c^{(k-1)}, \varphi_c^{(k)}) \end{aligned} \quad (5.22)$$

with, by convention, $\varphi_c^{(0)} = 0 < \varphi_c^{(k-1)} < \varphi_c^{(k)} < \varphi_c^{(N_c+1)} = 1$, for $k = 2, \ldots, N_c$. Without loss of generality, one has assumed that $\partial Q/\partial\varphi \leq dQ^*/d\varphi$ for $\varphi \in [0, \varphi_c^{(1)}]$. With this notation, the Lyapunov function (5.20) is rewritten as

$$\mathcal{V}(\rho) = \sum_{k=1}^{N_c+1} (-1)^k \int_{\varphi_c^{(k-1)}}^{\varphi_c^{(k)}} \left(\frac{\partial Q}{\partial \varphi} - \frac{dQ^*}{d\varphi}\right) d\varphi = 2 \sum_{k=1}^{N_c} (-1)^k \left[Q(\varphi_c^{(k)}) - Q^*(\varphi_c^{(k)})\right] , \quad (5.23)$$

since $Q(0) - Q^*(0) = Q(1) - Q^*(1) = 0$. The total variation distance is then the sum of the highest (and the lowest) value differences between the two quantile functions Q and Q^* (Figure 5.4).

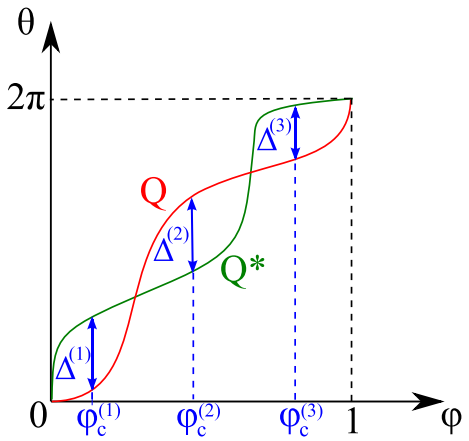

Figure 5.4: The Lyapunov function (5.23) is the total variation distance between two quantile density functions, a distance which is equal to the sum $\mathcal{V} = 2\sum_k \Delta^{(k)}$ of the highest value differences $|Q - Q^*|$.

5.3.3 Time evolution of the Lyapunov function

The candidate (5.20) is a good Lyapunov function. Its time evolution along the solutions of (5.8)-(5.9) depends on the derivative of the iPRC. In particular, monotonicity properties of the iPRC lead to a monotone time evolution of the Lyapunov function. The result is summarized in Theorem 5.3.1.

Theorem 5.3.1. *Let $\rho(\theta,t) \in C^0(L^1(0,2\pi),\mathbb{R}^+)$ be a strictly positive solution of (5.8)-(5.9). If the stationary density (5.11) exists and if either $Z''(\theta) \geq 0$ $\forall\theta \in [0,2\pi]$ or $Z''(\theta) \leq 0$ $\forall\theta \in [0,2\pi]$, then the Lyapunov function (5.20) satisfies*

$$J(0,t) \min_{\theta\in[0,2\pi]} \Big(K\,Z'(\theta)\Big)\mathcal{V}(\rho) \leq \dot{\mathcal{V}}(\rho) \leq J(0,t) \max_{\theta\in[0,2\pi]} \Big(K\,Z'(\theta)\Big)\mathcal{V}(\rho)\,. \tag{5.24}$$

Proof. For the sake of simplicity, the time variable t is omitted in the sequel. Furthermore, one supposes

$$\left.\frac{\partial Q}{\partial\varphi}\right|_0 \leq \left.\frac{dQ^*}{d\varphi}\right|_0$$

without loss of generality, since the proof for the other case follows on similar lines. Under this assumption, the critical points satisfy (5.21) and (5.22).

Since $0 < \rho(\theta,t) < \infty$ $\forall t \in \mathbb{R}^+$, one has $q(\varphi,t) < \infty$ $\forall t \in \mathbb{R}^+$ and the Lyapunov function is well-defined. If $\rho = \rho^*$, then $\mathcal{V} = 0$ and (5.24) is trivially verified. If $\rho \neq \rho^*$, the quantile densities q and q^* do not coincide and there exists at least one critical point, so that the Lyapunov function is given by (5.23).

Next, the time derivative can be written as

$$\dot{\mathcal{V}}(\rho) = 2\sum_{k=1}^{N_c}(-1)^k \left.\frac{\partial Q}{\partial t}\right|_{\varphi_c^{(k)}} . \tag{5.25}$$

Differentiating the expression $\theta \equiv Q(P(\theta,t),t)$ with respect to time t leads to

$$0 = \frac{dQ}{dt} = \frac{\partial Q}{\partial t} + \frac{\partial Q}{\partial \varphi}\frac{\partial P}{\partial t}$$

or

$$\frac{\partial Q}{\partial t} = -\frac{\partial P}{\partial t}\frac{\partial Q}{\partial \varphi} = -\frac{\partial P}{\partial t}\frac{1}{\rho(Q(\varphi))} ,$$

given (5.18). Furthermore,

$$\frac{\partial P}{\partial t} = \int_0^\theta \left.\frac{\partial \rho}{\partial t}\right|_s ds = -\int_0^\theta \left.\frac{\partial J}{\partial \theta}\right|_s ds = J_0 - J(\theta)$$

and the expression (5.25) becomes

$$\dot{\mathcal{V}}(\rho) = 2\sum_{k=1}^{N_c}(-1)^k \frac{J(Q(\varphi_c^{(k)})) - J_0}{\rho(Q(\varphi_c^{(k)}))} .$$

Since it follows from (5.18) that the critical values satisfy

$$\rho(Q(\varphi_c^{(k)})) = \rho^*(Q^*(\varphi_c^{(k)})) , \quad k = 1,\ldots,N_c , \tag{5.26}$$

one obtains, given (5.2), (5.6), and (5.11),

$$\begin{aligned}\dot{\mathcal{V}}(\rho) &= 2\sum_{k=1}^{N_c}(-1)^k \left[v(Q(\varphi_c^{(k)})) - \frac{J_0}{\rho^*(Q^*(\varphi_c^{(k)}))}\right] \\ &= 2\sum_{k=1}^{N_c}(-1)^k \left[\omega + K\,Z(Q(\varphi_c^{(k)}))J_0 - \frac{\omega J_0}{J^*} - K\,Z(Q^*(\varphi_c^{(k)}))J_0\right] .\end{aligned} \tag{5.27}$$

The boundary condition (5.9) yields a monotone relationship between the values $\rho(0)$ and $\rho(2\pi)$, that is, $\rho(0) > \rho^*(0)$ if and only if $\rho(2\pi) > \rho^*(2\pi)$. Apart from the case $\rho(0) = \rho^*(0)$, $\rho(2\pi) = \rho^*(2\pi)$, the number N_c of critical points, which satisfy (5.26), is even, owing to the continuity of ρ and Q (ρ^* and Q^*). Consequently, the terms $(-1)^k(\omega - \omega J_0/J^*)$ in (5.27) cancel each other. In the particular case $\rho(0) = \rho^*(0)$, N_c is not necessarily even but it follows from (5.9) that $J_0 = J^*(0) = J^*$ and the above-mentioned terms are equal to zero. As a consequence, one obtains

$$\begin{aligned}\dot{\mathcal{V}}(\rho) &= 2\,J_0 \sum_{k=1}^{N_c}(-1)^k K \left[Z(Q(\varphi_c^{(k)})) - Z(Q^*(\varphi_c^{(k)}))\right] \\ &= 2\,J_0 \sum_{k=1}^{N_c}(-1)^k K\,Z'(\xi_k) \left[Q(\varphi_c^{(k)}) - Q^*(\varphi_c^{(k)})\right] \\ &\triangleq 2J_0 \sum_{k=1}^{N_c} T^{(k)} ,\end{aligned} \tag{5.28}$$

where the second equality is obtained through the mean value theorem, with $\xi_k \in [Q(\varphi_c^{(k)}), Q^*(\varphi_c^{(k)})]$ or $\xi_k \in [Q^*(\varphi_c^{(k)}), Q(\varphi_c^{(k)})]$.

It remains to consider separately each term $T^{(k)}$ in the sum (5.28). For the sake of simplicity, we first consider the case $K\,Z'' \geq 0$. Denoting $(-1)^k[Q(\varphi_c^{(k)}) - Q^*(\varphi_c^{(k)})]$ by $\Delta^{(k)}Q$, we also distinguish two cases: $\Delta^{(k)}Q > 0$ and $\Delta^{(k)}Q \leq 0$.

Case $\boldsymbol{\Delta^{(k)}Q > 0}$. One has

$$T^{(k)} = K\,Z'(\xi_k)\Delta^{(k)}Q \leq \max_{\theta\in[0,2\pi]} \Big(K\,Z'(\theta)\Big)\Delta^{(k)}Q \tag{5.29}$$

and

$$T^{(k)} = K\,Z'(\xi_k)\Delta^{(k)}Q \geq \min_{\theta\in[0,2\pi]} \Big(K\,Z'(\theta)\Big)\Delta^{(k)}Q\,. \tag{5.30}$$

Case $\boldsymbol{\Delta^{(k)}Q \leq 0}$. We need to consider the addition of the term $T^{(k)}$ with the term $T^{(k-1)}$ or $T^{(k+1)}$. By (5.22), one gets

$$-\Delta^{(k-1)}Q < \Delta^{(k)}Q \;\leq\; 0\,, \tag{5.31}$$
$$-\Delta^{(k+1)}Q < \Delta^{(k)}Q \;\leq\; 0\,. \tag{5.32}$$

It follows that

$$T^{(k-1)} + T^{(k)} = K\,Z'(\xi_{k-1})\Delta^{(k-1)}Q + K\,Z'(\xi_k)\Delta^{(k)}Q \leq K\,Z'(\xi_k)\left(\Delta^{(k-1)}Q + \Delta^{(k)}Q\right), \tag{5.33}$$

The assumption $K\,Z'' \geq 0$ implies $K\,Z'(\xi_{k-1}) \leq K\,Z'(\xi_k)$, with $\xi_{k-1} \leq \xi_k$ and the above inequality then follows from (5.31). In addition, (5.31) also implies that the right hand in inequality (5.33) is the multiplication of $K\,Z'$ with the positive quantity $\Delta^{(k-1)}Q + \Delta^{(k)}Q$. Hence, (5.33) can be rewritten as

$$T^{(k-1)} + T^{(k)} \leq \max_{\theta\in[0,2\pi]} \Big(K\,Z'(\theta)\Big)\left(\Delta^{(k-1)}Q + \Delta^{(k)}Q\right). \tag{5.34}$$

Similarly, considering the addition of the terms $T^{(k)}$ and $T^{(k+1)}$ and using (5.32), one obtains

$$T^{(k)} + T^{(k+1)} \geq \min_{\theta\in[0,2\pi]} \Big(K\,Z'(\theta)\Big)\left(\Delta^{(k)}Q + \Delta^{(k+1)}Q\right). \tag{5.35}$$

Next, the inequalities (5.29) and (5.34) imply that the expression (5.28) can be rewritten as

$$\dot{\mathcal{V}}(\rho) = 2J_0 \sum_{k=1}^{N_c} T^{(k)} \leq J_0 \max_{\theta\in[0,2\pi]} \Big(K\,Z'(\theta)\Big)\mathcal{V}(\rho)\,. \tag{5.36}$$

In the case $\Delta^{(k)}Q \leq 0$, the two terms $T^{(k)}$ and $T^{(k-1)}$ are considered together. The additional $T^{(k-1)}$ itself corresponds to the case $\Delta^{(k-1)}Q > 0$, and does not require to be associated in turn with another term. In addition, there is no boundary problem since the term $T^{(1)}$ satisfies $\Delta^{(1)}Q > 0$, given (5.22) and $Q(0) = Q^*(0) = 0$.

Similarly, the inequalities (5.30) and (5.35) lead to

$$\dot{\mathcal{V}}(\rho) = 2J_0 \sum_{k=1}^{N_c} T^{(k)} \geq J_0 \min_{\theta\in[0,2\pi]} \Big(K\,Z'(\theta)\Big)\mathcal{V}(\rho)\,. \tag{5.37}$$

In the case $K\,Z'' \leq 0$, the inequalities (5.34) and (5.35) are reversed, that is, the sum $T^{(k-1)} + T^{(k)}$ has a lower-bound and the sum $T^{(k)} + T^{(k+1)}$ has an upper-bound. Hence, the inequalities (5.36) and (5.37) still hold, which completes the proof. □

If there is no coupling or if the iPRC is constant, (5.8) is a (marginally stable) standard transport equation (see Remark 5.2.1) and Theorem 5.3.1 implies that the Lyapunov function is constant along the solutions of (5.8). This is in agreement with the fact that the total variation distance is a conserved quantity for most of the systems of conservation laws [99]. But whereas the distance is constant with a standard transport equation, the distance is not constant under the influence of the coupling: the nonlinear coupling term in (5.8), which depends on $K\,Z'$, induces a variation (5.24) of the Lyapunov function. A monotone decreasing function $K\,Z$ implies a decreasing Lyapunov function along the solutions. This is discussed in detail in the next section.

A parallel with the analysis of finite populations has emphasized the importance of considering (i) *quantile densities instead of densities* and (ii) *a L^1 distance (total variation distance) instead of a L^2 distance*. The importance of these two points is illustrated in the two following paragraphs.

Quantile density vs. density function. The Lyapunov function (5.20) is induced by the total variation distance between *quantile densities*. An alternative choice would be the total variation distance between *density functions*, that is,

$$\mathcal{V}_{\rm bis}(\rho) = \int_0^{2\pi} |\rho - \rho^*|\, d\theta \quad \forall \rho \geq 0 \in C^0([0, 2\pi])\,. \tag{5.38}$$

Introducing the analog notation to (5.21), the critical phases $\theta_c^{(k)}$ $(k = 1, \ldots, N_c)$ are defined as the values satisfying

$$\rho(\theta_c^{(k)}, t) = \rho^*(\theta_c^{(k)}, t)\,. \tag{5.39}$$

The Lyapunov function (5.38) is rewritten as

$$\mathcal{V}_{\rm bis}(\rho) = \sum_{k=1}^{N_c+1} (-1)^k \int_{\theta_c^{(k-1)}}^{\theta_c^{(k)}} (\rho - \rho^*) d\theta$$

and its time derivative is given by

$$\dot{\mathcal{V}}_{\rm bis} = \sum_{k=1}^{N_c+1} (-1)^k \int_{\theta_c^{(k-1)}}^{\theta_c^{(k)}} \frac{\partial \rho}{\partial t} d\theta = \sum_{k=1}^{N_c+1} (-1)^k \left[J(\theta_c^{(k-1)}) - J(\theta_c^{(k)}) \right], \tag{5.40}$$

where we used (5.1). A simple argument shows that the Lyapunov function cannot be strictly decreasing along the solutions of (5.8). Indeed, for any density satisfying $\rho(0) = \rho^*(0)$, one must also have $J_0 = J^*(0) = J^*$ since it follows from (5.9) that there is a bijection between the values $\rho(0)$ and J_0. But then, (5.2) and (5.39) imply that $J(\theta_c^{(k)}) = J^*(\theta_c^{(k)}) = J^*$ for all k and the derivative (5.40) leads to $\dot{\mathcal{V}}_{\rm bis} = 0$. Even though one actually shows that $\dot{\mathcal{V}} \leq 0$, La

Salle principle (see [55]) cannot be used to prove the stability, since it is not obvious to prove the precompactness of the trajectories.

This argument shows that a direct application of the total variation distance on density functions does not lead to a good candidate Lyapunov function for the PDE (5.8). A key point is to apply the total variation distance on *quantile functions* instead.

$\mathbf{L^1}$ distance vs. $\mathbf{L^2}$ distance. The Lyapunov function (5.20) is induced by a L^1 *distance*. An alternative choice would be a Lyapunov function induced by a (more common) L^2 *distance*, that is $\mathcal{V}_{\text{ter}} = \|q - q^*\|_{L^2}$. However, straightforward computations (not presented here) show that this candidate Lyapunov function satisfies $\dot{\mathcal{V}}_{\text{ter}}(\rho) > 0$ for some ρ. Actually, the analysis of finite populations gives clear insight that a L^1 distance must be considered, instead of the L^2 distance. As an illustration, condition (4.6), necessary for the contraction under the 2-norm, is increasingly conservative as the number of oscillators grows, and it is particularly so in the extreme case of infinite populations.

5.4 Convergence analysis for monotone oscillators

The result of Theorem 5.3.1 has a strong implication in the case of monotone iPRC. It implies that the Lyapunov function (5.20) has a monotone time evolution if the iPRC is monotone. In this situation, the Lyapunov function either converges to a lower bound or to an upper bound. These two bounds correspond to the two particular behaviors which characterize the dichotomy. They are given by

$$0 \leq \mathcal{V}(\rho) \leq \|q\|_{L^1} + \|q^*\|_{L^1} = Q(1) - Q(0) + Q^*(1) - Q^*(0) = 4\pi\,.$$

At the lower bound, the function is equal to zero if and only if the density is the asynchronous (stationary) density (5.11). On the other hand, the Lyapunov function tends to the upper bound 4π if the density ρ tends to a Dirac function (synchronous state).

5.4.1 Exponential convergence to the asynchronous state

Theorem 5.3.1 will be used to study convergence to the asynchronous state for monotone decreasing functions $K\,Z(\theta)$. However, in order to apply (5.24) along the solutions, we need to show independently that the flux $J_0(t)$ remains strictly positive and bounded for all time. This condition will restrict the set of admissible initial conditions. In particular, the initial conditions have to ensure that $0 < J_0 < \infty$ when any oscillator crosses $\theta = 2\pi$ for the first time. [This is equivalent to preventing the initial absorptions of the oscillators in finite populations (see below).] Formally, we consider the characteristic curves $\Lambda_\theta(t)$ defined by $\dot{\Lambda}_\theta = v(\Lambda_\theta(t), t)$, $\Lambda_\theta(0) = \theta \in [0, 2\pi]$, $\Lambda_\theta(\bar{t}_\theta) = 2\pi$ (Figure 5.5).

The (strictly positive) initial density $\rho(\theta, 0) > 0$ must be such that the value of the flux at the intersection of the characteristic curves with $\theta = 2\pi$ is strictly positive and bounded, that is

$$\rho(\theta,0) > 0 \quad \Rightarrow \quad 0 < J\big(\Lambda_\theta(\bar{t}_\theta) = 2\pi, \bar{t}_\theta\big) = J_0(\bar{t}_\theta) < \infty \quad \forall\, \theta \in [0, 2\pi]\,. \tag{5.41}$$

Condition (5.41) is the condition that is imposed on the initial conditions to ensure that the flux satisfies $0 < J_0(t) < \infty$ for $t \in [0, \bar{t}_0]$. But if the flux is bounded for $t \in [0, \bar{t}_0]$, then

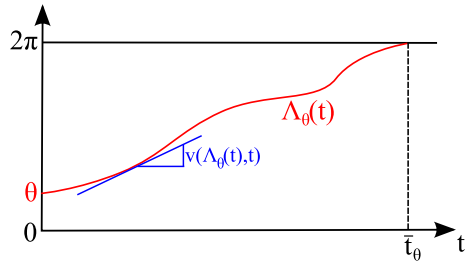

Figure 5.5: The characteristic curve $\Lambda_\theta(t)$ is defined by $\dot{\Lambda}_\theta = v(\Lambda_\theta(t), t)$, with the initial value $\Lambda_\theta(0) = \theta$, and reaches 2π at time $\bar{t}_\theta$.

the flux is bounded for all time and Theorem 5.3.1 can be applied to prove the exponential decreasing of the Lyapunov function. The result is summarized in the following proposition.

Proposition 5.4.1. *Consider the transport PDE (5.8)-(5.9) and assume that $Z(\theta)$ is such that (i) the stationary density (5.11) exists, (ii) $K\,Z'(\theta) < 0\ \forall\theta \in [0, 2\pi]$, and (iii) either $Z''(\theta) \geq 0\ \forall\theta \in [0, 2\pi]$ or $Z''(\theta) \leq 0\ \forall\theta \in [0, 2\pi]$. Then all solutions $\rho(\theta, t) \in C^0(L^1(0, 2\pi), \mathbb{R}^+)$ with an initial condition satisfying (5.41) exponentially converge to the asynchronous state and the Lyapunov functional (5.20) is exponentially decreasing along them.*

Proof. One considers a characteristic curve $\Lambda(t)$, with $\Lambda(\underline{t}) = 0$ and $\Lambda(\bar{t}) = 2\pi$. Solving the total derivative equation (5.10) on $\Lambda(t)$ yields

$$\rho(0, \underline{t}) \exp\left(-\int_{\underline{t}}^{\bar{t}} J_0(t)\, K\, Z'(\Lambda(t))\, dt\right) = \rho(2\pi, \bar{t})\,.$$

Next, using (5.2) and expressing the integral in the space variable Λ along the characteristic curve leads to

$$\frac{J_0(\underline{t})}{\omega + K\,Z(0)\,J_0(\underline{t})} \exp\left(-\int_0^{2\pi} \frac{J_0}{\omega + K\,Z(\Lambda)\,J_0} K\,Z'(\Lambda)\,d\Lambda\right) = \frac{J_0(\bar{t})}{\omega + K\,Z(2\pi)\,J_0(\bar{t})}\,.$$

If the flux is constant on $[\underline{t}, \bar{t}]$, then $J_0(t) = J_m = J_M$, with $J_m \triangleq \min_{t\in[\underline{t},\bar{t}]} J_0(t)$ and $J_M \triangleq \max_{t\in[\underline{t},\bar{t}]} J_0(t)$. Otherwise, since $K\,Z'$ is negative, replacing J_0 in the integral of the above expression by the bounds J_m and J_M and computing the integral yield the strict inequalities

$$\frac{J_0(\underline{t})}{\omega + K\,Z(0)\,J_0(\underline{t})} \frac{\omega + K\,Z(0)\,J_m}{\omega + K\,Z(2\pi)\,J_m} < \frac{J_0(\bar{t})}{\omega + K\,Z(2\pi)\,J_0(\bar{t})} < \frac{J_0(\underline{t})}{\omega + K\,Z(0)\,J_0(\underline{t})} \frac{\omega + K\,Z(0)\,J_M}{\omega + K\,Z(2\pi)\,J_M}\,.$$

By definition, $J_m \leq J_0(\underline{t}) \leq J_M$ and one obtains

$$\frac{J_m}{\omega + K\,Z(2\pi)\,J_m} < \frac{J_0(\bar{t})}{\omega + K\,Z(2\pi)\,J_0(\bar{t})} < \frac{J_M}{\omega + K\,Z(2\pi)\,J_M}$$

or equivalently

$$J_m < J_0(\bar{t}) < J_M\,. \tag{5.42}$$

Within any interval $[\underline{t}, \bar{t}]$, the flux remains either constant or satisfies (5.42). By induction, there holds

$$J_{\min} \leq J_0(t) \leq J_{\max} \quad \forall t > 0\,,$$

with $J_{\min} \triangleq \min_{t\in[0,\bar{t}_0]} J_0(t)$ and $J_{\max} \triangleq \max_{t\in[0,\bar{t}_0]} J_0(t)$. In addition, the initial condition (5.41) implies that $J_{\min} > 0$ and $J_{\max} < \infty$.

Since $\rho(\theta, 0) > 0$, the exponential evolution of the density along (all) the characteristic curves implies that the density remains strictly positive for all $t > 0$. The result of Theorem 5.3.1 is then applied and yields

$$J_{\min} \min_{\theta\in[0,2\pi]} \Big(K\,Z'(\theta)\Big)\mathcal{V}(\rho) \leq \dot{\mathcal{V}}(\rho) \leq J_{\max} \max_{\theta\in[0,2\pi]} \Big(K\,Z'(\theta)\Big)\mathcal{V}(\rho)$$

or, equivalently,

$$-\,J_{\max} \max_{\theta\in[0,2\pi]} \Big|K\,Z'(\theta)\Big|\mathcal{V}(\rho) \leq \dot{\mathcal{V}}(\rho) \leq -J_{\min} \min_{\theta\in[0,2\pi]} \Big|K\,Z'(\theta)\Big|\mathcal{V}(\rho) \leq 0$$

since $K\,Z' < 0$. It follows that the Lyapunov function is exponentially decreasing, which concludes the proof. □

Proposition 5.4.1 is a strong result showing that, provided that the function $K\,Z(\theta)$ is decreasing, the solution $\rho(\cdot, t)$ remains, for all time, in a particular set of functions $\{\rho|\mathcal{V}(\rho) < C\}$, with the constant $C > 0$. Inside this set, the solution eventually converges at exponential rate toward the stationary solution ρ^*, corresponding to $\mathcal{V}(\rho^*) = 0$.

The restriction (5.41) on the initial condition is rather weak for decreasing functions $K\,Z(\theta)$, as shown by the following proposition.

Proposition 5.4.2. *Assume that $K\,Z'(\theta) < 0\ \forall\theta \in [0, 2\pi]$. If $K\,Z(2\pi) \leq 0$, then (5.41) is always satisfied. If $K\,Z(2\pi) > 0$, then (5.41) is satisfied if*

$$\rho(\theta, 0) < \frac{1}{K\,Z(\theta)} \quad \forall\theta \in [0, 2\pi]\,. \tag{5.43}$$

Proof. **Case $\mathbf{K\,Z(2\pi) \leq 0}$.** Using the boundary condition (5.9), the condition $0 < J_0(\bar{t}_\theta) < \infty$ is turned into a condition on $\rho(2\pi, \bar{t}_\theta)$ and (5.41) is equivalent to

$$\rho(\theta, 0) > 0 \quad \Rightarrow \quad \rho(2\pi, \bar{t}_\theta) > 0 \quad \forall\,\theta \in [0, 2\pi]\,. \tag{5.44}$$

For $\theta = 2\pi$, condition (5.44) is satisfied, since $\bar{t}_{2\pi} = 0$. Next, we proceed by induction on θ: given θ and assuming that (5.44) is satisfied for all $\tilde{\theta} > \theta$, we prove that (5.44) also holds at θ. The total derivative equation (5.10) is well-defined on the characteristic curve $\Lambda_\theta(t)$ since $0 < J_0(t) < \infty$ for all $t < \bar{t}_\theta$. Solving (5.10) along the characteristic curve yields

$$\rho(2\pi, \bar{t}_\theta) = \rho(\theta, 0)\,\exp\left(-\int_0^{\bar{t}_\theta} J_0(t)\,K\,Z'(\Lambda_\theta(t))\,dt\right) \tag{5.45}$$

and $\rho(\theta, 0) > 0$ implies $\rho(2\pi, \bar{t}_\theta) > 0$. Condition (5.41), equivalent to (5.44), is then always satisfied.

Case $K\,Z(2\pi) > 0$. Using (5.9), the condition $0 < J_0(\bar{t}_\theta) < \infty$ is turned into a condition on $\rho(2\pi, \bar{t}_\theta)$ and (5.41) is equivalent to

$$\rho(\theta, 0) > 0 \quad \Rightarrow \quad 0 < \rho(2\pi, \bar{t}_\theta) < \frac{1}{K\,Z(2\pi)} \quad \forall\, \theta \in [0, 2\pi]\,. \tag{5.46}$$

The strict condition $\rho(\theta, 0) > 0$ always implies $\rho(2\pi, \bar{t}_\theta) > 0$, as in the case $K\,Z(2\pi) \leq 0$. Hence, we focus on the additional upper bound on the density $\rho(2\pi, \bar{t}_\theta)$. For $\theta = 2\pi$, condition (5.43) implies (5.46), since $\bar{t}_{2\pi} = 0$. Next, we proceed by induction on θ: given θ and assuming that (5.46) is satisfied for all $\tilde{\theta} > \theta$, we prove that (5.46) also holds at θ (provided that condition (5.43) is satisfied). Using (5.45) with condition (5.43) leads to

$$\rho(2\pi, \bar{t}_\theta) < \frac{1}{K\,Z(\theta)} \exp\left(- \int_0^{\bar{t}_\theta} J_0(t)\, K\, Z'(\Lambda_\theta(t))\, dt \right) .$$

Expressing the integral in the space variable along the characteristic curve yields

$$\rho(2\pi, \bar{t}_\theta) < \frac{1}{K\,Z(\theta)} \exp\left(- \int_\theta^{2\pi} \frac{J_0}{\omega + K\,Z(\Lambda_\theta)\,J_0} K\, Z'(\Lambda_\theta)\, d\Lambda_\theta \right) .$$

Since $K\,Z'$ is negative, the flux J_0 can be replaced by its maximal value, that is, $J_0 \to \infty$ and the above inequality leads to

$$\rho(2\pi, \bar{t}_\theta) < \frac{1}{K\,Z(\theta)} \exp\left(- \int_\theta^{2\pi} \frac{1}{Z(\Lambda_\theta)}\, Z'(\Lambda_\theta)\, d\Lambda_\theta \right) . \tag{5.47}$$

The relation (5.47) is well-defined since $Z(\theta) \neq 0$ for all $\theta \in [0, 2\pi]$. Finally, computing the integral in (5.47) implies that $\rho(2\pi, \bar{t}_\theta) < 1/[K\,Z(2\pi)]$. Condition (5.41), equivalent to (5.46), is then satisfied. This concludes the proof. □

When the conditions of Proposition 5.4.2 are not satisfied, condition (5.41) may fail to hold, in which case the flux blows-up (finite escape time to infinity). In the case $K\,Z(2\pi) > 0$, there is a positive feedback between the flux and the velocity: a high value of J_0 increases the velocity through the coupling, which in turn increases the flux. When the density approaches the critical value

$$\rho(2\pi, t) = \frac{1}{K\,Z(2\pi)}\,, \tag{5.48}$$

the flux is high enough to blow-up through the positive feedback.

This finite escape time phenomenon is related to the absorption phenomenon observed for finite populations. For finite populations, the initial condition (5.43) of Proposition 5.4.2 can be rewritten as

$$\frac{1}{N\,\Delta\theta} < \frac{\Delta x}{K\,\Delta\theta}\,,$$

where Δx and $\Delta\theta$ are respectively the state distance and the phase distance between two successive oscillators. The initial condition then imposes a minimal distance $\Delta x > K/N = \epsilon$ between any two oscillators, so that an absorption cannot occur.

5.4.2 Finite time convergence to a synchronous state

For increasing functions $K\,Z(\theta)$, Theorem 5.3.1 implies that the Lyapunov function (5.20) is strictly increasing, and a synchronous behavior is observed in finite time, for any initial condition. Either the flux $J_0(t)$ becomes infinite in finite time or the density $\rho(0,t)$ becomes infinite in finite time. The behavior is similar to the behavior of finite populations, where synchronization is achieved in finite time through the absorption phenomenon.

The finite time convergence to synchronization is established in Proposition 5.4.3. As a preliminary to this result, we need the following lemma.

Lemma 5.4.1. *The Lyapunov function (5.20) satisfies*

$$\mathcal{V} = \|q - q^*\|_{L^1} \leq 4\pi - 2\,q_{min}$$

with

$$q_{min} = \min\left(\min_{\varphi\in[0,1]} q(\varphi),\, \min_{\varphi\in[0,1]} q^*(\varphi)\right).$$

Proof. The proof of Lemma 5.4.1 can be found in Appendix A.3. □

Through Theorem 5.3.1 and the preceding lemma, the following proposition establishes the finite time convergence to the synchronous state.

Proposition 5.4.3. *Consider the transport PDE (5.8)-(5.9) and assume that $Z(\theta)$ is such that (i) the stationary density (5.11) exists, (ii) $K\,Z'(\theta) > 0\ \forall\theta \in [0,2\pi]$, and (iii) either $Z''(\theta) \geq 0\ \forall\theta \in [0,2\pi]$ or $Z''(\theta) \leq 0\ \forall\theta \in [0,2\pi]$. Then all solutions converge in finite time to a synchronous state. That is, if $K\,Z(0) \geq 0$, the flux satisfies $J(0,t_{fin}) = \infty$, or if $K\,Z(0) < 0$, the density satisfies $\rho(0,t_{fin}) = \infty$, with $t_{fin} < \infty$.*

Proof. An infinite flux $J_0(t)$ or a infinite density $\rho(0,t)$ is obtained when the density $\rho(2\pi,t)$ reaches a critical value. If $K\,Z(0) \geq 0$, the value $K\,Z(2\pi)$ is positive since $K\,Z$ is increasing. Hence, the flux J_0 becomes infinite when the density $\rho(2\pi,t)$ exceeds the critical value (5.48). If $K\,Z(0) < 0$, the velocity (5.6) at $\theta = 0$ is equal to zero when the flux reaches the value $J_0(t) = \omega/|K\,Z(0)|$ or equivalently, given (5.9), when the density reaches the value

$$\rho(2\pi,t) = \frac{1}{K\,Z(2\pi) - K\,Z(0)}\,. \tag{5.49}$$

With a velocity equal to zero at $\theta = 0$, the relationship (5.2) implies that the density is infinite at $\theta = 0$. (If $K\,Z(0) < 0$ along with $K\,Z(2\pi) > 0$, the reader will notice that the value (5.48) has no importance, since (5.48) is greater than (5.49).)

Next, we show that the density $\rho(2\pi,t)$ must necessarily reach the critical value (5.48) or (5.49) in finite time t_{fin}. Let us consider a characteristic curve $\Lambda(t)$, with $\Lambda(\underline{t}) = 0$ and $\Lambda(\bar{t}) = 2\pi$ and assume that the synchronous state is not reached within $[\underline{t},\bar{t}]$, so that $\rho(\theta,t) > 0 \in C^0(L^1(0,2\pi),[\underline{t},\bar{t}])$. Applying Theorem 5.3.1 and integrating (5.24), one has

$$\min_{\theta\in[0,2\pi]}\Big(K\,Z'(\theta)\Big)\int_{\underline{t}}^{\bar{t}} J_0(t)\,dt \leq \int_{\mathcal{V}(\underline{t})}^{\mathcal{V}(\bar{t})} \frac{1}{\mathcal{V}}\,d\mathcal{V} \leq \max_{\theta\in[0,2\pi]}\Big(K\,Z'(\theta)\Big)\int_{\underline{t}}^{\bar{t}} J_0(t)\,dt\,.$$

Since $[\underline{t}, \overline{t}]$ is the time interval corresponding to the complete evolution of an oscillator from $\theta = 0$ to $\theta = 2\pi$, the integral of the flux J_0 in the above equation is equal to one and it follows that

$$\exp\left(\min_{\theta\in[0,2\pi]}\Big(K\,Z'(\theta)\Big)\right) \leq \frac{\mathcal{V}(\overline{t})}{\mathcal{V}(\underline{t})} \leq \exp\left(\max_{\theta\in[0,2\pi]}\Big(K\,Z'(\theta)\Big)\right) .$$

The condition $K\,Z' > 0$ implies that the Lyapunov function strictly increases within the time interval $[\underline{t}, \overline{t}]$. Considering n successive intervals $[0, \overline{t}_1]$, ..., $[\underline{t}_n, \overline{t}_n]$, with $\underline{t}_{i+1} = \overline{t}_i$, one obtains

$$\frac{\mathcal{V}(\overline{t}_n)}{\mathcal{V}(0)} \geq \exp\left(n \min_{\theta\in[0,2\pi]}\Big(K\,Z'(\theta)\Big)\right) .$$

Hence, a given value $\overline{\mathcal{V}} > \mathcal{V}(0)$ is reached within at most $n_{\max}$ time intervals, with

$$n_{\max} \leq \frac{\log\left(\overline{\mathcal{V}}/\mathcal{V}(0)\right)}{\min_{\theta\in[0,2\pi]}\Big(K\,Z'(\theta)\Big)} .$$

Since the time length of each interval $[\underline{t}_k, \overline{t}_k]$ $(k = 1, \ldots, n_{\max})$ is finite, any value $\overline{\mathcal{V}} < 4\pi$ is reached in finite time. By Lemma 5.4.1, $\mathcal{V} = \overline{\mathcal{V}}$ implies that $q_{\min} \leq (4\pi - \overline{\mathcal{V}})/2$. When considering values $\overline{\mathcal{V}}$ close to 4π, the minimum of the quantile density q reaches in finite time any given value close to zero. Given (5.18), this implies that the maximum of the density ρ_M reaches in finite time any given value (provided that the critical value (5.48) or (5.49) is not already reached). In particular, the value

$$\rho_M = \rho_c \exp\left(\max_{\theta\in[0,2\pi]}\Big(K\,Z'(\theta)\Big)\right) , \tag{5.50}$$

with ρ_c denoting the critical value (5.48) or (5.49), is reached in finite time. Then, the maximum value ρ_M (obtained at θ_M at time t_M) decreases along the characteristic curve $\Lambda(t)$, with $\Lambda(t_M) = \theta_M$. Solving the total derivative equation (5.10), one shows that the variation along the characteristic curve is bounded:

$$\rho(2\pi, t_{\text{fin}}) = \rho_M \exp\left(-\int_{t_M}^{t_{\text{fin}}} J_0(t)\,K\,Z'(\Lambda(t))dt\right) \geq \rho_M \exp\left(-\max_{\theta\in[0,2\pi]}\Big(K\,Z'(\theta)\Big)\right) ,$$

where the inequality is obtained since the integral of J_0 on $[t_M, t_{\text{fin}}]$ is less than one. With ρ_M given by (5.50), the density exceeds the critical value in finite time t_{fin}, which concludes the proof. □

Proposition 5.4.3 shows that oscillators with monotone increasing functions $K\,Z$ converge to a synchronous behavior corresponding to a solution with a finite escape time to infinity. If the coupling is excitatory $(0 \leq K\,Z(0) < K\,Z(2\pi))$, the flux J_0 blows-up and is infinite at time t_{fin}, as well as the velocity $v(2\pi, t_{\text{fin}})$. This behavior corresponds to the absorption phenomenon occurring in finite populations of oscillators (see also the end of Section 5.4.1). If the coupling is inhibitory $(K\,Z(0) < 0)$, the velocity $v(0, t)$ reaches the value zero at time t_{fin} and the oscillators accumulate at $\theta = 0$, yielding an infinite density $\rho(0, t_{\text{fin}})$.

5.5 Implications for infinite populations of oscillators

The results of Section 5.4 are quite technical. In this section, their implications on the behavior of (monotone) oscillators are discussed with more details.

5.5.1 Parallel with finite populations

The results of Proposition 5.4.1 and Proposition 5.4.3 apply to oscillators characterized by a monotone iPRC. In the case of integrate-and-fire oscillators, the results thereby apply to oscillators with a monotone F (including the popular LIF oscillators), drawing a parallel with the results of Chapter 4 for finite populations.

When $K\,Z' > 0$ ($K\,dF/dx < 0$), the oscillators achieve synchrony.

Theorem 5.5.1. *Consider a continuum of identical pulse-coupled integrate-and-fire oscillators $\dot{x} = F(x)$ characterized by (i) a monotone property $K\,dF/dx < 0$ and (ii) an iPRC with a curvature of constant sign. Then, provided that the asynchronous state exits (cf. Corollary 5.2.1), the continuum converges to the synchronous state in finite time.*

When $K\,Z' < 0$ ($K\,dF/dx > 0$), the oscillators converge to the asynchronous state.

Theorem 5.5.2. *Consider a continuum of identical pulse-coupled integrate-and-fire oscillators $\dot{x} = F(x)$ characterized by (i) a monotone property $K\,dF/dx > 0$ and (ii) an iPRC with a curvature of constant sign. Then, provided that the asynchronous state exits (cf. Corollary 5.2.1), either the initial conditions do not fulfill* (5.41) *and the flux tends to infinity in finite time, or the continuum exponentially converges to the asynchronous state.*

The curvature condition on the iPRC is verified for the LIF oscillators [(2.10) in Section 2.3.3]. We note that this condition corresponds to the curvature condition on the scalar firing map (see Remark 5.5.1). In addition, the condition is also satisfied by the iPRC (2.2) of oscillators close to a homoclinic bifurcation (Example 2.3.1), so that the result also applies to Morris-Lecar oscillators (under particular sets of parameters).

Theorem 5.5.1 and Theorem 5.5.2 are the exact analogs of Theorem 4.1.1 and Theorem 4.2.3. While the results of Theorem 5.5.1 and Theorem 5.5.2 are stability results for continuous-time transport equations (infinite populations), the results of Theorem 4.1.1 and Theorem 4.2.3 are stability results for the equivalent discrete-time firing maps (finite populations). The above results therefore establish a strong link between a discrete-time approach and a continuous-time approach.

Remark 5.5.1. The results of finite populations impose conditions on the particular PRC Z_ϵ (3.3), and not on the iPRC Z. As a consequence, compared with the results of infinite populations, the results of finite populations rely on assumptions slightly less conservative. For instance, it follows from (3.9) and (3.10) that the monotonicity condition $|h'| < 1$ ($Z'_\epsilon < 0$) is equivalent to $Z(\theta) > Z(\theta + Z_\epsilon(\theta))$, which is less conservative than $Z' < 0$. Similarly, elementary computations show that a curvature condition $h'' \geq 0$ ($Z''_\epsilon \geq 0$) is equivalent to $Z'(\theta) < Z'(\theta + Z_\epsilon(\theta))$, which is less conservative than $Z'' > 0$. ◇

The results reinforce the numerical observations presented in Section 5.2.1 and prove that the behaviors of monotone oscillators are dichotomic, not only for finite populations but also

for infinite populations. Hence, the continuum approximation of large networks of pulse-coupled oscillators leads to coherent results and is a relevant approximation.

5.5.2 Transmission delays and non-instantaneous coupling

In the present dissertation, we mainly focus on an *instantaneous* impulsive coupling, where a given oscillator influences the other oscillators only at the very instant when $\theta = 0$. However, other studies have considered transmission time delays, with a *non-instantaneous* coupling. For instance, [3, 117] considered LIF oscillators ($F(x) = S + \gamma\, x$, $\gamma < 0$) characterized by the dynamics

$$\dot{x}_k = F(x_k) + K \int_{\infty}^{t} E(t-\tau)\, J_0(\tau)\, d\tau\,. \tag{5.51}$$

The coupling is realized by means of a series of smoothed finite-width pulses $E(t)$ corresponding to α-functions $E(t) = \alpha^2\, t\, \exp(\alpha(t))$, instead of a series of δ-like pulses. The α-function is a common synaptic response widely used in computational neuroscience. When $\alpha \to \infty$, the α-functions tend to Dirac functions ($E(t) \to \delta(t)$) and the dynamics (5.51) is equivalent to (5.5). The model investigated in this chapter is recovered and thereby appears as the limit case (instantaneous coupling) of the model studied in [3, 117] (non-instantaneous coupling). In particular, the stability results presented in this chapter are in accordance with the local stability results of [3, 117], for $\alpha \gg 1$.

In [117], the study of (5.51) shows that transmissions delays influence the behavior of the oscillators, which is not necessary dichotomic. Under a critical value α_c, that is, for slow transmissions and wide pulses, a Hopf bifurcation occurs and a periodic flux (firing pattern) is observed instead of the asynchronous state, a situation that corresponds to a quasiperiodic behavior of the individual oscillators. This behavior, different from the dichotomic behavior presented in this chapter, is triggered by transmission delays. In Chapter 6, we show that a similar behavior is obtained when considering particular non-monotone integrate-and-fire dynamics.

In spite of the evident interest of a model with transmission delays, we have restricted attention to instantaneous coupling, an approximation that is relevant for many realistic systems characterized by negligible transmission time delays. In addition, considering a non-instantaneous coupling presents some drawbacks that are not encountered with an instantaneous coupling.

First, the theoretical results are weaker in the case of a non-instantaneous coupling. While the stability analysis for a non-instantaneous coupling merely relies on a local linearization of the dynamics in the neighborhood of the equilibrium, a global approach is proposed here for the instantaneous coupling.

Furthermore, it is shown in [128] that some high frequency modes are not captured by the thermodynamic limit ($N \to \infty$) for the model (5.51), so that the stability properties are not preserved through the continuum approximation. The ratio α/N, which should be kept constant, actually tends to zero when $N \to \infty$. In contrast, the case of an instantaneous coupling is characterized by the ratio $\alpha/N = \infty$, so that the ratio remains constant in the thermodynamic limit. It turns out that, in this case, the thermodynamic limit is a correct approximation and the obtained stability results are in agreement with the behavior

of finite populations (as it is mentioned in Section 5.5.1). This reinforces the interest of the instantaneous coupling.

5.5.3 Adding noise

Noise is often introduced in models of pulse-coupled oscillators networks. A common stochastic component can play the role of a coupling that leads to organized collective behaviors. For instance, uncoupled oscillators driven by common independent Gaussian white noises [79] or by random Poisson impulses [23, 80] can achieve perfect synchrony, a phenomenon called *noise-induced synchronization*.

In addition, noise can also introduce some heterogeneity in the network, approximating discrepancies between non-identical oscillators. The continuum limit is particularly appropriate to investigate such a stochastic extension, since the law of large numbers implies that the density of oscillators is identical to the probability density induced by the stochastic dynamics. In this framework, the evolution of the density is dictated by a generalized continuity equation, known as the *Fokker-Planck equation*.

In the case of noisy pulse-coupled oscillators, it was shown in [3] that noise stabilizes the asynchronous state. In addition, we showed that a strong coupling reduces the effect of noise, a logical fact highlighting that strongly coupled non-identical oscillators behave as identical oscillators. Those preliminary results are not detailed in the present dissertation, because the study of noisy oscillators is beyond the scope of the thesis.

5.6 Conclusion

Finite and infinite populations of monotone oscillators exhibit an equivalent dichotomic behavior, which illustrates the strong parallel existing between the two situations. In particular, the global results of Chapter 4 are extended to the case of infinite populations, a process that yields a Lyapunov function induced by a total variation distance between quantile densities. In a more general context, the result provides an original Lyapunov function for a particular class of PDE's.

The case of monotone pulse-coupled oscillators is completely studied, both for finite and infinite populations. In the next chapter, we study oscillators that have no monotonicity property, such as QIF oscillators.

Chapter 6

Beyond monotone oscillators

While a wealth of studies have investigated many extensions of pulse-coupled monotone (LIF) oscillators, few studies have considered non-monotone pulse-coupled oscillators, aside from rare examples [16]. In particular, even though the QIF model is widely used (e.g. [14, 41]), there is no study of QIF oscillators with a pure impulsive coupling, to the author's knowledge. In this chapter, we therefore address the problem of non-monotone pulse-coupled integrate-and-fire oscillators, with a particular attention to the QIF model, a main motivation of the thesis.

A remarkable result is that the *dichotomic behavior* proved for monotone oscillators persists with QIF oscillators. In this case, the dichotomic behavior of the oscillators is dictated by the average properties of the (non-monotone) QIF dynamics. Interestingly, a *non-dichotomic* behavior is however observed with a specific "QIF-like" model, suggesting that the dichotomic behavior proved for two oscillators does not always extend to $N > 2$ oscillators.

Chapter 4 already shows that generalizing the global study of two monotone oscillators to larger populations (to higher dimensions) is not a simple task. The dichotomic behavior of QIF oscillators, although clearly suggested by numerical simulations, has remained a standing conjecture (QIF conjecture) for the entire duration of this thesis. Even a local stability analysis has proved elusive so far. Beyond the original motivations for considering non-monotone dynamics, this situation enhances the interest of studying non-monotone oscillators from a mathematical point of view.

In the chapter, we report both on several advances for the QIF conjecture and on related results for "QIF-like" oscillators. The chapter is organized as follows. In Section 6.1, we show how the dichotomic behavior of two "QIF-like" oscillators can be extended to larger networks. Section 6.2 highlights the difficulties that emerge with the study of large populations of non-monotone oscillators and suggests that a local analysis is sufficient to determine the behavior of the oscillators. In Section 6.3, we investigate the transition between the two dichotomic behaviors: a conservative limit case. The main advances on the QIF conjecture, which rely on a local stability analysis, are presented in Section 6.4. In Section 6.5, we propose an example of "QIF-like" oscillators that are not characterized by a dichotomic behavior, but by a more complex non-dichotomic behavior. Finally, the dichotomic behavior of infinite populations is considered in Section 6.6.

The main contributions of the chapter are the local stability results, on the one hand providing sufficient conditions to ensure that the behavior is dichotomic, and on the other hand

highlighting situations that cannot exhibit a dichotomic behavior. Some results presented in this chapter are published in [70] and in [74].

6.1 Dichotomic behavior: from two oscillators to large populations

Two pulse-coupled "QIF-like" oscillators (satisfying Assumption 1) are characterized by a dichotomic behavior (Proposition 3.3.2). The dichotomic behavior is a *global behavior*: depending on the conditions summarized in Table 6.1, the fixed point of the scalar firing map is either globally stable (phase-locked behavior) or globally anti-stable (synchronization). For $N > 2$ oscillators, we define the dichotomic behavior in the same way, as a *global behavior* that results from the global stability (phase-locked clustering) or anti-stability (synchronization) of the fixed point, according to the conditions summarized in Table 6.1.

Equivalent conditions	Phase-locked behavior (stable fixed point)	Synchronization (anti-stable fixed point)
Thresholds	$\underline{x} + \overline{x} > 0$	$\underline{x} + \overline{x} < 0$
Evolution function (2.4)	Concave-up in the mean	Concave-down in the mean
$Z(\theta) = Z_e(\theta - \overline{\theta})$ (2.14)	$\overline{\theta} < \pi$	$\overline{\theta} > \pi$
$h(\cdot + \Delta) = h^{-1}(\cdot) - \Delta$ (3.12)	$\Delta > 0$	$\Delta < 0$

Table 6.1: Equivalent conditions for the dichotomic behavior of "QIF-like" oscillators.

A first glimpse to understand the dichotomic behavior in large populations of "QIF-like" oscillators is the following observation. When "reversing" the thresholds $\underline{x}$ and $\overline{x}$, the firing map becomes similar to the inverse firing map.

Property 7. *Consider two models (a) and (b) that both have the same dynamics satisfying Assumption 1, but with different thresholds satisfying* $\underline{x}_{(a)} = -\overline{x}_{(b)}$ *and* $\overline{x}_{(a)} = -\underline{x}_{(b)}$ *(opposite values* $\underline{x} + \overline{x}$*). Then, the corresponding scalar firing maps satisfy* $h_{(b)} = h_{(a)}^{-1}$.

Proof. It follows from (2.15) and (2.17) that

$$\phi_{(b)}(x) = \frac{2\pi}{\omega} - \phi_{(a)}(x) \quad \text{and} \quad \phi_{(b)}^{-1}(\theta/\omega) = -\phi_{(a)}\Big((2\pi - \theta)/\omega\Big)\,,$$

so that (2.4) implies

$$f_{(b)}(\theta) = -f_{(a)}(2\pi - \theta) \quad \text{and} \quad f_{(b)}^{-1}(x) = 2\pi - f_{(a)}^{-1}(-x)\,.$$

Then, one has

$$h_{(b)} = f_{(b)}^{-1}\Big(f_{(b)}(2\pi - \theta) + \epsilon\Big) = 2\pi - f_{(a)}^{-1}\Big(-f_{(b)}(2\pi - \theta) - \epsilon\Big) = 2\pi - f_{(a)}^{-1}(\theta)\Big(f_{(a)} - \epsilon\Big) = h_{(a)}^{-1}\,.$$

□

Property 7 is the analog of Property 4 showing that the two models have mirrored iPRC's.

For higher dimensions, a noticeable difference is that $\mathbf{H_{(b)}} \neq \mathbf{H_{(a)}^{-1}}$: the equality holds, up to a linear change of coordinates. This is summarized as follows:

Proposition 6.1.1. *Consider the models (a) and (b) defined in Property 7. Then, the multidimensional firing maps satisfy*

$$\mathbf{H_{(b)}} = \mathbf{T^{-1}} \mathbf{H_{(a)}^{-1}} \mathbf{T}\,, \tag{6.1}$$

where $\mathbf{T} = \mathbf{PL}$*, with* $\mathbf{L}$ *given by* (3.29) *and with the permutation matrix*

$$\mathbf{P} = \begin{pmatrix} \mathbf{0} & & 1 \\ & \iddots & \\ 1 & & \mathbf{0} \end{pmatrix}.$$

Proof. We use the particular structure (3.28) of the firing map. It follows from Property 7 that $\mathbf{N_{(b)}} = \mathbf{N_{(a)}^{-1}}$. In addition, $\mathbf{N}$ is a repeated nonlinearity and is thus invariant under the permutation change of coordinates $\mathbf{P}$. Then, one obtains

$$\mathbf{H_{(b)}} = \mathbf{N_{(b)}} \mathbf{L} = \mathbf{N_{(a)}^{-1}} \mathbf{L} = \mathbf{P^{-1}} \mathbf{N_{(a)}^{-1}} \mathbf{P}\, \mathbf{L}\,.$$

It is easy to show that $\mathbf{LPL} = \mathbf{P}$ and one has finally

$$\mathbf{H_{(b)}} = (\mathbf{L^{-1}} \mathbf{P^{-1}} \mathbf{L^{-1}})\, \mathbf{N_{(a)}^{-1}} \mathbf{PL} = \mathbf{L^{-1}} \mathbf{P^{-1}}\, \mathbf{H_{(a)}^{-1}}\, \mathbf{PL} = \mathbf{T^{-1}} \mathbf{H_{(a)}^{-1}} \mathbf{T}\,.$$

□

Remark 6.1.1. The permutation matrix satisfies $\mathbf{P^{-1}} = \mathbf{P}$, so that the transformation matrix also satisfies $\mathbf{T^{-1}} = \mathbf{T}$. ◇

Property 7 and Proposition 6.1.1 give a first insight of the dichotomic behavior mechanism. When the thresholds are "reversed", the successive iterations of the new scalar firing map $h_{(b)}$ are the backward iterations of the former scalar firing map $h_{(a)}$. For higher dimensions, the successive iterations of firing map $\mathbf{H_{(b)}}$ are the backward iterations of the firing map $\mathbf{H_{(a)}}$, up to a change of coordinates. In particular, *when the thresholds are reversed, the stability of the fixed point is also reversed.* Depending on the thresholds (see Table 6.1), the firing map has two opposite time evolutions, resulting in two opposite behaviors with opposite stability. However, the property is not sufficient to prove the dichotomic behavior, since it does not imply a global convergence (or divergence) to the fixed point.

In addition, the two properties show a difference between the scalar firing map and its multidimensional generalization. Property 7 does not directly extend to higher dimensions but requires a change of variables, a fact which suggests that the stability analysis of the scalar case is not directly extended to higher dimensions (see also Section 6.3). Hence, generalizing the study of two oscillators to larger populations is not trivial: there is an increase of complexity between the stability analysis of the scalar firing map and the stability analysis of the multidimensional firing map.

6.2 Difficulties and limitations

For "QIF-like" oscillators, it is not obvious whether the dichotomic behavior shown with two oscillators still persist in larger populations. While large populations of QIF oscillators always seem to exhibit a dichotomic behavior, other "QIF-like" models exhibit non-dichotomic behaviors (Section 6.5). In other words, the known dichotomic behavior of the scalar firing map does not directly extend to higher dimensions, but depends on finer properties of the scalar firing map.

Numerical simulations clearly suggest that large populations of QIF oscillators have a dichotomic behavior. However, a global stability analysis showing that QIF oscillators have a (global) dichotomic behavior has so far remained an open problem, leading to the following conjecture.

Conjecture 1 ((Global) QIF conjecture)**.** *The behavior of QIF oscillators is always dichotomic. That is, for all $N_g \geq 2$, the fixed point of the $(N_g - 1)$-dimensional firing map is a global attractor whenever $\underline{x} + \overline{x} > 0$ and a global repeller whenever $\underline{x} + \overline{x} < 0$.*

It is obvious that the conjecture is verified in the case $\underline{x} > 0$ or in the case $\overline{x} < 0$, corresponding to a monotone dynamics (with known global stability results).

In this section, we explain why a global stability analysis is a problem that is more involved in the case of non-monotone dynamics. In addition, we show that a local analysis in the neighborhood of the fixed point is sufficient to have a good insight of the behaviors.

6.2.1 What is lost with non-monotone dynamics

In the case of monotone oscillators, the firing map is characterized by global stability results: the monotonicity property of the dynamics implies that the firing map is a contraction (Chapter 4). In contrast, when the dynamics is not monotone, the firing map is not a contraction, so that a global analysis is much more intricate (as illustrated in Figure 6.1).

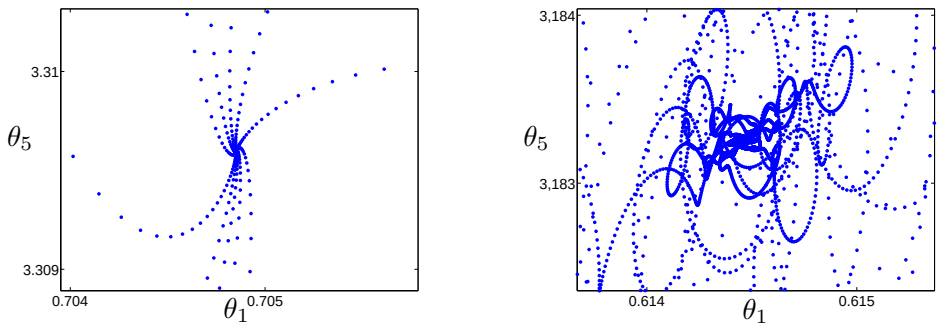

(a) Monotone dynamics

(b) Non-monotone QIF dynamics

Figure 6.1: The trajectory of the $(N_g - 1)$-dimensional firing map is more complex when the dynamics is not monotone. The figures represent a projection of the trajectory of the firing map in the neighborhood of the fixed point, with $\epsilon = 0.01$, $N_g = 10$, and with the dynamics (a) $\dot{x} = 0.2 + x$, $x \in [0, 1]$ and (b) $\dot{x} = 0.2 + x^2$, $x \in [-1, 1.5]$.

The global analysis of monotone oscillators fully exploits the special structure of the firing map. The (1-norm) distance between two trajectories is not modified by the linear map $\mathbf{L}$. In addition, the distance captures the monotonicity property of the nonlinear map $\mathbf{N}$: it is characterized by a monotone (increasing or decreasing) variation at each iteration of the nonlinear map. Thus, the distance is a quantity that has a monotone evolution at each iteration of the firing map $\mathbf{H} = \mathbf{N} \circ \mathbf{L}$.

For non-monotone oscillators, a similar approach does not work. Even though the same distance could be used with the same efficiency with respect to the linear map $\mathbf{L}$, difficulties arise with the nonlinear map $\mathbf{N}$. Indeed, the nonlinear map has no monotonicity property: it is contracting in a region of the state space and expanding in the complementary region. Then, the distance is not characterized by a monotone variation at each iteration.

With the monotonicity property, it is sufficient to consider only one iteration of the firing map to show the contraction. Without the monotonicity property, the contraction must be captured over several iterations $\mathbf{H}^n = \mathbf{N} \circ \mathbf{L} \circ \cdots \circ \mathbf{N} \circ \mathbf{L}$. The linear map is interpreted as a mixing map that spreads the trajectories over the whole state space, alternately in the contracting and expanding regions. As a result, the map is contracting (or expanding) in the mean over the successive iterations. For a $(N_g - 1)$-dimensional firing map, the property $(-\mathbf{L})^{N_g} = \mathbf{I}$ suggests that it could be necessary to consider $n = N_g$ iterations, that is, to consider the return map $\mathbf{R} = \mathbf{H}^{N_g}$.

The main difficulty is the mixing effect induced by the linear map, a process that is repeated at each iteration. Since the two maps $\mathbf{N}$ and $\mathbf{L}$ are not commutative, it is not obvious how to capture the contraction property of the nonlinear map while preserving the invariance of the linear map over more than one iteration. So far, the global analysis of the firing map has remained an open question (see Conjecture 1).

Remark 6.2.1 (Absorptions and clusters)**.** Another difference is that the result of Proposition 4.1.1 does not apply to non-monotone dynamics. After the initial phase of absorptions (described by the algorithm of Section 3.4.1), nothing precludes the clusters to aggregate through further absorptions. It is therefore more difficult to predict the final number of clusters N_g as well as the dimension $N_g - 1$ of the firing map dictating the evolution of the network. ◇

6.2.2 A local analysis for a global behavior

In Section 6.1, we have defined the dichotomic behavior as a global behavior of the oscillators. However, as explained in Section 6.2.1, it is difficult to obtain global stability results in the case of non-monotone dynamics. In this section, an intuitive argument shows that a *local analysis* in the neighborhood of the fixed point is actually convenient to describe the *global dichotomic behavior*.

We investigate how a set $\mathcal{A}$ of the state space is mapped by the firing map to the set

$$\mathbf{H}(\mathcal{A}) \triangleq \left\{ \boldsymbol{\Theta} \in [0, 2\pi]^{N_g - 1} \,|\, \mathbf{H}^{-\mathbf{1}}(\boldsymbol{\Theta}) \in \mathcal{A} \right\} .$$

For "QIF-like" oscillators, the overall behavior of the firing map is known. The following property shows that there exists a large set including the domain (3.21) that is invariant, either under the map $\mathbf{H}$ or under the map $\mathbf{H}^{-\mathbf{1}}$.

Property 8. *Consider a dynamics satisfying Assumption 1. Then, the corresponding* (N_g-1)*-dimensional firing map* ($N_g > 2$) *satisfies*

$$\begin{cases} \mathbf{H}(\tilde{\mathcal{U}}) \subset \tilde{\mathcal{U}} & \text{if } \underline{x} + \overline{x} > 0\,, \\ \tilde{\mathcal{U}} \subset \mathbf{H}(\tilde{\mathcal{U}}) & \text{if } \underline{x} + \overline{x} < 0\,, \end{cases}$$

where $\tilde{\mathcal{U}} \triangleq \left\{ \boldsymbol{\Theta} \in [0, h^{-1}(0)]^{N_g-1} \,|\, \theta_k < \theta_{k+1}, k = 1, \ldots, N_g - 2 \right\}$.

Proof. It is trivial that $\mathbf{L}\boldsymbol{\Theta} \in [0, h^{-1}(0)]^{N_g-1}$. Then, one has $\mathbf{H}(\boldsymbol{\Theta}) = \mathbf{N}(\mathbf{L}\boldsymbol{\Theta}) \in [0, h(0)]^{N_g-1}$. If $\underline{x} + \overline{x} > 0$, $\Delta > 0$ and it follows from Property 6 that $h^{-1}(0) = h(\Delta) + \Delta > h(0)$. Since $\mathbf{H}$ preserves the phase ordering, one verifies that $\mathbf{H}(\tilde{\mathcal{U}}) \subset \tilde{\mathcal{U}}$. For $\underline{x} + \overline{x} < 0$, the proof follows on similar lines. □

Remark 6.2.2. Property 8 is not valid with the natural domain of the firing map $\mathcal{U}$ (3.21), but with a larger set $\tilde{\mathcal{U}} \supset \mathcal{U}$. For instance, it is not true that $\mathbf{H}(\mathcal{U}) \subset \mathcal{U}$ if $\underline{x} + \overline{x} > 0$. Indeed, for some $\boldsymbol{\Theta} \in \mathcal{U}$, an absorption could occur, so that $\mathbf{H}(\boldsymbol{\Theta}) \notin \mathcal{U}$. ◇

Property 8 shows that the overall behavior of the firing map over $\tilde{\mathcal{U}}$ only depends on the sign of $\underline{x} + \overline{x}$. Whatever the "QIF-like" dynamics, the set $\tilde{\mathcal{U}}$ shrinks whenever $\underline{x} + \overline{x} > 0$ and stretches whenever $\underline{x} + \overline{x} < 0$. Interestingly, the overall behavior is always in agreement with the global behavior of the scalar firing map, and therefore with a dichotomic behavior (see Table 6.1).

The firing map is not characterized by a contraction property, as it is for monotone oscillators, but is characterized by an *average contraction* property. The firing map is *contracting in the mean* when $\underline{x} + \overline{x} > 0$, while it is *expanding in the mean* when $\underline{x} + \overline{x} < 0$.

Property 8 characterizes the behavior of the firing map, far from the fixed point. Then, a local stability analysis in the vicinity of the fixed point complements the study of the global behavior. A local analysis is not only significant to clearly suggest the global dichotomic behavior, but it is also sufficient to detect situations where the behavior cannot be dichotomic. When local stability is in agreement with the overall behavior, it suggests that the fixed point has global stability properties (dichotomic behavior). On the other hand, when local stability contradicts the overall behavior, it is sufficient to show that the fixed point is neither a global attractor nor a global repeller (non-dichotomic behavior) (Figure 6.2). In the latter case, the global dichotomic behavior of the scalar firing map does not extend to the multidimensional firing map.

In the sequel, local stability analysis confirms the (conjectured) dichotomic behavior for QIF oscillators and for exponential integrate-and-fire oscillators $\dot{x} = S \exp(x^2)$ (Section 6.4). The analysis also shows that piecewise linear integrate-and-fire oscillators $\dot{x} = S + \gamma|x|$ do not exhibit a dichotomic behavior (Section 6.5).

6.3 A conservative limit case

As a preamble to the study of the dichotomic behavior in large networks of "QIF-like" oscillators, we discuss the limit case characterized by $\underline{x} + \overline{x} = 0$ (or equivalently by $\Delta = 0$, $\overline{\theta} = \pi$, and by an function f with a zero mean-curvature). Even though it is a very particular

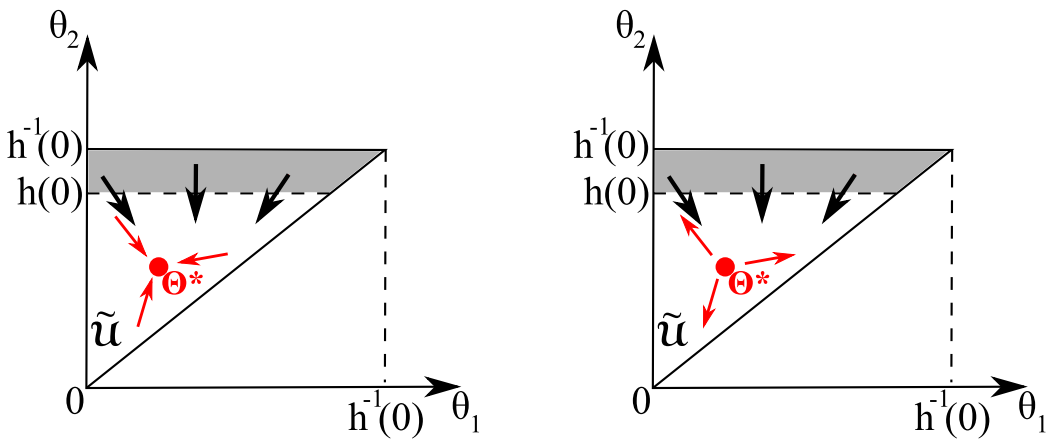

(a) Dichotomic behavior

(b) Non-dichotomic behavior

Figure 6.2: When $\underline{x} + \overline{x} > 0$, the overall behavior of the firing map suggests global stability (here in two dimensions). A local analysis complements the overall behavior of the firing map. (a) A locally stable fixed point is compatible with global stability (dichotomic behavior). (b) A locally unstable fixed point shows that the behavior is neither globally stable nor globally anti-stable (non-dichotomic behavior).

situation, the study is worth of interest: it provides an insight of the problem complexity for large populations of non-monotone oscillators, but is completely tractable through local analysis.

In the sequel, the parameters and values corresponding to the limit case are written with the "ˇ".

6.3.1 Quasiperiodic behavior

Since the limit case is characterized by $\Delta = 0$, it follows from Property 6 that $\check{h} = \check{h}^{-1}$: the trajectories of the scalar firing map are 2-periodic orbits. In a network of two clusters, a cluster has always the same phase at each firing of the other cluster.

For higher dimensions, however, the behavior of the firing map is not 2-periodic. Even though the nonlinear map satisfies $\check{\mathbf{N}} = \check{\mathbf{N}}^{-\mathbf{1}}$, one has the inequality $\check{\mathbf{H}} \neq \check{\mathbf{H}}^{-\mathbf{1}}$. Indeed, the two models (a) and (b) of Proposition 6.1.1 are identical, so that (6.1) implies $\check{\mathbf{H}} = \mathbf{T}^{-\mathbf{1}}\check{\mathbf{H}}^{-\mathbf{1}}\mathbf{T}$. Because of the transformation $\mathbf{T}$, two iterations of $\check{\mathbf{H}}$ do not yield the identity (Figure 6.3).

At least in the vicinity of the fixed point, numerical simulations show that the trajectories of the (discrete-time) firing map are *quasiperiodic trajectories on a dense orbit* (Figure 6.4). Several iterations of the firing map $\check{\mathbf{N}} \circ \mathbf{L} \circ \cdots \circ \check{\mathbf{N}} \circ \mathbf{L}$ never map a point $\boldsymbol{\Theta}$ to itself. The linear map $\mathbf{L}$ prevents successive nonlinear maps $\check{\mathbf{N}} = \check{\mathbf{N}}^{-\mathbf{1}}$ from combining to yield $\check{\mathbf{N}} \circ \check{\mathbf{N}} = \mathbf{I}$. Because of the (mixing) linear map, the firing map has no periodicity property, but seems to exhibit an aperiodic behavior.

In large networks, the clusters have a quasiperiodic behavior. At each firing of the same cluster, the other clusters have not fixed phases, but slightly drift away from their previous positions.

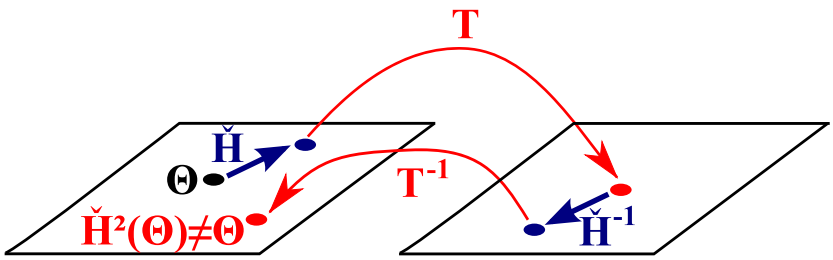

Figure 6.3: Two iterations of the firing map — that is, $\check{\mathbf{H}} \circ \check{\mathbf{H}} = \check{\mathbf{H}} \circ \mathbf{T}^{-1}\check{\mathbf{H}}^{-1}\mathbf{T}$ — do not map a point $\boldsymbol{\Theta}$ to itself. The mapping of the inverse $\check{\mathbf{H}}^{-1}$ is realized in other coordinates determined by the linear transformation $\mathbf{T}$.

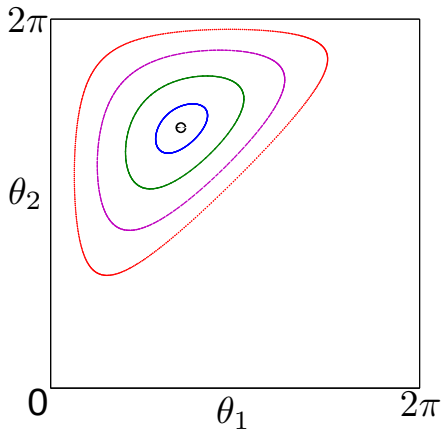

Figure 6.4: For different initial conditions, the trajectories of the discrete-time firing map are dense orbits encircling the fixed point (here in two dimensions).

Remark 6.3.1 (Monotone dynamics)**.** In contrast, the limit case for monotone dynamics is characterized by $dF/dx = 0$ and has a periodic behavior. In this situation, the scalar firing map is given by $\check{h}(\theta) = 2\pi - \theta + \epsilon$, so that the nonlinear map is $\check{\mathbf{N}} = (2\pi + \epsilon)\mathbf{1} - \mathbf{I}$, with $\mathbf{1} = (1, \cdots, 1)^T$. After N_g iterations of the $(N_g - 1)$-dimensional firing map $\check{\mathbf{N}} \circ \mathbf{L}$, all the cross terms induced by $(2\pi - \epsilon)\mathbf{1}$ cancel, while the last term $(-\mathbf{L})^{N_g} = \mathbf{I}$. Hence, the orbits are N_g-periodic, a simpler behavior than the quasiperiodic behavior of non-monotone dynamics.

For infinite populations, the equivalent situation is characterized by a constant iPRC. The continuum of oscillators evolves according to a standard transport equation whose solution is periodic (Remark 5.2.1). ◇

6.3.2 Marginal stability

The limit case is a conservative case: the fixed point is not a stable attractor nor an unstable repeller, but a *marginally stable center*. The Jacobian matrix at the fixed point has a palindromic characteristic polynomial with all its roots on the unit circle. This is the statement of Proposition 6.3.1.

A palindromic polynomial $p(z)$ is a polynomial with symmetric coefficients $p_k = p_{n-k}$. In full generality, such a polynomial has the following property: if λ is a root of p, then so is $1/\lambda$. With additional conditions, the roots can lie on the unit circle [62, 96]. In the case we are interested in, the polynomial coefficients are sorted and the following lemma shows that the roots are on the unit circle.

Lemma 6.3.1. *Let $p(z)$ be a polynomial with real coefficients*

$$p(z) = p_n z^n + p_{n-1} z^{n-1} + p_{n-2} z^{n-2} + \cdots + p_2 z^2 + p_1 z + p_0 \,,$$

such that

- $p_k = p_{n-k}$ $\forall k$,
- $p_n \geq p_{n-1} \geq \ldots p_{\lfloor n/2 \rfloor} > 0$, *with $\lfloor n/2 \rfloor$ denoting the integer part of $n/2$.*

Then all n roots of p are distinct and lie on the unit circle.

Proof. The proof, which is due to J. Hendrickx and A. Megretski, is not detailed in the present manuscript. The trick of the proof is to multiply the polynomial by $(z-1)$. Then it is straightforward to show that there exist $\lfloor n/2 \rfloor$ distinct values $\theta \in (0, \pi)$ such that $p(e^{\theta}) = p(e^{-\theta}) = 0$. If n is odd, -1 is the nth root. □

Remark 6.3.2. Beyond its present application to the local stability analysis of the firing map, the result of Lemma 6.3.1 on palindromic polynomials has noticeable implications. The result implies that the trigonometric equation

$$a_n \cos n\theta + a_{n-1} \cos(n-1)\theta + \cdots + a_1 \cos\theta + a_0 = 0 \,,$$

with $a_n \geq a_{n-1} \geq \cdots \geq a_0 > 0$, has n distinct real solutions on $[0, \pi]$. Equivalently, linear combinations of Chebyshev polynomials [90] have n roots on $[-1, 1]$, if the weighted coefficients are sorted.

To the author's knowledge, Lemma 6.3.1 is a new result among the numerous studies on the zeros of palindromic polynomials (e.g. [62, 96]) and on the zeros of linear combinations of Chebyshev polynomials (e.g. [8]). ◇

With Lemma 6.3.1, the result of Proposition 6.3.1 is proved.

Proposition 6.3.1. *If the dynamics satisfies Assumption 1 with thresholds such that $\underline{x} + \overline{x} = 0$, then the fixed point of the $(N_g - 1)$-dimensional firing map is locally marginally stable, for all $N_g \geq 2$.*

Proof. The characteristic polynomial of the $(N_g - 1) \times (N_g - 1)$ Jacobian matrix at the fixed point is given by (see (4.1))

$$\check{p}(z) = \sum_{k=0}^{N_g-1} \check{p}_k \, z^k = z^{N_g-1} + \check{h}'_{N_g-2} z^{N_g-2} + \check{h}'_{N_g-3} \check{h}'_{N_g-2} z^{N_g-3} + \cdots + \prod_{k=1}^{N_g-2} \check{h}'_k z + \prod_{k=0}^{N_g-2} \check{h}'_k \,,$$

with $\check{h}'_0 = |\check{h}'(\check{\theta}^*_{N_g-1})|$ and $\check{h}'_k = |\check{h}'(\check{\theta}^*_{N_g-1} - \check{\theta}^*_k)|$ for $k = 1, \ldots, N_g - 2$.

Next, one shows that the characteristic polynomial $\check{p}(z)$ is palindromic. First, the fixed point satisfies $\check{\mathbf{H}}^{-\mathbf{1}}(\check{\mathbf{\Theta}}^*) = \check{\mathbf{\Theta}}^*$. Then, it follows from the relationship $\check{\mathbf{H}} = \mathbf{T}^{-\mathbf{1}}\check{\mathbf{H}}^{-\mathbf{1}}\mathbf{T}$ that $\check{\mathbf{H}}(\mathbf{T}\check{\mathbf{\Theta}}^*) = \mathbf{T}\check{\mathbf{\Theta}}^*$. Since the fixed point is unique (Proposition 3.4.1), one has the equality $\mathbf{T}\check{\mathbf{\Theta}}^* = \check{\mathbf{\Theta}}^*$, or equivalently, $\mathbf{L}\check{\mathbf{\Theta}}^* = \mathbf{P}\check{\mathbf{\Theta}}^*$. Then, it follows that

$$\check{h}'_k = \left|\check{h}'(\check{\theta}^*_{N_g-1} - \check{\theta}^*_k)\right| = \left|\check{h}'(\check{\theta}^*_{N_g-1-k})\right| = \left|\check{h}'\Big(h(\check{\theta}^*_{N_g-1} - \check{\theta}^*_{N_g-2-k})\Big)\right| \qquad k = 1, \dots, N_g - 2$$

and

$$\check{h}'_0 = \left|\check{h}'\Big(\check{h}(\check{\theta}^*_{N_g-1} - \check{\theta}^*_{N_g-2})\Big)\right| .$$

Property $\check{h} = \check{h}^{-1}$ implies that

$$\check{h}'(\theta) = (\check{h}^{-1}(\theta))' = \Big[\check{h}'\Big(\check{h}^{-1}(\theta)\Big)\Big]^{-1} = \Big[\check{h}'\Big(\check{h}(\theta)\Big)\Big]^{-1}$$

and, therefore,

$$\check{h}'_k\, \check{h}'_{N_g-2-k} = 1 \qquad k = 0, \dots, N_g - 2 \,. \tag{6.2}$$

Hence, one has $\check{p}_k = \check{p}_{N_g-2-k}$ and the polynomial is palindromic.

In addition, it follows from (3.14) of Property 6 that $\check{h}'_k < 1 \;\forall k > \lfloor (N_g-1)/2 \rfloor$, so that $\check{p}_{N_g-1} \geq \check{p}_{N_g-2} \geq \cdots \geq \check{p}_{\lfloor (N_g-1)/2 \rfloor} > 0$. Then, Lemma 6.3.1 implies that all the eigenvalues (roots of $\check{p}(z)$) lie on the unit circle, which completes the proof. □

Proposition 6.3.1 shows that, whatever the "QIF-like" dynamics, the limit case is characterized by a marginally stable fixed point, a conservative behavior between the two opposite behaviors ($\underline{x} + \overline{x} > 0$ and $\underline{x} + \overline{x} < 0$). In addition, the local stability analysis is completely tractable. Interestingly, this is in contrast with the open problems encountered in the situations $\underline{x} + \overline{x} \lesseqgtr 0$.

6.4 Advances on the QIF conjecture

As shown in Conjecture 1, the global stability analysis of QIF oscillators is an open problem. Interestingly, even a local stability analysis is elusive, so that the local stability problem yields a second conjecture on the dichotomic behavior of QIF oscillators. We report on several advances on this second conjecture.

6.4.1 A second conjecture

We claim that the local stability of the QIF oscillators is in agreement with a dichotomic behavior. After deriving a general expression for the characteristic polynomial of the Jacobian matrix, we conjecture that, in the case of QIF oscillators, all the eigenvalues are inside the unit disk whenever $\underline{x} + \overline{x} > 0$.

In full generality, the characteristic polynomial of the $(N_g - 1) \times (N_g - 1)$ Jacobian matrix at the fixed point is given by

$$p(z) = \sum_{k=0}^{N_g-1} p_k\, z^k = z^{N_g-1} + \sum_{k=0}^{N_g-2} z^k \prod_{j=k}^{N_g-2} h'_j \,, \tag{6.3}$$

with $h'_0 = |h'(\theta^*_{N_g-1})|$ and $h'_k = |h'(\theta^*_{N_g-1} - \theta^*_k)|$ for $k = 1, \ldots, N_g - 2$.

From the fixed point equation, it follows that

$$\left\{\begin{array}{lcl} f(\theta^*_1) & = & f(2\pi - \theta^*_{N_g-1}) + \epsilon \\ f(\theta^*_2) & = & f(2\pi - \theta^*_{N_g-1} + \theta^*_1) + \epsilon \\ & \vdots & \\ f(\theta^*_{N_g-1}) & = & f(2\pi - \theta^*_{N_g-1} + \theta^*_{N_g-2}) + \epsilon \end{array}\right. . \tag{6.4}$$

Then, (3.10) implies

$$h'_j = \frac{F(f(\theta^*_{j+1}) - \epsilon)}{F(f(\theta^*_{j+1}))} = \frac{F(x^*_{j+1})}{F(x^*_{j+1} + \epsilon)}\,, \tag{6.5}$$

where one has introduced the notation $x^*_j = f(\theta^*_j) - \epsilon$.

In addition, the x^*_i's can be determined through the fixed point equation. Given (6.4), one writes

$$\left\{\begin{array}{lcl} f^{-1}(x^*_1) & = & 2\pi - \theta^*_{N_g-1} = 2\pi - f^{-1}(x^*_{N_g-1} + \epsilon) \\ f^{-1}(x^*_2) & = & 2\pi - \theta^*_{N_g-1} + \theta^*_1 = 2\pi - f^{-1}(x^*_{N_g-1} + \epsilon) + f^{-1}(x^*_1 + \epsilon) \\ & \vdots & \\ f^{-1}(x^*_n) & = & 2\pi - \theta^*_{N_g-1} + \theta^*_{N_g-2} = 2\pi - f^{-1}(x^*_{N_g-1} + \epsilon) + f^{-1}(x^*_{N_g-2} + \epsilon) \end{array}\right. ,$$

and it follows from the definition of f [see (2.5) and (2.4)] that the x^*_j's are determined by

$$\left\{\begin{array}{lcl} \int_{\underline{x}}^{x^*_1} \frac{1}{F(s)}\, ds & = & \int_{x^*_{N_g-1}+\epsilon}^{\overline{x}} \frac{1}{F(s)}\, ds \\ \int_{x^*_1+\epsilon}^{x^*_2} \frac{1}{F(s)}\, ds & = & \int_{x^*_{N_g-1}+\epsilon}^{\overline{x}} \frac{1}{F(s)}\, ds \\ & \vdots & \\ \int_{x^*_{N_g-2}+\epsilon}^{x^*_{N_g-1}} \frac{1}{F(s)}\, ds & = & \int_{x^*_{N_g-1}+\epsilon}^{\overline{x}} \frac{1}{F(s)}\, ds \end{array}\right. . \tag{6.6}$$

With a QIF dynamics, numerical simulations suggest great evidence that the eigenvalues — that is, the roots of (6.3) — are asymptotically stable whenever $\underline{x} + \overline{x} > 0$, a fact that reinforces Conjecture 1 on the dichotomic behavior of QIF oscillators. The following conjecture, summarizing (6.3), (6.5), and (6.6), is a weak (local) version of Conjecture 1.

Conjecture 2 (Local QIF conjecture)**.** *For the QIF model $F(x) = S + x^2$ and for all $N_g \geq 2$, the fixed point of the $(N_g - 1)$-dimensional firing map is locally stable if and only if $\underline{x} + \overline{x} > 0$. In other words, all the roots of the polynomial*

$$p(z) = z^{N_g-1} + \sum_{k=0}^{N_g-2} z^k \prod_{j=k+1}^{N_g-1} \frac{F(x^*_j)}{F(x^*_j + \epsilon)}\,, \tag{6.7}$$

with

$$\int_{\underline{x}}^{x^*_1} \frac{1}{F(x)}\, dx = \int_{x^*_j+\epsilon}^{x^*_{j+1}} \frac{1}{F(x)}\, dx = \int_{x^*_{N_g-1}+\epsilon}^{\overline{x}} \frac{1}{F(x)}\, dx \qquad 1 \leq j \leq N_g - 2\,, \tag{6.8}$$

are inside the unit disk if and only if $\underline{x} + \overline{x} > 0$.

When $\underline{x}+\overline{x}=0$, it is straightforward that (6.7) is a palindromic polynomial, corresponding to the conservative limit case studied in Section 6.3.2.

The proof of Conjecture 2 should rely on two points: (i) extract from (6.8) the essential properties of the x_j^*'s, and (ii) use the resulting properties of (6.7) to determine the location of the roots. In the sequel, we present some advances on Conjecture 2.

6.4.2 The case of three clusters

A network of $N_g=3$ clusters, with a QIF dynamics, is characterized by a dichotomic behavior. Indeed, Conjecture 2 can be solved for a polynomial of degree $N_g-1=2$.

We consider the function $F_\epsilon(x)=F(x)/F(x+\epsilon)$, which plays a key role in the local stability analysis, since it determines the coefficients of the polynomial (6.7). As shown in Figure 6.5, the graph of $F_\epsilon(\cdot)$, which corresponds to a QIF dynamics, has two extrema for the values

$$\begin{aligned} x_e^{(1)} &= \frac{-\epsilon-\sqrt{\epsilon^2+4S}}{2}, \\ x_e^{(2)} &= \frac{-\epsilon+\sqrt{\epsilon^2+4S}}{2}. \end{aligned} \tag{6.9}$$

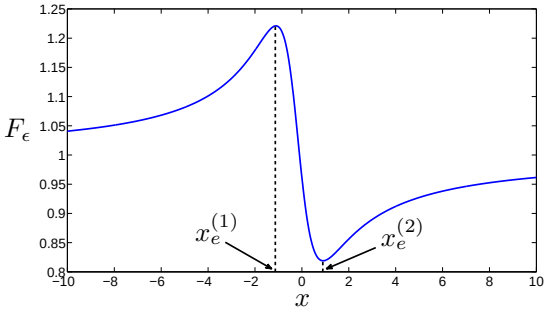

Figure 6.5: For the QIF model $F(x)=S+x^2$, the function $F_\epsilon(x)=F(x)/F(x+\epsilon)$ has two extrema, at $x=x_e^{(1)}$ and $x=x_e^{(2)}$.

The QIF model is characterized by a noticeable property: the two values (6.9) satisfy

$$\int_{-\infty}^{x_e^{(1)}} \frac{1}{F(x)}dx = \frac{1}{2}\int_{x_e^{(1)}+\epsilon}^{x_e^{(2)}} \frac{1}{F(x)}dx = \int_{x_e^{(2)}+\epsilon}^{\infty} \frac{1}{F(x)}dx = \frac{1}{\sqrt{S}}\arctan\left(\frac{-\epsilon+\sqrt{\epsilon^2+4S}}{2\sqrt{S}}\right). \tag{6.10}$$

In the case of $N_g-1=2$, the property is of great interest when compared with (6.8) and Conjecture 2 can be solved.

Proposition 6.4.1. *For the QIF model, the fixed point of the 2-dimensional firing map is locally stable if and only if* $\underline{x}+\overline{x}>0$.

Proof. We consider the different positions of x_1^* and x_2^* with respect to the extremum values $x_e^{(1)}$ and $x_e^{(2)}$, when $\underline{x}+\overline{x}>0$.

- $\mathbf{x_1^* \leq x_e^{(1)}}$ **and** $\mathbf{x_2^* \leq x_e^{(2)}}$
  With these conditions, we have $x_1^* + x_2^* \leq -\epsilon$. It follows from condition (6.8), that is

$$\int_{\underline{x}}^{x_1^*} \frac{1}{F(x)} dx = \int_{x_1^*+\epsilon}^{x_2^*} \frac{1}{F(x)} dx = \int_{x_2^*+\epsilon}^{\overline{x}} \frac{1}{F(x)} dx \,, \tag{6.11}$$

  that $x_1^* + (x_2^* + \epsilon) > 0$ since $\underline{x} + \overline{x} > 0$ and since $1/F(x)$ is even. However, this is in contradiction with the above condition. The situation is thus impossible.

- $\mathbf{x_e^{(1)} \leq x_1^* < x_2^* \leq 0}$
  Since $x_1^* + \epsilon < x_2^*$, the conditions imply $x_1^* + x_2^* + \epsilon < 2x_2^* \leq 0$. But again, it follows from (6.11) and $\underline{x} + \overline{x} > 0$ that $x_1^* + x_2^* + \epsilon > 0$. There is a contradiction and the situation is impossible.

- $\mathbf{x_1^* \leq x_e^{(1)}}$ **and** $\mathbf{x_2^* \geq x_e^{(2)}}$
  It follows from (6.11) that

$$\int_{x_e^{(1)}+\epsilon}^{x_e^{(2)}} \frac{1}{F(x)} dx \leq \int_{x_1^*+\epsilon}^{x_2^*} \frac{1}{F(x)} dx = \int_{x_2^*+\epsilon}^{\overline{x}} \frac{1}{F(x)} dx \leq \int_{x_e^{(2)}+\epsilon}^{\infty} \frac{1}{F(x)} dx.$$

  This is in contradiction with the relationship (6.10) imposing

$$\int_{x_e^{(1)}+\epsilon}^{x_e^{(2)}} \frac{1}{F(x)} dx > \int_{x_e^{(2)}+\epsilon}^{\infty} \frac{1}{F(x)} dx.$$

  The situation is thus impossible.

- $\mathbf{0 \leq x_1^* < x_2^*}$
  In this case, $F_\epsilon(x) < 1 \; \forall x \in [\underline{x}, \overline{x}]$. By the Eneström-Kakeya theorem [48], the two roots of the polynomial (6.7), that is

$$p(z) = z^2 + F_\epsilon(x_2^*) z + F_\epsilon(x_1^*) F_\epsilon(x_2^*) \,, \tag{6.12}$$

  are inside the unit disk.

- $\mathbf{x_e^{(1)} \leq x_1^* \leq 0 \leq x_2^* \leq x_e^{(2)}}$
  It follows from $\underline{x} + \overline{x} > 0$ and (6.11) that $x_1^* + x_2^* + \epsilon > 0$. In addition, for any situation $x_1^* + x_2^* + \epsilon = 0$, one easily shows that $F_\epsilon(x_1^*) F_\epsilon(x_2^*) = 1$. Then, we consider without loss of generality a transition from $x_1^* + x_2^* + \epsilon = 0$ to $x_1^* + x_2^* + \epsilon > 0$ where x_1^* remains constant while x_2^* increases. Since $dF_\epsilon/dx < 0$ for all $x \in (x_e^{(1)}, x_e^{(2)})$, it follows that $F_\epsilon(x_1^*) F_\epsilon(x_2^*) < 1$. As $F_\epsilon(x_2^*) < 1$ holds, the polynomial (6.12) has all its roots inside the unit disk.

- $\mathbf{x_e^{(1)} \leq x_1^* \leq 0}$ **and** $\mathbf{x_2^* \geq x_e^{(2)}}$
  Since $F_\epsilon(x_2^*) < 1$, it remains to show that $F_\epsilon(x_1^*) F_\epsilon(x_2^*) < 1$ in order to prove that the polynomial (6.12) has all its roots inside the unit circle.

  We first consider the case $\overline{x} = \infty$. Since $x_e^{(1)} + \epsilon = -x_e^{(2)}$, it follows from (6.10) that

$$\int_0^{x_e^{(2)}} \frac{1}{F(x)} dx = \int_{x_e^{(2)}+\epsilon}^{\infty} \frac{1}{F(x)} dx.$$

Then, (6.11) implies that $x_1^* = -\epsilon$ when $x_2^* = x_e^{(2)}$. If $x_1^* > -\epsilon/2$, then $F_\epsilon(x_1^*) < 1$ and it directly follows that $F_\epsilon(x_1^*)F_\epsilon(x_2^*) < 1$. As a consequence, we only focus on the critical interval $(x_1^*, x_2^*) \in \mathcal{I} = [-\epsilon, -\epsilon/2] \times [x_e^{(2)}, x_\star^{(2)}]$, where $x_\star^{(2)} > x_e^{(2)}$ is computed from (6.11) such that $x_2^* = x_\star^{(2)}$ when $x_1^* = -\epsilon/2$ (Figure 6.6). When varying the threshold $\underline{x}$, the variation of x_1^* as a function of x_2^* is obtained from (6.11) and we have

$$x_1^*(x_2^*) = \frac{(x_2^*)^2 - \epsilon x_2^* - S - \epsilon^2}{2x_2^* + \epsilon}.$$

The equation $F_\epsilon(x_1^*(x_2^*))F_\epsilon(x_2^*) = 1$ has two real roots

$$x_2^* = \begin{cases} \left(-\epsilon - \sqrt{\epsilon^2 + 3S}\right)/3 & < 0 \\ \left(-\epsilon + \sqrt{\epsilon^2 + 3S}\right)/3 & < x_e^{(2)} \end{cases},$$

so that $F_\epsilon(x_1^*)F_\epsilon(x_2^*) \neq 1$ for every pair $(x_1^*, x_2^*) \in \mathcal{I}$. Since the product is continuous on $\mathcal{I}$ and $F_\epsilon(-\epsilon/2)F_\epsilon(x_\star^{(2)}) = F_\epsilon(x_\star^{(2)}) < 1$, one obtains that $F_\epsilon(x_1^*)F_\epsilon(x_2^*) < 1 \; \forall (x_1^*, x_2^*) \in \mathcal{I}$.

Next, we show that the proof still holds for any $\overline{x} < \infty$. Without loss of generality, we consider a transition from $\overline{x} = \infty$ to $\overline{x} < \infty$, where the value x_1^* remains constant while the value x_2^* decreases. Since $dF_\epsilon/dx > 0$ for $x > x_e^{(2)}$, the product $F_\epsilon(x_1^*)F_\epsilon(x_2^*)$ decreases and still satisfies $F_\epsilon(x_1^*)F_\epsilon(x_2^*) < 1$ when $\overline{x} < \infty$.

□

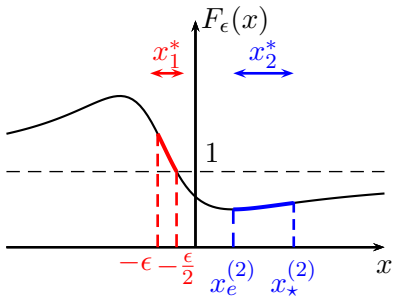

Figure 6.6: The critical interval $\mathcal{I}$, with $-\epsilon \leq x_1^* \leq -\epsilon/2$ and $x_e^{(2)} \leq x_2^* \leq x_\star^{(2)}$.

Proposition 6.4.1 shows that the clustering configuration of $N_g = 3$ clusters (of QIF oscillators) is locally stable when $\underline{x} + \overline{x} > 0$. The (local) conjecture on the dichotomic behavior of the QIF oscillators is then verified for three clusters.

To prove local stability in dimensions $N_g - 1 > 2$, a similar argument fails. The proof of Proposition 6.4.1 uses Property (6.10), which can only be related to the conditions (6.8) when $N_g - 1 = 2$. As a consequence, there is no hope to generalize the proof to higher dimensions and a general proof of Conjecture 2 must rely on a different approach.

6.4.3 Curvature of the scalar firing map: a sufficient condition

With the condition $h''(\theta) < 0 \; \forall \theta$, a local stability analysis is tractable and suggests that the behavior is dichotomic. This result solves Conjecture 2 for a certain range of parameters and shows that exponential integrate-and-fire oscillators have always a dichotomic behavior.

As a preliminary to this result, we need the following lemma.

Lemma 6.4.1. *Let*

$$p(z) = a_n b_n z^n + a_{n-1} b_{n-1} z^{n-1} + \cdots + a_0 b_0. \tag{6.13}$$

If the following conditions hold:

- $a_n > a_{n-1} > \cdots > a_0 > 0$,
- $b_{n-k} = b_k \ \forall k$,
- *The sequence* $\{b_0, b_1, \ldots, b_n\}$ *is positive and convex, i.e.* $b_k > 0$ *for all* k *and* $b_k - b_{k-1} \leq b_{k+1} - b_k$ *for* $k = 1, \ldots, n-1$,

then all roots of $p(z)$ *are strictly inside the unit disk.*

Proof. The proof is not detailed here. Refer to [70] for a detailed sketch of the proof and to [71] for the complete proof. □

The coefficients b_j are the coefficients of a palindromic polynomial, so that Lemma 6.4.1 is a generalization of Lemma 6.3.1.

Under the assumption $h''(\theta) < 0 \ \forall \theta$, the local stability of the multidimensional firing maps is established through Lemma 6.4.1.

Theorem 6.4.1. *Provided that the dynamics satisfies Assumption 1 and that the corresponding scalar firing map verifies* $h''(\theta) < 0 \ \forall \theta \in [0, 2\pi]$*, the fixed point of the* $(N_g - 1)$*-dimensional firing map* $(N_g > 2)$ *is locally stable if and only if* $\underline{x} + \overline{x} > 0$.

Proof. The derivative h' is related to F_ϵ through (3.10) and $h'' < 0 \ \forall \theta \in [0, 2\pi]$ implies $dF_\epsilon/dx < 0 \ \forall x \in [\underline{x}, \overline{x}]$.

First, let's consider an upper threshold $\breve{\overline{x}} = -\underline{x}$ so that we have the conservative limit case $\underline{x} + \breve{\overline{x}} = 0$. To this situation corresponds the coefficients $\breve{h}'_j$ (see Section 6.3.2). If one increases the upper threshold to recover the initial value $\overline{x}$ (that is, to recover $\underline{x} + \overline{x} > 0$), (6.8) implies that all the values x_j^* increase. Since F_ϵ is decreasing, it follows from (6.5) that the values h'_j decrease and can therefore be expressed as the decomposition

$$h'_j = \alpha_j \breve{h}'_j, \quad j = 0, \cdots, N_g - 2\,, \tag{6.14}$$

with $0 < \alpha_j < 1$. In addition, it follows from the assumption $h'' < 0$ that

$$0 < \breve{h}'_j < \breve{h}'_{j-1}, \quad j = 1, \cdots, N_g - 2\,. \tag{6.15}$$

Next, we show that the characteristic polynomial (6.3) is of the form of (6.13). Setting $a_{N_g-1} = b_{N_g-1} = 1$ and

$$a_k = \prod_{j=k}^{N_g-2} \alpha_j, \quad b_k = \prod_{j=k}^{N_g-2} \breve{h}'_j, \quad k = 0, \cdots, N_g - 2\,,$$

the inequality $0 < \alpha_j < 1$ leads to $a_{N_g-1} > a_{N_g-2} > \cdots > a_0 > 0$ and (6.2) implies $b_{N_g-1-k} = b_k$. Finally, it follows from $(\breve{h}'_k - 1)^2 \geq 0$ and $\breve{h}'_{k-1} > \breve{h}'_k$ (6.15) that $\breve{h}'_k \breve{h}'_{k-1} + 1 - 2\breve{h}'_k \geq 0$. Since $\breve{h}'_k = b_k / b_{k+1}$, one has the convexity condition $b_k - b_{k-1} \leq b_{k+1} - b_k$ for $k = 1, \cdots, N_g - 2$. Since the characteristic polynomial (6.3) satisfies the assumptions of Lemma 6.4.1, all the eigenvalues are inside the unit disk and the fixed point is locally stable, which concludes the proof. □

Through Theorem 6.4.1, the curvature condition on the scalar firing map appears as a sufficient condition to ensure that the behavior of large networks is dichotomic. In other words, this is a sufficient condition on the scalar firing map to extend the stability properties of the scalar firing map to higher dimensions.

Theorem 6.4.1 yields important corollaries. Even though the QIF model does not satisfy the property $h''(\theta) < 0 \ \forall \theta \in [0, 2\pi]$ in full generality, Theorem 6.4.1 solves Conjecture 2 when the thresholds are between two bounds. The first corollary is summarized as follows:

Corollary 6.4.1. *For the QIF model and for all $N_g \geq 2$, the fixed point of the $(N_g - 1)$-dimensional firing map is locally stable if and only if $\underline{x} + \overline{x} > 0$, provided that $\underline{x} > x_e^{(1)}$ and $\overline{x} < x_e^{(2)}$ [see (6.9)].*

Proof. The function $F_\epsilon(x)$ is strictly decreasing for all $x \in (x_e^{(1)}, x_e^{(2)})$. Then, (3.10) implies that $h''(\theta) < 0 \ \forall \theta \in [0, 2\pi]$ if $[\underline{x}, \overline{x}] \subset (x_e^{(1)}, x_e^{(2)})$. The result follows from Theorem 6.4.1. □

The second Corollary clearly suggests that oscillators with an exponential integrate-and-fire dynamics always exhibit a dichotomic behavior. This is of interest since they have a dynamics similar to the dynamics of QIF oscillators.

Corollary 6.4.2. *For the exponential vector field $F(x) = S \exp(x^2)$ and for all $N_g \geq 2$, the fixed point of the $(N_g - 1)$-dimensional firing map is locally stable if and only if $\underline{x} + \overline{x} > 0$.*

Proof. The function $F_\epsilon(x) = \exp\big(-(2\epsilon x + \epsilon^2)\big)$ is strictly decreasing on $\mathbb{R}$. Then, (3.10) implies that $h''(\theta) < 0 \ \forall \theta \in [0, 2\pi]$ and the result follows from Theorem 6.4.1. □

Asymptotic limit of measures. The curvature condition $h'' < 0$ is sufficient to solve the local stability problem. Interestingly, the condition is also sufficient to obtain global results in dimension $N_g - 1 = 2$. The following proposition characterizes the asymptotic limit of the Lebesgue measure of a set, under the iterations of the firing map.

Proposition 6.4.2. *Consider a dynamics satisfying Assumption 1 and such that the scalar firing map satisfies $h''(\theta) < 0 \ \forall \theta$. Then, for any set $\mathcal{A} \subseteq \mathcal{U}$, the corresponding 2-dimensional firing map ($N_g > 2$) satisfies*

$$\begin{cases} \lim_{n\to\infty} \mu_L \left[\mathbf{H}^{\mathbf{n}}(\mathcal{A})\right] = 0 & \text{if } \underline{x} + \overline{x} > 0\,, \\ \lim_{n\to\infty} \mu_L \left[\mathbf{H}^{-\mathbf{n}}(\mathcal{A})\right] = 0 & \text{if } \underline{x} + \overline{x} < 0\,, \end{cases}$$

where μ_L is the Lebesgue measure.

Proof. We first consider the case $\underline{x} + \overline{x} > 0$. With the Jacobian matrix $\mathbf{J}$, one has

$$\mu_L \left[\mathbf{H}^{\mathbf{n}}(\mathcal{A})\right] = \int_{\mathcal{A}} \prod_{k=0}^{n-1} \det \Big[\mathbf{J}\big(\mathbf{H}^{\mathbf{k}}(\mathbf{\Theta})\big)\Big] \ \mu(d\mathbf{\Theta}) = \int_{\mathcal{A}} \prod_{k=0}^{n-1} |h'(\theta_1^{(k)})\, h'(\theta_2^{(k)})| \, \mu_L(d\theta_1 d\theta_2)\,,$$

where $\mathbf{\Theta}^{(k)} = (\theta_1^{(k)}, \theta_2^{(k)})$, $k \in \mathbb{N}$, is a trajectory of

$$\begin{aligned} \theta_1^{(k+1)} &= h(\theta_2^{(k)}) \\ \theta_2^{(k+1)} &= h(\theta_2^{(k)} - \theta_1^{(k)}) \end{aligned}$$

with the initial condition $(\theta_1^{(0)}, \theta_2^{(0)}) = (\theta_1, \theta_2)$. Then, one writes

$$\begin{aligned}\mu_L\left[\mathbf{H^n}(\mathcal{A})\right] &= \int_{\mathcal{A}} \left|h'(\theta_1^{(0)})\, h'(\theta_2^{(n-1)})\right| \prod_{k=0}^{n-2} \left|h'(\theta_1^{(k+1)})\, h'(\theta_2^{(k)})\right| \, \mu_L(d\theta_1 d\theta_2)\,, \\ &= \int_{\mathcal{A}} \left|h'(\theta_1^{(0)})\, h'(\theta_2^{(n-1)})\right| \prod_{k=0}^{n-2} \left|h'(h(\theta_2^{(k)}))\, h'(\theta_2^{(k)})\right| \, \mu_L(d\theta_1 d\theta_2)\,, \\ &\leq \left[\max_{\theta} \Big(\left|h'(\theta)\, h'(h(\theta))\right| \Big)\right]^n \max\Big(\left|h'(\theta_1^{(0)})\, h'(\theta_2^{(n-1)})\right| \Big)\, \mu_L[\mathcal{A}]\,.\end{aligned} \tag{6.16}$$

Next, Property 6 yields $h\big(h(\theta)+\Delta\big) = \theta - \Delta$ with $\Delta > 0$ and it follows that

$$\left|h'\big(h(\theta)+\Delta\big)\, h'(\theta)\right| = 1$$

Since $h' < 0$ and $h'' < 0$, one has $\left|h'\big(h(\theta)+\Delta\big)\right| > \left|h'\big(h(\theta)\big)\right|$ so that $\left|h'(\theta)\, h'\big(h(\theta)\big)\right| < 1 \ \forall \theta$, which implies that

$$\max_{\theta} \Big(\left|h'(\theta)\, h'\big(h(\theta)\big)\right| \Big) \triangleq C_1 < 1\,. \tag{6.17}$$

In addition, Property 8 implies that $\mathbf{H}(\tilde{\mathcal{U}}) \subset \tilde{\mathcal{U}}$ so that $\theta_2^{(n-1)} \in [0, h^{-1}(0)]$ and $h'(\theta_2^{(n-1)})$ is bounded. Then, one has

$$\max\Big(\left|h'(\theta_1^{(0)})\, h'(\theta_2^{(n-1)})\right| \Big) = \max_{\theta \in [0, h^{-1}(0)]} \Big(\left|h'(\theta)\right|^2 \Big) \triangleq C_2 < \infty\,. \tag{6.18}$$

Injecting (6.17) and (6.18) in (6.16) yields $\mu_L\left[\mathbf{H^n}(\mathcal{A})\right] \leq C_1^n\, C_2\, \mu_L[\mathcal{A}]$, and $\mu_L\left[\mathbf{H^n}(\mathcal{A})\right] \to 0$ when $n \to \infty$.

The proof for the case $\underline{x} + \overline{x} < 0$ relies on the proof for the case $\underline{x} + \overline{x} > 0$. Consider the firing maps $\mathbf{H_{(a)}}$ and $\mathbf{H_{(b)}}$ corresponding respectively to $\underline{x}_{(a)} + \overline{x}_{(a)} < 0$ and to the reversed thresholds $\underline{x}_{(b)} + \overline{x}_{(b)} = -\big(\underline{x}_{(a)} + \overline{x}_{(a)}\big) > 0$. Then, Proposition 6.1.1 implies that

$$\mu_L[\mathbf{H^n_{(b)}}(\mathcal{A})] = \mu_L[(\mathbf{T^{-1}H_{(a)}T})^n(\mathcal{A})] = \mu_L[\mathbf{T^{-1}H^{-n}_{(a)}T}(\mathcal{A})] = \mu_L[\mathbf{H^{-n}_{(a)}}(\mathcal{A})]\,,$$

since one easy shows that the Lebesgue measure is invariant under $\mathbf{L}$ and therefore under $\mathbf{T} = \mathbf{PL}$. The first part of the proof shows that $\mu_L[\mathbf{H^n_{(b)}}(\mathcal{A})] \to 0$ when $n \to \infty$, and so does $\mu_L[\mathbf{H^{-n}_{(a)}}(\mathcal{A})]$. This completes the proof. □

This global result confirms the dichotomic behavior highlighted by the local result of Theorem 6.4.1, for QIF oscillators (in some situations) and for exponential oscillators. When $\underline{x} + \overline{x} < 0$, Proposition 6.4.2 implies that *a network of three oscillators (or clusters) achieve synchrony for almost every initial condition.* The proof relies on a measure-based framework similar to the approach used in [75] to prove synchronization of monotone oscillators. When $\underline{x} + \overline{x} > 0$, Proposition 6.4.2 does not prove global convergence to the phase-locked clustering configuration, but implies that a closed dense orbit cannot be a limit set of the trajectories. This precludes the existence of closed dense orbits, a phenomenon that is precisely observed when the behavior is not dichotomic (Section 6.5).

For higher dimensions $N_g - 1$, the argument of Proposition 6.4.2 does not hold. Indeed, if the dimension is greater than 2, the key property (6.17) is not sufficient to prove the result. However, such a measure-based approach is closely related to ergodic theory and to operator-theoretic methods (Perron-Frobenius operator) [64] that seem to be promising to obtain new advances on the QIF problem.

6.5 When the behavior is not dichotomic

When local stability is in contradiction with the overall behavior of the firing map (cf. Section 6.2.2), the fixed point has no global stability property and the behavior is not dichotomic. In this section, we discuss a criterion, derived from the local analysis, that determines whether a model has a dichotomic behavior or not. In addition, we provide a concrete example where a network of "QIF-like" pulse-coupled oscillators does not exhibit a dichotomic behavior, showing that the dichotomic behavior is not a general property of the "QIF-like" oscillators, but a more subtle property that is not observed for every model. Non-dichotomic behaviors are described in the rest of the section.

6.5.1 A criterion for the dichotomic behavior ?

In Section 6.4.3, we have seen that the curvature condition $h'' < 0 \ \forall\theta$, equivalent to the condition $dF_\epsilon/dx < 0 \ \forall x$, is sufficient to ensure that the local stability is in accordance with a dichotomic behavior. This result suggests that the length of the interval

$$\mathcal{D} \triangleq \{x | dF_\epsilon/dx < 0\}$$

could be a good criterion to estimate whether the dichotomic behavior holds for a dynamics $\dot{x} = F(x)$.

- When $\mathcal{D} = \mathbb{R}$ (the case of exponential oscillators), the length of $\mathcal{D}$ is infinite and local stability results suggest that the behavior is always dichotomic (Theorem 6.4.1).
- If the interval $\mathcal{D}$ is short — it is not possible to have $\mathcal{D} = \emptyset$ — then one can find values $x_k^* \notin \mathcal{D}$, $k \in \{1, 2\}$, and a simple argument shows that a dichotomic behavior does not always hold in dimension $N_g - 1 = 2$. This is summarized in the following proposition, which provides a sufficient condition to ensure that the behavior is not dichotomic.

Proposition 6.5.1. *Let a dynamics $\dot{x} = F(x)$ satisfy Assumption 1. If there exists a real $X > \epsilon/2$ such that the values x_1^* and x_2^* satisfying*

$$\int_{-X}^{x_1^*} \frac{1}{F(x)} dx = \int_{x_1^*+\epsilon}^{x_2^*} \frac{1}{F(x)} dx = \int_{x_2^*+\epsilon}^{X} \frac{1}{F(x)} dx \tag{6.19}$$

are not in $\mathcal{D}$, then the 2-dimensional firing map is not dichotomic for thresholds $\underline{x} \approx -X$ and $\overline{x} \approx X$. That is, the fixed point is locally unstable when $\underline{x} + \overline{x} > 0$.

Proof. The hypothesis implies that there exist values $\{x_1^*, x_2^*\}$, corresponding to the conservative limit case $F_\epsilon(x_1^*)F_\epsilon(x_2^*) = 1$, such that $x_k^* \notin \mathcal{D}$ for $k = \{1, 2\}$. Then, a slight increase of $\overline{x}$ to get $\underline{x} + \overline{x} \gtrsim 0$ increases the values x_k^*, so that $F_\epsilon(x_1^*)F_\epsilon(x_2^*) \gtrsim 1$ since $dF_\epsilon/dx > 0$ in the neighborhood of x_k^*. The characteristic polynomial (6.12) implies that the fixed point is unstable for $\underline{x} + \overline{x} \gtrsim 0$, which contradicts a dichotomic behavior. □

The piecewise linear vector field $F(x) = S + \gamma|x|$ is characterized by a short interval $\mathcal{D}$ (as suggested in Figure 6.7) and satisfies the hypothesis of Proposition 6.5.1. Then, *piecewise linear oscillators can exhibit a non-dichotomic behavior.* This is summarized in the following corollary.

Corollary 6.5.1. *For $F(x) = S + \gamma|x|$ with thresholds $\underline{x} + \overline{x} \approx 0$, the behavior of the 2-dimensional firing map is not dichotomic.*

Proof. For piecewise linear dynamics, one has $\mathcal{D} = (-\epsilon, 0)$. It follows from (6.19) that $x_1^* + \epsilon < 0$ and $x_2^* > 0$ so that $x_k^* \notin \mathcal{D}$, $k \in \{1, 2\}$, for any $\overline{x} \in \mathbb{R}^+$. Then, the proof follows from Proposition 6.5.1. □

The reader will note that a non-dichotomic behavior is not a particular behavior that results from the discontinuity of dF/dx at $x = 0$. Indeed, the proof of Corollary 6.5.1 clearly shows that smoothing $F(x)$ in a small neighborhood of $x = 0$ — so that $F \in C^\infty$ — does not change the result. In addition, Proposition 3.3.2 implies that two piecewise linear oscillators *always* exhibit a dichotomic behavior, in spite of the discontinuous dynamics.

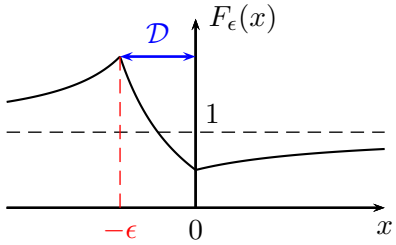

Figure 6.7: The function F_ϵ for the piecewise linear vector field $F(x) = S + \gamma|x|$ has a short interval $\mathcal{D} = (-\epsilon, 0)$.

The length of the interval $\mathcal{D}$ is a good criterion to determine whether a dichotomic behavior holds. We have found a sufficient condition on large intervals to ensure that the behavior is dichotomic ($\mathcal{D} = \mathbb{R}$) as well as a sufficient condition on short intervals to ensure that the behavior is not dichotomic (see Proposition 6.5.1). However, finding out a necessary and sufficient condition on the length of $\mathcal{D}$ to ensure that the behavior is dichotomic is so far an open question.

The QIF dynamics has a medium-length interval $\mathcal{D}$ and satisfies none of both sufficient conditions. The QIF model corresponds to an intermediate situation between two known models: between the exponential model (dichotomic behavior) and the piecewise linear model (non-dichotomic behavior). This intermediate situation makes the analysis of the QIF oscillators difficult.

6.5.2 Non-dichotomic behavior

When the behavior is not dichotomic, the fixed point of the firing map has no global stability property. Whereas local stability implies that the trajectories are attracted in the neighborhood of the fixed point, the overall behavior implies that the trajectories are repelled far from the fixed point, and vice versa. It is therefore obvious that the non-dichotomic dynamics is more complex.

In the sequel, we describe the non-dichotomic behaviors, considering piecewise linear integrate-and-fire oscillators.

Two dimensions For the piecewise linear dynamics with thresholds $\underline{x} + \overline{x} \approx 0$, the phase portrait of the 2-dimensional firing map clearly shows the existence of a closed dense orbit, which is either an ω-limit set[1] of the trajectories ($\underline{x}+\overline{x} > 0$) or an α-limit set[2] of the trajectories ($\underline{x} + \overline{x} < 0$).

- When $\underline{x} + \overline{x} > 0$, the fixed point is locally unstable while the overall behavior is contracting, a situation characterized by a stable dense orbit. For any initial conditions, the trajectories converge to the dense orbit and the behavior is quasiperiodic [Figure 6.8 (a)].

- When $\underline{x}+\overline{x} < 0$, the fixed point is locally stable while the overall behavior is expanding, a situation characterized by an unstable dense orbit that corresponds to the boundary of the basin of attraction of the fixed point. Consequently, two behaviors can be observed, depending on the initial condition. For an initial condition inside the basin of attraction, the trajectory asymptotically converges to the fixed point. On the other hand, for an initial condition outside the basin of attraction, the trajectory converges to the boundary of the domain (absorption) [Figure 6.8 (b)].

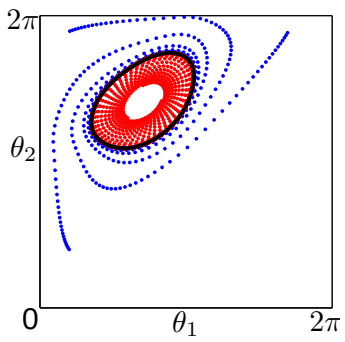

(a) Stable dense orbit ($\underline{x} + \overline{x} > 0$)

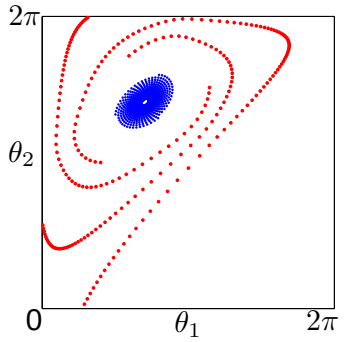

(b) Unstable dense orbit ($\underline{x} + \overline{x} < 0$)

Figure 6.8: When the behavior is not dichotomic, the fixed point has no global property and a closed dense orbit is observed ($\dot{x} = S + |x|$, $\epsilon = 0.1$, $\overline{x} = 1$). (a) For $\underline{x} = -0.9$ (case $\underline{x} + \overline{x} > 0$), the two trajectories converge to the closed dense orbit (black). (b) For $\underline{x} = -1.2$ (case $\underline{x} + \overline{x} < 0$), a closed dense orbit is unstable: the trajectories either converge to the fixed point (blue) or to the boundary of the domain (red).

The behavior is different from the dichotomic behavior. With thresholds $\underline{x} + \overline{x} > 0$, the behavior of three clusters is quasiperiodic. With thresholds $\underline{x} + \overline{x} < 0$, the behavior depends on the initial condition: (i) the three clusters converge to the phase-locked configuration or (ii) an absorption occurs and the two remaining clusters synchronize.

[1] The ω-limit set of a point $\boldsymbol{\Theta} \in \mathcal{U}$ is defined as the set $\bigcap_{\overline{n}>0} \mathrm{cl}\left(\bigcup_{n>\overline{n}} \mathbf{H^n}(\boldsymbol{\Theta})\right)$, where cl denotes the closure of the set.

[2] The α-limit set of a point $\boldsymbol{\Theta} \in \mathcal{U}$ is defined as the set $\bigcap_{\overline{n}>0} \mathrm{cl}\left(\bigcup_{n>\overline{n}} \mathbf{H^{-n}}(\boldsymbol{\Theta})\right)$.

Higher dimensions. When the behavior is non-dichotomic in higher dimensions, the fixed point is a saddle-focus, so that a unidimensional dense orbit is still observed (Figure 6.9).

- When $\underline{x} + \overline{x} > 0$, the fixed point has two unstable eigenvalues and the two unstable directions force convergence to the stable dense orbit. The behavior is quasiperiodic [Figure 6.9 (a)].
- When $\underline{x} + \overline{x} < 0$, the fixed point has two stable eigenvalues. But contrary to the 2-dimensional case, the fixed point remains unstable since the other directions are unstable. The basin of attraction of the fixed point, delimited by the dense orbit, has zero measure. Then, almost every trajectory converges to the boundary of the domain and synchronization is achieved for almost every initial condition.

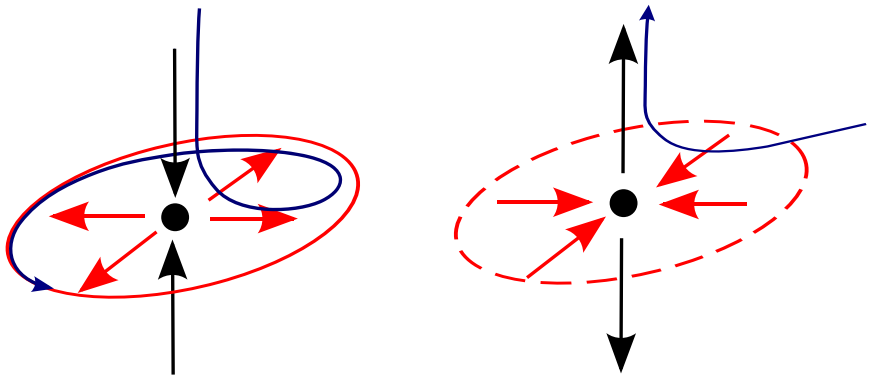

(a) Stable dense orbit ($\underline{x}+\overline{x} > 0$) (b) Unstable dense orbit ($\underline{x} + \overline{x} < 0$)

Figure 6.9: In higher dimensions, the fixed point is a saddle-focus. (For the sake of clarity, the discrete-time trajectory is represented as a continuous one, in three dimensions.) (a) The trajectory converges to the unidimensional dense orbit. (b) The trajectory converges neither to the dense orbit nor to the fixed point.

Hopf bifurcations The closed dense orbit observed along with a non-dichotomic behavior is always characterized by the same stability as the fixed point when the behavior is dichotomic. In addition, Proposition 6.5.1 shows that the behavior is non-dichotomic for values $\underline{x}+\overline{x} \approx 0$, but does not preclude that the behavior be dichotomic for higher values. This suggests that a non-dichotomic behavior is the result of a Hopf bifurcation that occurs when decreasing the value $|\underline{x} + \overline{x}|$ from a high value.

- In the case $\underline{x}+\overline{x} > 0$, a *supercritical bifurcation* occurs: the stable fixed point is turned into a (unstable) saddle-focus with a stable closed orbit.
- In the case $\underline{x}+\overline{x} < 0$, a *subcritical bifurcation* occurs: the unstable fixed point is turned into a (unstable) saddle-focus with an unstable closed orbit.

In the studies on LIF pulse-coupled oscillators with delayed transmissions [117], similar Hopf bifurcations are observed for high coupling delays (seen also Section 5.5.2). Introducing delays

actually suppresses the monotonicity and the symmetry properties of the oscillators dynamics (see Section 7.2.3), so that it is not surprising that a dichotomic behavior does not persist with important delays. In contrast, the present section shows that the dichotomic behavior can be lost even with symmetric and non-delayed "QIF"-like dynamics.

Remark 6.5.1. In peculiar situations, the behavior is never dichotomic, even for the case $|\underline{x} + \overline{x}| \gg 0$ that is characterized by a periodic behavior. A Hopf bifurcation is not observed, but the periodic behavior becomes a quasiperiodic behavior when the closed dense orbit appears. ◇

Conservative limit case. Since the behavior is non-dichotomic for values $\underline{x}+\overline{x} \approx 0$, it is of interest to consider the conservative limit case $\underline{x} + \overline{x} = 0$. The behavior in the neighborhood of the fixed point is similar to the behavior observed in the dichotomic case (Section 6.3.1): the fixed point, which is a marginal stable center, is encircled by a family of closed dense orbits. However, the trajectories far from the fixed point can exhibit very complex patterns (Figure 6.10) that contrast with the simple dynamics corresponding to a dichotomic behavior (Figure 6.4).

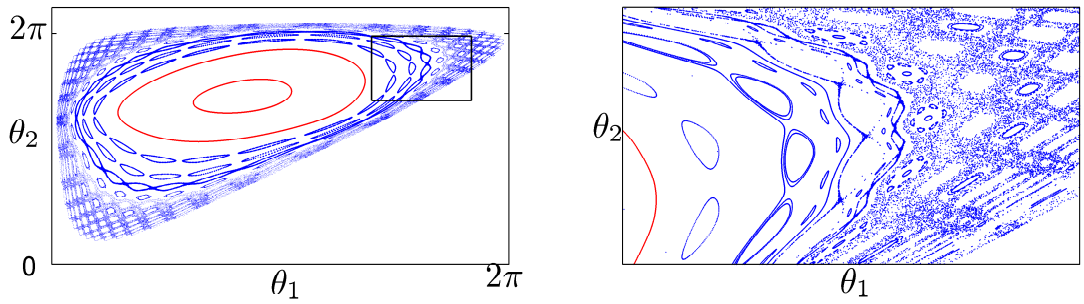

(a) (b)

Figure 6.10: The trajectories of the 2-dimensional firing map exhibit complex evolutions. ($\dot{x} = 0.3 + |x|$, $\epsilon = 0.2$). (a) Near the fixed point, closed dense orbits encircle the fixed point (red trajectories). (b) A zoom far from the fixed point shows complex patterns (blue trajectories).

6.6 Infinite populations

The previous sections give clear insight that determining the dichotomic behavior of QIF and "QIF-like" oscillators from the scalar firing map $h(\cdot)$ is a difficult question. In this section, we focus on infinite populations of oscillators, investigating whether the continuum approximation may lead to some advances on the conjectures that prevail with finite populations.

Numerical simulations clearly suggest that the behavior of infinite populations is in agreement with the behavior of finite populations. For instance, infinite populations of QIF oscillators always exhibit a dichotomic behavior (convergence to either synchronous state or asynchronous state). In contrast, infinite populations of piecewise linear integrate-and-fire oscillators may exhibit a non-dichotomic behavior.

Unfortunately, it appears that the local stability problem is still elusive, so that the continuum approximation does not help to solve the QIF conjectures. However, the developments on the local analysis presented in the section are important preliminaries for the results presented in Chapter 7.

6.6.1 Local analysis

To investigate the dichotomic behavior of the "QIF-like" oscillators, we linearize the PDE (5.1)-(5.3) around the stationary solution (5.11) and derive an eigenvalue equation for the local analysis of the stationary solution.

The derivation of the eigenvalue equation is classical and follows similar lines as in [3, 117]. For the sake of simplicity, a new phase variable is introduced, which satisfies

$$\frac{d\vartheta}{d\theta} = \frac{2\pi J^*}{\omega + K\, Z(\theta)\, J^*}\,, \tag{6.20}$$

with $\vartheta = 0$ (resp. $\vartheta = 2\pi$) corresponding to $\theta = 0$ (resp. $\theta = 2\pi$). The new phase is such that the oscillators have a constant velocity $\dot{\vartheta} = 2\pi J^*$ under the asynchronous regime $J_0 = J^*$. Next, the phase dynamics (5.6) is rewritten as

$$\dot{\vartheta} = \frac{d\vartheta}{d\theta} v(\theta, t) = 2\pi J^* + (J_0 - J^*) K\, Z_\vartheta(\vartheta)\,. \tag{6.21}$$

The function

$$Z_\vartheta(\vartheta) = \frac{d\vartheta}{d\theta} Z(\theta) = \frac{2\pi J^*\, Z(\theta)}{\omega + J^*\, K\, Z(\theta)} \tag{6.22}$$

is interpreted as an iPRC related to phase ϑ and corresponds to the oscillators phase sensitivity to a perturbation of the asynchronous regime. Defining the density ρ_ϑ so that $\rho_\vartheta\, d\vartheta = \rho\, d\theta$, one has

$$J = \dot{\vartheta}\, \rho_\vartheta\,. \tag{6.23}$$

Next, considering the small variations $j = J - J^*$ (and $j_0 = J_0 - J^*$) around the stationary solution, (6.21)-(6.23) are linearized and the density can be expressed as

$$\rho_\vartheta = \frac{1}{2\pi} + \frac{1}{2\pi\, J^*} j - \frac{K}{4\pi^2\, J^*} Z_\vartheta(\vartheta)\, j_0\,. \tag{6.24}$$

The continuity equation

$$\frac{\partial \rho_\vartheta}{\partial t} = -\frac{\partial J}{\partial \vartheta}\,,$$

which is equivalent to (5.1), becomes through (6.24) the linear PDE

$$\frac{\partial j}{\partial t} = -2\pi J^* \frac{\partial j}{\partial \vartheta} + \frac{K}{2\pi} Z_\vartheta(\vartheta) \frac{dj_0}{dt}\,. \tag{6.25}$$

To compute the eigenspectrum of the equation, an exponential solution $j(\vartheta, t) = \bar{j}(\vartheta)\, \exp(\lambda t)$ is injected in (6.25). The linear differential equation for a mode $\bar{j}$ has the solution

$$\bar{j}(\vartheta) = \bar{j}(0)\, e^{-\lambda\vartheta/(2\pi\, J^*)} \left(1 + \frac{K\,\lambda}{4\pi^2\, J^*} \int_0^\vartheta Z_\vartheta(s)\, e^{\lambda s/(2\pi\, J^*)} ds\right)\,. \tag{6.26}$$

Finally, evaluating (6.26) in $\vartheta = 2\pi$ and using the boundary condition (5.3), we obtain the eigenvalue equation

$$e^{\lambda/J^*} - 1 = \frac{K\,\lambda}{4\pi^2\,J^*} \int_0^{2\pi} Z_\vartheta(\vartheta)\, e^{\lambda\vartheta/(2\pi\,J^*)} d\vartheta\,. \tag{6.27}$$

The eigenvalue equation (6.27) has an infinity of solutions λ_n ($n \in \mathbb{Z}$) whose real parts determine the stability of the asynchronous state. When the real parts of the eigenvalues are all negative, the asynchronous state is locally stable. When they are all positive, all the modes are unstable and the flux tends to a Dirac function. When $Z(\theta)$ (and therefore $Z_\vartheta(\vartheta)$) is constant (for instance in the uncoupled case $K = 0$), the eigenvalues are $\lambda_n = i\,n\,2\pi J^*$ and all lie on the imaginary axis: the asynchronous state is marginally stable (see also Remark 5.2.1).

Local analysis provides a useful insight to determine whether the behavior of the infinite population is dichotomic. When the behavior is dichotomic, the eigenmodes are either all stable or all unstable (depending on the value $\underline{x} + \overline{x}$ and on the coupling K). In other words, the real part of all the eigenvalues must have the same sign.

As a preliminary result, the following proposition provides general properties of the eigenvalues.

Proposition 6.6.1. *1.* $0 \triangleq \lambda_0$ *is a solution of* (6.27)*;*
2. If λ_n *is a solution of* (6.27)*, then its complex conjugate* $\lambda_n^\dagger \triangleq \lambda_{-n}$ *is also a solution;*
3. There exist solutions satisfying $\Im\{\lambda_n\} \to \infty$ *which tend to*

$$\lambda_\infty \triangleq J^* \log\left(\frac{\omega + J^*\,K\,Z(2\pi)}{\omega + J^*\,K\,Z(0)}\right) + i\,n\,2\pi J^* \quad (n \to \infty)\,.$$

Proof. The first two points are trivial. The latter is proved as follows. Integrating by parts the right hand of (6.27) yields

$$e^{\lambda/J^*} - 1 = \frac{K}{2\pi}\left[Z_\vartheta(2\pi)e^{\lambda/J^*} - Z_\vartheta(0)\right] - \frac{K}{2\pi}\int_0^{2\pi} \frac{dZ_\vartheta}{d\vartheta}\, e^{\lambda\vartheta/(2\pi\,J^*)} d\vartheta\,. \tag{6.28}$$

Considering that $\Im\{\lambda\} \to \infty$, the Riemann-Lebesgue lemma [18] implies that the integral in (6.28) vanishes. Then it follows from (6.22) that (6.28) writes

$$e^{\lambda/J^*} = \frac{\omega + J^*\,Z(2\pi)}{\omega + J^*\,Z(0)}\,.$$

The solution of this equation is λ_∞, which concludes the proof. □

Proposition 6.6.1 implies that the real part $\Re\{\lambda_\infty\}$ has the same sign as $K[Z(2\pi) - Z(0)]$. Then, it follows from (2.6) that "QIF-like" oscillators are characterized by stable high frequency modes — that is, $\Re\{\lambda_\infty\} < 0$ — when $K(\underline{x} + \overline{x}) > 0$. This is in agreement with the stability conditions presented in Table 6.1, conditions that correspond to a dichotomic behavior with an excitatory coupling $K > 0$. As a consequence, the stability of the high frequency modes, which depends on the sign of $K(\underline{x} + \overline{x})$ only, always supports a dichotomic behavior. However, since the eigenvalues of lower frequency can have real parts of opposite sign, the result is not sufficient to ensure that a dichotomic behavior holds.

The result of Proposition 6.6.1 (infinite populations) can be related with the result of Property 8 (finite populations). Indeed, both results show that some stability properties — overall behavior for finite populations or high frequency modes for infinite populations — are always in agreement with a dichotomic behavior.

In the same idea, Proposition 6.1.1 has also its analog result:

Proposition 6.6.2. *Consider two models (a) and (b) that both have the same "QIF-like" dynamics satisfying Assumption 1, but with different thresholds satisfying* $\underline{x}_{(a)} = -\overline{x}_{(b)}$ *and* $\overline{x}_{(a)} = -\underline{x}_{(b)}$ *(opposite values* $\underline{x} + \overline{x}$*). Then, the respective eigenvalues, solutions of* (6.27)*, satisfy* $\Re\{\lambda_{n,(a)}\} = -\Re\{\lambda_{n,(b)}\}$*.*

Proof. Property 4 implies $Z_{(a)}(\theta) = Z_{(b)}(2\pi - \theta)$ and it follows from (6.20) and (6.22) that one has also $Z_{\vartheta,(a)}(\vartheta) = Z_{\vartheta,(b)}(2\pi - \vartheta)$. In addition, one easily shows that the stationary flux J^* is the same for the two models. Then, the eigenvalue equation (6.27) for $Z_{\vartheta,(a)}$ can be rewritten as

$$e^{\lambda/J^*} - 1 = \frac{K\,\lambda}{4\pi^2\,J^*} \int_0^{2\pi} Z_{\vartheta,(b)}(2\pi - \vartheta)\, e^{\lambda\vartheta/(2\pi\,J^*)} d\vartheta$$

or, after a change of variables,

$$e^{-\lambda/J^*} - 1 = \frac{K\,(-\lambda)}{4\pi^2\,J^*} \int_0^{2\pi} Z_{\vartheta,(b)}(\vartheta)\, e^{-\lambda\vartheta/(2\pi\,J^*)} d\vartheta\,.$$

If $\lambda_{n,(a)}$ is an eigenvalue for $Z_{\vartheta,(a)}$, then $-\lambda_{n,(a)} \triangleq \lambda_{-n,(b)}$ is an eigenvalue for $Z_{\vartheta,(b)}$. Since Proposition 6.6.1 implies $\lambda_{-n,(b)} = \lambda^{\dagger}_{n,(b)}$, one has $\Re\{\lambda_{n,(a)}\} = -\Re\{\lambda_{n,(b)}\}$, which completes the proof. □

Proposition 6.6.2 shows how models satisfying Assumption 1 are the most likely to exhibit dichotomy: two opposite values $\underline{x} + \overline{x}$ (corresponding to two mirrored iPRC's) yield two behaviors with opposite stability.

In spite of the above results, a complete local stability analysis of the continuum model cannot be achieved, so that the continuum approximation fails to prove the QIF conjecture. Whether the model satisfies Assumption 1 or not, the whole set of solutions of (6.27) can only be obtained numerically: it is impossible to obtain an analytical characterization of all the eigenvalues. (In the next chapter, an analytical characterization of the eigenvalues becomes available, through the weak coupling limit.)

Remark 6.6.1 (Conservative limit case)**.** In the limit case $\underline{x} + \overline{x} = 0$, an infinite number of eigenvalues lie on the imaginary axis. The asynchronous state is marginally stable, a behavior that is in agreement with the behavior described in Section 6.3.

In the conservative limit case, one has $\overline{\theta} = \pi$ and the oscillators have a symmetric iPRC $Z(\theta) = Z(2\pi - \theta)$. Given the resulting symmetry of $Z_\vartheta(\vartheta) = Z_{\vartheta,e}(\vartheta - \pi)$, with $Z_{\vartheta,e}(\cdot)$ an even function, the eigenvalue equation (6.27) is written as

$$e^{\lambda/(2J^*)} - e^{-\lambda/(2J^*)} = \frac{K\,\lambda}{4\pi^2\,J^*} \int_{-\pi}^{\pi} Z_{\vartheta,e}(\vartheta)\, e^{\lambda\vartheta/(2\pi\,J^*)} d\vartheta\,.$$

Assuming a purely imaginary solution $\lambda = i|\lambda|$, the equation becomes

$$\sin\left(\frac{|\lambda|}{2\,J^*}\right) = \frac{K\,|\lambda|}{4\pi^2\,J^*} \int_0^{\pi} Z_{\vartheta,e}(\vartheta)\, \cos\left(\frac{|\lambda|\vartheta}{2\pi\,J^*}\right) d\vartheta$$

and has an infinity of solutions. A symmetric iPRC $Z(\theta) = Z(2\pi - \theta)$ is a necessary condition to ensure an infinity of eigenvalues on the imaginary axis. ◇

6.6.2 Dichotomic and non-dichotomic behaviors

As mentioned in Chapter 5, there is a perfect parallel between the behavior of finite populations and the corresponding behavior of infinite populations: finite and infinite populations exhibit a similar behavior under identical assumptions.

Dichotomic behavior. Numerical simulations of the PDE, as well as the numerical solutions of the eigenvalue equation (6.27), clearly suggest that the dichotomic behavior of QIF oscillators and of exponential integrate-and-fire oscillators persists in the continuum limit. The behavior is not described in this section since it is similar to the dichotomic behavior of infinite populations of monotone oscillators (see Figure 5.1 and Figure 5.2).

Non-dichotomic behavior. For piecewise linear integrate-and-fire oscillators, one recovers the (non-dichotomic) behavior of finite populations (Section 6.5.2). For high values $\underline{x} + \overline{x}$ ($\overline{\theta} \approx 0$), the asynchronous state is stable, as for oscillators with a dichotomic behavior. When $\underline{x}+\overline{x}$ is decreased under a critical value, the system undergoes a supercritical Hopf bifurcation and the flux oscillates under the influence of the second (unstable) mode (Figure 6.11).

It is noticeable that the situation of periodic flux corresponds to a quasiperiodic behavior of finite populations. Actually, even in infinite populations, a single oscillator in the continuum does not fire in phase with the flux but has a quasiperiodic behavior. While macroscopic quantities evolve periodically, microscopic quantities evolve in a quasiperiodic way. A similar situation was initially described in [60, 117] for LIF oscillators with delayed transmissions.

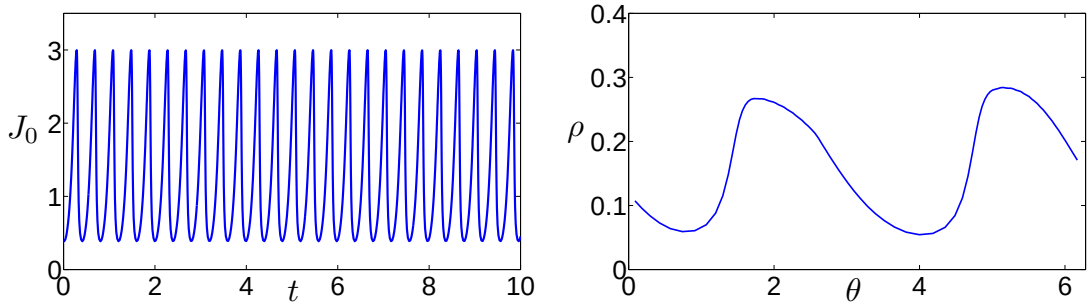

(a) Flux (b) Density

Figure 6.11: Near the Hopf bifurcation, (a) the flux is periodic and (b) there are two high density regions, in which the oscillators tend to gather. (The oscillators have the dynamics $\dot{x} = 1 + |x|$, with $\underline{x} = -0.6$, $\overline{x} = 1$, and $K = 0.5$.)

An important observation is the phenomenon of clustering. Under the influence of the unstable mode, Figure 6.11 (b) clearly shows that the oscillators tend to gather into 2 clusters. The phenomenon is accentuated for $\underline{x}+\overline{x} \approx 0$ ($\overline{\theta} \approx \pi$), a situation where no stable limit cycle is observed, so that the unstable mode strongly affects the behavior. The (second) unstable

mode grows exponentially and the flux tends to a series of Dirac functions, characterized by two Dirac functions per period [Figure 6.12 (a)]. In this situation, the continuum of oscillators clearly splits into two distinct clusters [Figure 6.12 (b)].

The present clustering behavior is different from the clustering behavior of finite populations, which is described in Chapter 4. In the present case, it is not a consequence of an absorption phenomenon, but a (more inherent) consequence of the non-dichotomic dynamics of the oscillators. In addition, the number of clusters does not depend on the initial conditions, but is determined by the number n of the unstable mode.

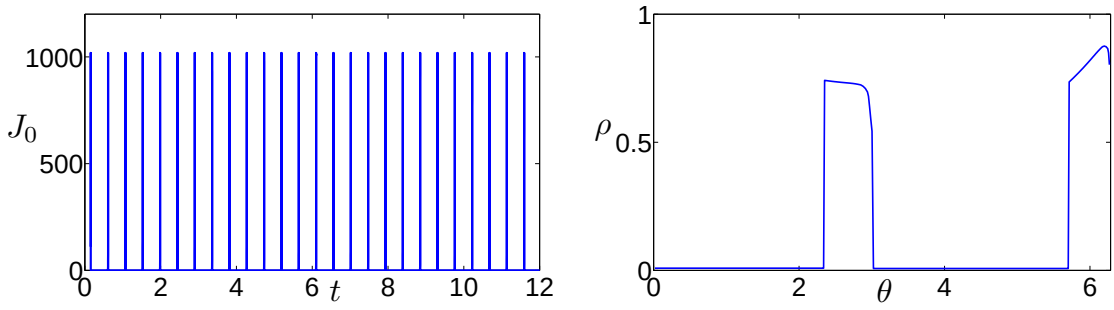

(a) Flux (b) Density

Figure 6.12: For $\underline{x}+\overline{x} \approx 0$, (a) the flux is a series of Dirac functions, with two Dirac functions per oscillator period ($T \approx 0.9$), and (b) the oscillators gather in two clusters. (The dynamics is the same as in Figure 6.11, except for $\underline{x} = -0.8$.)

6.7 Conclusion

This chapter, which was devoted to the study of "QIF-like" oscillators, has showed that a local analysis is significant to capture the global dichotomic behavior of the oscillators and sufficient to detect situations characterized by a non-dichotomic behavior. Interestingly, the local analysis suggests that the dichotomic behavior still persists in large populations of QIF oscillators whereas it does not persist with piecewise linear oscillators, in which case the population may exhibit rich and complex non-dichotomic behaviors. As a consequence, the dichotomic behavior is not an obvious and regular property of large populations of "QIF-like" oscillators.

The stability problem of the QIF oscillators is a standing conjecture that holds both for finite and infinite populations. However, the stability problem is solved with other models. On the one hand, finer assumptions on the firing map ensure the dichotomic behavior of exponential integrate-and-fire oscillators. On the other hand, strong conditions ensure the non-dichotomic behavior of piecewise linear integrate-and-fire oscillators. The QIF oscillators, that satisfy none of these conditions, appear as an intermediate situation between the two simpler situations, an intermediate situation for which the conjecture is "surrounded" by the results obtained for smaller networks and/or for the other dynamics (Table 6.2).

A promising approach to solve the QIF conjecture is to exploit the strong average properties of the firing map. In the present chapter, the property of the dynamics have been

considered only over one iteration of the firing map. However, it could be of interest to focus on a larger time horizon by considering statistical time averages over several iterations through operator-theoretic methods (Perron-Frobenius operator).

In the next chapter, we simplify the study of "QIF-like" oscillators by considering the weak coupling limit. This approximation is more amenable to local stability analysis and solves the (local) QIF conjecture. In addition, the weak coupling approximation is suitable for averaging techniques that may capture the average properties of the dynamics.

Number of clusters	Monotone (LIF, etc.)	Exponential, QIF with bounded $[\underline{x}, \overline{x}]$	QIF
$N_g = 2$			
$N_g = 3$			
$N_g > 3$			

Table 6.2: Summarizing the results obtained for the dichotomic behavior of different integrate-and-fire models, the table shows that the QIF conjecture (white cell) is "surrounded" by the other global results (dark gray cells) and local results (light gray cells).

Chapter 7

Weak coupling limit and averaging

As highlighted in Chapter 6, the study of large networks of non-monotone pulse-coupled oscillators is not trivial. The analysis of the remarkable dichotomic behavior of QIF oscillators is elusive, both for finite and infinite populations, leading to a standing conjecture not only for the global analysis but also for the local analysis. In the present chapter, we show that the weak coupling approximation overcomes all these difficulties and solves the QIF conjecture. Through a weak coupling assumption, local analysis is completely tractable and yields an explicit criterion for the dichotomic behavior of the oscillators. In particular, while Chapter 6 suggests that the continuum limit does not help to solve the conjectures, the weak coupling approximation shows that the continuum limit is more amenable to study in the case of general models of pulse-coupled oscillators.

Beyond local results, networks of weakly (pulse-coupled) oscillators are amenable to averaging techniques. As shown in [58], averaging the dynamics of the oscillators yields an *averaged model* that is similar to the Kuramoto model [4, 59, 104]. Since the averaging techniques capture the average properties of the network in a better way than the firing map does, a global analysis of the averaged model is more tractable. For instance, the results of Chapter 4 are exploited to show that the averaged model has strong contraction properties, a global result that can be related to *consensus problems* in multiagent systems. In addition, averaging is a promising approach to the global stability problem.

The chapter is organized as follows. In Section 7.1, we derive the stability criteria for the behaviors of finite and infinite populations. The two criteria are applied in Section 7.2 to solve the local QIF conjecture and to highlight the dichotomic behavior in infinite populations of "QIF-like" oscillators. In addition, the section is also devoted to the study of delayed transmissions and to the study of more complex dynamics (e.g. Hodgkin-Huxley model). In Section 7.3, we consider the averaged dynamics of the pulse-coupled oscillators both for monotone and QIF dynamics.

The main contributions of the chapter are (i) the two stability criteria, that are efficiently applied to solve a QIF conjecture and to study extensions of the original model and (ii) the contraction property of the averaged dynamics of monotone oscillators. Some results presented in this chapter are published in [74].

7.1 Local analysis of finite and infinite populations

In the preceding chapter, the local stability analysis is limited because the eigenvalue equation has no analytical solution (both for finite and infinite populations). Only qualitative properties of the eigenvalues can be derived from the eigenvalue equation. In contrast, an analytical characterization of the eigenvalues becomes available when the coupling is weak. Indeed, the eigenvalue equation for a weak coupling ($\epsilon \approx 0$, $K \approx 0$) can be linearized around the known solutions of the uncoupled case ($\epsilon = K = 0$), a process that provides an explicit expression of the eigenvalues. Through this process, similar stability criteria are obtained for finite and infinite populations, showing the strong parallel between finite and infinite populations.

Under the weak coupling assumption, absorptions never occur so that a cluster is never observed. Thus, one always considers $N_g = N$ throughout the present chapter.

7.1.1 A stability criterion for finite populations

In this section, we consider the characteristic polynomial (6.7) and we investigate how the eigenvalues corresponding to the uncoupled case are modified when a weak coupling is added. This yields a general criterion for the stability of finite populations of weakly pulse-coupled oscillators.

The coefficients of (6.7) are linearized around the values corresponding to the uncoupled case. In the uncoupled case, the fixed point is the splay state $\theta_j^* = j2\pi/N$ ($x_j^* = f(j2\pi/N)$), according to (6.4). Then, one has

$$\frac{F(x_j^*)}{F(x_j^*+\epsilon)} = 1 - \epsilon \frac{dF}{dx}(x_j^*)\frac{1}{F(x_j^*)} + \mathcal{O}(\epsilon^2) = 1 + \epsilon Z'\left(j\frac{2\pi}{N}\right) + \mathcal{O}(\epsilon^2)\,, \tag{7.1}$$

where the last equality follows from (2.9). [Equality (7.1) can also be obtained through (3.9) and (6.5). Indeed, (3.3) implies $Z_\epsilon \approx \epsilon\, Z$ for a weak coupling and one has $h(\theta) = 2\pi - \theta + \epsilon\, Z(2\pi - \theta)$.] Next, the coefficients of the polynomial are given by

$$p_k = \prod_{j=k+1}^{N-1} \frac{F(x_j^*)}{F(x_j^*+\epsilon)} = 1 + \epsilon \sum_{j=k+1}^{N-1} Z'\left(j\frac{2\pi}{N}\right) + \mathcal{O}(\epsilon^2)$$

an expression that involves the first derivative of the iPRC. Then, for a weak coupling $\epsilon \ll 1$, (6.7) is rewritten as

$$p(z) = \sum_{k=0}^{N-1} z^k + \epsilon \sum_{k=0}^{N-2} \sum_{j=k+1}^{N-1} Z'\left(j\frac{2\pi}{N}\right) z^k\,. \tag{7.2}$$

The first sum is the characteristic polynomial for the uncoupled oscillators; the second sum appears as a perturbation of the first sum.

At this stage, an important trick is to multiply (7.2) by $(z-1)$ — as in the proof of Lemma 6.3.1. Such a modification, whose motivation is intuitively explained in Section 7.1.3,

dramatically simplifies the polynomial (7.2). Indeed, we obtain

$$\begin{aligned}(z-1)\,p(z) &= z^N - 1 + \epsilon \sum_{k=0}^{N-2} \sum_{j=k+1}^{N-1} Z'\left(j\frac{2\pi}{N}\right)(z^{k+1}-z^k)\,,\\ &= z^N - 1 + \epsilon \sum_{k=1}^{N-1} \sum_{j=k}^{N-1} Z'\left(j\frac{2\pi}{N}\right) z^k - \epsilon \sum_{k=0}^{N-2} \sum_{j=k+1}^{N-1} Z'\left(j\frac{2\pi}{N}\right) z^k\,,\\ &= z^N - 1 + \epsilon \sum_{k=1}^{N-1} Z'\left(k\frac{2\pi}{N}\right) z^k - \epsilon \sum_{k=1}^{N-1} Z'\left(k\frac{2\pi}{N}\right)\,.\end{aligned}$$

The polynomial is thus the polynomial $z^N - 1$ perturbed according to

$$(z-1)\,p(z) = z^N - 1 + \epsilon\, e(z)\,,$$

where the perturbation polynomial $e(z) = e_N z^N + e_{N-1} z^{N-1} + \cdots + e_0$ has the coefficients

$$\begin{aligned} e_0 &= -\sum_{k=1}^{N-1} Z'\left(k\frac{2\pi}{N}\right)\,,\\ e_k &= Z'\left(k\frac{2\pi}{N}\right) \qquad k = 1,\ldots,N-1\,,\\ e_N &= 0\,. \end{aligned} \tag{7.3}$$

In the sequel, we analyze the sensitivity of the eigenvalues to the perturbation. Since the roots of $z^N - 1$ lie on the unit circle, we investigate whether all the roots λ_n, $n = 0,\ldots,N-1$, move into the unit circle under the effect of the (infinitesimal) perturbation $\epsilon\, e(z)$. First, the roots must satisfy

$$\frac{d}{d\epsilon}\left[\lambda_n^N - 1 + \epsilon\, e(\lambda_n)\right] = \left(\lambda_n^{N-1} + \epsilon \sum_{k=1}^{N} e_k \lambda_n^{k-1}\right)\frac{d\lambda_n}{d\epsilon} + e(\lambda_n) = 0\,.$$

For $\epsilon = 0$, the roots are $\lambda_n = e^{in2\pi/N}$ and move under the perturbation according to the direction

$$\left.\frac{d\lambda_n}{d\epsilon}\right|_{\epsilon=0} = -\sum_{k=0}^{N} e_k\, e^{i\frac{2\pi(k+1)n}{N}}\,.$$

This direction points inward if and only if

$$\Re\left\{\left(\sum_{k=0}^{N} e_k\, e^{i\frac{2\pi(k+1)n}{N}}\right)\left(e^{i\frac{2\pi n}{N}}\right)^{\dagger}\right\} = \Re\left\{\sum_{k=0}^{N} e_k\, e^{i\frac{2\pi kn}{N}}\right\} \geq 0 \quad \forall n \in \{0,\ldots,N-1\}\,. \tag{7.4}$$

[We note that the condition is equivalent to $\Re\{\mathbf{V}.(e_0 \ldots e_N)^T\} \geq 0$, where $\mathbf{V}$ is the Vandermonde matrix of the roots $\exp(i\frac{2\pi n}{N})$.]

Finally, injecting (7.3) in (7.4), we obtain the following criterion for the stability of the fixed point of the firing map.

Criterion 1. *Under the assumption of weak coupling, all the eigenvalues (roots of* (6.7)*) are stable if and only if*

$$-\sum_{k=1}^{N-1} Z'\left(k\frac{2\pi}{N}\right) + \sum_{k=1}^{N-1} Z'\left(k\frac{2\pi}{N}\right)\cos\left(\frac{kn2\pi}{N}\right) \geq 0 \quad \forall n \in \{0,\dots,N-1\}\,. \tag{7.5}$$

All the eigenvalues are unstable if the inequality is inverted.

For the value $n = 0$, the above expression is always equal to zero. Actually, this situation corresponds to the root $z = 1$ that we have previously introduced by multiplying the polynomial by $(z - 1)$. Since this root does not vary under the effect of the coupling, it is logical that its sensitivity to the perturbation is equal to zero.

It is noticeable that local stability of finite populations requires *little information on the iPRC*. Indeed, Criterion 1 imposes conditions on the derivative of the iPRC at $N - 1$ given phase values only: $\theta = 2\pi/N, 4\pi/N, \dots, 2\pi(N-1)/N$. The other values have no influence on the local stability.

Criterion 1 is of paramount importance to determine the behavior of weakly pulse-coupled oscillators. If the criterion is satisfied, it indicates a dichotomic behavior. When the criterion is not satisfied for some values n, the corresponding eigenvalues are not stable, while the other eigenvalues are stable, a situation that is characteristic of a non-dichotomic behavior.

The stability criterion is very general, since it imposes no condition on the iPRC. In particular, it applies to oscillators that do not satisfy Assumption 1, and even to pulse-coupled oscillators that do not have an integrate-and-fire dynamics.

7.1.2 A stability criterion for infinite populations

To complement the previous result, we introduce a stability criterion equivalent to Criterion 1, but for infinite populations of weakly pulse-coupled oscillators.

In the uncoupled case, the stationary density (5.11) is a constant $\rho^* = J^*/\omega$ and it follows that $2\pi\, J^* = \omega$ since ρ^* is normalized on $[0, 2\pi]$. Then, (6.20) implies $\vartheta = \theta$ and (6.22) leads to $Z_\vartheta(\vartheta) = Z(\theta)$. In addition, the eigenvalues, solutions of (6.27) with $K = 0$, are given by $\lambda_n = i\, n\, \omega$.

For a weak coupling $K \ll 1$, the eigenvalue equation (6.27) is linearized around the solutions of the uncoupled case. Considering the small variations $\lambda_n = i\, n\, \omega + \delta\lambda_n$ and $J^* = \omega/2\pi + \delta J^*$, the linearization of (6.27) leads to

$$\frac{2\pi}{\omega}\delta\lambda_n - i\frac{4\pi^2\, n}{\omega}\delta J^* = i\frac{n\, K}{2\pi}\int_0^{2\pi} e^{i\, n\theta} Z(\theta)\, d\theta + \mathcal{O}(K^2)\,. \tag{7.6}$$

Taking the real part of (7.6) finally yields

$$\Re\{\delta\lambda_n\} = \Re\{\lambda_n\} = -\frac{K\, n\omega}{4\pi^2}\int_0^{2\pi} Z(\theta)\, \sin(n\theta)\, d\theta + \mathcal{O}(K^2)\,,$$

or equivalently

$$\Re\{\lambda_n\} = \frac{K\, n\omega}{2\pi}\Im\{\hat{Z}_n\} + \mathcal{O}(K^2)\,, \tag{7.7}$$

with $\hat{Z}_n$ the nth Fourier coefficient of the iPRC, that is

$$\hat{Z}_n = \frac{1}{2\pi}\int_0^{2\pi} Z(\theta)\, e^{-in\theta}\, d\theta\,.$$

The result is summarized in the following criterion.

Criterion 2. *Under the assumption of weak coupling, all the eigenvalues (solutions of* (6.27)*) are stable if and only if*

$$K\int_0^{2\pi} Z(\theta)\,\sin(n\theta)\,d\theta \geq 0 \quad \Big(or\ K\,\Im\{\hat{Z}_n\} \leq 0\Big) \quad \forall n \geq 0\ (n \in \mathbb{N})\,. \tag{7.8}$$

All the eigenvalues are unstable if the inequality is inverted.

For the value $n = 0$, the above expression is always equal to zero. This situation corresponds to the eigenvalue $\lambda_0 = 0$.

Contrary to Criterion 1, Criterion 2 is in fact not new: the expression (7.7) appears in [3, 60] to study the local stability of weakly pulse-coupled LIF oscillators. However, Criterion 2 is general, so that we will fully exploit the result to study more general oscillators, including the QIF oscillators. In Section 7.2, we solve the (local) QIF conjectures not only for infinite populations, through Criterion 2 but also for finite populations through Criterion 1.

7.1.3 Parallel between finite and infinite populations

The results of Chapter 4 and Chapter 5 on monotone oscillators underline the strong parallel between the analysis of finite populations and the analysis of infinite populations. In addition, Chapter 6 shows the same coherence for the dichotomic behavior of finite and infinite populations of "QIF-like" oscillators. As a brief digression, we still put emphasis on this elegant analogy, highlighting the strong relations between a discrete-time system for finite populations (the firing map) and a continuous-time system for infinite populations (the transport PDE).

Eigenvalues. In the uncoupled case $\epsilon = K = 0$, for finite populations, the eigenvalues of the time-Discrete firing map, roots of (6.7), are given by $\lambda_D = \exp(i\,n2\pi/N)$. For infinite populations, in contrast, the eigenvalues of the time-Continuous transport equation, solutions of (6.27), are given by $\lambda_C = i\,n\,2\pi J^*$. This suggests a relationship between the eigenvalues of the discrete-time and continuous-time systems:

$$\lambda_D \equiv \exp\left(\frac{\lambda_C}{NJ^*}\right)\,. \tag{7.9}$$

Through this relationship, the eigenvalue equation (6.27) with $K = 0$ is rewritten as the polynomial

$$\lambda_D^N - 1 = 0\,. \tag{7.10}$$

Interestingly, the characteristic polynomial (6.7) with $\epsilon = 0$ is not (7.10) but

$$\lambda_D^{N-1} + \lambda_D^{N-2} + \cdots + \lambda_D + 1 = 0\,. \tag{7.11}$$

While $\lambda_D = 1$ ($\lambda_C = 0$) is an eigenvalue for (7.10), it is not an eigenvalue for (7.11). But if this eigenvalue is introduced in the polynomial, that is, if (7.11) is multiplied by $(\lambda - 1)$, then the two polynomials become identical.

For finite populations, the dimension of the system $(N-1)$ is not equal to the number of oscillators N, since the oscillator firing at phase $\theta = 0$ is artificially removed. This reduced dimension corresponds to a "modified dynamics" for which a global analysis (such as in Chapter 4) is more tractable. Surprisingly, for the local stability, an elegant mathematical expression is lost with the modified dynamics (see (7.11)). As a consequence, reintroducing a rigid (marginally stable) mode through the additional eigenvalue simplifies the local analysis (see (7.10)). The proof of Lemma 6.3.1 and the derivation of Criterion 1 are illustrations of such a simplification.

In full generality, the eigenvalue equation (6.27) for infinite populations is closely related to the characteristic polynomial (6.7) for finite populations. Indeed, according to (7.9), the eigenvalue equation (6.27) is interpreted as the polynomial (6.7) of infinite degree and multiplied by $(z-1)$.

Stability criterion. To complement the above discussion, it is also easy to see that Criterion 2 is the continuous analog of Criterion 1. Indeed, integrating (7.8) by parts and considering an excitatory coupling $K > 0$ yield

$$-\int_0^{2\pi} Z'(\theta)\, d\theta + \int_0^{2\pi} Z'(\theta)\, \cos(n\theta)\, d\theta \geq 0\,,$$

an inequality that is similar to (7.5). While local stability of finite populations only depends on $N-1$ values of the iPRC, local stability of infinite populations depends on $N \to \infty$ values, that is, it depends on the iPRC over the whole interval $[0, 2\pi]$.

The two criteria show that local stability is closely related to the derivative of the iPRC. According to Criterion 1, local stability of finite populations depends on the Fourier coefficients of a discrete sample of $Z'(\theta)$. Similarly, local stability of infinite populations is also related to the Fourier coefficients of $Z'(\theta)$, since (7.7) yields

$$\Re\{\lambda_n\} = \frac{K\,\omega}{2\pi}\,[Z(2\pi) - Z(0)] - \frac{K\,\omega}{2\pi}\Re\{\hat{Z}'_n\} = \frac{K\,\omega}{2\pi}\left(\hat{Z}'_0 - \Re\{\hat{Z}'_n\}\right)\,.$$

These observations are in agreement with the results of Chapter 5, which highlight the key role of the derivative of the iPRC.

The main difference between Criterion 1 and Criterion 2 is that Criterion 2 is easier to use: it is simpler to handle integrals instead of series. In the case of large numbers N, we will therefore prefer Criterion 2, which is more amenable to analytical calculations.

7.2 Dichotomic behavior of weakly coupled oscillators

Criterion 1 and Criterion 2 are powerful results to study the dichotomic behavior of weakly pulse-coupled oscillators: when the criteria show that all the eigenvalues have the same stability, they support a dichotomic behavior of the oscillators. A noticeable result is that the stability criteria prove the dichotomic behavior of QIF oscillators for finite and infinite populations, so that the QIF conjecture is solved in the weak coupling limit. Through Criterion

2, one also recovers, in the case of infinite populations, all the results known for finite populations of "QIF-like" oscillators (see Chapter 6). In addition, the stability criterion applies to more general situations: oscillators with delayed transmissions and oscillators that have not an integrate-and-fire dynamics (such as the realistic Hodgkin-Huxley and Fitzhugh-Nagumo oscillators).

7.2.1 Weakly coupled QIF oscillators have a dichotomic behavior

In this section, we solve the (local) QIF conjecture both for finite and infinite populations, showing that weakly pulse-coupled QIF oscillators always exhibit a dichotomic behavior.

Finite populations. The main result, obtained through Criterion 1, is given in Proposition 7.2.1. As a preliminary to this result, we need the following lemma.

Lemma 7.2.1. *Consider $N \in \mathbb{N}$ with $N \geq 2$ and $a \in (0,1)$. Then, for all $n = 1, \ldots, N-1$,*

$$\frac{\sin\left(\frac{N-1}{N}a\pi\right)}{\sin\left(\frac{a\pi}{N}\right)} - \frac{1}{2}(-1)^n \left(\frac{\sin\left(\frac{N-1}{N}(n\pi + a\pi)\right)}{\sin\left(\frac{1}{N}(n\pi + a\pi)\right)} + \frac{\sin\left(\frac{N-1}{N}(n\pi - a\pi)\right)}{\sin\left(\frac{1}{N}(n\pi - a\pi)\right)} \right) > 0\,. \tag{7.12}$$

Proof. The proof of Lemma 7.2.1 can be found in Appendix A.4. □

Proposition 7.2.1. *For weakly pulse-coupled QIF oscillators and for all $N \geq 2$, the fixed point of the $(N-1)$-dimensional firing map is locally stable if and only if $\underline{x} + \overline{x} > 0$.*

Proof. According to Table 2.1, the iPRC of QIF oscillators is given by $Z(\theta) = \frac{\omega}{S}\cos^2\left(\frac{\sqrt{S}}{\omega}(\theta - \overline{\theta})\right)$.

Using the equality

$$\sum_{k=1}^{N-1} \sin(k\,x + b) = \frac{\sin\left(\frac{N-1}{2}x\right)}{\sin(x/2)} \sin\left(\frac{N\,x}{2} + b\right)\,,$$

straightforward but lengthy computations of (7.5) yield

$$\begin{aligned} &-\sum_{k=1}^{N-1} Z'\left(k\frac{2\pi}{N}\right) + \sum_{k=1}^{N-1} Z'\left(k\frac{2\pi}{N}\right)\cos\left(\frac{kn2\pi}{N}\right) \\ &= \frac{1}{\sqrt{S}}\sin\left(\frac{2\sqrt{S}}{\omega}(\pi - \overline{\theta})\right) \\ &\quad \times \left[\frac{\sin\left(\frac{N-1}{N}\frac{2\sqrt{S}}{\omega}\pi\right)}{\sin\left(\frac{1}{N}\frac{2\sqrt{S}}{\omega}\pi\right)} - \frac{1}{2}(-1)^n \left(\frac{\sin\left(\frac{N-1}{N}(n\pi + \frac{2\sqrt{S}}{\omega}\pi)\right)}{\sin\left(\frac{1}{N}(n\pi + \frac{2\sqrt{S}}{\omega}\pi)\right)} + \frac{\sin\left(\frac{N-1}{N}(n\pi - \frac{2\sqrt{S}}{\omega}\pi)\right)}{\sin\left(\frac{1}{N}(n\pi - \frac{2\sqrt{S}}{\omega}\pi)\right)} \right) \right]. \end{aligned} \tag{7.13}$$

In addition, one easily shows that (see Table 2.1)

$$\omega > 2\sqrt{S}\,, \qquad 2\sqrt{S}|\pi - \overline{\theta}|/\omega < \pi\,. \tag{7.14}$$

Lemma 7.2.1 with $a = 2\sqrt{S}/\omega < 1$ implies that the sign of (7.13) is given by the sign of $\sin\left(\frac{2\sqrt{S}}{\omega}(\pi - \overline{\theta})\right)$. Then, it follows from (7.14) that (7.13) is positive for $\overline{\theta} < \pi$, or equivalently for $\underline{x} + \overline{x} > 0$ (see Property 4 and Table 6.1). Criterion 1 is thus satisfied if and only if $\underline{x} + \overline{x} > 0$, which completes the proof. □

Through Proposition 7.2.1, Conjecture 2 is proved under the assumption of weak coupling. This is a noticeable advance on the open problems arising from the study of QIF oscillators.

The proof of Proposition 7.2.1, as well as the proof of Lemma 7.2.1, is tedious. In contrast, the next paragraph shows that an equivalent proof for infinite populations is more straightforward.

Infinite populations. Infinite populations of weakly pulse-coupled QIF oscillators also exhibit a dichotomic behavior. The result, obtained through Criterion 2, is summarized in the following proposition.

Proposition 7.2.2. *For a continuum of weakly pulse-coupled QIF oscillators, the asynchronous state is locally stable if and only if* $K\,(\overline{x}+\underline{x})>0$.

Proof. According to Table 2.1, the iPRC of QIF oscillators is given by $Z(\theta)=\frac{\omega}{S}\,\cos^2\left(\frac{\sqrt{S}}{\omega}(\theta-\overline{\theta})\right)$. Then, straightforward computations of (7.8) lead to

$$K\int_0^{2\pi} Z(\theta)\,\sin(n\theta)\,d\theta = K\frac{2\pi\,n\,\omega^3\,\sin(4\pi^2\sqrt{S}/\omega)}{S(\omega^2n^2-4S)}\sin\left[\frac{2\sqrt{S}}{\omega}\left(\pi-\overline{\theta}\right)\right]\,,\quad n>0\,.$$

It follows from (7.14) that the above expression is positive for $K\,(\pi-\overline{\theta})>0$, or equivalently for $K\,(\underline{x}+\overline{x})>0$ (see Property 4 and Table 6.1). Criterion 2 is thus satisfied if and only if $K\,(\underline{x}+\overline{x})>0$, which completes the proof. □

Proposition 7.2.2 extends the result of Proposition 7.2.1 to infinite populations. In contrast with the lengthy proof of Proposition 7.2.1, the proof of Proposition 7.2.2 is much more straightforward, a simplification that illustrates the interest of approximating a large population by its continuum limit.

7.2.2 "QIF-like" oscillators

In Chapter 6, some results have been obtained on the dichotomic behavior of finite populations of "QIF-like" oscillators. In contrast, no equivalent result has been obtained for infinite populations. In this section, we apply Criterion 2 to study the behavior of infinite populations of "QIF-like" oscillators and we recover the results known in the case of finite populations. This still reinforces the parallel between finite and infinite populations.

Curvature of the iPRC. Section 6.4.3 provides a sufficient condition on the curvature of the firing map to ensure that the behavior is dichotomic, in the case of finite populations. The following proposition complements the result for infinite populations.

Proposition 7.2.3. *Consider a continuum of weakly pulse-coupled integrate-and-fire oscillators which (i) satisfy Assumption* (1) *and (ii) have an iPRC satisfying* $Z''(\theta)<0\ \forall\theta\in[0,2\pi]$. *Then, the asynchronous state is locally stable if and only if* $K\,(\overline{x}+\underline{x})>0$.

Proof. It follows from Property 4 that the iPRC can be rewritten as (2.14), with $Z_e''(\theta)<0$. Then, we define

$$I_n(\overline{\theta})\triangleq\int_0^{2\pi} Z(\theta)\,\sin(n\theta)\,d\theta=\int_0^{2\pi} Z_e(\theta-\overline{\theta})\,\sin(n\theta)\,d\theta$$

and compute the variation of $I_n(\overline{\theta})$ ($n > 0$) corresponding to a variation of the symmetry point $\overline{\theta}$. This yields

$$\frac{dI_n}{d\overline{\theta}} = -\int_0^{2\pi} Z_e'(\theta - \overline{\theta})\,\sin(n\theta)\,d\theta = \frac{1}{n}\left(Z_e'(2\pi - \overline{\theta}) - Z_e'(-\overline{\theta}) - \int_0^{2\pi} Z_e''(\theta - \overline{\theta})\,\cos(n\theta)\,d\theta\right)$$
$$< \frac{1}{n}\left(Z_e'(2\pi - \overline{\theta}) - Z_e'(-\overline{\theta}) - \int_0^{2\pi} Z_e''(\theta - \overline{\theta})\,d\theta\right) = 0\,.$$

When $\overline{\theta} = \pi$ (conservative limit case), the 2π-periodic function $Z(\cdot)$ is even, so that $I_n(\overline{\theta}) = 0$. Then, it follows that $I_n(\overline{\theta}) > 0\ \forall n > 0$ for $\overline{\theta} < \pi$, or equivalently for $\underline{x} + \overline{x} > 0$ (see Property 4 and Table 6.1). Criterion 2 is thus satisfied if and only if $K\,(\underline{x} + \overline{x}) > 0$, which completes the proof. □

Provided they have a concave-down iPRC, infinite populations of "QIF-like" oscillators exhibit a dichotomic behavior. One easily verifies — through (2.9) — that the result applies to exponential integrate-and-fire oscillators.

The curvature condition on the iPRC is the analog of a curvature condition on the firing map, so that Proposition 7.2.3 for infinite populations corresponds to Theorem 6.4.1 for finite populations.

Piecewise linear oscillators. Previous results show that finite populations of piecewise linear integrate-and-fire oscillators are not always characterized by a dichotomic behavior. Through Criterion 2, we show that it is still the case for infinite populations, confirming the numerical experiments presented in Section 6.6.2.

According to Table 2.1, the iPRC of piecewise linear integrate-and-fire oscillators is given by $Z(\theta) = \frac{\omega}{S}\,\exp(-\frac{\gamma}{\omega}|\theta - \overline{\theta}|)$. In the weak coupling limit, straightforward computations of (7.7) yield the eigenvalues

$$\Re\{\lambda_n\} = \frac{K\,n^2\,\omega^3}{2\pi^2 S(\gamma^2 + n^2\omega^2)}\left[-\frac{\gamma}{n}\sin(n\,\overline{\theta}) + \omega\,e^{-\pi\gamma/\omega}\sinh\left(\frac{\gamma}{\omega}(\overline{\theta} - \pi)\right)\right]\,.$$

The second term of the right hand, which dominates for $n \gg 1$, has a constant sign for all n. However, the first term is not negligible for lower values n and has a sign which depends on n. For some parameters, the values $\Re\{\lambda_n\}$ with a low n can be both positive and negative, depending on n (see Figure 7.1), so that there is always at least one unstable eigenvalue. As in the case of a finite population, the behavior is not dichotomic.

7.2.3 Transmission delays

In the weak coupling limit, considering transmission delays is a straightforward extension of the model. In particular, for infinite populations, we show that Criterion 2 is perfectly suited to consider a distribution of time delays and leads to an elegant formulation of the stability. We investigate whether delays modify or preserve the dichotomic behavior of the oscillators.

Transmissions delays can be induced by a non-instantaneous coupling, characterized by smoothed pulses $E(t)$ instead of δ-like pulses (see e.g. α-functions in Section 5.5.2). Then, as shown in [118], oscillators with delayed transmissions are equivalent to oscillators with no delay but characterized by the equivalent iPRC

$$Z_d(\theta) = \int_0^{\infty} Z(\theta + \xi)\,E(\xi/\omega)\,d\xi\,, \tag{7.15}$$

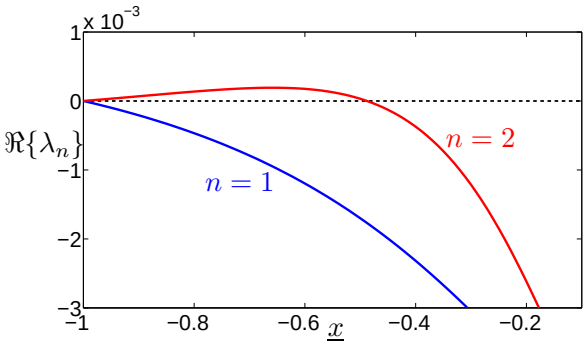

Figure 7.1: Piecewise linear oscillators have not a dichotomic behavior. When $\underline{x} < -0.5$, one has $\Re\{\lambda_2\} > 0$ while $\Re\{\lambda_1\} < 0$. (The parameters are $S = 1$, $\gamma = 1$, $K = 0.005$, and $\overline{x} = 1$.)

where Z is assumed to be 2π-periodic.

For infinite populations, an equivalent framework is to consider a distribution of delays. When the transmission between the oscillators is delayed by $t = \tau$, an oscillator receives a pulse when the emitting oscillator is at phase $\xi = \omega\tau$. If the delay is weak and constant, it is equivalent to consider oscillators with no delay, but characterized by the shifted iPRC $Z_d(\theta) = Z(\theta + \xi)$ [60]. If the delays are not constant, but randomly distributed, the phase lags ξ are also randomly distributed with a probability density function $g(\xi)$. Then, for infinite populations, [69] shows that oscillators with delayed transmissions are equivalent to oscillators with no delay but characterized by the equivalent iPRC

$$Z_d(\theta) = \int_0^\infty Z(\theta + \xi)\, g(\xi)\, d\xi\,. \tag{7.16}$$

The comparison between (7.15) and (7.16) implies that, for infinite populations, *a smoothed pulse is equivalent to a distribution of delays*, according to the relationship $g(\xi) \equiv E(\xi/\omega)$. As a consequence, the following results on (randomly distributed) delays equivalently apply to smoothed pulses.

In the case of infinite populations, Criterion 2 is applied to the equivalent iPRC obtained with transmission delays.

- For a constant delay, the Fourier coefficients of the equivalent iPRC are given by $\hat{Z}_{d,n} = \hat{Z}_n \exp(in\xi)$, so that Criterion 2 implies stability provided that

$$K\,\Im\{\hat{Z}_{d,n}\} = K\,\Big(\Im\{\hat{Z}_n\}\cos(n\xi) + \Re\{\hat{Z}_n\}\sin(n\xi)\Big) \geq 0 \quad \forall n \geq 0\,. \tag{7.17}$$

- For delays distributed according to the distribution $g(\xi)$, with a support in $[0, 2\pi]$, relationship (7.16) implies $Z^d(\theta) = Z_d(\theta) \odot g(2\pi - \theta)$, where $\odot$ is the circular convolution on $[0, 2\pi]$. The Fourier coefficients of the equivalent iPRC are $\hat{Z}_{d,n} = \hat{Z}_n\, \hat{g}_n^\dagger$, so that Criterion 2 implies stability provided that

$$K\,\Im\{\hat{Z}_{d,n}\} = K\,\Big(\Im\{\hat{Z}_n\}\Re\{\hat{g}_n\} - \Re\{\hat{Z}_n\}\Im\{\hat{g}_n\}\Big) \geq 0 \quad \forall n \geq 0\,. \tag{7.18}$$

Delayed transmissions affect the stability properties of the network and the oscillators can consequently lose their dichotomic behavior. For instance, (7.17) implies that if the stability criterion is satisfied for the model without delay (i.e. $K\,\Im\{\hat{Z}_n\} \geq 0$), then the stability criterion is likely not to be satisfied when a delay is introduced (i.e. $K\,\Im\{\hat{Z}_{n,d}\} < 0$ for some n). As explained above, delays (or equivalently smoothed pulses) modify the iPRC so that even monotone LIF oscillators can lose their monotonicity properties and can exhibit non-dichotomic behaviors (see [60, 117] and Section 5.5.2).

Interestingly, while distributions of delays usually preclude the dichotomic behavior of the oscillators, particular distributions can preserve a dichotomic behavior or even induce a dichotomic behavior in (initially) non-dichotomic models.

Delays preserving a dichotomic behavior. Particular distributions do not modify the stability property of the oscillators: they are so that $\Im\{\hat{Z}_{n,d}\} \geq 0$ whenever $\Im\{\hat{Z}_n\} \geq 0$. In this case, the delays preserve the dichotomic behavior of the oscillators. This is illustrated in the following examples.

Example 7.2.1 (Even distributions)**.** When the delay distribution is even, that is $g(2\pi-\xi) = g(\xi)$, one has $\Im\{\hat{g}_n\} = 0$ so that condition (7.18) is rewritten as

$$K\,\Im\{\hat{Z}_n\}\,\Re\{\hat{g}_n\} \geq 0 \quad \forall n \geq 0\,. \tag{7.19}$$

Provided that the values $\Re\{\hat{g}_n\} \geq 0$ for all $n > 0$ [see Figure 7.2 (a)], stability of the model without delay ($K\,\Im\{\hat{Z}_n\} \geq 0$) implies stability of the model with delays (7.19). ◇

Example 7.2.2 (Odd distributions)**.** When the delay distribution is odd, that is $g(2\pi-\xi) = -g(\xi)$, one has $\Re\{\hat{g}_n\} = 0\ \forall n > 0$ so that condition (7.18) is rewritten as

$$K\,\Re\{\hat{Z}_n\}\,\Im\{\hat{g}_n\} \leq 0 \quad \forall n \geq 0\,.$$

Provided that the values $\Im\{\hat{g}_n\} \geq 0$ for all $n > 0$ [see Figure 7.2 (b)], stability of the model with delay is determined by the sign of the coefficients $\Re\{\hat{Z}_n\}$ (instead of $\Im\{\hat{Z}_n\}$). If they are all positive, or all negative, a dichotomic behavior is preserved. ◇

(a) Even distribution (b) Odd distribution

Figure 7.2: (a) The even delay distribution g satisfies $\Im\{\hat{g}_n\} = 0$ and $\Re\{\hat{g}_n\} \geq 0$ for all $n > 0$. Then, the delays do not modify the stability property of the network. (b) The odd delay distribution g satisfies $\Re\{\hat{g}_n\} = 0$ and $\Im\{\hat{g}_n\} \geq 0$ for all $n > 0$. Then, stability depends on the coefficients $\Re\{\hat{Z}_n\}$.

Delays inducing a dichotomic behavior. The delay distribution can modify the iPRC in such a way that non-dichotomic oscillators exhibit a dichotomic behavior. Indeed, the delay distribution can be so that (7.18) is satisfied, even though (7.8) is not satisfied for Z. This is illustrated in the the following example.

Example 7.2.3 (Piecewise linear oscillators)**.** Networks of piecewise linear oscillators, with delayed transmissions, can exhibit a dichotomic behavior. The non-dichotomic behaviors of (non-delayed) piecewise linear oscillators arise because Criterion 2 is not satisfied for $n = 2$. If the delay distribution is the even distribution presented in Figure 7.2 (a), then one easily computes that $\Re\{\hat{g}_n\} = 0$ for all n even. In particular, the case $n = 2$ corresponds to a zero value in condition (7.19), condition that is therefore satisfied. Thus, the behavior of delayed piecewise linear oscillators is dichotomic. ◇

7.2.4 General models

The weak coupling limit is relevant not only for integrate-and-fire oscillators but also for more general (pulse-coupled) models of oscillators, including realistic biological models. Indeed, the phase reduction of multidimensional dynamics in the neighborhood of a limit cycle is valid only under the weak coupling assumption. In addition, to the weak coupling limit are associated Criterion 1 and Criterion 2, that can apply to very realistic iPRC's, however complex they are.

General models of oscillators do not exhibit a (global) dichotomic behavior, as defined in the previous chapters. Since the oscillators are not integrate-and-fire oscillators, their dynamics does not involve the thresholds $\underline{x}$ and $\overline{x}$ that determine the dichotomic behavior. In addition, in contrast with "QIF-like" oscillators, a local stability analysis gives no guarantee about the global stability of the trajectories. However, local analysis is still of interest to investigate whether locally stable phase-locked configurations (or asynchronous states) are observed within the network.

In the sequel, we apply Criterion 1 and Criterion 2 to two realistic neuron models: the well-known Hodgkin-Huxley (HH) model [45, 50] (see also Example 2.1.1) and the Fitzhugh-Nagumo (FN) model [34, 50, 78] (see also Example 2.1.2), whose respective iPRC is given in Figure 2.4. (The phase $\theta = 0$, which defines the precise firing instant when a pulse is sent out, is assigned to the maximal value of the membrane voltage on the limit cycle.)

For weakly pulse-coupled HH oscillators or FN oscillators, a phase-locked configuration is never observed with finite populations and, similarly, an asynchronous state is never observed with infinite populations. Indeed, Figure 7.3 shows that Criterion 1 and Criterion 2 are never satisfied with these models. Except for FN oscillators with $N = 5$, several stable eigenvalues coexist along with several unstable eigenvalues. This suggests that the behavior could be more complex than the non-dichotomic behavior of "QIF-like" oscillators, for which only two eigenvalues have an opposite stability with respect to all the others (see Section 6.5.2). Further investigations require numerical experiments that are beyond the scope of the present dissertation.

Local stability of finite populations (Criterion 1) is coherent with local stability of infinite populations (Criterion 2). More precisely, a finite population with few oscillators is well-approximated by an infinite population. For instance, Figure 7.3 (c) and Figure 7.3 (d) are similar and coherent, similar for the low frequency eigenvalues and coherent since the infinite

spectrum of Figure 7.3 (d) has no influence on the behavior (the imaginary part of the high frequency eigenvalues rapidly decreases to zero, when n increases). This observation shows that the behavior of only $N = 20$ oscillators is equivalent to the behavior of an infinite population.

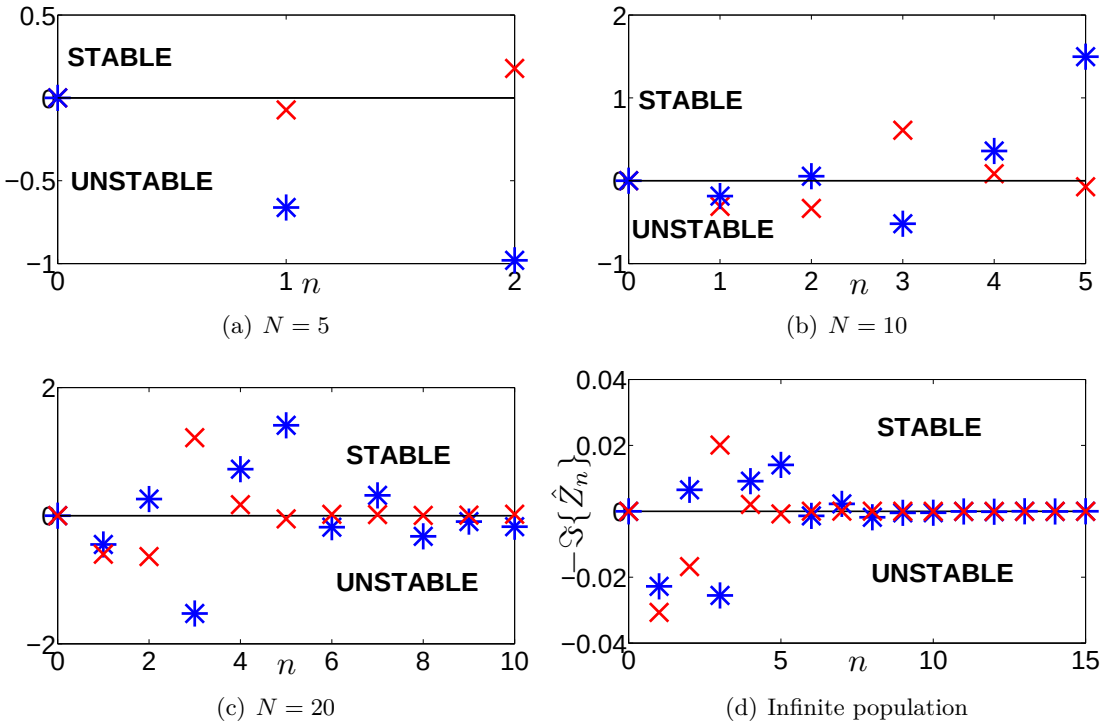

(a) $N = 5$ (b) $N = 10$

(c) $N = 20$ (d) Infinite population

Figure 7.3: The eigenvalues are not all stable, whether for the HH model (red cross markers) or the FN model (blue star markers). (a,b,c) In the case of finite populations, the markers correspond to the values (7.5) of Criterion 1 for every $n < N/2$ (the other values are identical to the first values). (d) In the case of infinite populations, the markers correspond to the values (7.8) of Criterion 2. (For the sake of clarity, the values corresponding to the FN model have been divided by 5.)

The above results have underlined that the phase-locked configuration (or the asynchronous state) is always unstable. Indeed, Criterion 1 and Criterion 2 are not satisfied. However, in some situations, the criteria are satisfied. For instance, close to a Hopf bifurcation (observed with the FN model) or a Bautin bifurcation (observed with the HH model), the iPRC is well-approximated by a sinusoidal function (see [13]) and has therefore only one nonzero Fourier coefficient, so that the criteria can be satisfied.

For infinite populations, local stability of the asynchronous state is also obtained with particular delay distributions. For instance, consider an even distribution ($\Im\{\hat{g}_n\} = 0$) satisfying $\Re\{\hat{g}_n\} = C\,\Im\{\hat{Z}_n\}$, $n > 0$, where C is a positive constant (with $g(\theta) > 0\ \forall\theta$ and $\hat{g}_0 = 1$). Then, it follows from (7.19) that Criterion 2 is satisfied. This is illustrated with HH oscillators in Figure 7.4.

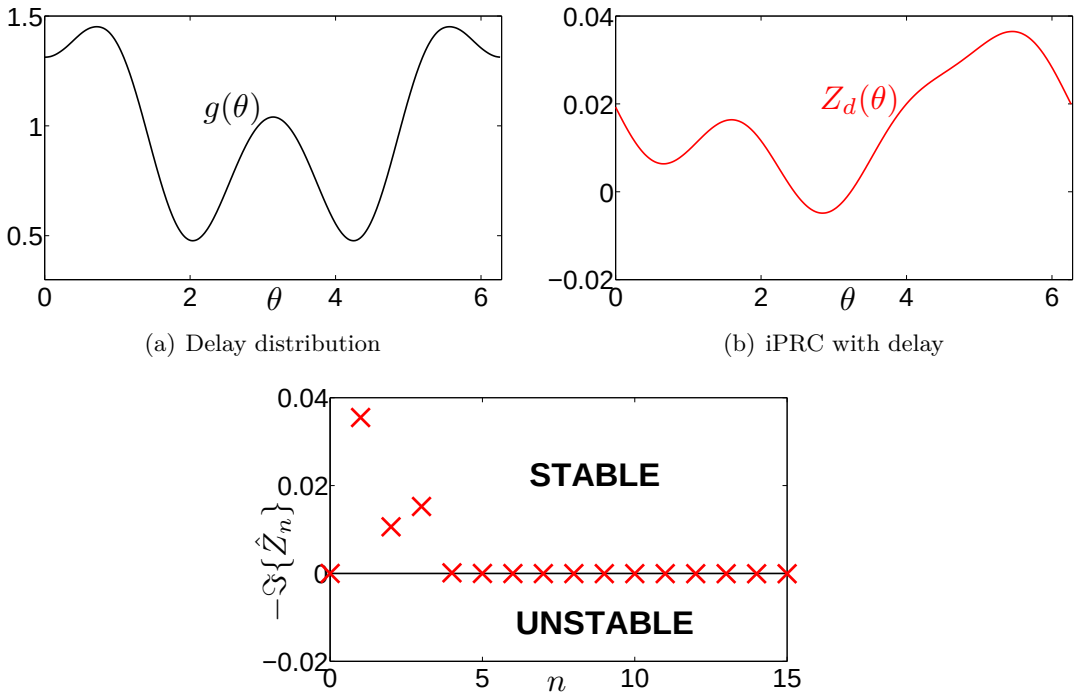

(a) Delay distribution

(b) iPRC with delay

(c) Stability of the eigenmodes

Figure 7.4: For infinite populations of HH oscillators, the asynchronous state is locally stable with a particular delay distribution. (a) The delay distribution is even and satisfies $\Re\{\hat{g}_n\} = 6\,\Im\{\hat{Z}_n\}$. (b) The delays yield an iPRC that satisfies Criterion 2: (c) Condition (7.8) is positive for all $n > 0$.

7.3 Averaging

In the weak coupling limit, averaging techniques can be applied to the dynamics of the pulse-coupled oscillators and lead to a very general averaged model, whose particular case is the well-known Kuramoto model. In this context, the results obtained in the previous chapters are exploited to derive new results on the general averaged model on the one hand and to derive a new formulation of the QIF conjecture on the other hand.

7.3.1 Averaged phase dynamics

When averaging techniques (see [55] for an overview) are applied to weakly coupled oscillators, the averaged phase dynamics has a universal form, characterized by a coupling that depends on the phase differences between the oscillators [47, 58]. The averaged phase dynamics is given by

$$\dot{\theta}_k = \omega + \sum_{\substack{j=1 \\ j\neq k}}^{N} \Gamma(\theta_k - \theta_j)\,, \tag{7.20}$$

where $\Gamma(\cdot)$ is the 2π-periodic *coupling function*. A well-known model of the form (7.20) is the Kuramoto model [59].

Example 7.3.1 (Kuramoto model)**.** The Kuramoto model is characterized by the coupling function $\Gamma(\theta) = -K/N \sin(\theta)$, a function that can be considered as the first odd Fourier harmonic of more complex coupling functions. The constant K is the coupling strength.

The measure of synchrony

$$\mathcal{V}(\mathbf{\Theta}) = \left\| \sum_{k=1}^{N} e^{i\theta_k} \right\|^2$$

is a quadratic Lyapunov function for the model. It follows that the global behavior is very simple:

- When the coupling is excitatory ($K > 0$), the oscillators achieve perfect synchrony;
- When the coupling is inhibitory ($K < 0$), the oscillators globally converge toward an incoherent state characterized by

$$\sum_{k=1}^{N} e^{i\theta_k} = 0\,.$$

In spite of the simple behavior of the identical Kuramoto oscillators, the model is however worth of interest. Indeed, the study of non-identical Kuramoto oscillators, though amenable to mathematical analysis, leads to intricate open problems. Investigating heterogeneous populations in the Kuramoto model is a major issue on which there is an extensive literature [4, 104]. ◇

The analysis of identical Kuramoto oscillators is trivial because the coupling function is odd, that is $\Gamma(\theta) = -\Gamma(2\pi - \theta)$. Indeed, when the coupling function is odd, the system is a gradient system, therefore characterized by strong global stability properties [47].

In contrast, the analysis is more involved in the case of pulse-coupled oscillators. In this case, the coupling function is expressed as a function of the iPRC and is therefore not odd: the system is no longer a gradient system. The derivation of the coupling function is explained in the following paragraph, adapted from [60].

In the weak coupling limit, (3.3) implies that $Z_\epsilon \approx \epsilon Z$. In addition, the phases can be decomposed as $\theta_k = \omega t + \zeta_k$, where ζ_k is a slow phase deviation from the uniform natural oscillation $\omega\, t$. Then, the pulse-coupled phase dynamics (3.2) is rewritten as

$$\dot{\zeta}_k = \epsilon\, Z\left((\omega t + \zeta_k) \bmod 2\pi\right) \sum_{\substack{j=1 \\ j\neq k}}^{N} \sum_{l=0}^{\infty} \delta(t - t_l^{(j)})\,.$$

The modulo operation is introduced because we consider that the iPRC is defined in $[0, 2\pi]$ only. Next, averaging the above dynamics over a period $\Delta T \approx 2\pi/\omega$ and under fixed ζ_k, we obtain

$$\dot{\zeta}_k = \frac{1}{\Delta T} \int_t^{t+\Delta T} \epsilon\, Z\left((\omega s + \zeta_k) \bmod 2\pi\right) \sum_{\substack{j=1 \\ j\neq k}}^{N} \sum_{l=0}^{\infty} \delta(s - t_l^{(j)})\, ds = \frac{\omega}{2\pi} \epsilon \sum_{\substack{j=1 \\ j\neq k}}^{N} \left(Z(\omega t^{(j)} + \zeta_k) \bmod 2\pi \right),$$

since each oscillator fires once over the period. The firing times satisfy $\omega t^{(j)} + \zeta_j = 0$, so that one finally gets

$$\dot{\zeta}_k = \epsilon \frac{\omega}{2\pi} \sum_{\substack{j=1 \\ j \neq k}}^{N} Z\big((\zeta_k - \zeta_j) \bmod 2\pi\big)$$

or equivalently

$$\dot{\theta}_k = \omega + \epsilon \frac{\omega}{2\pi} \sum_{\substack{j=1 \\ j \neq k}}^{N} Z\big((\theta_k - \theta_j) \bmod 2\pi\big)\,.$$

Thus, the averaged dynamics is of the form (7.20), with a coupling function related to the iPRC according to

$$\Gamma(\theta) = \epsilon \frac{\omega}{2\pi} Z(\theta \bmod 2\pi)\,. \tag{7.21}$$

Apart from the conservative limit case $\underline{x} + \overline{x} = 0$, the coupling function is discontinuous, that is $\Gamma(0^-) \neq \Gamma(0^+)$. However, it is important to note that the 2π-periodicity condition imposes $\Gamma(0) = \Gamma(2\pi)$ (Figure 7.5). If the condition is not satisfied, synchronized states are ill-defined.

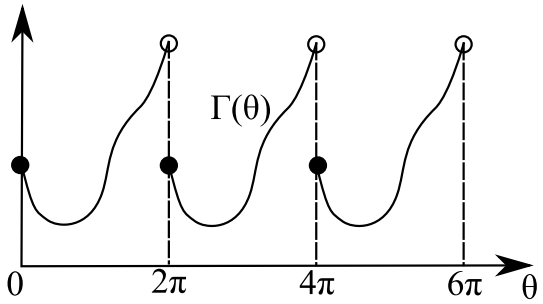

Figure 7.5: The coupling function of the pulse-coupled oscillators is discontinuous but satisfies the 2π-periodicity condition, so that $\Gamma(0) = \Gamma(2\pi)$.

7.3.2 Links to pulse-coupled oscillators

In the case of pulse-coupled oscillators, the study of the averaged phase dynamics is valuable. Inspired by the results obtained on monotone pulse-coupled oscillators (Chapter 4), we show that the averaged dynamics has a strong contraction property when the coupling function is monotone. In addition, we obtain an elegant reformulation of the (global) QIF conjecture.

Monotone oscillators

Networks of monotone pulse-coupled oscillators are characterized by a strong contraction property (Chapter 4). Since the iPRC of the oscillators is monotone, the coupling function of the averaged dynamics (7.20) is monotone on $(0, 2\pi)$, according to (7.21). This suggests a general property related to consensus problems: the general phase dynamics (7.20) with a monotone coupling function on $(0, 2\pi)$ is characterized by a contraction property.

As explained in [76], the study of phase oscillators that evolve according to (7.20) within a *semicircle* is equivalent to a trivial consensus problem on the real line. [For instance, the oscillators with phases within the interval $(-\pi/2, \pi/2)$ are mapped to the real line through the change of coordinates $\theta \mapsto x = \tan(\theta)$.] Then, a simple argument shows that, if the coupling function is monotone increasing, the convex hull of the individual oscillators can only shrink along the solution of (7.20), that is, the distance $\max\{\theta_k\} - \min\{\theta_k\}$ decreases. As a consequence, all the oscillators asymptotically reach a *consensus value*: they achieve perfect synchrony.

We emphasize that, when the oscillators are not within a semicircle, the above argument fails since the problem is *not equivalent to a consensus problem on the real line*. Actually, the whole N-torus $\mathbb{T}^N$ is not a convex set and a distance between the oscillators (such as the "min-max" distance) cannot capture the collective behavior of the oscillators (an extensive survey on consensus problems on the circle — in contrast with consensus on the real line — can be found in [95]).

In the sequel, we address the above issue, exploiting the global results presented in Chapter 4 (in particular Theorem 4.2.2) and thereby extending the known result of a trivial consensus problem on the real line to a more significant result on the N-torus. In particular, we show that the phase dynamics has a strong contraction property with respect to a 1-norm, a result that can be compared with the result of [83] showing that a quadratic Lyapunov function does not exist for consensus algorithms on the real line (with time-dependent connectivity).

In the previous chapters, the pulse-coupled oscillators are described through a phase difference with respect to the firing oscillator (at phase $\theta = 0$). To exploit the results of Chapter 4, the phase dynamics (7.20) is similarly expressed in terms of phase differences, in a rotating frame associated with an oscillator (without loss of generality, we choose oscillator 1). Denoting the phase differences by $\tilde{\theta}_k = \theta_{k+1} - \theta_1$ for $k = 1, \dots, N-1$, we obtain the $N-1$ equations

$$\dot{\tilde{\theta}}_k = \Gamma(\tilde{\theta}_k) + \sum_{\substack{j=1 \\ j \neq k}}^{N-1} \Gamma(\tilde{\theta}_k - \tilde{\theta}_j) - \sum_{j=1}^{N-1} \Gamma(-\tilde{\theta}_j)\,. \tag{7.22}$$

Whereas the dynamics (7.20) is invariant with respect to a rigid rotation of the oscillators, the change of coordinates removes the marginally stable rigid mode. Moreover, a trajectory $\tilde{\Theta}$ is not defined in $\mathbb{T}^N$, but in the cone $\mathcal{C} = \{\tilde{\boldsymbol{\Theta}} \in (0, 2\pi)^{N-1} | \tilde{\theta}_k < \tilde{\theta}_{k+1}\}$, an open set that is the equivalent of $\mathcal{U}$ (3.21).

The dynamics (7.22) has several fixed points (Figure 7.6). The only fixed point in the interior of the cone $\mathcal{C}$ corresponds to the phase-locked configuration of the oscillators. Given the periodicity of the coupling function, it is the splay state

$$\tilde{\theta}_k^* = k\frac{2\pi}{N}\,. \tag{7.23}$$

The other fixed points are in the boundary of $\mathcal{C}$, where at least two oscillators are synchronized. The (unique) synchronized configuration of all the oscillators is represented by N different fixed points

$$\begin{cases} \theta_k^* = 0 & \text{for } k < j \\ \tilde{\theta}_k^* = 2\pi & \text{for } k \geq j \end{cases} \qquad j = 1, \dots, N\,. \tag{7.24}$$

Finally, the last fixed points, denoted by P_k in Figure 7.6, correspond to phase-locked configurations characterized by two or more synchronized oscillators, that is, characterized by $\tilde{\theta}_k = 0$, $\tilde{\theta}_k = 2\pi$, or $\tilde{\theta}_k = \tilde{\theta}_{k+1}$ for at least one subscript k. They are $2^N - 2 - N$ saddle points.

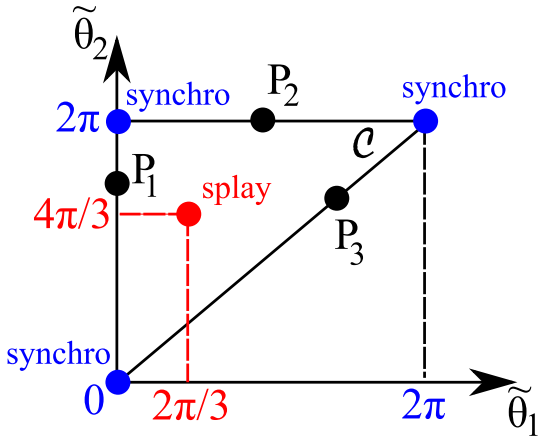

Figure 7.6: The dynamics (7.22) has several fixed points on the cone $\mathcal{C}$ (here in two dimensions, i.e. $N - 1 = 2$). The splay state $(2\pi/3, 4\pi/3)$ is the only fixed point in the interior of $\mathcal{C}$. The synchronized state corresponds to the three fixed points $(0, 0)$, $(0, 2\pi)$, and $(2\pi, 2\pi)$. There are other unstable fixed points in the boundary of $\mathcal{C}$.

Next, we claim that the dynamics (7.22) is a contraction on the cone $\mathcal{C}$ with respect to the 1-norm (4.10) previously used with monotone pulse-coupled oscillators.

Theorem 7.3.1. *Consider a coupling function that satisfies either* $\Gamma''(\theta) \geq 0$ $\forall \theta \in (0, 2\pi)$ *or* $\Gamma''(\theta) \leq 0$ $\forall \theta \in (0, 2\pi)$. *If* $\Gamma'(\theta) < 0$ $\forall \theta \in (0, 2\pi)$, *then the dynamics* (7.22) *is contracting on* $\mathcal{C}$ *for the* 1*-norm* (4.10), *that is*

$$\frac{d}{dt} \left\| \tilde{\mathbf{\Theta}}(t) - \tilde{\mathbf{\Psi}}(t) \right\|_{(1)} < 0 \,,$$

where $\tilde{\mathbf{\Theta}}(\cdot)$ *and* $\tilde{\mathbf{\Psi}}(\cdot)$ *are two distinct solutions of* (7.22) *in* $\mathcal{C}$. *If* $\Gamma'(\theta) > 0$ $\forall \theta \in (0, 2\pi)$, *the dynamics is expanding, that is*

$$\frac{d}{dt} \left\| \tilde{\mathbf{\Theta}}(t) - \tilde{\mathbf{\Psi}}(t) \right\|_{(1)} > 0 \,.$$

Proof. The proof has some similarity to the proof of Theorem 5.3.1. Owing to its length, it is deferred to Appendix A.5. □

Contraction properties of dynamical systems are usually considered with respect to quadratic metrics [6, 7, 67]. For instance, networks of diffusively coupled oscillators have been studied through a (quadratic) contraction argument [121]. In contrast, numerical experiments show that the contraction property of (7.22) cannot be captured through a quadratic norm. Theorem 7.3.1 underlines the importance of considering a 1-norm instead of a quadratic norm.

The result of Theorem 7.3.1 is also in contrast to the quadratic norm that characterizes the dynamics of Kuramoto oscillators (Example 7.3.1). However, the dichotomic behavior

of monotone oscillators is identical to the dichotomic behavior of Kuramoto oscillators. The result is a corollary of Theorem 7.3.1.

Corollary 7.3.1. *Consider a network of N phase oscillators with the dynamics* (7.20)*. Provided that the coupling function has a curvature of constant sign on* $(0, 2\pi)$*, for almost every initial condition,*

- *the oscillators asymptotically converge to the splay state configuration*

$$\theta_k^*(t) = \theta_0 + \Omega\, t + (k-1)\frac{2\pi}{N} \qquad \text{with } \Omega \text{ and } \theta_0 \text{ constant } \forall k \tag{7.25}$$

  if the coupling function is strictly decreasing on $(0, 2\pi)$*;*

- *the oscillators achieve perfect synchrony in finite time if the coupling function is strictly increasing on* $(0, 2\pi)$*.*

Proof. We first consider the case of a decreasing coupling function. Let $\mathbf{\Phi}$ denote the flow of (7.22), that is, $\mathbf{\Phi}(\tilde{\mathbf{\Theta}}, t)$ is a solution of (7.22), with $\mathbf{\Phi}(\tilde{\mathbf{\Theta}}, 0) = \tilde{\mathbf{\Theta}}$. Theorem 7.3.1 implies that

$$\left\|\mathbf{\Phi}(\tilde{\mathbf{\Theta}}, t) - \mathbf{\Phi}(\tilde{\mathbf{\Psi}}, t)\right\|_{(1)} < \left\|\tilde{\mathbf{\Theta}} - \tilde{\mathbf{\Psi}}\right\|_{(1)} \qquad \forall t \text{ small enough}\,.$$

Then, for any small fixed Δt, the discrete-time mapping $\tilde{\mathbf{\Theta}} \mapsto \mathbf{\Phi}(\tilde{\mathbf{\Theta}}, \Delta t)$ is a contraction in $\mathcal{C}$. From the contraction mapping theorem (see e.g. [55]), the solutions of (7.22) asymptotically converge to (7.23), for every initial condition in $\mathcal{C}$ (see also the developments in [7]). As a consequence, for all initial conditions (except a zero-measure set corresponding to the boundary of $\mathcal{C}$), the trajectories of the original dynamics (7.20) asymptotically converge to

$$\theta_{k+1}^*(t) = \theta_1^*(t) + \tilde{\theta}_k^* = \theta_1^*(t) + k\frac{2\pi}{N}\,, \qquad k \neq 1\,. \tag{7.26}$$

It follows from (7.20) that the velocity of θ_1^* is constant: $\dot{\theta}_1^* = \omega + \sum_{j=1}^{N-1} \Gamma(j2\pi/N) \triangleq \Omega$. Then, $\theta_1^* = \theta_0 + \Omega t$ and (7.26) corresponds to the splay state (7.25), which concludes the first part of the proof.

In the case of an increasing coupling function, Theorem 7.3.1 implies that the distance between a trajectory (in $\mathcal{C}$) and, say the fixed point (7.23), must monotonically increase. Then, the trajectory converges toward the boundary of $\mathcal{C}$, which corresponds to the synchronization of two oscillators. A straightforward computation shows that the trajectory approaches the boundary with the finite velocity $\Gamma(2\pi^-) - \Gamma(0^+)$ (e.g. $\dot{\tilde{\theta}}_k - \dot{\tilde{\theta}}_{k+1} = \Gamma(2\pi^-) - \Gamma(0^+)$ in the vicinity of the boundary $\tilde{\theta}_k = \tilde{\theta}_{k+1}$). Then, the trajectory reaches the boundary in finite time [see Figure 7.7 (a)]. In addition, for almost every initial condition, it cannot converge to a (unstable) saddle node P_k.

Since two synchronized oscillators remain synchronized forever, the boundary of $\mathcal{C}$ is an invariant set: the trajectory subsequently evolves within a $(N-2)$-dimensional cone $\mathcal{C}'$, lying in the boundary of $\mathcal{C}$ and delimited by $(N-3)$-dimensional subsets corresponding to another synchronization of two oscillators. The reduced dynamics governing the evolution of the trajectory in $\mathcal{C}'$ satisfies the contraction property of Theorem 7.3.1 (see Remark A.5.1 in Appendix A.5). Then, a same argument as above proves that, for almost every initial

condition, the trajectory converges in finite time to the $(N-3)$-dimensional boundary of $\mathcal{C}'$, leading to a second synchronization of two oscillators.

The argument can be repeated and after $N-1$ successive synchronization of pairs of oscillators, the network achieves synchrony in finite time. [See Figure 7.7 (b)]. □

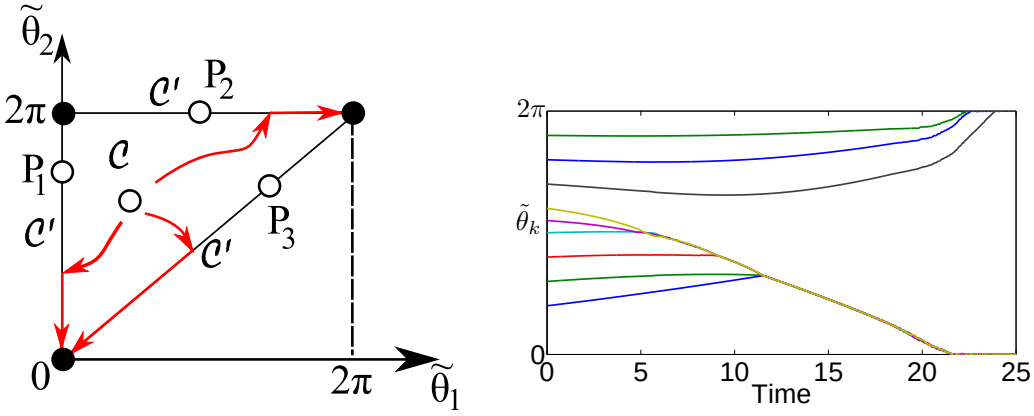

(a) $N = 3$ (b) $N = 10$

Figure 7.7: (a) The trajectories (in red) reach the boundary of $\mathcal{C}$ in finite time. Then, they evolve in $\mathcal{C}'$ and converge to the synchronization state. (b) Several pairwise synchronizations occur, until the network achieves perfect synchrony.

Whether on a semicircle or not, the oscillators always exhibit the same behavior. For instance, with a monotone increasing coupling function, the oscillators always achieve synchrony (consensus). The simple results of consensus on the real line (or equivalently on the semicircle) are extended to more general results that hold for any configurations in the whole N-torus.

As Theorem 7.3.1 and its corollary extend the results of Chapter 4 for finite populations, similar results could also generalize the results of Chapter 5 for infinite populations. This issue is not addressed in this manuscript.

QIF oscillators

Now that the contraction property of monotone oscillators (Chapter 4) has been extended to the general phase dynamics (7.20), we investigate whether interesting links can also be drawn in the case of "QIF-like" oscillators (Chapter 6).

In Section 7.2.1, the local QIF conjecture (Conjecture 2) is solved in the weak coupling limit. However, the global QIF conjecture (Conjecture 1) is still unsolved, even in the weak coupling limit. In this context, we suggest that an "averaged version" of the global QIF conjecture could be more tractable.

An averaged phase dynamics of the form (7.20) is interpreted as a continuous-time equivalent of the discrete-time return map $\mathbf{R} = \mathbf{H}^N$. Hence, it fully exploits the average properties of the dynamics, that are of paramount importance in the case of QIF oscillators.

According to Table 2.1, the iPRC of QIF oscillators is given by

$$Z(\theta) = \frac{\omega}{S}\,\cos^2\left(\frac{\sqrt{S}}{\omega}(\theta-\overline{\theta})\right) = \frac{\omega}{2S}\,\left(1+\cos\left(\frac{2\sqrt{S}}{\omega}(\theta-\overline{\theta})\right)\right)\,.$$

Denoting $a \triangleq 2\sqrt{S}/\omega$, (7.21) implies that the coupling function related to the pulse-coupled QIF oscillators is given by

$$\Gamma(\theta) = \frac{\epsilon\,\omega^2}{4\pi\,S}\left(1+\cos\Big(a((\theta \bmod 2\pi)-\overline{\theta})\Big)\right)\,.$$

Removing the constant term as well as the multiplicative constant, that correspond to a rigid motion of the oscillators, we obtain the averaged dynamics

$$\dot{\theta}_k = \omega + \sum_{\substack{j=1\\ j\neq k}}^{N} \cos\Big(a\Big((\theta_k-\theta_j) \bmod 2\pi\Big) - a\overline{\theta}\Big)\,. \tag{7.27}$$

The averaged dynamics (7.27) of weakly pulse-coupled QIF oscillators has an elegant form. From (7.14), it follows that $a < 1$ and the coupling function thereby results from the shift and the dilatation of a 2π-periodic cosine function, whose values are taken within $(0, 2\pi)$.

In the limit case $a = 1$, (7.27) becomes the dynamics

$$\dot{\theta}_k = \omega + \sum_{\substack{j=1\\ j\neq k}}^{N} \cos\Big(\theta_k-\theta_j-\overline{\theta}\Big) \tag{7.28}$$

and corresponds (up to a sign) to a dynamics of Josephson-junction arrays that has been extensively studied in [122]. The authors showed that the dynamics is characterized by $N-3$ constants of motion, so that it can be reduced to a 3-dimensional dynamics, whatever the number of oscillators. When $\overline{\theta} = \pi$, the 3-dimensional system is an integrable Hamiltonian system. When $\overline{\theta} \neq \pi$, the Hamiltonian function induces a Lyapunov function that forces global convergence to the phase-locked splay state ($\overline{\theta} < \pi$) or to the synchronized state ($\overline{\theta} > \pi$).

The results of [122] are in agreement with Conjecture 1 on the dichotomic behavior of the QIF oscillators. The integrable Hamiltonian system is obtained with $\overline{\theta} = \pi$, a situation that corresponds to the conservative limit case $\underline{x} + \overline{x} = 0$. In addition, phase-locking (resp. synchronization) is obtained for $\overline{\theta} < \pi$ (resp. $\overline{\theta} > \pi$), a situation that corresponds to $\underline{x}+\overline{x} > 0$ (resp. $\underline{x} + \overline{x} < 0$) (see Table 6.1).

However, the above results do not directly apply to the study of QIF oscillators. Indeed, the dynamics (7.28) has a continuous coupling function $\Gamma(\theta) = \cos(\theta - \overline{\theta})$, a limit situation ($a = 1$) that corresponds to the extreme case $\underline{x} = -\infty$, $\overline{x} = \infty$. In full generality, the modulo function in the averaged QIF dynamics (7.27) introduces a discontinuity that makes the analysis more difficult.

Owing to the simple expression of (7.27) and to its close link to the results of [122], a global analysis of (7.27) is an equivalent and elegant reformulation of the global QIF conjecture (Conjecture 1) for weakly coupled QIF oscillators.

Conjecture 3 ((Weak coupling) QIF conjecture)**.** *The behavior of weakly coupled QIF oscillators is always dichotomic. That is, the averaged dynamics*

$$\dot{\theta}_k = \omega + \sum_{\substack{j=1 \\ j\neq k}}^{N} \cos\Big(a\Big((\theta_k - \theta_j) \bmod 2\pi\Big) - a\overline{\theta}\Big)\,, \qquad a < 1\,.$$

leads to synchronization for $\overline{\theta} > \pi$ *and to splay state for* $\overline{\theta} < \pi$*.*

7.4 Conclusion

A weak coupling assumption simplifies the dynamics of the pulse-coupled integrate-and-fire oscillators. In particular, efficient criteria are derived for local stability of both finite and infinite populations, a result that solves the local QIF conjecture.

To the weak coupling assumption are associated efficient techniques to average the dynamics of the oscillators. In the case of monotone oscillators, the averaged dynamics has a strong contraction property, a result that complements known results related to consensus problems. For QIF oscillators, the averaged dynamics yields a simple reformulation of the global QIF conjecture.

The averaged dynamics of the pulse-coupled oscillators is a classical model of coupled oscillators, a particular case of which is the well-known Kuramoto model. The stability problem of weakly pulse-coupled oscillators is therefore equivalent to the stability problem of a "Kuramoto-like" model. This clearly suggests that the general analysis of pulse-coupled oscillators (without the weak coupling assumption), such as presented in Chapters 4-6, is more involved than the analysis of classical models of coupled oscillators like the Kuramoto model.

Chapter 8

Conclusions and perspectives

The present dissertation is a study of the collective behaviors in networks of pulse-coupled oscillators. While an extensive literature considers only *leaky* integrate-and-fire oscillators, the present study investigates *other integrate-and-fire dynamics*, including the well-known *quadratic* integrate-and-fire dynamics. The study highlights that a *dichotomic behavior* is frequently observed: the oscillators either achieve perfect synchrony (periodic behavior with low firing frequency) or converge toward a phase-locked clustering configuration (periodic behavior with high firing frequency).

We conclude the dissertation with some remarks and perspectives.

8.1 Concluding remarks

1-norm for monotone oscillators. One of the main contribution of the dissertation is the global contraction result obtained for monotone oscillators. In Chapter 4, the study of monotone pulse-coupled oscillators stresses the importance of a 1-norm to prove the contraction. In addition, the result is successfully exploited in Chapter 5 for the study of a continuum of monotone oscillators (L^1-Lyapunov function) and in Chapter 7 for the study of "monotone Kuramoto-like" oscillators (1-norm contraction). In a general context, the dissertation could potentially open new avenues in stability theory, connecting the monotonicity property of a system to its contraction with respect to a suitable 1-norm.

Standing conjectures for QIF oscillators. When the oscillators dynamics has no monotonicity property (e.g. QIF oscillators), studying the network appears to be a complex issue. Even though numerical experiments clearly suggest the (global) dichotomic behavior of the QIF oscillators, the corresponding stability problem is an open problem. However, it is a key point that a local stability analysis, still elusive in full generality, is relevant to (partially) solve the QIF conjectures (Chapter 6).

Three conjectures have been formulated throughout the dissertation.

- Conjecture 1 (Section 6.2): the *global QIF conjecture* on the global stability of pulse-coupled QIF oscillators.

- Conjecture 2 (Section 6.4.1): the *local QIF conjecture* on the local stability of pulse-coupled QIF oscillators.
- Conjecture 3 (Section 7.3.2): the *weak coupling QIF conjecture* on the global stability of weakly pulse-coupled QIF oscillators.

From two oscillators to large populations. Two "QIF-like" oscillators always exhibit a dichotomic behavior. Interestingly, the property is not necessary satisfied in larger populations. As an illustration, it was shown that a Hopf bifurcation can occur in large populations of piecewise linear oscillators, which leads to a non-dichotomic behavior. The study of the dichotomic behavior therefore illustrates that the (stability) property of a low-dimensional system (i.e. the scalar firing map) does not necessarily extend to its higher dimensional analog (i.e. the multidimensional firing map). Hence, the network size, which determines the dimensionality of the system, plays a role in the collective behavior of the oscillators.

From large populations to infinite populations. The properties of two coupled oscillators do not necessarily extend to large populations. In contrast, one observes a perfect coherence between large populations and infinite populations regarding the dichotomic behavior. Given this coherence, either a large population or an infinite population, whatever the most tractable for the context, is equivalently relevant to investigate the collective behavior of the network. At a more general level, a concurrent study of the two equivalent populations reveals an elegant parallel between a discrete-time map and a continuous-time PDE, a parallel that motivates, in particular, the use of quantile density functions (Chapter 5).

Weak coupling. Studying non-monotone pulse-coupled oscillators is an involved problem. Interestingly, the (local) stability problem is tractable under the assumption of weak coupling: a simple condition on the iPRC determines the network stability, however complex the oscillator dynamics may be. Hence, a weak coupling assumption, though restrictive, leads to significant advances in the study of pulse-coupled oscillators characterized by a general dynamics. In addition, weakly coupled oscillators are amenable to averaging techniques that establish a parallel between pulse-coupled oscillators and "Kuramoto-like" oscillators. Then, the stability results obtained for pulse-coupled models are naturally extended to "Kuramoto-like" models.

8.2 Perspectives for future research

So far a global stability analysis of non-monotone oscillators is an open problem that raises interesting research questions. For instance, it is unclear how the strong global results obtained with monotone oscillators could be extended to non-monotone oscillators, and whether a 1-norm based approach is still relevant in this case.

As highlighted in the present dissertation, a promising lead is to consider the average behavior of the network over a given time period, an attempt to exploit the possible "monotonicity in the mean" of the dynamics. In this context, averaging techniques have been considered in the dissertation, yielding an elegant reformulation of the problem that might be worth further investigation. In addition, investigating statistical averages of the network

dynamics through operator-theoretic methods (e.g. Perron-Frobenius operator) also seems to be a promising perspective.

In addition to the interesting QIF conjecture, several extensions of the model investigated in the thesis could be considered for future research.

The dissertation paves the way for the study of general dynamics of pulse-coupled oscillators. As a natural continuation, further research could focus on particular oscillator dynamics motivated by real applications that involve impulsive coupling (neuroscience, animal behaviors, earthquake dynamics, etc.). For these application-oriented dynamics, the study of the collective behaviors should imply appropriate methods that are not developed yet.

A second interesting extension is the study of excitable dynamics instead of oscillator dynamics. For instance, a QIF dynamics $\dot{x} = S + x^2$, where S is negative, does not exhibit an oscillatory regime but an excitatory regime. The issue is motivated not only by various applications (see e.g. neuroscience) but also by several mathematical aspects. Indeed, preliminary results have shown that the collective behaviors of excitable QIF units are slightly more complex than those of QIF oscillators: non-uniqueness of the phase-locked behavior, resting state when the coupling is weak, etc. In addition, a further step could possibly highlight novel collective behaviors in mixed populations of both oscillators and excitable units.

Finally, the study of non-identical oscillators leads to intricate problems in many coupled oscillator models and is still in its infancy in the particular case of pulse-coupled oscillators. The robustness of synchronization against the network heterogeneity has been investigated only in few studies on LIF oscillators. Very conservative conditions for synchronization have been established in simple cases, but the complex partial synchronization behavior is still not well-understood. In case of clustering, the numerical experiments presented in the dissertation underline the robustness of the clusters against the oscillators heterogeneity, a result that could be validated through a mathematical analysis. The analysis could rely either on an infinite population model, where the heterogeneity is randomly distributed according to a density of oscillators, or on a stochastic model, where heterogeneity is induced by the noise.

To conclude. In applied mathematics, it is surprising that some problems look trivial at first sight and finally turn out to be more involved and more captivating than expected. Networks of pulse-coupled oscillators are such an example. Their study unveils rich and complex behaviors, leads to exciting open problems, requires the development of new mathematical tools along with fundamental results, and raises promising perspectives for future research.

Appendix A

Proofs

A.1 Proof of Lemma 4.2.1

It is obvious that $\|\mathbf{D}_{N_g-1}^{(0,1)}\|_{(2)} = 0$. For $n < N_g - 1$, the value $\|\mathbf{D}_n^{(0,1)}\|_{(2)}^2$ is obtained by solving the optimization problem

$$\min\ -\mathbf{x^T}\mathbf{D}_n^{(0,1)}\mathbf{Q}\mathbf{D}_n^{(0,1)}\mathbf{x^T} \quad \text{such that} \quad \mathbf{x^T}\mathbf{Q}\mathbf{x} \leq 1\,.$$

The global minimizer $\mathbf{x}^\star$ satisfies

$$(-\mathbf{D}_n^{(0,1)}\mathbf{Q}\mathbf{D}_n^{(0,1)} + \lambda\mathbf{Q})\mathbf{x}^\star = 0\,,$$

with $\lambda \geq 0$ and $\lambda(\|\mathbf{x}^\star\|_{(2)} - 1) = 0$ ([37, 103]). Straightforward but lengthy computations lead to the values

$$\lambda = \frac{N_g + n(N_g - 1 - n)}{N_g}$$

and

$$x_k^\star = \frac{a_k}{\Big[n(n+1)a_1^2 - 2n(N_g - 1 - n)a_1 a_{N_g-1} + (N_g - 1 - n)(N_g - n)a_{N_g-1}^2\Big]^{1/2}}\,,$$

with

$$\begin{cases} a_1 = 1/[\lambda(n+1)]\,, & \\ a_{N_g-1} = 1/[\lambda(N_g - 1 - n)]\,, & \\ a_k = k\,a_1 & \text{for } k = 2, \ldots, n\,, \\ a_{N_g-k} = k\,a_{N_g-1} & \text{for } k = 2, \ldots, N_g - 1 - n\,. \end{cases}$$

Next, the norm is given by

$$\|\mathbf{D}_n^{(0,1)}\|_{(2)} = \sqrt{\mathbf{x}^{\star T}\mathbf{D}_n^{(0,1)}\mathbf{Q}\mathbf{D}_n^{(0,1)}\mathbf{x}^\star} = \sqrt{1 + \frac{n(N_g - 1 - n)}{N_g}}\,. \tag{A.1}$$

A derivation of (A.1) with respect to n shows that the norm has a maximum value for $n = (N_g - 1)/2$. (If N_g is even, the maximum value is not reached, since n is an integer.) Hence, one has finally

$$\max_{n \in \{0, \ldots, N_g - 1\}} \|\mathbf{D}_n^{(0,1)}\|_{(2)} \leq \frac{N_g + 1}{2\sqrt{N_g}}\,.$$

A.2 Proof of Lemma 4.2.2

It is obvious that $\|\mathbf{D}_{N_g-1}^{(0,1)}\|_{(1)} = 0$. For $n < N_g - 1$, the norm is obtained by solving

$$\|\mathbf{D}_n^{(0,1)}\|_{(1)} = \max_{\mathbf{x}} \frac{|x_{n+1}| + \sum_{k=n+1}^{N_g-2} |x_{k+1} - x_k| + |x_{N_g-1}|}{|x_1| + \sum_{k=1}^{N_g-2} |x_{k+1} - x_k| + |x_{N_g-1}|}\,.$$

Observing that

$$|x_{n+1}| = \left| x_1 + \sum_{k=1}^{n} (x_{k+1} - x_k) \right| \leq |x_1| + \sum_{k=1}^{n} |x_{k+1} - x_k|\,,$$

it follows that $\|\mathbf{D}_n^{(0,1)}\|_{(1)} \leq 1$. Choosing a vector $\mathbf{x}$ such that $0 < x_1 \leq \cdots \leq x_{N_g-1}$ yields

$$\frac{\|\mathbf{D}_n^{(0,1)}\mathbf{x}\|_{(1)}}{\|\mathbf{x}\|_{(1)}} = \frac{2\,x_{N_g-1}}{2\,x_{N_g-1}} = 1$$

and, consequently, $\|\mathbf{D}_n^{(0,1)}\|_{(1)} = 1$.

A.3 Proof of Lemma 5.4.1

Given (5.23), the Lyapunov function is written as

$$\mathcal{V} = \sum_{k=1}^{N_c+1} (-1)^k \int_{\varphi_c^{(k-1)}}^{\varphi_c^{(k)}} (q - q^*)\, d\varphi\,.$$

The highest value is obtained when $q^*(\varphi) = q_{\min}$ for $\varphi \in [\varphi_c^{(k-1)}, \varphi_c^{(k)}]$, with k even, and $q(\varphi) = q_{\min}$ for $\varphi \in [\varphi_c^{(k-1)}, \varphi_c^{(k)}]$, with k odd. This leads to the inequality

$$\mathcal{V} \leq \sum_{\substack{k=1 \\ k \text{ even}}}^{N_c+1} \int_{\varphi_c^{(k-1)}}^{\varphi_c^{(k)}} q\, d\varphi - q_{\min} \sum_{\substack{k=1 \\ k \text{ even}}}^{N_c+1} (\varphi_c^{(k)} - \varphi_c^{(k-1)}) + \sum_{\substack{k=1 \\ k \text{ odd}}}^{N_c+1} \int_{\varphi_c^{(k-1)}}^{\varphi_c^{(k)}} q^*\, d\varphi - q_{\min} \sum_{\substack{k=1 \\ k \text{ odd}}}^{N_c+1} (\varphi_c^{(k)} - \varphi_c^{(k-1)})\,. \tag{A.2}$$

Moreover, one has

$$\sum_{\substack{k=1 \\ k \text{ even}}}^{N_c+1} \int_{\varphi_c^{(k-1)}}^{\varphi_c^{(k)}} q\, d\varphi + q_{\min} \sum_{\substack{k=1 \\ k \text{ odd}}}^{N_c+1} (\varphi_c^{(k)} - \varphi_c^{(k-1)}) \leq \int_0^1 q\, d\varphi = Q(1) - Q(0) = 2\pi\,, \tag{A.3}$$

and

$$\sum_{\substack{k=1 \\ k \text{ odd}}}^{N_c+1} \int_{\varphi_c^{(k-1)}}^{\varphi_c^{(k)}} q^*\, d\varphi + q_{\min} \sum_{\substack{k=1 \\ k \text{ even}}}^{N_c+1} (\varphi_c^{(k)} - \varphi_c^{(k-1)}) \leq \int_0^1 q^*\, d\varphi = Q^*(1) - Q^*(0) = 2\pi\,. \tag{A.4}$$

Next, injecting (A.3) and (A.4) in inequality (A.2) yields

$$\mathcal{V} \leq 2\pi - 2\,q_{\min} \sum_{\substack{k=1 \\ k \text{ odd}}}^{N_c+1} (\varphi_c^{(k)} - \varphi_c^{(k-1)}) + 2\pi - 2\,q_{\min} \sum_{\substack{k=1 \\ k \text{ even}}}^{N_c+1} (\varphi_c^{(k)} - \varphi_c^{(k-1)})$$

or

$$\mathcal{V} \leq 4\pi - 2\,q_{\min}(\varphi_c^{(N_c+1)} - \varphi_c^{(0)}) = 4\pi - 2\,q_{\min}\,.$$

A.4 Proof of Lemma 7.2.1

One first verifies that (7.12) is well-defined, since $a \in (0,1)$ and $N \geq 2$ imply that $\sin \frac{a\pi}{N} \neq 0$ and $\sin\left(\frac{1}{N}(n\pi \pm a\pi)\right) \neq 0$. Next, note that

$$\frac{\sin\left(\frac{N-1}{N}a\pi\right)}{\sin\frac{a\pi}{N}} = \frac{\sin a\pi\,\cos\frac{a\pi}{N} - \sin\frac{a\pi}{N}\,\cos a\pi}{\sin\frac{a\pi}{N}} = \frac{\sin a\pi}{\tan\frac{a\pi}{N}} - \cos a\pi\,.$$

Then, the left hand side (LHS) of (7.12) can be rewritten as

$$\begin{aligned}\text{LHS} = \frac{\sin a\pi}{\tan\frac{a\pi}{N}} - \cos a\pi - \frac{1}{2}(-1)^n \Bigg(& \frac{\sin(n\pi + a\pi)}{\tan\left(\frac{1}{N}(n\pi + a\pi)\right)} - \cos(n\pi + a\pi) \\ & + \frac{\sin(n\pi - a\pi)}{\tan\left(\frac{1}{N}(n\pi - a\pi)\right)} - \cos(n\pi - a\pi)\Bigg)\,,\end{aligned}$$

where we assume that $(n\pi \pm a\pi)/N \neq \pi/2 + k\pi$, $k \in \mathbb{Z}$ (the opposite case is considered at the end of the proof).

Since $\cos(n\pi \pm a\pi) = (-1)^n \cos(a\pi)$ and $\sin(n\pi \pm a\pi) = \pm(-1)^n \sin(a\pi)$, one obtains

$$\begin{aligned}\text{LHS} &= \sin a\pi \left(\frac{1}{\tan\frac{a\pi}{N}} - \frac{1}{2}\left(\frac{1}{\tan\left(\frac{1}{N}(n\pi + a\pi)\right)} - \frac{1}{\tan\left(\frac{1}{N}(n\pi - a\pi)\right)}\right)\right)\,, \\ &= \sin a\pi \left(\frac{1}{\tan\frac{a\pi}{N}} - \frac{1}{2}\left(\frac{1 - \tan\frac{n\pi}{N}\,\tan\frac{a\pi}{N}}{\tan\frac{n\pi}{N} + \tan\frac{a\pi}{N}} - \frac{1 + \tan\frac{n\pi}{N}\,\tan\frac{a\pi}{N}}{\tan\frac{n\pi}{N} - \tan\frac{a\pi}{N}}\right)\right)\,, \\ &= \sin a\pi \left(\frac{1}{\tan\frac{a\pi}{N}} + \frac{\tan\frac{a\pi}{N} + \tan^2\frac{n\pi}{N}\,\tan\frac{a\pi}{N}}{\tan^2\frac{n\pi}{N} - \tan^2\frac{a\pi}{N}}\right)\,.\end{aligned}$$

It follows from $a \in (0,1)$ and $N \geq 2$ that

$$\begin{aligned}\sin a\pi &> 0\,. \\ \tan\frac{a\pi}{N} &> 0\,. \\ \tan^2\frac{n\pi}{N}\,\tan\frac{a\pi}{N} &> 0\,.\end{aligned}$$

Then, it remains to show that $\tan^2\frac{n\pi}{N} - \tan^2\frac{a\pi}{N} > 0$, or equivalently $\left|\tan\frac{n\pi}{N}\right| > \left|\tan\frac{a\pi}{N}\right|$, an inequality that follows from

$$\left|\tan\frac{n\pi}{N}\right| \geq \left|\tan\frac{N-1}{N}\pi\right| = \left|\tan\frac{\pi}{N}\right| > \left|\tan\frac{a\pi}{N}\right|\,.$$

Then, equality (7.12) is verified.

We above assumed that $(n\pi \pm a\pi)/N \neq \pi/2 + k\pi$, $k \in \mathbb{Z}$. Next, we consider the situations where this inequality is not verified and show that (7.12) is still satisfied.

1. The equality $(n\pi + a\pi)/N = \pi/2 + k\pi$ implies

$$n + a = \frac{N}{2} + Nk = \frac{1}{2} + \frac{N-1}{2} + kN\,,$$

so that one must have $a = 1/2$ and $n = (N-1)/2 + kN$ (with N odd). In this case, (7.12) is rewritten as

$$\text{LHS} = \sin a\pi \left(\frac{1}{\tan \frac{a\pi}{N}} + \frac{1}{2} \frac{1}{\tan\left(\frac{N-2}{2N}\pi\right)} \right) .$$

It follows from $\frac{N-2}{2N}\pi < \pi/2$ that LHS > 0.

2. Similarly, the equality $(n\pi - a\pi)/N = \pi/2 + k\pi$ implies $a = 1/2$ and $n = (N+1)/2 + kN$ (with N odd). In this case, (7.12) is rewritten as

$$\text{LHS} = \sin a\pi \left(\frac{1}{\tan \frac{a\pi}{N}} - \frac{1}{2} \frac{1}{\tan\left(\frac{N+2}{2N}\pi\right)} \right) .$$

It follows from $\pi/2 < \frac{N+2}{2N}\pi \leq \pi$ that LHS > 0.

A.5 Proof of Theorem 7.3.1

For the sake of clarity, we omit the time variable t and the tilde "˜" for the phases. We prove the contraction property in the case $\Gamma' < 0$. In addition, without loss of generality, we suppose that $\Gamma'' \leq 0$ and, considering the two trajectories $\boldsymbol{\Theta} = (\theta_1, \ldots, \theta_{N-1})$ and $\boldsymbol{\Psi} = (\psi_1, \ldots, \psi_{N-1})$, we assume that $\theta_1 - \psi_1 \leq 0$. The proof of the other cases follows on similar lines.

The distance induced by the 1-norm (4.10) between the two trajectories is written as

$$\|\boldsymbol{\Theta} - \boldsymbol{\Psi}\|_{(1)} = |\theta_1 - \psi_1| + \sum_{j=1}^{N-2} |\theta_{j+1} - \psi_{j+1} - (\theta_j - \psi_j)| + |\theta_{N-1} - \psi_{N-1}|\,.$$

One can remove the absolute values to obtain

$$\|\boldsymbol{\Theta} - \boldsymbol{\Psi}\|_{(1)} = \sum_{k=1}^{N_c} (-1)^k \left(\theta_{\mathcal{K}(k)} - \psi_{\mathcal{K}(k)}\right) . \tag{A.5}$$

The subscripts $\mathcal{K}(k)$ correspond to N_c *critical oscillators* ($1 \leq N_c \leq N-1$) whose phases are characterized by a change of the sign of $\theta_{j+1} - \psi_{j+1} - (\theta_j - \psi_j)$. Formally, the map $\mathcal{K} : \{1, \ldots, N_c\} \mapsto \{1, \ldots, N-1\}$ is defined such that $\mathcal{K}(k-1) < \mathcal{K}(k)$ and such that

$$\left[\theta_{\mathcal{K}(k)+1} - \psi_{\mathcal{K}(k)+1} - \left(\theta_{\mathcal{K}(k)} - \psi_{\mathcal{K}(k)}\right)\right] \left[\theta_{\mathcal{K}(k)} - \psi_{\mathcal{K}(k)} - \left(\theta_{\mathcal{K}(k)-1} - \psi_{\mathcal{K}(k)-1}\right)\right] < 0\,,$$

with $\theta_0 = \psi_0 = \theta_N = \theta_N = 0$. The index $\mathcal{K}(k)$ corresponds to a maximum of $\theta_j - \psi_j$ when k is even and to a minimum when k is odd (Figure A.1). In particular, one has

$$(-1)^k \left(\theta_{\mathcal{K}(k)} - \psi_{\mathcal{K}(k)}\right) > (-1)^k \left(\theta_{\mathcal{K}(k\pm1)} - \psi_{\mathcal{K}(k\pm1)}\right) , \tag{A.6}$$

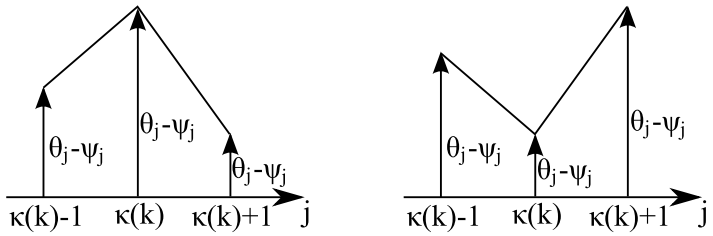

(a) k even (b) k odd

Figure A.1: The critical oscillators correspond to extremal values of $\theta_j - \psi_j$.

assuming that $\theta_{\mathcal{K}(0)} = \psi_{\mathcal{K}(0)} = \theta_{\mathcal{K}(N_c+1)} = \psi_{\mathcal{K}(N_c+1)} = 0$.

The time derivative of (A.5) yields

$$\frac{d}{dt} \left\| \mathbf{\Theta} - \mathbf{\Psi} \right\|_{(1)} = \sum_{k=1}^{N_c} (-1)^k \left(\dot{\theta}_{\mathcal{K}(k)} - \dot{\psi}_{\mathcal{K}(k)} \right) \triangleq \sum_{k=1}^{N_c} T^{(k)} \,. \tag{A.7}$$

Next, we consider separately each term $T^{(k)}$. It follows from (7.22) that

$$T^{(k)} = (-1)^k \Bigg[\Gamma(\theta_{\mathcal{K}(k)}) - \Gamma(\psi_{\mathcal{K}(k)}) + \sum_{\substack{j=1 \\ j \neq \mathcal{K}(k)}}^{N-1} \Gamma(\theta_{\mathcal{K}(k)} - \theta_j) - \Gamma(\psi_{\mathcal{K}(k)} - \psi_j) - \sum_{j=1}^{N-1} \Gamma(-\theta_j) - \Gamma(-\psi_j) \Bigg] .$$

Using the mean value theorem, we obtain

$$\begin{aligned} T^{(k)} = & \underbrace{\Gamma'(\xi_{\mathcal{K}(k)})(-1)^k \left(\theta_{\mathcal{K}(k)} - \psi_{\mathcal{K}(k)} \right)}_{\triangleq T^{(k)}_{\mathcal{K}(k)}} \\ & + \sum_{\substack{j=1 \\ j \neq \mathcal{K}(k)}}^{N-1} \underbrace{\Gamma'(\xi_{\mathcal{K}(k),j})(-1)^k \left(\theta_{\mathcal{K}(k)} - \psi_{\mathcal{K}(k)} - (\theta_j - \psi_j) \right)}_{\triangleq T^{(k)}_j} \\ & + (-1)^k \underbrace{\left(- \sum_{j=1}^{N-1} \Gamma(-\theta_j) - \Gamma(-\psi_j) \right)}_{\triangleq T_\Sigma} , \end{aligned} \tag{A.8}$$

with $\xi_{\mathcal{K}(k)} \in [\theta_{\mathcal{K}(k)}, \psi_{\mathcal{K}(k)}]$ or $\xi_{\mathcal{K}(k)} \in [\psi_{\mathcal{K}(k)}, \theta_{\mathcal{K}(k)}]$ and $\xi_{\mathcal{K}(k),j} \in [(\theta_{\mathcal{K}(k)} - \theta_j) \bmod 2\pi, (\psi_{\mathcal{K}(k)} - \psi_j) \bmod 2\pi]$ or $\xi_{\mathcal{K}(k),j} \in [(\psi_{\mathcal{K}(k)} - \psi_j) \bmod 2\pi, (\theta_{\mathcal{K}(k)} - \theta_j) \bmod 2\pi]$. Since $\Gamma'' \leq 0$, the values satisfy

$$\xi_{\mathcal{K}(k)} \leq \xi_{\mathcal{K}(k+1)} \qquad k < N_c \tag{A.9}$$

$$\xi_{\mathcal{K}(k),j} \leq \xi_{\mathcal{K}(k+1),j} \qquad k < N_c \quad j \neq \{\mathcal{K}(k), \mathcal{K}(k+1)\} \,, \tag{A.10}$$

$$\xi_{\mathcal{K}(N_c),j} \leq \xi_{\mathcal{K}(1),j} \qquad j \neq \{\mathcal{K}(1), \mathcal{K}(N_c)\} \,. \tag{A.11}$$

Because of the discontinuity of Γ, it is noticeable that these relationships are not valid if a trajectory is in the boundary of $\mathcal{C}$.

Disregarding the terms T_Σ, we show that each positive term $T_j^{(k)}$ of $T^{(k)}$ (in (A.8)) can be associated with a term $T_j^{(k+1)}$ of $T^{(k+1)}$ so that the addition of both terms $T_j^{(k)} + T_j^{(k+1)}$ is negative.

- If the term $T_{\mathcal{K}(k)}^{(k)} \geq 0$, it is associated with the term $T_{\mathcal{K}(k+1)}^{(k+1)}$. It follows from (A.9) and from $\Gamma'' \leq 0$ that $\Gamma'(\xi_{\mathcal{K}(k+1)}) \leq \Gamma'(\xi_{\mathcal{K}(k)}) < 0$. In addition, (A.6) implies

$$-(-1)^{k+1}\left(\theta_{\mathcal{K}(k+1)} - \psi_{\mathcal{K}(k+1)}\right) < (-1)^k\left(\theta_{\mathcal{K}(k)} - \psi_{\mathcal{K}(k)}\right) \leq 0\,.$$

  Then, we obtain $T_{\mathcal{K}(k)}^{(k)} + T_{\mathcal{K}(k+1)}^{(k+1)} < 0$.

- If the term $T_j^{(k)} \geq 0$ for any $j \neq \mathcal{K}(k)$, it is associated with the term $T_j^{(k+1)}$, $j \neq \mathcal{K}(k+1)$. According to (A.6), one has never $T_j^{(k)} \geq 0$ for $j = \mathcal{K}(k+1)$. It follows from (A.10) and from $\Gamma'' \leq 0$ that $\Gamma'(\xi_{\mathcal{K}(k+1),j}) \leq \Gamma'(\xi_{\mathcal{K}(k),j}) < 0$. In addition, (A.6) implies

$$-(-1)^{k+1}\left(\theta_{\mathcal{K}(k+1)} - \psi_{\mathcal{K}(k+1)} - (\theta_j - \psi_j)\right) < (-1)^k\left(\theta_{\mathcal{K}(k)} - \psi_{\mathcal{K}(k)} - (\theta_j - \psi_j)\right) \leq 0\,.$$

  Then, we obtain $T_j^{(k)} + T_j^{(k+1)} < 0$.

For $k = N_c$, the terms of $T^{(k)}$ cannot be associated with the terms of $T^{(k+1)}$. Then, it remains to consider the terms $T_j^{(N_c)}$ and the terms $(-1)^k T_\Sigma$. We distinguish two cases: the case N_c even and the case N_c odd.

Case $\mathbf{N_c}$ even. The addition of the N_c terms $(-1)^k T_\Sigma$ yields

$$\sum_{k=1}^{N_c} (-1)^k T_\Sigma = 0\,.$$

In addition, the relationship (A.6) implies

$$\theta_{\mathcal{K}(1)} - \psi_{\mathcal{K}(1)} < 0 \qquad \theta_{\mathcal{K}(N_c)} - \psi_{\mathcal{K}(N_c)} > 0 \tag{A.12}$$

so that the term $T_{\mathcal{K}(N_c)}^{(N_c)} < 0$.

If the term $T_j^{(N_c)} \geq 0$ for any $j \neq \mathcal{K}(N_c)$, it is associated with the term $T_j^{(1)}$, $j \neq \mathcal{K}(1)$. According to (A.6), one has never $T_j^{(N_c)} \geq 0$ for $j = \mathcal{K}(1)$. It follows from (A.11) and from $\Gamma'' \leq 0$ that $\Gamma'(\xi_{\mathcal{K}(1),j}) \leq \Gamma'(\xi_{\mathcal{K}(N_c),j}) < 0$. In addition, the inequalities (A.12) imply

$$-(-1)^1\left(\theta_{\mathcal{K}(1)} - \psi_{\mathcal{K}(1)} - (\theta_j - \psi_j)\right) < (-1)^{N_c}\left(\theta_{\mathcal{K}(N_c)} - \psi_{\mathcal{K}(N_c)} - (\theta_j - \psi_j)\right) \leq 0\,.$$

Then, we obtain $T_j^{(N_c)} + T_j^{(1)} < 0$.

Case $\mathbf{N_c}$ odd. The addition of the N_c terms $(-1)^k T_\Sigma$ yields

$$\sum_{k=1}^{N_c} (-1)^k T_\Sigma = -T_\Sigma = -\sum_{j=1}^{N-1} \Gamma'(\xi_{-j})\,(\theta_j - \psi_j)$$

with $\xi_{-j} \in [2\pi - \theta_j, 2\pi - \psi_j]$ or $\xi_{-j} \in [2\pi - \psi_j, 2\pi - \theta_j]$. Since $\Gamma'' \leq 0$, the values satisfy

$$\xi_{\mathcal{K}(N_c),j} \leq \xi_{-j} \leq \xi_{\mathcal{K}(1),j}\,. \tag{A.13}$$

If the term $-\Gamma'(\xi_{-j})(\theta_j - \psi_j) \geq 0$, it is associated with the term $T_j^{(1)}$. It follows from (A.13) and from $\Gamma'' \leq 0$ that $\Gamma'(\xi_{\mathcal{K}(1),j}) \leq \Gamma'(\xi_{-j}) < 0$. In addition, the relationship (A.6) implies

$$\theta_{\mathcal{K}(1)} - \psi_{\mathcal{K}(1)} < 0 \qquad \theta_{\mathcal{K}(N_c)} - \psi_{\mathcal{K}(N_c)} < 0 \tag{A.14}$$

so that

$$-(-1)^1 \left(\theta_{\mathcal{K}(1)} - \psi_{\mathcal{K}(1)} - (\theta_j - \psi_j)\right) < -(\theta_j - \psi_j) \leq 0\,.$$

Then, we obtain $-\Gamma'(\xi_{-j})(\theta_j - \psi_j) + T_j^{(1)} < 0$.

Next, (A.14) implies that the term $T_{\mathcal{K}(N_c)}^{(N_c)} < 0$.

If the term $T_j^{(N_c)} \geq 0$ for any $j \neq \mathcal{K}(N_c)$, it is associated with the term $-\Gamma'(\xi_{-j})(\theta_j - \psi_j)$. It follows from (A.13) and from $\Gamma'' \leq 0$ that $\Gamma'(\xi_{-j}) \leq \Gamma'(\xi_{\mathcal{K}(N_c),j}) < 0$. In addition, (A.14) implies

$$\theta_j - \psi_j < (-1)^{N_c} \left(\theta_{\mathcal{K}(N_c)} - \psi_{\mathcal{K}(N_c)} - (\theta_j - \psi_j)\right) \leq 0\,.$$

Then, we obtain $T_j^{(N_c)} - \Gamma'(\xi_{-j})(\theta_j - \psi_j) < 0$.

Finally, every term of (A.7)-(A.8) is either negative or can be associated to a unique term such that the addition of both is negative. Thus, one has

$$\frac{d}{dt} \left\| \boldsymbol{\Theta} - \boldsymbol{\Psi} \right\|_{(1)} = \sum_{k=1}^{N_c} T^{(k)} < 0\,.$$

For the other situations ($\Gamma'' \geq 0$, $\Gamma' < 0$), the proof follows on similar lines (except that the terms of $T^{(k)}$ might be associated with the terms of $T^{(k-1)}$ instead).

Remark A.5.1. The contraction property is not verified if one trajectory is in the boundary of $\mathcal{C}$. However, it is noticeable that a reduced dynamics governing the evolution of trajectories in the boundary of $\mathcal{C}$ still satisfies the contraction property of Theorem 7.3.1. In other words, the $(N-2)$-dimensional dynamics obtained

- when $\tilde{\theta}_1 = 0$, i.e.

$$\dot{\tilde{\theta}}_k = 2\Gamma(\tilde{\theta}_k) + \sum_{\substack{j=2 \\ j \neq k}}^{N-1} \Gamma(\tilde{\theta}_k - \tilde{\theta}_j) - \sum_{j=2}^{N-1} \Gamma(-\tilde{\theta}_j) - \Gamma(0) \quad k = 2, \ldots, N-1\,;$$

- or when $\tilde{\theta}_{N-1} = 2\pi$, i.e.

$$\dot{\tilde{\theta}}_k = 2\Gamma(\tilde{\theta}_k) + \sum_{\substack{j=1 \\ j \neq k}}^{N-2} \Gamma(\tilde{\theta}_k - \tilde{\theta}_j) - \sum_{j=1}^{N-2} \Gamma(-\tilde{\theta}_j) - \Gamma(0) \quad k = 1, \ldots, N-2\,;$$

- or when $\tilde{\theta}_n = \tilde{\theta}_{n+1}$, $n = 1, \ldots, N-2$, i.e.

$$\begin{cases} \dot{\tilde{\theta}}_k = \Gamma(\tilde{\theta}_k) + \sum\limits_{\substack{j=1 \\ j \neq \{k,n,n+1\}}}^{N-1} \Gamma(\tilde{\theta}_k - \tilde{\theta}_j) + 2\Gamma(\tilde{\theta}_k - \tilde{\theta}_n) - \sum\limits_{\substack{j=1 \\ j \neq \{n,n+1\}}}^{N-2} \Gamma(-\tilde{\theta}_j) - 2\Gamma(-\tilde{\theta}_n) \qquad k \neq \{n, n+1\} \\ \dot{\tilde{\theta}}_n = \Gamma(\tilde{\theta}_n) + \sum\limits_{\substack{j=1 \\ j \neq \{n,n+1\}}}^{N-1} \Gamma(\tilde{\theta}_n - \tilde{\theta}_j) + \Gamma(0) - \sum\limits_{\substack{j=1 \\ j \neq \{n,n+1\}}}^{N-2} \Gamma(-\tilde{\theta}_j) - 2\Gamma(-\tilde{\theta}_n) \end{cases}$$

is characterized by a contraction property with respect to the 1-norm (A.5). The proof, which is a straightforward corollary of the proof of Theorem 7.3.1, is left to the reader. ◇

Bibliography

[1] L. F. Abbott, *Lapicque's introduction of the integrate-and-fire model neuron (1907)*, Brain Research Bulletin **50** (1999), no. 5-6, 303–304.

[2] L. F. Abbott and T. B. Kepler, *Model neurons: From Hodgkin-Huxley to Hopfield*, Statistical Mechanics of Neural Networks (L. Garrido, ed.), Springer Berlin / Heidelberg, 1990, pp. 5–18.

[3] L. F. Abbott and C. van Vreeswijk, *Asynchronous states in networks of pulse-coupled oscillators*, Physical Review E **48** (1993), 1483–1490.

[4] J. A. Acebron, L. L. Bonilla, C. J. P. Vicente, F. Ritort, and R. Spigler, *The Kuramoto model: A simple paradigm for synchronization phenomena*, Reviews of Modern Physics **77** (2005), no. 1, 137–185.

[5] D. Aeyels and F. De Smet., *A model for the dynamical process of cluster formation*, Proceedings of 7th IFAC Symposium on Nonlinear Control Systems, August 2007.

[6] N. Aghannan and P. Rouchon, *An intrinsic observer for a class of Lagrangian systems*, IEEE Transactions on Automatic Control **48** (2003), no. 6, 936–944.

[7] E. M. Aylward, P. A. Parrilo, and J. J. E. Slotine, *Stability and robustness analysis of nonlinear systems via contraction metrics and SOS programming*, Automatica **44** (2008), no. 8, 2163–2170.

[8] H. Bavinck, *On the zeros of certain linear combinations of Chebyshev polynomials*, Journal of Computational and Applied Mathematics **65** (1995), no. 1-3, 19–26.

[9] E. M. Boczko, C. S. Stowers, T. Gedeon, and T. R. Young, *ODE, RDE and SDE models of cell cycle dynamics and clustering in yeast*, Journal of Biological Dynamics **4** (2010), no. 4, 328–345.

[10] S. Bottani, *Synchronization of integrate and fire oscillators with global coupling*, Physical Review E **54** (1996), no. 3, 2334–2350.

[11] P. C. Bressloff, *Mean-field theory of globally coupled integrate-and-fire neural oscillators with dynamic synapses*, Physical Review E **60** (1999), no. 2, 2160–2170.

[12] P. C. Bressloff and S. Coombes, *A dynamical theory of spike train transitions in networks of integrate-and-fire oscillators*, Siam Journal on Applied Mathematics **60** (2000), no. 3, 820–841.

[13] E. Brown, J. Moehlis, and P. Holmes, *On the phase reduction and response dynamics of neural oscillator populations*, Neural Computation **16** (2004), no. 4, 673–715.

[14] N. Brunel and P. E. Latham, *Firing rate of the noisy quadratic integrate-and-fire neuron*, Neural Computation **15** (2003), no. 10, 2281–2306.

[15] J. Buck, *Synchronous rhythmic flashing of fireflies .2*, Quarterly Review Of Biology **63** (1988), no. 3, 265–289.

[16] M. Calamai, A. Politi, and A. Torcini, *Stability of splay states in globally coupled rotators*, Physical Review E **80** (2009), no. 3, 036209.

[17] F. M. Callier and C. A. Desoer, *Multivariable feedback systems*, New York: Springler-Verlag, 1982.

[18] H. S. Carslaw, *Introduction to the theory of Fourier's series and integrals*, Dover, 1983.

[19] Y.-C. Chang and J. Juang, *Stable synchrony in globally coupled integrate-and-fire oscillators*, SIAM Journal on Applied Dynamical Systems **7** (2008), 1445–1476.

[20] A. Cima, A. Gasull, and F. Manosas, *The discrete Markus-Yamabe problem*, Nonlinear Analysis-Theory Methods & Applications **35** (1999), no. 3, 343–354.

[21] J. M. Coron, G. Bastin, and B. d'Andrea Novel, *Dissipative boundary conditions for one-dimensional nonlinear hyperbolic systems*, Siam Journal on Control and Optimization **47** (2008), no. 3, 1460–1498.

[22] J. M. Coron, B. d'Andrea Novel, and G. Bastin, *A strict Lyapunov function for boundary control of hyperbolic systems of conservation laws*, IEEE Transactions on Automatic Control **52** (2007), no. 1, 2–11.

[23] P. Danzl, R. Hansen, G. Bonnet, and J. Moehlis, *Partial phase synchronization of neural populations due to random Poisson inputs*, Journal of Computational Neuroscience **25** (2008), no. 1, 141–157.

[24] F. De Smet and D. Aeyels, *Coexistence of stable stationary behavior and partial synchrony in an all-to-all coupled spiking neural network*, Physical Review E **82** (2010), no. 6, 066208.

[25] M. Denker, M. Timme, M. Diesmann, F. Wolf, and T. Geisel, *Breaking synchrony by heterogeneity in complex networks*, Physical Review Letters **92** (2004), no. 7, 074103.

[26] A. Diaz-Guilera, A. Arenas, A. Corral, and C. J. Pérez, *Stability of spatio-temporal structures in a lattice model of pulse-coupled oscillators*, Physica D **103** (1997), 419–429.

[27] G. Drion, L. Massotte, R. Sepulchre, and V. Seutin, *How modeling can reconcile apparently discrepant experimental results: The case of pacemaking in dopaminergic neurons*, PLoS Comput Biol **7** (2011), no. 5, e1002050.

[28] R. Dror, C. C. Canavier, R. J. Butera, J. W. Clark, and J. H. Byrne, *A mathematical criterion based on phase response curves for stability in a ring of coupled oscillators*, Biological Cybernetics **80** (1999), no. 1, 11–23.

[29] N. Dunford and J. T. Schwartz, *Linear Operators, Part I: General Theory*, Wiley, 1958.

[30] R. Eckhorn, R. Bauer, W. Jordan, M. Brosch, W. Kruse, M. Munk, and H. J. Reitboeck, *Coherent oscillations: A mechanism of feature linking in the visual cortex? Multiple electrode and correlation analyses in the cat*, Biological Cybernetics **60** (1988), no. 2, 121–130.

[31] G. B. Ermentrout, *Type I membranes, phase resetting curves, and synchrony*, Neural Computation **8** (1996), no. 5, 979–1001.

[32] G. B. Ermentrout and N. Kopell, *Parabolic bursting in an excitable system coupled with a slow oscillation*, Siam Journal on Applied Mathematics **15** (1986), 3457–3466.

[33] U. Ernst, K. Pawelzik, and T. Geisel, *Delay-induced multistable synchronization of biological oscillators*, Physical Review E **57** (1998), no. 2, 2150–2162.

[34] R. FitzHugh, *Impulses and physiological states in models of nerve membrane*, Biophysical Journal **1** (1961), 445–466.

[35] W. Gerstner and W. Kistler, *Spiking neuron models*, Cambridge University Press, Cambridge, England, 2002.

[36] P. Goel and G. B. Ermentrout, *Synchrony, stability, and firing patterns in pulse-coupled oscillators*, Physica D **163** (2002), 191–216.

[37] N. I. M. Gould, S. Lucidi, M. Roma, and P. L. Toint, *Solving the trust-region subproblem using the Lanczos method*, Siam Journal on Optimization **9** (1999), no. 2, 504–525.

[38] C.M. Gray, P. Konig, A.K. Engel, and W. Singer, *Oscillatory responses in cat visual cortex exhibit intercolumnar synchronization which reflects global stimulus properties*, Nature **338** (1989), 334–337.

[39] J. Guckenheimer and P. Holmes, *Nonlinear oscillations, dynamical systems, and bifurcations of vector fields*, New York: Springler-Verlag, 1983.

[40] M. Hafner, P. Sacré, L. Symul, H. Koeppl, and R. Sepulchre, *Multiple feedback loops in circadian cycles: robustness and entrainment as selection criteria*, Proceedings of the 7th International Workshop on Computational Systems Biology, June 2010, pp. 51–54.

[41] D. Hansel and G. Mato, *Asynchronous states and the emergence of synchrony in large networks of interacting excitatory and inhibitory neurons*, Neural Computation **15** (2003), no. 1, 1–56.

[42] D. Hansel, G. Mato, and C. Meunier, *Synchrony in excitatory neural networks*, Neural Computation **7** (1995), 307–337.

[43] R. Hegselmann and U. Krause, *Opinion dynamics and bounded confidence: models, analysis and simulation*, Journal of Artificial Societies and Social Simulation **5** (2002), no. 3.

[44] M. W. Hirsch, C. C. Pugh, and M. Shub, *Invariant manifolds*, Lecture Notes in Mathematics, vol. 583, Springler-Verlag, 1977.

[45] A. Hodgkin and A. Huxley, *A quantitative description of membrane current and its application to conduction and excitation in nerve*, Bulletin of Mathematical Biology **52** (1990), 25–71, 10.1007/BF02459568.

[46] J. J. Hopfield, *Neural networks and physical systems with emergent collective computational capabilities*, Proceedings of the National Academy of Science, vol. 79, 1982, pp. 2554–2558.

[47] F. C. Hoppensteadt and E. M. Izhikevich, *Weakly connected neural networks*, New York: Springler-Verlag, 1997.

[48] R. A. Horn and C. R. Johnson, *Matrix analysis*, Cambridge University Press, Cambridge, England, 1996.

[49] C. Huygens, *Horoloqium oscilatorium*, Apud F. Muquet, Parisiis, 1673, Translation: The pendulum clock (Iowa State University Press, Ames, 1986).

[50] E. M. Izhikevich, *Dynamical systems in neuroscience: The geometry of excitability and bursting*, MIT press, 2007.

[51] E.M. Izhikevich, *Simple model of spiking neurons*, IEEE Transactions on Neural Networks **14** (2003), 1569–1572.

[52] A. Jadbabaie, J. Lin, and A. S. Morse, *Coordination of groups of mobile autonomous agents using nearest neighbor rules*, IEEE Transactions On Automatic Control **48** (2003), no. 6, 988–1001.

[53] R. E. Kalman, *Lyapunov functions for the problem of Lur'e in automatic control*, Proceedings of the National Academy of Sciences **49** (1963), 201–205.

[54] J. Keener and J. Sneyd, *Mathematical physiology*, New York: Springler-Verlag, 1998.

[55] H. K. Khalil, *Nonlinear systems*, 2nd edition ed., Prentice Hall, 1996.

[56] C. Kirst, T. Geisel, and M. Timme, *Sequential desynchronization in networks of spiking neurons with partial reset*, Physical Review Letters **102** (2009), no. 6, 068101.

[57] B. W. Knight, *Dynamics of encoding in a population of neurons*, Journal of General Physiology **59** (1972), no. 6, 734–766.

[58] Y. Kuramoto, *Chemical oscillations, waves, and turbulence*, Springler-Verlag, 1984.

[59] ———, *Cooperative dynamics of oscillator community*, Progress of Theoretical Physics **Suppl. 79** (1984), 223–240.

[60] ———, *Collective synchronization of pulse-coupled oscillators and excitable units*, Physica D **50** (1991), no. 1, 15–30.

[61] ———, *Phase- and center-manifold reductions for large populations of coupled oscillators with application to non-locally coupled systems*, International Journal of Bifurcation and Chaos **7** (1997), no. 4, 789–805.

[62] P. Lakatos, *On zeros of reciprocal polynomials*, Publicationes Mathematicae-Debrecen **61** (2002), no. 3-4, 645–661.

[63] L. Lapicque, *Recherches quantitatives sur l'excitation électrique des nerfs traitée comme une polarisation*, Journal de physiologie et de pathologie générale **9** (1907), 620–638.

[64] A. Lasota and M. C. Mackey, *Chaos, fractals, and noise: stochastic aspects of dynamics*, Springler-Verlag, 1994.

[65] P. E. Latham, B. J. Richmond, P. G. Nelson, and S. Nirenberg, *Intrinsic dynamics in neuronal networks. I. Theory*, Journal of Neurophysiology **83** (2000), no. 2, 808–827, cited By (since 1996) 109.

[66] N. E. Leonard, D. A. Paley, F. Lekien, R. Sepulchre, D. M. Fratantoni, and R. E. Davis, *Collective motion, sensor networks, and ocean sampling*, Proceedings of the IEEE, special issue on the emerging technology of networked control systems **95** (2007), no. 1, 48–74.

[67] W. Lohmiller and J. J. E. Slotine, *On contraction analysis for nonlinear systems*, Automatica **34** (1998), no. 6, 683–696.

[68] J. H. G. Macdonald, *Lateral excitation of bridges by balancing pedestrians*, Proceedings of the Royal Society **465** (2009), no. 2104, 1055–1073.

[69] E. Mallada and Ao Tang, *Weakly pulse-coupled oscillators: Heterogeneous delays lead to homogeneous phase*, Proceedings of the 49th IEEE Conference on Decision and Control, December 2010, pp. 992–997.

[70] A. Mauroy, J. M. Hendrickx, A. Megretski, and R. Sepulchre, *Global analysis of firing maps*, Proceedings of the 19th International Symposium on Mathematical Theory of Networks and Systems, July 2010, pp. 1775–1782.

[71] ———, *Proof of Proposition 4 in "Global analysis of firing maps"*, http://www.inma.ucl.ac.be/∼hendrickx/availablepublications/MTNS 2010MHM-Sreport.pdf, 2010.

[72] A. Mauroy and R. Sepulchre, *Global analysis of a continuum model for pulse-coupled oscillators*, Submitted, http://arxiv.org/abs/1102.4511.

[73] ———, *Clustering behaviors in networks of integrate-and-fire oscillators*, Chaos **18** (2008), no. 3, 037122.

[74] ———, *Local stability results for the collective behaviors of infinite populations of pulse-coupled oscillators*, Proceedings of the 50th IEEE Conference on Decision and Control, December 2011.

[75] R. E. Mirollo and S. H. Strogatz, *Synchronization of pulse-coupled biological oscillators*, Siam Journal on Applied Mathematics **50** (1990), no. 6, 1645–1662.

[76] L. Moreau, *Stability of multiagent systems with time-dependent communication links*, IEEE Transactions on Automatic Control **50** (2005), no. 2, 169–182.

[77] C. Morris and H. Lecar, *Voltage oscillations in the barnacle giant muscle fiber*, Biophysical Journal **35** (1981), 193–213.

[78] J. Nagumo, S. Arimoto, and S. Yoshizawa, *An active pulse transmission line simulating nerve axon*, Proceedings of the IRE, vol. 50, 1962, pp. 2061–2070.

[79] H. Nakao, K. Arai, and Y. Kawamura, *Noise-induced synchronization and clustering in ensembles of uncoupled limit-cycle oscillators*, Physical Review Letters **98** (2007), no. 18, 184101.

[80] H. Nakao, K. Arai, K. Nagai, Y. Tsubo, and Y. Kuramoto, *Synchrony of limit-cycle oscillators induced by random external impulses*, Physical Review E **72** (2005), no. 2, 26220–1–13.

[81] D. Q. Nykamp and D. Tranchina, *A population density approach that facilitates large-scale modeling of neural networks: Analysis and an application to orientation tuning*, Journal of Computational Neuroscience **8** (2000), no. 1, 19–50.

[82] Z. Olami, H. J. Feder, and K. Christensen, *Self-organized criticality in a continuous, nonconservative cellular automaton modeling earthquakes*, Physical Review Letters **68** (1992), no. 8, 1244–1247.

[83] A. Olshevsky and J. N. Tsitsiklis, *On the nonexistence of quadratic Lyapunov functions for consensus algorithms*, IEEE Transactions on Automatic Control **53** (2008), no. 11, 2642–2645.

[84] P. Ostborn, *Phase transition to frequency entrainment in a long chain of pulse-coupled oscillators*, Physical Review E **66** (2002), no. 1, 016105.

[85] E. Parzen, *Nonparametric statistical data modeling*, Journal of the American Statistical Association **74** (1979), no. 365, 105–121.

[86] C. S. Peskin, *Mathematical aspects of heart physiology*, Courant Institute of Mathematical Sciences, New York University, New York, 1975.

[87] A. Polanski, *On absolute stability analysis by polyhedral Lyapunov functions*, Automatica **36** (2000), 573–578.

[88] L. Praly, *Topological orbital equivalence with asymptotic phase for a two time-scales discrete-time systems*, Mathematics of Control, Signals, and Systems **3** (1990), 225–253.

[89] A. Rantzer, *On the Kalman-Yakubovich-Popov lemma*, Systems & Control Letters **28** (1996), 7–10.

[90] M. O. Rayes, V. Trevisan, and P. S. Wang, *Factorization properties of Chebyshev polynomials*, Computers & Mathematics with Applications **50** (2005), no. 8-9, 1231–1240.

[91] C. W. Reynolds, *Flocks, herds, and schools: A distributed behavioral model*, Computer Graphics (ACM SIGGRAPH '87 Conference Proceedings) **2** (1987), no. 4, 25–34.

[92] M. B. H. Rhouma and H. Frigui, *Self-organization of pulse-coupled oscillators with application to clustering*, Transactions on Pattern Analysis and Machine Intelligence **23** (2001), no. 2, 180–195.

[93] J. Rinzel and G. B. Ermentrout, *Analysis of neural excitability*, Methods of Neuronal Modeling (C. Koch and I. Segev, eds.), MIT Press, Cambridge, 1998.

[94] A. Sarlette, *Geometry and symmetries in coordination control*, Ph.D. thesis, University of Liège, January 2009.

[95] A. Sarlette and R. Sepulchre, *Synchronization on the circle*, The complexity of dynamical systems: a multi-disciplinary perspective (J. Dubbeldam, K. Green, and D. Lenstra, eds.), Wiley & Sons, 2011.

[96] A. Schinzel, *Self-inversive polynomials with all zeros on the unit circle*, Ramanujan Journal **9** (2005), no. 1-2, 19–23.

[97] W. Senn and R. Urbanczik, *Similar nonleaky integrate-and-fire neurons with instantaneous couplings always synchronize*, Siam Journal on Applied Mathematics **61** (2000), no. 4, 1143–1155.

[98] R. Sepulchre, D. A. Paley, and N. E. Leonard, *Stabilization of planar collective motion: All-to-all communication*, IEEE Transactions on Automatic Control **52** (2007), no. 5, 811–824.

[99] D. Serre, *Sur la variation totale comme fonction de Liapunov pour un système de lois de conservation*, Comptes rendus de l'Académie des Sciences Paris **312, Série I** (1991), 919–922.

[100] A. Sherman, J. Rinzel, and J. Keizer, *Emergence of organized bursting in clusters of pancreatic beta-cells by channel sharing*, Biophysical Journal **54** (1988), no. 3, 411 – 425.

[101] M. H. Shih and J. W. Wu, *On a discrete version of the Jacobian conjecture of dynamical systems*, Nonlinear Analysis-Theory Methods & Applications **34** (1998), no. 5, 779–789.

[102] R. M. Smeal, G. B. Ermentrout, and J. A. White, *Phase-response curves and synchronized neural networks*, Philosophical Transactions of the Royal Society B: Biological Sciences **365** (2010), no. 1551, 2407–2422.

[103] D. C. Sorensen, *Minimization of a large-scale quadratic function: Subject to a spherical constraint*, Siam Journal on Optimization **7** (1997), no. 1, 141–161.

[104] S. H. Strogatz, *From Kuramoto to Crawford: exploring the onset of synchronization in populations of coupled oscillators*, Physica D **143** (2000), no. 1-4, 1–20.

[105] ———, *Exploring complex networks*, Nature **410** (2001), no. 6825, 268–276.

[106] ———, *Sync: The emerging science of spontaneous order*, Hyperion Press, 2003.

[107] B. Temple, *Systems of conservation laws with invariant submanifolds*, Transactions of the AMS **280** (1983), 781–795.

[108] M. Timme, F. Wolf, and T. Geisel, *Coexistence of regular and irregular dynamics in complex networks of pulse-coupled oscillators*, Physical Review Letters **89** (2002), no. 25, 258701.

[109] ———, *Prevalence of unstable attractors in networks of pulse-coupled oscillators*, Physical Review Letters **89** (2002), no. 15, 154105.

[110] ———, *Topological speed limits to network synchronization*, Physical Review Letters **92** (2004), no. 7, 074101.

[111] A. Tonnelier, H. Belmabrouk, and D. Martinez, *Event-driven simulations of nonlinear integrate-and-fire neurons*, Neural Computation **19** (2007), no. 12, 3226–3238.

[112] A. Treves, *Mean-field analysis of neuronal spike dynamics*, Network-Computation in Neural Systems **4** (1993), no. 3, 259–284.

[113] J. N. Tsitsiklis, *Problems in decentralized decision making and computation*, Ph.D. thesis, MIT, 1984.

[114] M. Tsodyks, I. Mitkov, and H. Sompolinsky, *Pattern of synchrony in inhomogeneous networks of oscillators with pulse interactions*, Physical Review Letters **71** (1993), 1280–1283.

[115] K. Tsumoto, H. Kitajima, T. Yoshinaga, K. Aihara, and H. Kawakami, *Bifurcations in Morris-Lecar neuron model*, Neurocomputing **69** (2006), no. 4-6, 293–316.

[116] P. J. Uhlhaas and W. Singer, *Neural synchrony in brain disorders: Relevance for cognitive dysfunctions and pathophysiology*, Neuron **52** (2006), no. 1, 155 – 168.

[117] C. van Vreeswijk, *Partial synchronization in populations of pulse-coupled oscillators*, Physical Review E **54** (1996), 5522–5537.

[118] C. van Vreeswijk, L. F. Abbott, and G. B. Ermentrout, *When inhibition not excitation synchronizes neural firing*, Journal of Computational Neuroscience **1** (1994), no. 4, 313–321.

[119] T. Vicsek, A. Czirok, E. Benjacob, I. Cohen, and O. Shochet, *Novel type of phase-transition in a system of self-driven particles*, Physical Review Letters **75** (1995), no. 6, 1226–1229.

[120] T. J. Walker, *Acoustic synchrony: two mechanisms in the snowy tree cricket*, Science **166** (1969), 891–894.

[121] W. Wang and J. J. E. Slotine, *On partial contraction analysis for coupled nonlinear oscillators*, Biological Cybernetics **92** (2005), no. 1, 38–53.

[122] S. Watanabe and S. H. Strogatz, *Constants of motion for superconducting Josephson arrays*, Physica D **74** (1994), no. 3-4, 197–253.

[123] K. Wiesenfeld, *New results on frequency-locking dynamics of disordered Josephson arrays*, Physica B **222** (1996), no. 4, 315–319.

[124] J. C. Willems, *The analysis of feedback systems*, MIT Press, 197.

[125] A. Winfree, *The geometry of biological time*, New York: Springler-Verlag, 2001 (Second Edition).

[126] V. A. Yakubovich, *Solution of certain matrix inequalities in the stability theory of nonlinear control systems*, Soviet. Math. Dokl. **3** (1962), 620–623.

[127] G. Zames and P. L. Falb, *Stability conditions for systems with monotone and slope-restricted nonlinearities*, SIAM Journal on Control **6** (1968), no. 1, 89–108.

[128] R. Zillmer, R. Livi, A. Politi, and A. Torcini, *Stability of the splay state in pulse-coupled networks*, Physical Review E **76** (2007), no. 4, 046102.